



## Copyright Undertaking

This thesis is protected by copyright, with all rights reserved.

**By reading and using the thesis, the reader understands and agrees to the following terms:**

1. The reader will abide by the rules and legal ordinances governing copyright regarding the use of the thesis.
2. The reader will use the thesis for the purpose of research or private study only and not for distribution or further reproduction or any other purpose.
3. The reader agrees to indemnify and hold the University harmless from and against any loss, damage, cost, liability or expenses arising from copyright infringement or unauthorized usage.

### IMPORTANT

If you have reasons to believe that any materials in this thesis are deemed not suitable to be distributed in this form, or a copyright owner having difficulty with the material being included in our database, please contact [lbsys@polyu.edu.hk](mailto:lbsys@polyu.edu.hk) providing details. The Library will look into your claim and consider taking remedial action upon receipt of the written requests.

**FINE ATMOSPHERIC PARTICLES (PM<sub>2.5</sub>) IN LARGE CITY  
CLUSTERS, CHINA: CHEMICAL COMPOSITIONS,  
TEMPORAL-SPATIAL VARIATIONS AND REGIONAL  
TRANSPORT**

**MING LI LI**

**Ph.D**

**The Hong Kong Polytechnic University**

**2017**

**The Hong Kong Polytechnic University**

**Department of Civil and Environmental Engineering**

**FINE ATMOSPHERIC PARTICLES (PM<sub>2.5</sub>) IN LARGE CITY  
CLUSTERS, CHINA: CHEMICAL COMPOSITIONS,  
TEMPORAL-SPATIAL VARIATIONS AND REGIONAL  
TRANSPORT**

**MING LI LI**

**A thesis submitted in partial fulfilment of the requirements for  
the degree of Doctor of Philosophy**

**November 2016**

## **CERTIFICATE OF ORIGINALITY**

I hereby declare that this thesis is my own work and that, to the best of my knowledge and belief, it reproduces no material previously published or written, nor material that has been accepted for the award of any other degree or diploma, except where due acknowledgement has been made in the text.

---

**MING LI LI**

## Abstract

With the aggravation of atmospheric environment, fine atmospheric particle ( $PM_{2.5}$ ) pollution has become one of the top environmental issues in China, due to its adverse impact on human health and climate. This project is aimed to investigate the current pollution statuses and pollution characteristics of  $PM_{2.5}$  in three large city clusters of China: the Pearl River Delta (PRD), the Yangtze River Delta (YRD) and North China.  $PM_{2.5}$  samples were simultaneously collected in the three regions over a one-year period to measure their chemical compositions (*e.g.*, trace metals, organic carbon and elemental carbon, lead isotopic compositions and water-soluble inorganic ions). The temporal-spatial and seasonal variations, sources and long-range transport of  $PM_{2.5}$ , the formation mechanism and regional transport of  $PM_{2.5}$  during pollution events, and the bioaccessibility and health risks of airborne trace metals in  $PM_{2.5}$  have been studied in this research.

In the three regions, the concentrations and chemical compositions of  $PM_{2.5}$  showed a decreasing trend in the order of urban > rural > remote site, and clear seasonal variations. Among the urban sites,  $PM_{2.5}$  pollution was most serious in North China (Beijing), followed by the YRD region (Shanghai, Nanjing and Hangzhou) and the PRD region (Guangzhou). Source appointment of chemical compositions of  $PM_{2.5}$  demonstrated that anthropogenic sources including coal combustion, heavy industries and traffic emissions were the major contributors to  $PM_{2.5}$  in the three regions. Long-range transport pathways and potential source regions of  $PM_{2.5}$  in the three regions were seasonally dependent. Different characteristics in the temporal-spatial and seasonal variations of  $PM_{2.5}$  among the three regions were driven by their local emissions, meteorological conditions and long-range transport pathways.

Trans-boundary transport of  $PM_{2.5}$  over the three regions was demonstrated by the PSCF model and the NAQPMS model. Meteorological conditions and regional transport play an important role in the formation of the three pollution events occurred in Shanghai during

autumn and winter. Secondary aerosols contributed the largest fraction to  $PM_{2.5}$  during the pollution events, suggesting the importance of secondary aerosol formation in driving  $PM_{2.5}$  pollution. The results indicated that the formation of  $PM_{2.5}$  pollution is related to emission sources, meteorological conditions and long-range transport of air pollutants.

High bioaccessibility for V, intermediate bioaccessibility for Mn, Cr and Ni, and low bioaccessibility for Pb and Zn were investigated in Guangzhou (GZ), Shanghai (SH) and Nanjing (NJ). Seasonally, the bioaccessibility of Mn, Pb and Zn were highest in winter. Compared with non-pollution days, the bioaccessibility of Mn, Pb, V and Zn in GZ, and Zn in SH and NJ were higher on pollution days. Carcinogenic and non-carcinogenic risks posed by airborne trace metals via inhalation exposure to children and adults were significantly higher on pollution days than those on non-pollution days during winter.

## **Publications from the Research Project**

- Ming, L.L., Jin, L., Li, J., Fu, P.Q., Yang, W.Y., Liu, D., Zhang, G., Wang, Z.F. and Li, X.D. 2017. PM<sub>2.5</sub> in the Yangtze River Delta, China: chemical compositions, seasonal variations and regional pollution events. *Environmental Pollution*. 223, 200-212.
- Wang, Y., Luo, C.L., Wang, S.R., Liu, J.W., Pan, S.H., Li, J., Ming, L.L., Zhang, G. and Li, X.D. 2014. Assessment of the air-soil partitioning of polycyclic aromatic hydrocarbons in a paddy field using a modified fugacity sampler. *Environmental Science & Technology*. 49, 284-291.
- Wang, Y., Wang, S.R., Luo, C.L., Li, J., Ming, L.L., Zhang, G. and Li, X.D. 2015. The effects of rice canopy on the air-soil exchange of polycyclic aromatic hydrocarbons and organochlorine pesticides using paired passive air samplers. *Environmental Pollution*. 200, 35-41.
- Wang, Y., Wang, S.R., Luo, C.L., Xu, Y., Pan, S.H., Li, J., Ming, L.L., Zhang, G. and Li, X.D. 2015. Influence of rice growth on the fate of polycyclic aromatic hydrocarbons in a subtropical paddy field: A life cycle study. *Chemosphere*. 119, 1233-1239.

## Acknowledgements

I would like to express my sincere thanks to my supervisor, Professor. X.D. Li. Without his patient guidance and full support throughout my PhD study and this project, the completion of this thesis would be unachievable. Through his guidance, I have gained stringent attitude and the ability to think independently, which are useful for my career development in environmental science.

I am very grateful to Mr. W.S. Lam, Ms. Carman Ip, Ms. Chloe Tang and Mr. Steven Poon for their help on field sampling and chemical analysis. I also want to thank the group members at the Hong Kong Polytechnic University including Dr. B.W. Chen, Dr. L. Cang, Dr. L.C. Fang, Dr. R.S. Ying, Dr. X.S. Luo, Dr. L. Jin, Ms. S.Y. Liang, Ms. Y.P. Zhao, Ms. J.W. Xie and Mr. N. Xiang, for their kind help and support. Special thanks to Prof. G. Zhang and Dr. J. Li, Guangzhou Institute of Geochemistry, Chinese Academy of Sciences (CAS), for their guidance and support throughout the project. Thanks to the students from the research group of Prof. G. Zhang (Guangzhou Institute of Geochemistry, Chinese Academy of Sciences), Prof. Z.G. Guo (Department of Environmental Science and Engineering, Fudan University), Prof. D.H. Lin (College of Environmental and Resource Sciences, Zhejiang University), and Dr. L. Cang (Institute of Soil Science, Chinese Academy of Sciences) for their help on the field sampling. Finally, I would like to thank my parents and husband, for their wholehearted support and encouragement.



2.2.4.4	Pb Isotopic Fingerprinting in Aerosols .....	20
2.2.4.5	Health Effect of Airborne Trace Metals .....	21
2.3	Bioaccessibility of Airborne Trace Metals .....	22
2.3.1	Assessment Methods for Bioaccessible Airborne Trace Metals .....	22
2.3.1.1	Water-soluble Fraction .....	22
2.3.1.2	Sequential Extraction .....	23
2.3.1.3	Simulated Human Body Fluids .....	23
2.3.2	Possible Influence Factors on Bioaccessibility of Airborne Trace Metals ..	24
2.4	Regional Transport of Atmospheric Particulate Particles.....	25
2.5	Research Emphasis of PM <sub>2.5</sub> .....	26
2.5.1	Emission Inventory of PM <sub>2.5</sub> and Air Pollutants .....	27
2.5.2	PM <sub>2.5</sub> Pollution in China .....	28
2.5.3	The Characteristics of Chemical Compositions in PM <sub>2.5</sub> .....	29
2.5.4	Haze Episode .....	32
2.5.5	PM <sub>2.5</sub> Studies in Remote Sites.....	34
2.6	Summary and Outlook .....	35

### **Chapter 3 - Methodology .....** **37**

3.1	Characteristics of the Study Region .....	37
3.1.1	The Pearl River Delta Region .....	37
3.1.2	The Yangtze River Delta Region.....	39
3.1.3	North China.....	40
3.2	Sampling Sites.....	41
3.2.1	Description of Sampling Sites in the PRD Region .....	43
3.2.2	Description of Sampling Sites in the YRD Region.....	44
3.2.3	Description of Sampling Sites in North China.....	46
3.3	Sampling Methods .....	46
3.3.1	Sampling Instruments .....	46
3.3.2	PM <sub>2.5</sub> Sampling .....	47
3.3.3	Overview of the Sampling .....	47
3.4	Chemical Analysis.....	50
3.4.1	Total Metal Concentration.....	50
3.4.2	Pb Isotopic Composition Analysis .....	52
3.4.3	Bioaccessible Fraction of Trace Metals .....	52
3.4.4	Water-soluble Ions Analysis.....	53
3.4.5	Carbonaceous Species.....	54
3.5	NAQPMS Model Description and Setup .....	54
3.6	Enrichment Factor .....	57
3.7	Meteorological Information .....	57
3.8	Back Trajectory Analysis .....	57
3.9	Potential Source Contribution Function .....	58
3.10	Health Risk Assessment of Airborne Trace Metals .....	59
3.11	Statistical Analysis .....	60

## **Chapter 4 - Concentrations and Chemical Compositions of PM<sub>2.5</sub> in the Pearl River Delta, the Yangtze River Delta and North China..... 61**

4.1 Data Validation-Sum of Chemical Species versus PM <sub>2.5</sub> Mass.....	61
4.2 An Overview of PM <sub>2.5</sub> Concentrations.....	63
4.3 Air Quality in Guangzhou, Shanghai, Nanjing and Beijing.....	66
4.4 Concentrations of Airborne Trace Metals in PM <sub>2.5</sub> .....	67
4.5 Lead Isotopic Compositions in PM <sub>2.5</sub> .....	71
4.6 Concentrations of Carbonaceous Species in PM <sub>2.5</sub> from Guangzhou, Shanghai and Beijing.....	73
4.7 Concentrations of Water-soluble Ions in PM <sub>2.5</sub> from Shanghai and Nanjing.....	75
4.8 Summary.....	77

## **Chapter 5 -Temporal-Spatial Variations and Source Appointment of PM<sub>2.5</sub> in the PRD, the YRD and North China..... 78**

5.1 Temporal and Spatial Variations of PM <sub>2.5</sub> .....	78
5.1.1 The PRD Region.....	78
5.1.2 The YRD Region.....	82
5.1.3 North China.....	88
5.1.4 Comparison among the Three Regions.....	93
5.2 Source Appointment of PM <sub>2.5</sub> .....	95
5.2.1 Enrichment Factor of Trace Metals.....	95
5.2.2 Sources of Pb in PM <sub>2.5</sub> .....	98
5.2.3 The Relationship between OC and EC.....	107
5.2.4 The Ratio of NO <sub>3</sub> <sup>-</sup> /SO <sub>4</sub> <sup>2-</sup> .....	109
5.3 Influent Factors for PM <sub>2.5</sub> Pollution.....	111
5.3.1 Emission Inventories and Source Contributions for Primary Atmospheric Pollutants.....	111
5.3.2 Meteorological Conditions.....	115
5.3.3 Impact of Long-range Transport.....	117
5.3.3.1 Potential Source Regions.....	117
5.3.3.2 Long-range Transport of Pb.....	124
5.4 Summary.....	127

## **Chapter 6 - Regional Transport of PM<sub>2.5</sub> in China: Analysis of Pollution Events ..... 129**

6.1 A Modeling Study of Regional Transport of PM <sub>2.5</sub> during a Severe and Long-lasting Pollution Event.....	129
6.1.1 Air Quality during the Pollution Event.....	129
6.1.2 Meteorological Conditions.....	132
6.1.3 The Evolution and Regional Transport of PM <sub>2.5</sub> -Modeling Results.....	134
6.2 Formation Mechanisms of Pollution Events in the YRD Region.....	136

6.2.1	Identification of Three Pollution Events in the YRD Region .....	136
6.2.2	Meteorological Conditions during Three Pollution Events.....	139
6.2.3	Regional Transport of PM <sub>2.5</sub> during Three Pollution Events–Modeling Results.....	142
6.2.4	Chemical Compositions during Three Pollution Events .....	146
6.2.4.1	Pollution Event 1 .....	147
6.2.4.2	Pollution Event 2 .....	149
6.2.4.3	Pollution Event 3 .....	150
6.2.4.4	Comparison the Three Pollution Events .....	150
6.3	Summary .....	152
<b>Chapter 7 - Bioaccessibility and Health Risks of Trace Metals in PM<sub>2.5</sub> in Large Cities of China using Simulated Lung Fluids.....</b>		<b>154</b>
7.1	Total and Bioaccessible Concentrations of Trace Metals in PM <sub>2.5</sub> .....	154
7.2	Bioaccessibility of Airborne Trace Metals .....	157
7.3	Seasonal Variations of Airborne Trace Metals Bioaccessibility .....	157
7.4	Bioaccessibility of Airborne Trace Metals on Pollution Days and Non-pollution Days.....	161
7.5	Health Risks Assessment of Airborne Trace Metals .....	165
7.6	Summary .....	171
<b>Chapter 8 - Conclusions and Recommendations.....</b>		<b>172</b>
8.1	Summary of Major Results .....	172
8.2	Recommendations .....	174
8.3	Limitations and Future Research.....	174
<b>References .....</b>		<b>176</b>
<b>Database of Original Results from All Experiments in the Study .....</b>		<b>200</b>

## List of Tables

Table 2-1 Concentration limits ( $\mu\text{g m}^{-3}$ ) for PM pollutants in the Chinese National Ambient Air Quality Standards (NAAQS), European (EU) and the World Health Organization (WHO) Air Quality Guidelines. ....	8
Table 2-2 The levels of some toxic metals with National Ambient Air Quality Standards (NAAQS) in China and WHO ( $\text{ng m}^{-3}$ ).....	16
Table 2-3 Various emission sources of metal elements in the air (Calvo et al., 2013). ....	19
Table 2-4 Annual mean concentrations of airborne trace metals ( $\text{ng m}^{-3}$ ) in $\text{PM}_{2.5}$ from the urban cities over China.....	31
Table 3-1 Overview of the sampling sites in the present study. ....	42
Table 3-2 The sampling program for $\text{PM}_{2.5}$ in the PRD, the YRD and North China. ....	49
Table 3-3 The temperature setting of aluminium heating block for acid digestion of filter samples. ....	51
Table 3-4 Composition ( $\text{g L}^{-1}$ ) of simulated lung fluids–Gamble’s solution.....	53
Table 4-1 The annual mean concentrations of $\text{PM}_{2.5}$ ( $\mu\text{g m}^{-3}$ ) in the nine sampling sites. ....	65
Table 4-2 The annual average concentrations (annual $\pm$ S.D.) of airborne trace metals and the mass ratios of crustal elements (Al, Fe, Ca, K and Mg), trace elements (Cr, Cu, Pb, Mn, Zn, V and Ni) and total metals to $\text{PM}_{2.5}$ mass (%) at the sampling sites from the PRD and YRD regions, and North China.....	69
Table 4-3 The annual and seasonal averages of Pb isotope compositions (mean $\pm$ S.D.) in $\text{PM}_{2.5}$ in the sampling sites from the PRD, the YRD and North China. ....	72
Table 4-4 Statistical description of the concentrations ( $\mu\text{g m}^{-3}$ ) and the mass ratios (%) of carbonaceous species, and the ratio of OC/EC and POC/SOC in Guangzhou, Shanghai and Beijing. ....	74
Table 4-5 The annual average concentrations of water-soluble ions ( $\mu\text{g m}^{-3}$ ) and their mass contributions to $\text{PM}_{2.5}$ mass (%), and the ratio of $\text{NO}_3^-/\text{SO}_4^{2-}$ in Shanghai and Nanjing.....	76
Table 5-1 The annual and seasonal averages of $\text{PM}_{2.5}$ and airborne trace metal concentrations in $\text{PM}_{2.5}$ in Guangzhou, Heshan and Hok Tsui.....	80

Table 5-2 The annual and seasonal average concentrations of PM <sub>2.5</sub> and airborne trace metals in the four sites in the YRD region. ....	84
Table 5-3 The annual and seasonal averages of PM <sub>2.5</sub> and airborne trace metals in Beijing and Mount Changbai. ....	90
Table 5-4 The Pb isotopic compositions of some known natural/anthropogenic sources and other environmental samples in the PRD region. ....	102
Table 5-5 The Pb isotopic compositions of some known natural/anthropogenic sources and other environmental samples in Shanghai. ....	103
Table 5-6 The Pb isotopic compositions of some known natural/anthropogenic sources and other environmental samples in North China. ....	104
Table 5-7 Emission inventory (kt) of primary atmospheric pollutants in the PRD, the YRD and Beijing. ....	114
Table 5-8 Emission of primary atmospheric pollutants and energy consumption in Guangzhou, Shanghai and Beijing during the year of 2013. ....	114
Table 5-9 Meteorological parameters in the year of 2013 in Guangzhou, Shanghai and Beijing. ....	116
Table 7-1 Total and Bioaccessible concentrations (ng m <sup>-3</sup> , annual mean ± S.D.), and bioaccessible fraction (%) of trace metals in PM <sub>2.5</sub> from Guangzhou, Shanghai and Nanjing. ....	156
Table 7-2 Correlation coefficients between PM <sub>2.5</sub> and bioaccessible trace metal concentrations in Guangzhou, Shanghai and Nanjing. ....	159
Table 7-3 Correlation coefficients between PM <sub>2.5</sub> concentration and trace metal bioaccessibility in Guangzhou, Shanghai and Nanjing. ....	159
Table 7-4 Related parameters for risk assessment calculation of airborne trace metals via inhalation exposure. ....	168
Table 7-5 Mean concentrations (ng m <sup>-3</sup> ) of bioaccessible trace metals in PM <sub>2.5</sub> in Guangzhou, Shanghai and Nanjing. ....	169
Table 7-6 Carcinogenic risk (CR) and non-carcinogenic risk (HQ) of airborne trace metals (annual mean concentrations) via inhalation exposure to children and adults in Guangzhou, Shanghai and Nanjing. ....	170

## List of Figures

Figure 2-1 The correlation between atmospheric particulate matters compositions, sources, properties, atmospheric interactions and transformation, climate and health effects [Source: (P öschl, 2005)].....	5
Figure 3-1 City cluster of the Pearl River Delta Region (Du et al., 2013).....	38
Figure 3-2 City cluster of the Yangtze River Delta Region.....	39
Figure 3-3 City cluster of North China Plain.....	40
Figure 3-4 The sampling sites in the PRD and YRD regions, and North China.....	41
Figure 3-5 The high-volume PM <sub>2.5</sub> sampler.....	47
Figure 3-6 The modeling domain.....	56
Figure 4-1. Scatter plots of sum of measured chemical species versus measured mass on quartz microfiber filters for PM <sub>2.5</sub> samples collected at (a) Guangzhou, (b) Shanghai and (c) Beijing.....	62
Figure 4-2 The annual averages of PM <sub>2.5</sub> concentrations in the nine sampling sites.....	65
Figure 4-3 The distributions of air quality grades (PM <sub>2.5</sub> concentration, µg m <sup>-3</sup> ) in frequencies in (a) Guangzhou; (b) Shanghai; (c) Nanjing; and (d) Beijing in the autumn, winter, spring and summer (0-35 µg m <sup>-3</sup> : excellent; 35-75 µg m <sup>-3</sup> : fine; 75-115 µg m <sup>-3</sup> : light pollution; 115-150 µg m <sup>-3</sup> : medium pollution; 150-250 µg m <sup>-3</sup> : severe pollution; 250-500 µg m <sup>-3</sup> : serious pollution).....	67
Figure 4-4 The mass ratios of crustal elements and trace elements to PM <sub>2.5</sub> mass in the nine sampling sites.....	70
Figure 5-1 Temporal variations of PM <sub>2.5</sub> concentrations (µg m <sup>-3</sup> ) over the sampling period in (a) Guangzhou and Heshan and (b) Hok Tsui.....	79
Figure 5-2 Temporal variations of OC and EC (µg m <sup>-3</sup> ) in Guangzhou during the high frequency sampling period in each season.....	81
Figure 5-3 Time series of PM <sub>2.5</sub> concentrations for the simultaneous samples in the YRD...	82
Figure 5-4 The linear regression of trace metal concentrations and PM <sub>2.5</sub> in Shanghai, Nanjing, Hangzhou and Ningbo in the YRD region: major elements (Al, Ca and	

Mg) and trace elements (Cu, Pb and Zn). .....	85
Figure 5-5 Temporal variations of OC and EC ( $\mu\text{g m}^{-3}$ ) in Shanghai during the high frequency sampling period in each season. ....	87
Figure 5-6 Temporal variations of PM <sub>2.5</sub> concentrations in Beijing in autumn (from 15 <sup>th</sup> October to 14 <sup>th</sup> November 2013), winter (from 2 to 21 January 2014), spring (from 12 <sup>th</sup> April to 12 <sup>th</sup> May 2014) and summer (30 <sup>th</sup> July to 28 <sup>th</sup> August 2014). .....	89
Figure 5-7 Temporal variations of OC and EC ( $\mu\text{g m}^{-3}$ ) in Beijing during the high frequency sampling period in each season. ....	91
Figure 5-8 Temporal variations of PM <sub>2.5</sub> concentrations in Mount Changbai.....	92
Figure 5-9 Mass contributions of POC, EC, SOC, crustal elements and trace elements to PM <sub>2.5</sub> in (a) Guangzhou; (b) Shanghai; and (c) Beijing. ....	94
Figure 5-10 The seasonal averages of enrichment factors (EF) for metal elements in PM <sub>2.5</sub> in the PRD region: (a) Guangzhou; (b) Heshan; and (c) Hok Tsui. ....	96
Figure 5-11 The seasonal averages of enrichment factors (EF) for metal elements in PM <sub>2.5</sub> in the YRD region: (a) Shanghai; (b) Nanjing; (C) Hangzhou; and (d) Ningbo. ....	96
Figure 5-12 The seasonal averages of enrichment factors (EF) for metal elements in PM <sub>2.5</sub> in North China: (a) Beijing and (b) Mount Changbai. ....	97
Figure 5-13 Comparison of <sup>206</sup> Pb/ <sup>207</sup> Pb and <sup>208</sup> Pb/ <sup>207</sup> Pb of PM <sub>2.5</sub> samples in this study and some known natural/anthropogenic sources and other environmental samples in (a) the PRD; (b) the YRD; and (c) North China. ....	101
Figure 5-14 Seasonal variations of Pb isotopic ratios ( <sup>206</sup> Pb/ <sup>207</sup> Pb and <sup>208</sup> Pb/ <sup>207</sup> Pb) and Pb concentrations (mg kg <sup>-1</sup> ) for PM <sub>2.5</sub> samples in (a) Guangzhou; (b) Heshan; and (c) Hok Tsui. ....	105
Figure 5-15 Seasonal variations of Pb isotopic ratios ( <sup>206</sup> Pb/ <sup>207</sup> Pb and <sup>208</sup> Pb/ <sup>207</sup> Pb) and Pb concentrations (mg kg <sup>-1</sup> ) for PM <sub>2.5</sub> samples in (a) Shanghai; (b) Nanjing; (c) Hangzhou; and (d) Ningbo. ....	105
Figure 5-16 Seasonal variations of Pb isotopic ratios ( <sup>206</sup> Pb/ <sup>207</sup> Pb and <sup>208</sup> Pb/ <sup>207</sup> Pb) and Pb concentrations (mg kg <sup>-1</sup> ) for PM <sub>2.5</sub> samples in (a) Beijing and (b) Mount Changbai. ....	106
Figure 5-17 Correlation between OC and EC concentrations in PM <sub>2.5</sub> in (a) Guangzhou; (b) Shanghai; and (c) Beijing during the four seasons. ....	108

Figure 5-18 Time series of $\text{NO}_3^-/\text{SO}_4^{2-}$ ratio in Shanghai and Nanjing.....	110
Figure 5-19 Cluster analysis of two-day backward trajectories of air masses during the four seasons in Guangzhou.....	119
Figure 5-20 Cluster analysis of two-day backward trajectories of air masses during the four seasons in Shanghai.....	120
Figure 5-21 Cluster analysis of two-day backward trajectories of air masses during the four seasons in Beijing.....	121
Figure 5-22 Maps of potential sources of $\text{PM}_{2.5}$ in Guangzhou during the four seasons. The darkness of red cells represents PSCF values. ....	122
Figure 5-23 Maps of potential sources of $\text{PM}_{2.5}$ in Shanghai during the four seasons.....	122
Figure 5-24 Maps of potential sources of $\text{PM}_{2.5}$ in Beijing during the four seasons.....	123
Figure 5-25 Comparison of annual means of Pb isotopic ratios in $\text{PM}_{2.5}$ from the nine sampling sites.....	126
Figure 5-26 Lead isotopic compositions of coal samples, cinder samples and ash samples from power plants in China (the dataset were provided by Dr. Xiangyang Bi from the State Key Laboratory of Biogeology and Environmental Geology, China University of Geosciences, Wuhan).....	126
Figure 6-1 Daily average $\text{PM}_{2.5}$ concentrations ( $\mu\text{g m}^{-3}$ ) in Guangzhou, Jiangmen (Heshan), Shanghai, Nanjing, Hangzhou, Ningbo and Beijing during the pollution event. .	131
Figure 6-2 Satellite image on 7 December 2013 in Eastern China ( <a href="http://earthobservatory.nasa.gov/NaturalHazards/view.php?id=82535">http://earthobservatory.nasa.gov/NaturalHazards/view.php?id=82535</a> ).....	131
Figure 6-3 Surface meteorological conditions from 5 to 12 December 2013 in Shanghai from the monitoring station (31.4N, 121.47E) (Real-time data display from ENVF Atmospheric & Environmental Real-time Database: <a href="http://envf.ust.hk/">http://envf.ust.hk/</a> ). ....	133
Figure 6-4 Vertical sounding plots on 6 December 2013 in Shanghai from the monitoring station (31.4N, 121.47E) (Real-time data display from ENVF Atmospheric & Environmental Real-time Database: <a href="http://envf.ust.hk/">http://envf.ust.hk/</a> ) (the blue line represents dew point and the red line represents temperature).....	133
Figure 6-5 The simulated daily average of surface $\text{PM}_{2.5}$ concentration ( $\mu\text{g m}^{-3}$ ) and wind vector ( $\text{m s}^{-1}$ ) in China during the severe pollution event: (a) on 5 December 2013; (b) on 7 December 2013; (c) on 9 December 2013; (d) on 11 December 2013; (e)	

on 12 December 2013; and (f) on 14 December 2013. ....	135
Figure 6-6 Temporal variations of PM <sub>2.5</sub> concentrations for the samples collected in Shanghai and Nanjing during high frequency sampling period. PE 1 = pollution event 1; PE 2 = pollution event 2 and PE 3 = pollution event 3.....	136
Figure 6-7 Time series of PM <sub>2.5</sub> concentrations in Shanghai during the processes of the three pollution events. ....	137
Figure 6-8 Time series of visibility in the monitoring station (31.4N, 121.47E) during the three pollution events (Real-time data display from ENVF Atmospheric & Environmental Real-time Database: <a href="http://envf.ust.hk/">http://envf.ust.hk/</a> ). ....	138
Figure 6-9 Time series of relative humidity in the monitoring station (31.4N, 121.47E) during the three pollution events (Real-time data display from ENVF Atmospheric & Environmental Real-time Database: <a href="http://envf.ust.hk/">http://envf.ust.hk/</a> ). ....	138
Figure 6-10 Surface meteorological conditions during the three pollution events in Shanghai from the monitoring station (31.4N, 121.47E) (Real-time data display from ENVF Atmospheric & Environmental Real-time Database: <a href="http://envf.ust.hk/">http://envf.ust.hk/</a> ). ....	140
Figure 6-11 One-day backward trajectories of air masses arriving at Shanghai at an altitude 1000 m during the process of the three pollution events (PE1, 2 and 3).....	141
Figure 6-12 The simulated daily average of surface PM <sub>2.5</sub> concentration ( $\mu\text{g m}^{-3}$ ) and wind vector ( $\text{m s}^{-1}$ ) in eastern China during the first pollution event (PE1): (a) on 5 November 2013; (b) on 6 November 2013; (c) on 7 November 2013; and (d) on 8 November 2013.....	143
Figure 6-13 The simulated daily average of surface PM <sub>2.5</sub> concentration ( $\mu\text{g m}^{-3}$ ) and wind vector ( $\text{m s}^{-1}$ ) in eastern China during the secondary pollution event (PE2): (a) on 6 December 2013; (b) on 8 December 2013; (c) on 9 December 2013; (d) on 11 December 2013; (e) on 12 December 2013; and (f) on 14 December 2013. ....	144
Figure 6-14 The simulated daily average of surface PM <sub>2.5</sub> concentration ( $\mu\text{g m}^{-3}$ ) and wind vector ( $\text{m s}^{-1}$ ) in eastern China during the third pollution event (PE3): (a) on 26 December 2013; (b) on 31 December 2013; (c) on 2 January 2014; and (d) on 4 January 2014. ....	145
Figure 6-15 Concentrations of the measured chemical compositions and the relative abundance of POC and SOC in PM <sub>2.5</sub> samples in Shanghai during PE1, 2 and 3.	146
Figure 6-16 Chemical composition of PM <sub>2.5</sub> samples collected before pollution event 1 (BPE 1), in pollution event (PE 1) and after pollution event (APE 1) in Shanghai. ....	148

Figure 6-17 Chemical composition of PM <sub>2.5</sub> during pollution event 2 (PE2) in Shanghai. .	148
Figure 6-18 Chemical composition of PM <sub>2.5</sub> samples collected before pollution event 3 (BPE 3), in pollution event (PE 3) and after pollution event (APE 3) in Shanghai. ....	148
Figure 6-19 Relative abundances of the measured chemical compositions in PM <sub>2.5</sub> samples in Shanghai during the three pollution events: PE1, 7-8 November 2013; PE2, 5-12 December 2013; and PE3, 25 December 2013-5 January 2014.....	152
Figure 7-1 Seasonal variations of bioaccessible concentrations for trace metals in PM <sub>2.5</sub> in (a) Guangzhou; (b) Shanghai; and (c) Nanjing. The boxes and whiskers denote the minimums, 25, 50, 75 percentiles and maximums; the dots denote the mean values. ....	160
Figure 7-2 Bioaccessibility (mean ± S.D.) of trace metals in PM <sub>2.5</sub> in four seasons in (a) Guangzhou; (b) Shanghai; and (c) Nanjing.....	160
Figure 7-3 Bioaccessible concentrations of trace metals during pollution and non-pollution days in Guangzhou in four seasons. ....	162
Figure 7-4 Bioaccessible concentrations of trace metals during pollution during pollution and non-pollution days in Shanghai in four seasons. ....	162
Figure 7-5 Bioaccessible concentrations of trace metals during pollution during pollution and non-pollution days in Nanjing in four seasons. ....	163
Figure 7-6 Bioaccessibility of trace metals during pollution and non-pollution days in Guangzhou in four seasons. ....	163
Figure 7-7 Bioaccessibility of trace metals during pollution and non-pollution days in Shanghai in four seasons. ....	164
Figure 7-8 Bioaccessibility of trace metals during pollution and non-pollution days in Nanjing in four seasons. ....	164
Figure 7-9 The ratios of (a) CR on pollution days to CR on non-pollution days and (b) HQ on pollution days to HQ on non-pollution days posed by airborne trace metals during winter in Guangzhou, Shanghai and Nanjing.....	167

# Chapter 1 - Introduction

## 1.1 Background

Elevated fine particles ( $PM_{2.5}$ ) in the atmosphere have become one of the top environmental concerns, due to their adverse effects on human health (Wessels et al., 2010) and climate change (Huang et al., 2012a).  $PM_{2.5}$  itself can get deep into human lungs when inhaled and may cause a wide range of health problems (Lanki et al., 2006; Wessels et al., 2010). The epidemiological association between human exposure to inhalable particles (*i.e.*,  $PM_{10}$ ) and increased incidence mortality rates due to lung cancer or cardiovascular diseases has been demonstrated by a number of studies (Corbett et al., 2007; Viana et al., 2008). Moreover, the adverse effect of fine particles also has been attributed to the toxicological effects of chemical compounds associated with fine particles (Gerlofs-Nijland et al., 2009; Uzu et al., 2011), such as organic carbon (OC) and elemental carbon (EC), water-soluble inorganic ions and metal elements (such as Fe, Cu, Pb, Zn, Ni and V). The inhalation of  $PM_{2.5}$  can therefore have long-term and serious impacts on human health.

In recent years, the occurrence of  $PM_{2.5}$  pollution has become increasingly frequent at a large scale in China (Fu et al., 2008; Hu et al., 2014), indicating that  $PM_{2.5}$  pollution is no longer confined in individual cities, but expanding over a large regional scale. Previous studies investigated the characteristics, chemical compositions, sources and formation mechanism of  $PM_{2.5}$  in some mega cities of China, such as Guangzhou, Shanghai, Nanjing and Beijing (Yao et al., 2002; Yang et al., 2005c; Wang et al., 2006b). However, very few investigations of  $PM_{2.5}$  have been conducted at a regional scale in China, such as those carried out in the Pearl River Delta (PRD) (Hagler et al., 2006) and the Beijing-Tianjin-Hebei (BTH) area (Zhao et al., 2013a). Therefore, it is imperative to generate a high-quality database of the concentration and chemical compositions of  $PM_{2.5}$  on region scales. The Pearl River Delta, the Yangtze River Delta (YRD) and the Beijing-Tianjin-Hebei regions are the most economically developed and rapidly urbanized city clusters in South, East and North China, respectively, which are characterized by

various characteristics and local emissions of air pollutants due to their different economic modes, meteorological conditions and other factors. Apart from local pollution, the three regions may also act as receptors and sources of large natural and anthropogenic emissions (Wang et al., 2008; Li et al., 2014) which could further make the aerosols more complex.  $PM_{2.5}$  have been individually studied at a regional scale (Hagler et al., 2006; Zhao et al., 2013a), but very few studies involving the synchronous sampling at different regions over a long-term period. Thus, simultaneously investigation on the pollution characteristics of  $PM_{2.5}$  in the three regions can help us to better understand the factors that influence air quality, and provide effective policy and strategy on the air pollution control.

Regional haze events with high  $PM_{2.5}$  concentrations occurred more frequently in the three regions recently (Fu et al., 2008; Tan et al., 2009; Zhao et al., 2013b; Wang et al., 2015). Previous studies investigated the meteorological conditions and aerosol physical, chemical and optical properties during haze episodes, and analyzed the key factors that affect the formation of haze (Ye et al., 2011; Huang et al., 2012a; Kang et al., 2013). However, the evolution and regional transport of air pollutants during haze have seldom studied (Wang et al., 2006d). A 3-D model, the Nested Air Quality Prediction Modeling System (NAQPMS), is a useful tool to understand the formation, evolution and transport of air pollutants (Wang et al., 2006d; Li et al., 2008; Li et al., 2014). This encourages us to integrate simultaneous field monitoring and modeling results of  $PM_{2.5}$  to better understand the formation, evolution and transport of haze events in the three regions, and possible regional transport of  $PM_{2.5}$  among the three regions.

The toxicity of  $PM_{2.5}$  has been studied predominantly through toxicological studies, but the mechanisms by which chemical components induces adverse health effects are still not fully understood. Many studies have been hypothesized that the toxicity of fine particles might be associated with the bioaccessible transition metals on the particle surface, such as iron (Fe), copper (Cu), vanadium (V), manganese (Mn), nickel (Ni) and zinc (Zn) (Heal et al., 2009; Charrier et al., 2014) which can enhance reactive oxygen species or free radical generation,

causing oxidative damage effects both to the lung (Lin et al., 2009) and other organs (Merolla and Richards, 2005). Furthermore, some toxic metals, such as cadmium (Cd), chromium (Cr) and lead (Pb), can also be carcinogenic for humans. Due to the rapid urbanization and industrialisation in China in recent decades, large quantities of trace metals have been emitted from various anthropogenic sources to the atmosphere (Luo et al., 2014). In China, investigations of airborne trace metals in  $PM_{2.5}$  tend to focus on urban areas in only one city (Hagler et al., 2007; Wang et al., 2007a; Chen et al., 2008; Bao et al., 2010), but very few researches are conducted simultaneously to measure trace metals in  $PM_{2.5}$  at regional scales. Moreover, these limited studies mainly focus on the total metal concentrations, while the bioaccessibility of trace metals in  $PM_{2.5}$  has rarely studied (Feng et al., 2009a). Consequently, the lack of data for the bioaccessibility of airborne trace metals in the three regions requires more research to understand their potential toxicity, and then provide insightful information regarding trace metal pollution control to policy makers.

## **1.2 Research Objectives**

This study is focused on characterization and comparison of  $PM_{2.5}$  in three large city clusters in China with distinctly different emissions and meteorological conditions: the PRD, the YRD and North China. In order to fill in those research gaps mentioned above, the objectives of the study are:

- 1) to study the concentrations and chemical compositions of  $PM_{2.5}$  in the three regions;
- 2) to characterize the temporal-spatial and seasonal variations, and sources of  $PM_{2.5}$ ;
- 3) to analyze the differences in pollution characteristics of  $PM_{2.5}$  among the three regions by studying the local emissions, meteorological conditions and long-range transport pathways;
- 4) to study the formation mechanism, evolution and regional transport of  $PM_{2.5}$  during pollution events; and
- 5) to evaluate the bioaccessibility and health risks of trace metals in  $PM_{2.5}$  in large cities of China.

### **1.3 Scope of Work**

In present work, PM<sub>2.5</sub> samples were simultaneously collected in the PRD, the YRD and North China over a one-year period. The chemical analysis for PM<sub>2.5</sub> include total and bioaccessible trace metals, water-soluble inorganic ions, organic carbon and elemental carbon and Pb isotopic compositions. HYbrid Single-Particle Lagrangian Integrated Trajectory (HYSPLIT) and Potential Sources Contribution Function (PSCF) model were used to identify the long-range transport and potential source regions of PM<sub>2.5</sub>. Based on the analysis of the temporal-spatial variations and sources of PM<sub>2.5</sub> in the three regions, factors including local emissions, meteorological conditions and long-range transport pathways that influence the characteristics of PM<sub>2.5</sub> have been studied. The formation mechanism, evolution and transport of PM<sub>2.5</sub> during pollution events were studied using the NAQPMS model and chemical composition analysis. Additionally, the bioaccessibility and health risks of trace metals in PM<sub>2.5</sub> have been evaluated. The outcome of this research will contribute to a better understanding of the pollution formation and transport of PM<sub>2.5</sub> at a regional scale, and to the formulation of effective policy on the regional air pollution control.

### **1.4 Organization**

This thesis is divided into eight chapters. The present chapter includes the background, objectives, scopes of this project, and the whole structure of this thesis. Chapter Two gives an integrated literature review. Chapter Three covers the details of sampling and methodology of this study. Chapter Four summaries and compares the concentrations and chemical compositions of PM<sub>2.5</sub> in the three regions. Chapter Five analyzes the temporal and spatial variations, sources and long-range transport pathways of PM<sub>2.5</sub> in the three regions, and investigates the possible factors that influence the characteristics of PM<sub>2.5</sub> pollution. Chapter Six studies the formation mechanism, evolution and regional transport of PM<sub>2.5</sub> during pollution events. The characteristics of bioaccessibility and health risks of airborne trace metals in PM<sub>2.5</sub> are evaluated in Chapter Seven. Finally, Chapter Eight gives the major findings in this study and some recommendations for future research.

## Chapter 2 - Literature Review

It is well known that atmospheric particulate matters (APM) are important for atmospheric physics and chemistry, the biosphere, climate and human health. As illustrated in Figure 2-1, the compositions, sources, properties, atmospheric interactions and transformation, climate and health effects of atmospheric particulate matters are closely related (Pöschl, 2005). Therefore, this review provides a comprehensive overview of sources, properties, chemical compositions and effects on climate and public health for APM and its pollution scenario and scientific research emphasis.

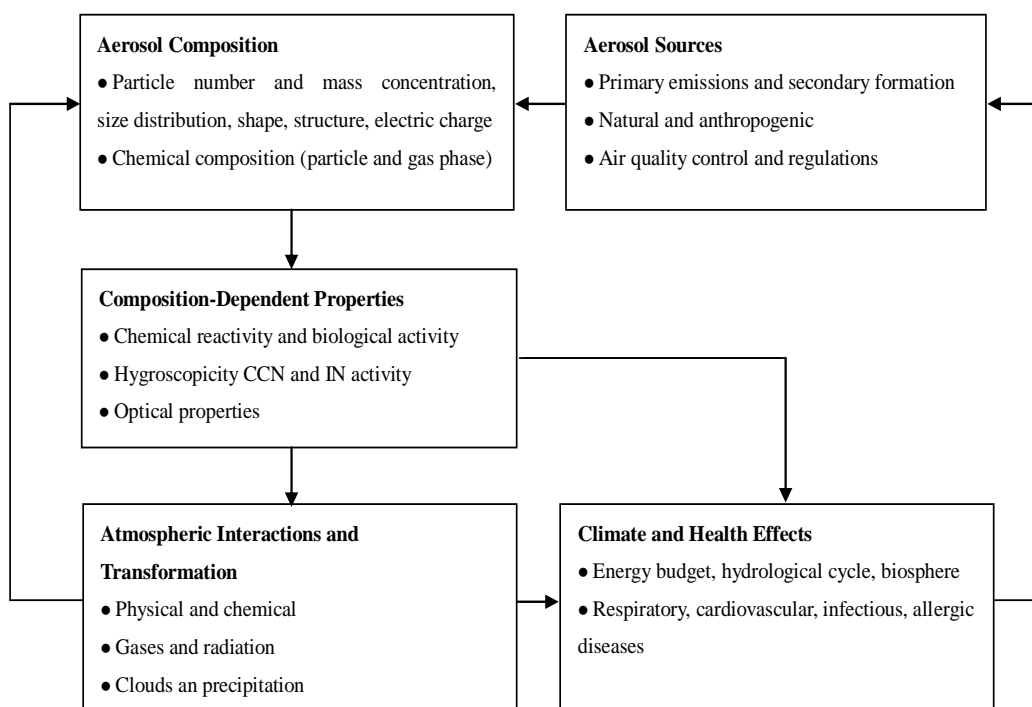


Figure 2-1 The correlation between atmospheric particulate matters compositions, sources, properties, atmospheric interactions and transformation, climate and health effects [Source: (Pöschl, 2005)].

## **2.1 Atmospheric Particulate Matters**

### **2.1.1 Definition**

Atmospheric particulate matters, also known as atmospheric particles or particulate matters (PM), are defined as a suspension of fine solid particles or liquid matters in the air, with particle size from  $10^{-7}$  to  $10^{-4}$  m in diameter (Seinfeld and Pandis, 2012). Atmospheric particulate matters are important constituents of the atmosphere system due to their role in atmospheric environment, climate and human health. Subtypes of atmospheric particle matters include suspended particulate matters (SPM), inhalable suspended particles ( $PM_{10}$ , particles with diameter of 10  $\mu\text{m}$  or less), fine particles ( $PM_{2.5}$ , particles with diameter of 2.5  $\mu\text{m}$  or less) and ultrafine particles ( $PM_{0.1}$ , particles with diameter of 0.1  $\mu\text{m}$  or less). Due to their small size, fine particles can be inhaled into and accumulate in the respiratory system, posing a potential threat to human health. Hence, the concerns regarding fine particles have attracted much scientific and public attention recently.

### **2.1.2 Physical and Chemical Properties**

The characteristics of APM, including physical, chemical and optical properties, are the key factors that influence climate and human health. Physical properties of APM include grain diameter, microscopic characteristics and size distribution. Regarding a single particle, the particle aerodynamic diameter ( $dp$ ) is sufficient to describe the particle size. However, for a polydisperse particle, the particle size distribution needs to be introduced to describe the particle size. Two approaches can be used to define the particle size distribution. One is characterized by the mass distribution of particles, and the other is obtained based on the particles number distribution. The mass distribution of particles usually shows two modes in most area: the accumulation mode (from 0.1 to 2  $\mu\text{m}$  in diameter) and the coarse mode (from 2 to 50  $\mu\text{m}$  in diameter). The particle number distribution is dominated by two modes: the nucleation mode (particles with diameter less than 10 nm) and the Aitken nuclei (particles with diameter from 10 to 100 nm) (Seinfeld and Pandis, 2012). Knowledge of the

particle size is important for the characteristics of APM. The role of APM in disease transmission is closely related to the particle size. Previous studies have suggested that coarse inhalable particles ( $PM_{10}$ ) can precipitate in the upper respiratory tract, whereas fine particles ( $PM_{2.5}$ ) could penetrate deeper into the lungs, and ultrafine particles ( $PM_{0.1}$ ) can reach further into alveolar regions (Wichmann and Peters, 2000; Voutsas and Samara, 2002). Moreover, the size distribution of particles is an important property to investigate the formation and growth mechanisms of ultrafine atmospheric particles (Kulmala et al., 2004).

Generally speaking, the major chemical compositions of APM are secondary inorganic ions (*i.e.*, sulfate, nitrate and ammonium), carbonaceous species (*e.g.*, organic carbon and elemental carbon), sea salts, organic compounds, and crustal and trace metals. The chemical compositions of APM mainly depend on their sources and meteorological conditions. For example, wind-blown mineral dusts tend to be made of mineral oxides and other crustal elements, while sea salts mainly consist of sodium chloride and other magnesium, sulfate, calcium, potassium. The chemical compositions and size distributions provide important information on the sources, formation mechanisms and toxicity of APM.

### **2.1.3 Sources of Atmospheric Particulate Matters**

Sources of particulate matters in the atmosphere can be natural or anthropogenic. The major natural sources of APM include volcanic eruptions, dust storms, forest and grassland fires, living vegetation, and sea spray. Atmospheric particulate matters can be anthropogenic originated from fossil fuels combustion by vehicles and power plants, and various industrial processes. On a global scale, atmospheric particles mainly derive from natural sources, such as dusts, biogenic emissions and sea salts (Carslaw et al., 2010). However, due to the increased emissions of atmospheric particles from fossil fuels combustion and industrial activities, anthropogenic emissions account for a major fraction of atmospheric particles in urban or rural areas (Pöschl, 2005; Rosenfeld, 2006; Kolb and Worsnop, 2012).

According to the particle formation mechanism, atmospheric particles can be defined as

primary particles and secondary particles. Primary particles contain particles that are directly emitted from natural sources such as volcanic eruptions, sea salts, mineral dusts and soot particles, and anthropogenic sources such as incomplete combustion of fossil fuels, industry processes, traffic emissions and biomass burnings. Whereas, secondary particles, including secondary inorganic particulate matter (SIM) and secondary organic particulate matter (SOM), are formed by gas-particle conversion processes in the atmosphere (*e.g.*, nucleation, condensation and heterogeneous chemical reactions) (Pöschl, 2005).

#### 2.1.4 Air Quality Standard of Atmospheric Particulate Matters

In order to control the atmospheric particulate matters, the policy makers established the concentrations limits for PM in the atmosphere. The new Chinese National Ambient Air Quality Standards (NAAQS) first regulated the standard for PM<sub>2.5</sub> in 2012. The regulations for PM<sub>10</sub> and PM<sub>2.5</sub> in the NAAQS, European (EU) and the World Health Organization (WHO) Air Quality Guidelines are shown in Table 2-1. By comparison, the Chinese NAAQS are less strict than the EU and WHO air quality standards.

Table 2-1 Concentration limits ( $\mu\text{g m}^{-3}$ ) for PM pollutants in the Chinese National Ambient Air Quality Standards (NAAQS), European (EU) and the World Health Organization (WHO) Air Quality Guidelines.

Pollutants	Averaging time	NAAQS <sup>a</sup>		EU <sup>b</sup>	WHO <sup>c</sup>
		Grade I	Grade II		
PM <sub>10</sub>	Annual	40	70	40	20
	Daily	50	150	50	50
PM <sub>2.5</sub>	Annual	15	35	25	10
	Daily	35	75	-	25

<sup>a</sup> <http://www.pm2d5.com>; <sup>b</sup>(Guerreiro et al., 2013); <sup>c</sup>(WHO, 2000)

### 2.1.5 Health and Climate Effects

Fine atmospheric particles ( $PM_{2.5}$ ) are small enough to penetrate the cell membranes of the respiratory tract and enter the blood circulation or move along olfactory nerves into the brain (Nemmar et al., 2002), causing a wide range of health problems such as respiratory and cardiovascular diseases, and lung cancer (Lanki et al., 2006; Wessels et al., 2010). The adverse effect of  $PM_{2.5}$  was not only due to a direct result of fine particles in the respiratory tissue or lung tissues, but also attributed to the toxicological effects of chemical compounds associated with particles (Gerlofs-Nijland et al., 2009; Uzu et al., 2011), such as polycyclic aromatic hydrocarbons (PAHs), organic carbon (OC) and elemental carbon (EC), water-soluble inorganic ions and metal elements (such as Fe, Cu, Pb, Zn, Ni and V). Researchers have conducted numerous studies on the toxicity of atmospheric particles predominantly through toxicological studies, but there is conflicting evidence in the literature regarding the predominant mechanism and the chemical compositions of fine particles which drive the inflammatory response. A widely accepted hypothesis is the oxidative damage originates from the surface of airborne particles that produce reactive oxygen species (ROS) such as transition metals (especially Fe, Cu, V, Zn) (Molinelli et al., 2002; Merolla and Richards, 2005; Heal et al., 2009) and polycyclic aromatic hydrocarbons (PAHs) (Gerlofs-Nijland et al., 2009), causing destructive effects both in the lung (Li et al., 2003; Tao et al., 2003) and internal organs (Merolla and Richards, 2005).

Effects of fine atmospheric particles on climate are generally classified as direct and indirect. Fine particles can directly affect visibility and scatter and absorb solar radiation (Pöschl, 2005; Rosenfeld, 2006). Due to high energy consumption and large emissions of atmospheric pollutants, the degradation of air quality and visibility was severe in some mega cities. Many previous studies have shown that elevated concentrations of  $PM_{2.5}$  in the air are the main cause of decreased visibility (Xiao et al., 2014; Zhang et al., 2015). Fine atmospheric particles in the atmosphere generally cause negative visual side effects to the human eye, such as smog and a yellowish tint to the air, which can cause difficulties in

transportation and people's daily life. The chemical compositions in  $PM_{2.5}$  such as sulfate, nitrate, organic and element carbon are known as the major species that influence visibility (Deng et al., 2008; Xiao et al., 2014). On the other hand, fine atmospheric particles can indirectly influence climate via their role as cloud condensation nuclei (CCN), by modifying optical properties of clouds, altering precipitation processes and indirectly affecting cloud particle interaction with solar and terrestrial radiation. All these effects combine to influence the atmospheric and oceanic circulation, and biogeochemical cycles (Pöschl, 2005).

## **2.2 Typical Chemical Compositions of $PM_{2.5}$**

The chemical compositions and their relative abundances in  $PM_{2.5}$  are various at different locations, times and meteorological conditions. This section will discuss some typical chemical compositions of  $PM_{2.5}$ , consisting of carbonaceous matters (organic carbon and element carbon), secondary organic aerosols, secondary inorganic aerosols and trace metals.

### **2.2.1 Carbonaceous Matters**

Carbonaceous matters are the dominant components of atmospheric particulate particles, and believed to have adverse effects on global climate (Ramanathan et al., 2001; Ramanathan and Carmichael, 2008) and human health (Schuetzle, 1983).

#### **2.2.1.1 Sources of Carbonaceous Matters**

Organic carbon (OC) and element carbon (EC) are the two main components of carbonaceous species in  $PM_{2.5}$ . EC is exclusively formed from primary sources such as fossil fuels combustion (*e.g.*, coal, gasoline and diesel) and biomass burning (*e.g.*, vegetation and wood), whereas OC can be either directly emitted from primary sources (*i.e.*, primary organic carbon, POC) including natural sources (*e.g.*, pollen, wind-blown soil and plant waxes) and incomplete fossil fuels combustion, or formed by photochemical oxidation of volatile precursors (*i.e.*, secondary organic carbon, SOC).

Anthropogenic emissions, such as fossil fuels combustion, vehicle exhausts and the burning of biomass (*e.g.*, crop residues, wood, and domestic waste), are the major sources of carbonaceous aerosols (Duan et al., 2004; Zhang et al., 2010; Zheng et al., 2011; Fu et al., 2012). In recent years, more studies investigated the important contribution of biomass burning to carbonaceous matters concentrations and compositions in South China (Zhang et al., 2010; Sang et al., 2011; Zhang et al., 2012b), East China (Huang et al., 2013; Liu et al., 2013) and North China (Wang et al., 2007b; Cheng et al., 2013). There are two main periods of open biomass burning in China: one is after the harvest in late spring, and the other follows the harvesting in autumn. These open burning activities are the major sources of OC and EC and some gases such as CO and NO<sub>x</sub> (Burling et al., 2010; Cheng et al., 2011; Zhang et al., 2013). Lu et al. (2011) reported that the emissions of EC and primary OC by fuel type were increased in China since 2000, and the contributions of biomass burning to primary OC and EC were 34-45% and 63-74% within the period from 1996 to 2010. In addition, the contributions of biomass burning emissions to primary OC (70%) and EC (40%) were relatively stable during the period from 2006 to 2010. Therefore, it is important to study how the biomass burning activities affect air quality and to what extent they contribute to the carbonaceous matters in PM<sub>2.5</sub> in China.

### **2.2.1.2 Source Apportionment for Carbonaceous Matters**

It is difficult to identify and quantify the sources of carbonaceous matters in PM<sub>2.5</sub> because they are originated from various sources that are temporal and spatial dependence. Several methods, such as water soluble potassium (K<sup>+</sup>), the ratio of OC/EC, levoglucosan (C<sub>6</sub>H<sub>10</sub>O<sub>5</sub>) and radiocarbon (<sup>14</sup>C), have been developed to identify the emission sources of carbonaceous matters in PM<sub>2.5</sub>.

Organic carbon and K<sup>+</sup> are the typical components of biomass burning particles (Duan et al., 2004; Reche et al., 2012). OC accounted for about two-thirds of biomass burning particle mass. K<sup>+</sup> has been used as tracer element for the qualitative identification of biomass burning (Urban et al., 2012). However, some other sources of K<sup>+</sup> (such as crustal dust, sea

salt and the dust from smelting activities) can disturb the contribution of biomass burning. Levoglucosan ( $C_6H_{10}O_5$ ) is the pyrolysis product from carbohydrates, such as starch and cellulose (Simoneit et al., 1999). Moreover, other combustion processes, such as fossil fuels combustion, do not produce levoglucosan (Elias et al., 2001). Hence, levoglucosan is a unique and the most commonly used tracer to indicate biomass burning processes (Zhang et al., 2008a; Sang et al., 2011; Urban et al., 2012), and to assess the contribution of biomass burning to the total carbonaceous matters in  $PM_{2.5}$  (Gelencsér et al., 2007; Claeys et al., 2010; Kumagai et al., 2010). Levoglucosan is usually measured by gas chromatography-mass spectrometry (GC-MS) (Urban et al., 2012) or high-performance liquid chromatography (HP-LC) (Schkolnik et al., 2005; Yttri et al., 2007). However, both of the two methods require complex sample pre-treatments and/or analytical procedures. Recently, a new method named high-performance anion-exchange chromatography coupled to pulsed amperometric detection (HPAEC-PAD) was developed by Engling et al. (2006), which can directly quantify levoglucosan and various other carbohydrates in aerosol samples with simple pre-treatment method (Sang et al., 2011; Cheng et al., 2013). The ratios of OC to EC provide information in the emission sources of carbonaceous matters in  $PM_{2.5}$ . The ratios OC/EC were detected in some typical emission sources, such as wood kitchen emissions (32.9-81.6), combustion (16.8-40.0), residential coal smoke (2.5-10.5), biomass burning (7.7) and vehicular exhausts (1.0-4.2) (Feng et al., 2009b). Several studies used the levoglucosan to OC ratios, levoglucosan to  $PM_{2.5}$  ratios,  $K^+$  to OC ratios and  $K^+$  to  $PM_{2.5}$  ratios to identify the contribution of biomass burning. Sang et al. (2011) estimated that the contributions of biomass burning to OC were in the range of 6.5-11% using the levoglucosan to OC ratios from  $PM_{2.5}$  samples. The ratio of  $K^+$  to OC was used to estimate the contribution of biomass burning to OC measured in Beijing by Duan et al. (2004). Cheng et al. (2013) compared the levoglucosan and  $K^+$  concentrations in  $PM_{2.5}$  samples, suggesting that it was acceptable to use  $K^+$  as a biomass burning tracer during summer in Beijing. However, the limitations of these methods lacking the knowledge of the characteristics of emission sources (*e.g.*, fossil fuel emissions and biomass burning) and the differences between primary and secondary sources for carbonaceous matters in  $PM_{2.5}$ .

Compared with the methods mentioned above, radiocarbon ( $^{14}\text{C}$ ) analysis provides the direct differences in the characteristics between modern carbon sources and fossil fuel sources (Liu et al., 2013; Liu et al., 2014). The ratio of  $^{14}\text{C}$  to  $^{12}\text{C}$  of carbonaceous matters in  $\text{PM}_{2.5}$  is completely absent in fossil fuel sources due to their long half-life with 5,730 years, while is relatively constant in modern carbon sources as natural origins (*e.g.*, wild fires, plant wax and pollen) and anthropogenic origins (*e.g.*, meat cooking and domestic and prescribed burning). Thus, radiocarbon ( $^{14}\text{C}$ ) measurements in APM samples provide unambiguous differentiation among the emission sources of carbonaceous matters. This method has been conducted in China recently to quantify the contribution of fossil fuel and contemporary sources of OC and EC. Liu et al. (2013) reported the seasonal contributions of fossil fuel vs biomass burning and biogenic sources on OC and EC at a background site in East China using the combination of OC/EC separation and  $^{14}\text{C}$  analysis. Furthermore,  $^{14}\text{C}$  analysis technique is also helpful to understand the formation mechanisms of SOC during haze events (Liu et al., 2014).

### **2.2.2 Secondary Organic Particulate Matters**

Secondary organic particulate matters (SOM) account for a large fraction of organic matters in  $\text{PM}_{2.5}$  and are spatially and seasonally depended (Feng et al., 2009b; Zhou et al., 2012). SOM are formed from chemical reactions and gas-to-particle conversion of volatile organic compounds (VOCs) that can condense to form new particles or coagulate with existing particles. The formation processes of SOM may involve three pathways: 1) new particle formation: from semi-volatile organic compounds (SVOCs) by gas-phase reactions and from the participation of the SVOCs in the nucleation; 2) gas-particle partitioning: formation of SVOCs by gas-particle reactions and uptake by existing aerosols or cloud particles; and 3) heterogeneous reactions: formation of low-volatility or nonvolatile organic compounds (LVOSCs, NVOCs) by chemical reaction of VOCs or SVOCs at the surface or in the bulk of aerosol or cloud particles (Pöschl, 2005). Several laboratory and field experiments have found that aerosol acidity play an important role in the enhancement of SOM formation from oxidation of VOC (Surratt et al., 2007; Zhang et al., 2007). Recent studies have

suggested that acid-catalysed heterogeneous reactions on atmospheric aerosols can lead to significant increase in SOM mass in both the laboratory (Surratt et al., 2007) and the field (Zhou et al., 2012).

A number of reviews summarized the analytical techniques for the determination and quantification of SOM chemical compositions recently. Three categories of analysis techniques can be classified: indirect methods (quantify the total SOM from the difference between the measured total organic matters and estimated primary organic matters), off-line techniques, such as gas chromatography-mass spectrometry (GC-MS), liquid chromatography-Mass Spectrometry (LC-MS), nuclear magnetic resonance (NMR) and Fourier transform infrared (FTIR) spectroscopy, and on-line techniques such as aerosol mass spectrometry (AMS) (Hallquist et al., 2009). Off-line techniques can detect the individual chemical species or functional groups in SOM, while on-line techniques have fast acquisition times and provide near real-time data. Significant gaps still remain in the formation mechanisms and chemical compositions of SOM, so continuing laboratory and field research on SOM is required.

### **2.2.3 Secondary Inorganic Particulate Matters**

Secondary inorganic particulate matters (SIM), including sulfate ( $\text{SO}_4^{2-}$ ), nitrate ( $\text{NO}_3^-$ ) and ammonium ( $\text{NH}_4^+$ ), are the main chemical compositions of  $\text{PM}_{2.5}$  and the major concerns of the chemical composition of  $\text{PM}_{2.5}$  source apportionment. Sulphur dioxide ( $\text{SO}_2$ ), nitrogen oxides ( $\text{NO}_2$ ) and ammonia ( $\text{NH}_3$ ) are the gaseous precursors of SIM in PM. The major sources of  $\text{SO}_2$  and  $\text{NO}_2$  are fossil fuel combustion in coal-burning power plants, traffic, ships and industries, while ammonia is mainly emitted from agricultural activities. Generally, SIAM are formed by the conversion of inorganic gases such as  $\text{SO}_2$ ,  $\text{NO}_2$  and  $\text{NH}_3$  into particulate phase sulfate, nitrate and ammonium. Several studies have investigated the formation mechanisms of SIAM in  $\text{PM}_{2.5}$ . Sulfate is mainly formed from the gas-phase reactions between  $\text{SO}_2$  and OH radical followed by nucleation and condensational growth, or originated from the heterogeneous reactions of  $\text{SO}_2$  on the surface of crustal particles or

cloud droplets (Wang et al., 2012a; Clements et al., 2013). Nitrate is primarily produced by the reactions of gaseous or liquid  $\text{HNO}_3$  with  $\text{NH}_3$  or by heterogeneous reactions of  $\text{N}_2\text{O}_5$  on aerosol surface (Pathak et al., 2009; He et al., 2012). Ammonium formation in  $\text{PM}_{2.5}$  is often combined with the formation of sulfates and nitrates (Pathak et al., 2004). Several studies have emphasized the important roles of secondary inorganic components on the chemical properties of  $\text{PM}_{2.5}$  (e.g., aerosol acidity) (Gioda et al., 2011) and climate (Hillamo et al., 1998). Few currently available toxicological studies highlighted that the possible indirect adverse effects of SIM in PM are (1) increase the bioavailability of metallic species; (2) enhance lung deposition of toxic compounds; and (3) catalyze the formation of organic matters (Reiss et al., 2007).

#### **2.2.4 Trace Metals**

Trace metals are the important components of  $\text{PM}_{2.5}$ , which have attracted much attention due to their adverse impacts on human health (Ghio, 1999; Adamson et al., 2000; Riley et al., 2003; Nel, 2005) and environmental ecosystem (Okubo et al., 2013). The research progresses of trace metals in  $\text{PM}_{2.5}$  are discussed in this section, including size distributions, spatial and temporal distributions, source identification and health effects.

##### **2.2.4.1 Essential Trace Metals and Toxic Metals in the Atmosphere**

Some metal elements such as Cu, Co, Fe, Mn, Mo and Zn are essential nutrients for plants, and Cu, Co, Fe, Mn, Mo, Zn, Cr, Ni and V are essential elements for animal nutrition. These vital elements are necessary to ensure the health for humans and other organisms. However, all the essential trace metals are considered to be toxic if ingested or inhaled at sufficiently high levels and for long enough periods. Trace metals such as As, Pb, Cd and Hg are classified as toxic elements which have potential toxic effects on human health. Hence, the inhalation of airborne trace metals can have long-term and serious impacts on human health, causing damage to the nervous system and internal organs (Ghio, 1999; Nel, 2005). Table 2-2 shows the limited levels of some toxic metals in the atmosphere.

Table 2-2 The levels of some toxic metals with National Ambient Air Quality Standards (NAAQS) in China and WHO ( $\text{ng m}^{-3}$ ).

Toxic elements	NAAQS (GB3095-2012)	WHO (2000) <sup>a</sup>
V	1000	1000
Cr (VI)	0.025	0.25
Mn	150	150
Ni	20	25
As	6	6.6
Cd	5	5
Hg	50	1000
Pb	500	500

<sup>a</sup> (WHO, 2000)

#### 2.2.4.2 Size Distribution of Trace Metals in Atmospheric Particulate Matters

Size distribution of airborne trace metals not only affect the toxicity of metals to humans by inhalation, but also control the dispersion of metals in the air and the deposition of metals to the Earth's surface (Spurný, 2000). There were a few studies analysed the metal contents in different sizes of atmospheric particles (Milford and Davidson, 1985; Waheed et al., 2011). Results of these researches generally suggested that 70-90% of metals are concentrated in the  $\text{PM}_{10}$  particles, and noted that the finer the particle size, the more metals contained. It has been found that several toxic metals, including arsenic (As), cadmium (Cd), nickel (Ni), lead (Pb), vanadium (V), zinc (Zn), cobalt (Co), chromium (Cr), mercury (Hg), manganese (Mn), and their compounds, are associated with fine particles in the atmosphere. Waheed et al. (2011) noted that the airborne toxic metals (such as Pb, Cd, Se, Sn, Bi and Zn) in Shanghai are concentrated in the alveolar fraction (particles with diameter less than  $1 \mu\text{m}$ ). Knowledge of the size distribution of airborne trace metals is useful to study the sources, long-range transport and atmospheric deposition of airborne trace metals and their potential toxicity to humans (Pakkanen et al., 2001; Waheed et al., 2011). It is now commonly accepted that

metal elements associated with particles less than 1  $\mu\text{m}$  tend to result from high temperature combustion sources, while large particles with diameter greater than 10  $\mu\text{m}$  are likely derive from the suspending of surface soils, road dusts and fugitive dusts (Schroeder et al., 1987). For health reason and air pollution control, mass concentration and size distribution of trace metals in PM must be determined. Some studies have investigated the size distribution of trace metals in PM<sub>2.5</sub> (Birmili et al., 2006; Duan et al., 2014). Duan et al. (2014) reported the size distribution of heavy metals in PM<sub>2.5</sub> during haze episode in Beijing. They found that Pb, Cd, and Zn exhibited in accumulation mode (with particle size from 0.1 to 2  $\mu\text{m}$ ), and V, Mn and Cu existed mostly in both coarse mode (with particle size greater than 2  $\mu\text{m}$ ) and accumulation mode, while Ni and Cr resided in all of the coarse, accumulation and nucleation mode (with particle size less than 0.1  $\mu\text{m}$ ).

#### **2.2.4.3 Sources and Source Identification of Airborne Trace Metals**

Both natural and anthropogenic sources result in the release of trace metals into the atmosphere. The mainly natural and anthropogenic sources of airborne trace metals are listed in Table 2-3 (Calvo et al., 2013). The major natural sources of airborne trace metals are windblown dusts, forest fires, volcanogenic particles, vegetation and sea salt sprays. For example, about 60-80% natural emissions of Cu, Pb, Ni and Zn are normally from eroded soil particles, and 60% natural emissions of Cd are from volcanogenic particles. Vegetative exudates clearly represent an important source of airborne metals which account for about 20% of Zn from natural sources. Forest fires and sea salt sprays only represent less than 10% of natural emissions of trace metals (Nriagu, 1979). Major anthropogenic metals emissions are generally considered to be from smelting of metallic ores, iron and steel industries, non-ferrous metal industries and fossil fuels combustion. The fly ash from oil-fired thermal generating station has been found to contain V, Ni, Fe, Zn, Pb and Cu (Schroeder et al., 1987). The combustion of coal in most types of coal-fired power plants is a very important source of Fe, Zn, Pb, V, Cr and Mn (Schroeder et al., 1987). Due to the rapid urbanisation and economic development in megalopolis, the anthropogenic emissions of metals in the

atmosphere have been continuously increasing (Ye et al., 2003; Chen et al., 2008).

In terms of source identification of airborne trace metals, methodologies such as size differentiation, enrichment factors (EF), principal component analysis (PCA), chemical mass balance model (CMB) and positive matrix factorization (PMF) can be used. Enrichment factors is the most commonly used method, which can be used to identify the origins of metals from crustal or anthropogenic sources (Chen et al., 2008; Cao et al., 2009; Schleicher et al., 2011). It can also be used in remote areas to provide evidence concerning the nature and extent of long range transport of anthropogenic emissions (Schroeder et al., 1987). Lu et al. (2012) investigated the chemical elements in  $PM_{2.5}$  in Shanghai and found that Si, K, Ca, Fe, Mn, Rb, and Sr were from crustal sources, and S, Cl, Cu, Zn, As, Se, Br, and Pb from anthropogenic sources. However, this method cannot distinguish the specific anthropogenic sources of trace metals in the atmosphere. CMB and PMF model has widely used for source apportionment. CMB and PMF models are two kinds of receptor models that are mathematical approaches used for quantifying the contribution of aerosol sources. The application of receptor models depends on the composition or fingerprints of aerosol sources. The CMB model requires the accurate database of all significant source emissions compositions which is difficult to establish, while the PMF model demands both concentration and user-provided uncertainty of sample species. Previous study has been compared the source contributions resolved by PMF and CMB models, and found that the source profiles obtained from PMF model were generally similar to measured source profiles (Rizzo and Scheff, 2007).

Table 2-3 Various emission sources of metal elements in the air (Calvo et al., 2013).

Source	Metal element
<b>Natural sources</b>	
Sea salt	Cl, Na, Na <sup>+</sup> , Cl <sup>-</sup> , Br, I, Mg and Mg <sup>2+</sup>
Crustal or geological tracers	Elements associated with feldspars, quartz, micas and their weathering products (mostly clay minerals), <i>i.e.</i> Si, Al, K, Na, Ca, Fe and associated trace elements such as Ba, Sr, Rb, and Li.
<b>Anthropogenic sources</b>	
Steel industry	Cr, Ni and Mo
Copper metallurgy	Cu and As
Ceramic industries	Ce, Zr and Pb
Heavy industry (refinery, coal mine, power stations)	Ti, V, Cr, Co, Ni, Zn, As and Sb
Petrochemical industry	Ni and V
Oil burning	V, Ni, Mn, Fe, Cr and As
Coal burning	Al, Sc, Se, Co, As, Ti, Th, S, Pb and Sb
Iron and steel industries	Mn, Cr, Fe, Zn, W and Rb
Non-ferrous metal industries	Zn, Cu, As, Sb, Pb and Al
Cement industry	Ca
Refuse incineration	K, Zn, Pb and Sb
Biomass burning	K and Br
Firework combustion	K, Pb, Ba, Sb and Sr
Vehicle tailpipe	Platinum group elements, Ce, Mo and Zn
Automobile gasoline	Ce, La, Pt
Mechanical abrasion of tyres	Zn
Mechanical abrasion of brakes	Ba, Cu and Sb

#### **2.2.4.4 Pb Isotopic Fingerprinting in Aerosols**

It is well known that lead is a highly toxic element for humans. Lead pollution in the atmosphere in China is a serious concern related to human health. Inhalation is the one of the main pathways of human exposure to Pb. Several studies showed that the blood lead levels (BLLs) of children in cities of China have decreased after the phasing out of leaded gasoline, however, the BLLs of children are still much higher than those in some developed countries (Zhang et al., 2009b; Chen et al., 2012). The major sources of airborne Pb in Chinese cities include vehicle exhausts, industrial emissions, coal combustion, suspension of soil dusts, and long-range transport of aerosols containing Pb. Liang et al. (2010) found that particles generated by coal combustion is the dominate source of airborne lead exposure to children in Shanghai after the banning of leaded gasoline.

In order to control Pb pollution in the atmosphere, it is important to determine the potential sources of airborne Pb. Pb isotopic fingerprinting is a useful technique in establishing the sources of lead in the environment. Previous studies have been successfully applied the Pb isotopic technique to trace the sources of Pb in different environmental samples, including sediments, soils, plants, atmospheric particles and aquatic organisms (Ip et al., 2007; Lee et al., 2007; Bi et al., 2013). The Pb isotopic technique has been conducted to evaluate the variations of Pb isotopic ratios and sources of atmospheric Pb pollution after phasing out leaded gasoline in China from 1997. The major source of Pb in the air was reported to be coal combustion rather than vehicle exhausts (Chen et al., 2005; Wang et al., 2006a; Chen et al., 2008). Zheng et al. (2004) reported the average concentration of airborne Pb in winter at Shanghai was  $515 \text{ ng m}^{-3}$ , indicating that a high concentration of Pb remains in the atmosphere after the phasing out of leaded gasoline. They also suggested that the major emission sources of airborne Pb in Shanghai were metallurgic dust, coal combustion and cement. Furthermore, Pb isotopic ratios have been used in assessing the long-range transport of anthropogenic Pb from mainland China to Taiwan (Hsu et al., 2006) and Japan (Nakano et al., 2006). However, the current Pb isotopic fingerprint in aerosol in China is expected to

bring further changes to Pb isotopic compositions in the atmosphere via the long-range transport because of the rapidly expanding of lead ores mining and atmospheric Pb pollution in China.

#### **2.2.4.5 Health Effect of Airborne Trace Metals**

The interest in trace metals in atmospheric particles has widely increased due to their adverse impacts on human health (Ghio, 1999; Riley et al., 2003; Nel, 2005). Some trace metals are non-degradable, and can accumulate in the atmospheric particulate matters. According to the International Agency for Research on Cancer (IARC), arsenic and arsenic compounds, cadmium and cadmium compounds, hexavalent chromium ( $\text{Cr}^{6+}$ ), and nickel compounds are carcinogenic to humans, inorganic lead compounds are probably carcinogenic to humans, and many other metals are possibly carcinogenic to humans. The inhalation of airborne toxic metals can therefore injure the health of human body (Ghio, 1999; Nel, 2005). Some research groups have reported the impact of individual trace metals on the toxicity in the lung. Adamson et al. (2000) found zinc was the toxic factor in the lung response to an aerosol sample. A strong correlation between V and Fe concentrations and cellular toxicity was observed by Okeson et al. (2013). Investigations in the toxic effects of mixtures of trace metals in particulate matters have attracted great interest. The impact of trace metals (*e.g.*, Zn, Cu, Ni, V, and Fe) individually and in combination on a rat lung epithelial cell line (RLE-6TN) was evaluated by Riley et al. (2003). They found that Zn appeared to diminish the negative impact of V and Cu, but has an additive effect with Ni.

Previous studies have found that oxidative damage to cells is primarily attributed to transition metals on the particle surface, which typically include Fe, V, Cr, Mn, Ni, Cu, Zn, and Ti (Merolla and Richards, 2005; Shao et al., 2006; Heal et al., 2009; Phillips et al., 2010; Uzu et al., 2011; Xiao et al., 2013). Some of these metals, such as Fe and Cu, are believed to contribute to particle-induced formations of ROS through the Fenton reaction, and then have been considered important for particle toxicity. The water-soluble fraction of PM, which is thought to have the greatest bioaccessibility, is commonly rich in bioaccessible trace metals

including transition metals (Molinelli et al., 2002). Shao et al. (2006) suggested that water-soluble Zn might be the major component responsible for oxidative damage of plasmid DNA. Furthermore, Xiao et al. (2013) indicated that water-soluble metals in PM<sub>2.5</sub> from Lanzhou, including Zn, Pb, Fe and Mn, might be the primary elements responsible for plasmid DNA damage.

### **2.3 Bioaccessibility of Airborne Trace Metals**

It is now widely recognized that the bioaccessibility of trace metals in PM is important for risk assessment of metal toxicity instead of total metal contents. Many factors influence the bioaccessibility of airborne metals, including particle source of origin (Desboeufs et al., 2005; Heal et al., 2005), metal speciation (Chester et al., 1989), water-soluble organic matter (Wozniak et al., 2013) and particle acidity (Desboeufs et al., 2005). In this section, the major assessment measurements and possible influential factors of bioaccessibility of trace metals in PM are discussed.

#### **2.3.1 Assessment Methods for Bioaccessible Airborne Trace Metals**

Quantification of bioaccessible fractions of airborne trace metals has not been standardized in the literature. Various methods have been used to extract the bioaccessible metal fractions, such as single step extraction with one leaching agent (*e.g.*, water, buffer, salt and chelating solutions) (Voutsas and Samara, 2002), sequential extraction (Al-Masri et al., 2006) and synthetic human body fluids extraction (Falta et al., 2008; Wiseman and Zereini, 2014).

##### **2.3.1.1 Water-soluble Fraction**

The water-soluble fraction of trace metals in PM is found to be positively correlated with the observed pulmonary toxicity (Adamson et al., 2000; Sun et al., 2001). Since particle-bound metals need to be dissolved and become free ions in the lung fluid, the water-soluble fraction of particle-bound metals is more likely to become bioaccessible and therefore may be potentially more harmful to humans (Birmili et al., 2006). Several studies used the

water-soluble fraction for risk assessment of airborne trace metals (Birmili et al., 2006). However, water does not mimic the human body conditions, thus this method cannot provide the real bioaccessibility of airborne trace metals.

### **2.3.1.2 Sequential Extraction**

Sequential extraction procedures are commonly used to estimate the speciation of trace metals in soil and sediments (Tessier et al., 1979), and also used to investigate trace metal speciation on airborne particles (Moloi et al., 2002; Al-Masri et al., 2006; Wang et al., 2007a; Feng et al., 2009a). Smichowski et al. (2005) have classified the sequential chemical extraction methods for airborne trace metals into water-soluble fraction, exchangeable fraction, carbonate fraction, Fe and Mn oxide fraction, organic matter fraction and the residual fraction based on different chemical fractionation procedures. The method of sequential extraction is time-consuming, but it can provide useful information about the origins, mobilization and bioaccessibility of airborne trace metals. For example, in the study by Al-Masri et al. (2006), Pb and Zn were found to be significantly associated with organic matter. Feng et al. (2009a) used the sequential extraction procedures to fractionate the airborne trace metals in PM<sub>2.5</sub> samples in South China. The results found that about 91% of Cd, 85% of Pb and 74% of As were in bioaccessible forms. Although the method of sequential leaching can provide useful information on bioaccessible fractionation of airborne trace metals, the influence of the operational conditions of each extraction step could change the original distribution of trace metal species in the aerosol sample.

### **2.3.1.3 Simulated Human Body Fluids**

In order to better investigate the bioaccessibility of airborne trace metals, some researchers used the simulated human body fluids as leaching agents (Twining et al., 2005; Falta et al., 2008; Mukhtar and Limbeck, 2011; Zereini et al., 2012; Wiseman and Zereini, 2014). Two leaching agents, synthetic gastric juice and synthetic lung fluid, are normally used. Mukhtar and Limbeck (2011) reported that the mean bioaccessible metal fractions varied between  $32 \pm$

14% (Ni) and  $97 \pm 36\%$  (Pb) in  $PM_{10}$  using the synthetic gastric juice. In addition, some studies used the synthetic lung fluid to simulate the lung environment for assessment of bioaccessibility of airborne metals (Zereini et al., 2012; Wiseman and Zereini, 2014). Two synthetic lung fluids were used as surrogates for different areas of potential exposure in the human lungs: Gamble's solution is representative of the interstitial fluid of the deep lung and artificial lysosomal fluid (ALF) is representative of the more acidic environment following phagocytosis by alveolar and interstitial macrophages within the lung (Mukhtar and Limbeck, 2013). The main differences between the two simulated lung fluids are the acidity (ALF, pH = 4.5-5.0; Gamble's solution, pH = 7.4) and the organic content (ALF has much higher organic content than Gamble's solution). Wiseman and Zereini (2014) compared the bioaccessibility of airborne trace metals in  $PM_{10}$ ,  $PM_{2.5}$  and  $PM_1$  using ALF and Gamble's solution. They found that higher bioaccessibility of airborne trace metals was observed in ALF due to the more acidity of ALF. The use of simulated human body fluid as leaching agents does provide more real bioaccessibility of airborne trace metals compared to using water as leaching agents, as these are more likely to reflect the real human body conditions (Mukhtar and Limbeck, 2013).

### **2.3.2 Possible Influence Factors on Bioaccessibility of Airborne Trace Metals**

Trace metals in the atmosphere derive from both natural and anthropogenic sources. Generally, a higher proportion of trace metal is water-soluble in anthropogenic particles than in crustal particles (Heal et al., 2005). Colin et al. (1990) found that the solubility of airborne trace metals was higher in air masses originated from anthropogenic and marine sources, whereas the insoluble fractions were higher in events in which crustal emission was the dominant source. Desboeufs et al. (2005) compared the solubility of metals from two kinds of matrix: alumino-silicated and carbonaceous particles. They found trace metals coming from carbonaceous particles dissolved easier than those in the alumino-silicated particles. The solubility of iron (Fe) in arid region soils, glacial weathering products and oil combustion products were investigated by Schroth et al. (2009). The results found that the solubility of

iron in oil combustion products (77-81%) was much higher than that in arid region soils (less than 1%) and glacial products (2-3%). These results indicate the important role of aerosol sources on the bioaccessible fraction of airborne trace metals.

The role of pH on the solubility of trace metals in soils is widely known (Basta and Tabatabai, 1992; McLean and Bledsoe, 1996). Various studies have shown that dissolved speciation of metals in rain water is pH-dependent (Colin et al., 1990). Desboeufs et al. (2005) suggested that the dissolution of the matrix network (Fe, Mn) highly influenced by pH. Aerosol acidity can affect the physical and chemical properties of atmosphere. The acidity of aerosol particles is mainly determined by the balance of acidic ionic components including sulfate ( $\text{SO}_4^{2-}$ ) and nitrate ( $\text{NO}_3^-$ ), and partly or fully neutralized ionic component ammonium ( $\text{NH}_4^+$ ). However, the correlation between the pH of atmospheric particulate matters and the solubility of airborne trace metals has seldom been studied (Al-Momani, 2003; Shi et al., 2011). In addition, the bioaccessibility of airborne trace metals may vary from region to region due to the spatial and temporal variability in the emission of natural and anthropogenic sources and chemical characteristics of aerosols, as well as regional differences in the meteorological conditions.

#### **2.4 Regional Transport of Atmospheric Particulate Particles**

Large amount of atmospheric particles can deteriorate the air quality in source regions, but also can be long-range transported from their initial source regions to other areas. The distribution and fate of atmospheric pollutants are strongly affected by air-mass sources and meteorological conditions during transportation (Niemi et al., 2006). Two major issues considering the regional transport of air pollutants are the term “long-range transport” (LRT) and monsoon activities.

It is well known that the LRT has promoted the regional and global air pollution. The trans-boundary transportation of pollutants associated with particulate matters have been widely investigated, including dusts (2010a; Hsu et al., 2010b; Feng et al., 2012),

carbonaceous species (Qu et al., 2008; Zhang et al., 2012b) and non-sea salt sulfate (Alexander et al., 2012; Sakata et al., 2012). The evidence on the possibility of long-range transport of airborne trace metals also has been found (Hsu et al., 2005; 2006; Lee et al., 2007). The outflow of airborne trace metals from continental Asia has been reported by many researches. Hsu et al. (2006) observed that the highest level of Pb isotopic ratios of aerosols in Taipei was measured during winter, identifying the long-range transport of airborne Pb from the Yangtze River Delta to Taiwan. Hsu et al. (2005) also found that low Cd/Pb and Zn/Pb ratios were observed in aerosols collected during the Asian dust period, which was attributed to long-range transportation. Lee et al. (2007) revealed that the enrichment of trace metals in South China coastal region (*e.g.*, Hong Kong and Guangzhou) was closely associated with the air masses from the northern inland areas of China by conducting the air back-trajectory analysis. Based on the previous observations, the concentrations of airborne trace metals in rural or remote areas might also be influenced by the long-range atmospheric transport from urban and industrial areas (Heal et al., 2005).

The long-range transport of air pollutants is dependent on monsoon activities which display seasonal variations of prevailing winds (Hsu et al., 2005; 2006; Lee et al., 2007). In general, the summer monsoon prevails in China during the period from May to August. It originates from three airflows: 1) the Indian summer monsoonal airflow; 2) the cross-equatorial airflow from Australian region flowing over Southeast Asia and the South China Sea; 3) the southeast monsoon coming from the southern flank of the subtropical high over the western Pacific (Ding, 1994). In contrast, the winter monsoon develops in Siberia and Northern China between late October and early May, and moves southeastward out of China.

## **2.5 Research Emphasis of PM<sub>2.5</sub>**

In this section, research statuses and research gaps of emission inventories of PM<sub>2.5</sub> and air pollutants, PM<sub>2.5</sub> pollution in China, characteristics of chemical compositions, haze episode and aerosol studies in regional background sites are summarized.

### 2.5.1 Emission Inventory of PM<sub>2.5</sub> and Air Pollutants

Estimating the emission inventory of air pollutants is the foundation for understanding their formation, transport and controlling air quality. In recent decades, the emissions of major air pollutants including sulphur dioxide (SO<sub>2</sub>), nitrogen oxides (NO<sub>x</sub>), carbon monoxide (CO), carbon dioxide (CO<sub>2</sub>), methane (CH<sub>4</sub>), ammonia (NH<sub>3</sub>), PM<sub>10</sub>, PM<sub>2.5</sub> and VOCs (Volatile Organic Compounds) have been estimated at global and regional scales by many studies (Zhang et al., 2009a; Huang et al., 2011; Zhao et al., 2012; Kurokawa et al., 2013). Regional emission inventories naturally include the estimates for areas in Asia, such as East, Southeast, South, and Central Asia (Kurokawa et al., 2013), and some specific regions in China, such as the Pearl River Delta (PRD) (Zheng et al., 2009), the Yangtze River Delta (YRD) (Huang et al., 2011) and Huabei region (Zhao et al., 2012). Kurokawa et al. (2013) estimated the emissions of major air pollutants and greenhouse gas during 2000 and 2008 in Asia. Asian emissions of PM<sub>2.5</sub> in the year of 2008 were estimated as 24.7 Tg. They found that the emissions of each species in 2008 were much higher than those in 2000, and China and India were the largest and second largest contributors to Asian emissions, respectively. Emission inventories of primary PM<sub>2.5</sub> have been established in some large regions of China. Zheng et al. (2009) estimated that 204.6 kt of primary PM<sub>2.5</sub> in the PRD region in the year of 2006 mainly originated from the industries, vehicle exhausts and power plants. Fu et al. (2013) reported that the emissions of PM<sub>2.5</sub> in the YRD region were 643 kt in the year of 2010, and 28.9% of the emissions were from industrial process.

Some of emission inventory studies were generally distributed at a low grid resolution, *e.g.*, 1 °latitude by 1 °longitude (Streets et al., 2003), 0.3 °latitude by 0.3 °longitude (Huang et al., 2011) and 0.25 ° latitude by 0.25 ° longitude (Kurokawa et al., 2013). Accurate and high resolution emission inventories are essential for better understanding pollution formation and transport, and forecasting air quality. Fu et al. (2013) estimated the emission inventories of primary air pollutants and chemical speciation in 2010 for the YRD region with 4 km × 4 km spatial grids based on high resolution information of point sources, population, road network

and land cover. Zhao et al. (2012) presented a high resolution emission inventory of primary air pollutant in the Huabei region, China for the year 2003 with 0.1 °latitude by 0.1 °longitude resolution. The high resolution emission inventories need to be conducted in more regions and focus on more air pollutants.

### **2.5.2 PM<sub>2.5</sub> Pollution in China**

Due to the dramatic increase in population, technological development, economic growth and urbanization over the past few decades in China, PM<sub>2.5</sub> pollution has been found to occur more frequently in China (Yang et al., 2005c; Wang et al., 2006b). The complexly chemical composition in PM<sub>2.5</sub> and widespread sources leads to complicated and serious PM<sub>2.5</sub> pollution pattern in China. Studies for PM<sub>2.5</sub> have been gradually conducted since 2000 in China, and mainly focused on the large cities in the PRD (Cao et al., 2003; Wang et al., 2006b), the YRD (Fu et al., 2008; Wang et al., 2013; Shen et al., 2014), Beijing-Tianjin-Hebei (BTH) (Duan et al., 2012; Zhao et al., 2013a) and North China Plain (NCP) (Hu et al., 2014). These cities are exposed to high levels of PM<sub>2.5</sub> concentrations from the investigation. For example, the annual mean concentration of PM<sub>2.5</sub> in urban site was 182 µg m<sup>-3</sup> in Beijing in 2001-2003 (Zhang et al., 2006), 103 µg m<sup>-3</sup> in Shanghai in 2009-2010 (Wang et al., 2013), 106 µg m<sup>-3</sup> in Nanjing in 2011-2012 (Shen et al., 2014) and 124 µg m<sup>-3</sup> in Guangzhou in winter time of 2004-2005 (Huang et al., 2007). In Shanghai, the annual average PM<sub>2.5</sub> concentration was about 60 µg m<sup>-3</sup> during 1999 to 2000 (Ye et al., 2003), while it reached 90 µg m<sup>-3</sup> during 2005 to 2006 (Feng et al., 2009a). In Nanjing, another metropolitan city of the YRD, the PM<sub>2.5</sub> concentrations were more than 4-6 times of the NAAQS (National Ambient Air Quality Standards) of the USA (65 µg m<sup>-3</sup>) during 2001 (Wang et al., 2003), and a high level of 103 µg m<sup>-3</sup> was observed during 2007 to 2008 (Yang et al., 2010). High PM<sub>2.5</sub> concentrations affect the air quality in cities and background sites due to the long-range atmospheric transportation. The annual average PM<sub>2.5</sub> concentration reached 58.2 ± 50.8 and 41.3 ± 20.0 µg m<sup>-3</sup> at the regional background station in the YRD during 2010 (Meng et al., 2012) and in the PRD in the winter of 2001 (Cao et al., 2003),

respectively. All of these reported annual averages of  $PM_{2.5}$  concentrations are several times higher than the Chinese NAAQS and the WHO Air Quality Guidelines. Compared with global  $PM_{2.5}$  concentrations, such as UAS (Abu-Allaban et al., 2007), Korea (Choi et al., 2012) and Greece (Samara et al., 2014),  $PM_{2.5}$  concentrations in China were much higher.

In addition, frequent occurrence of haze episodes characterized by high concentration of  $PM_{2.5}$  and reduced visibility has been reported at a large scale in China especially in the city clusters such as the PRD (Hagler et al., 2006), the YRD (Fu et al., 2008; Hu et al., 2014), and BTH (Zhao et al., 2013a) regions, indicating that  $PM_{2.5}$  pollution is no longer limited to mega cities, but expanding to much large regional scales. The characteristics of  $PM_{2.5}$  in China exhibited higher concentrations in North China than in South China due to relative large PM emissions and unfavorable meteorological conditions for air pollutants dispersion (Zhang and Cao, 2015). High  $PM_{2.5}$  concentrations are also regularly observed in Southeast China during summer due to biomass burning (Huang et al., 2012a; Cheng et al., 2014), and in West China during spring due to dust storms (Wu et al., 2012).  $PM_{2.5}$  concentrations in China are generally higher in winter than those in summer (Wang et al., 2002; Cao et al., 2012; Zhao et al., 2013a). The diurnal patterns of  $PM_{2.5}$  concentrations in China have been reported by Zhang and Cao (2015), with highest concentrations in the evening and lowest concentrations in the afternoon.

### **2.5.3 The Characteristics of Chemical Compositions in $PM_{2.5}$**

The observation of  $PM_{2.5}$  mass concentration is not enough in studying the effects of  $PM_{2.5}$  on human health and environment; it is more important to know the chemical compositions of  $PM_{2.5}$ . In China, the major chemical compositions of  $PM_{2.5}$  including the secondary inorganic species, carbonaceous species and mineral elements have been widely studied. Cao et al. (2012) investigated the chemical compositions of  $PM_{2.5}$  during winter and summer in 14 large cities over China. They reported that OC, EC,  $SO_4^{2-}$ ,  $NO_3^-$  and  $NH_4^+$  are the major contributors in  $PM_{2.5}$  in all of the cities during both winter and summer. Zhao et al. (2013a) reported that the secondary inorganic ions ( $SO_4^{2-}$ ,  $NO_3^-$  and  $NH_4^+$ ) contributed 24-43% of the

total PM<sub>2.5</sub> mass in the region of BTH, China. Relatively few studies have reported less proportion components in PM<sub>2.5</sub>, such as trace metals. As shown in Table 2-4, the concentrations of trace metals in PM<sub>2.5</sub> at several cities in China were summarized. However, these studies were mainly conducted in urban areas in one city, and there are no reports focusing on a simultaneous measurement of trace metals in PM<sub>2.5</sub> at a regional scale. Investigations of airborne trace metals in PM<sub>2.5</sub> are insufficient for a regional estimation.

Spatially, the concentrations of chemical species were generally higher in urban than in rural sites. For example, the concentrations of OC and EC were found 2-3 times higher in urban than in rural sites of the PRD region (Cao et al., 2004). OC and EC concentrations were also found to be higher in the inland cities (*e.g.*, Changchun, Xi'an, Wuhan and Chongqing) and lower in the coastal cities (*e.g.*, Hong Kong, Xiamen and Qingdao). Seasonally, the highest concentrations of most chemical species in PM<sub>2.5</sub> were found in winter (Cao et al., 2012; Cheng et al., 2012), while maximum concentrations of mineral elements were observed in spring in north and west China due to the dust storms (Yang et al., 2005b).

In addition, some studies focused on the size distributions of chemical compositions in the atmosphere. The size distribution of EC in the atmosphere can help to understand the role of EC in regional and global climate. Huang and Yu (2008) investigated the size distribution of elemental carbon in the atmosphere in a coastal urban area in the PRD region. They found that about 80% of EC existed in fine particles less than 3.2 µm in diameter. The mode at 0.42 µm could be attributed to fresh vehicle exhausts, while the mode at 0.75 µm was likely due to the particle growth from smaller EC particles. Furthermore, size distribution of water soluble ions is helpful to know the formation and transport of secondary aerosols (Xiu et al., 2004; Guo et al., 2010). Guo et al. (2010) found that 70-80% of sulfate (SO<sub>4</sub><sup>2-</sup>) in the summer of Beijing were ascribed to in-cloud process or aerosol droplet process. They also investigated that NO<sub>3</sub><sup>-</sup> in fine particles in the afternoon was probably Ca(NO<sub>3</sub>)<sub>2</sub> at 1-1.8 µm

Table 2-4 Annual mean concentrations of airborne trace metals (ng m<sup>-3</sup>) in PM<sub>2.5</sub> from the urban cities over China

	Shanghai, Baoshan (2009-2010)	Shanghai, Putuo (2009-2010)	Hangzhou (2006)	Guangzhou (2005-2006)	Tianjin (2009-2010)	Shijiazhuang (2009-2010)	Chengde (2009-2010)	Beijing (2009-2010)
Cd	3.00	1.00	-	5.01	-	10.0	-	-
Cr	31.0	9.00	13.0	2.78	10.0	10.0	10.0	20.0
Cu	29.0	15.0	76.0	71.8	140	40.0	20.0	40.0
Mn	132	66.0	46.0	23.6	100	120	60.0	70.0
Ni	27.0	9.00	7.00	12.5	10.0	10.0	-	10.0
Pb	133	59.0	128	196	220	300	110	140
Zn	465	236	651	477	750	680	280	320
References	Wang et al. (2013)	Wang et al. (2013)	Bao et al. (2010)	Lee (2007)	Zhao et al. (2013a)	Zhao et al. (2013a)	Zhao et al. (2013a)	Zhao et al. (2013a)

and  $\text{KNO}_3$  at 0.56-1  $\mu\text{m}$ , suggesting the reaction of  $\text{HNO}_3$  with soil particles was important in both coarse and fine particles.

#### **2.5.4 Haze Episode**

Haze is defined by the following conditions: (1) a daily mean visibility less than 10 km; (2) no precipitation; and (3) a daily mean relative humidity (RH) lower than 80% (Deng et al., 2008). The formation of haze is related to the meteorological conditions and high concentrations of atmospheric particulate matters emitted by anthropogenic sources and gas-to-particle conversion. Haze has attracted much scientific and public attention during the past decade for its adverse impact on visibility, public health and global climate (Yadav et al., 2003; Huang et al., 2012b; Kang et al., 2013). Haze episode in China has been substantially increased since the 1990s due to the increase of atmospheric particulate matters and gaseous pollutants (Fu et al., 2008; Huang et al., 2012b). Che et al. (2009b) investigated the haze trends over 31 provincial capitals in China from 1981 to 2005. They found that the annual haze increased significantly in 13 cities from the southern, southwestern and eastern provinces; and the high haze regions were found in the Sichuan Basin, north and east China. Furthermore, the occurrence of haze at a regional scale has been reported more frequently in China in recent years (Hua et al., 2015; Wang et al., 2015). Haze has increasingly become an important environmental issue in China.

Research of haze has been conducted in the major affected areas in China, such as the PRD region in South China, the YRD region in East China and North China Plain (Zhang et al., 2012a). Previous studies have investigated the meteorological conditions, aerosol physical, chemical and optical properties, and sources during the haze pollution episode, and have analyzed the key factors that affect the formation of haze (Ye et al., 2011; Huang et al., 2012a; Kang et al., 2013; Hua et al., 2015; Wang et al., 2015). Huang et al. (2012a) summarized the formation mechanisms and chemical compositions during three typical haze types (*i.e.*, secondary inorganic pollution, dust and biomass burning) in Shanghai. Kang et al.

(2013) observed a high ratio of  $\text{NO}_3^-/\text{SO}_4^{2-}$  in aerosol during a long-lasting haze episode occurred in Nanjing, indicating that traffic source became more important in the YRD region. Ye et al. (2011) suggested that the available  $\text{NH}_3$  played a vital role in the enhancement of particulate sulphate and nitrate during the haze episode. The importance of secondary organic aerosol formation in driving  $\text{PM}_{2.5}$  pollution during haze events was observed by Huang et al. (2014). In China, haze occurred more frequently in winter due to the large emissions of air pollutants and stagnant weather conditions (Gao et al., 2015; Wang et al., 2015). Recently, haze episodes were also observed in summer (Tan et al., 2009; Du et al., 2011) and fall (Hua et al., 2015). Furthermore, the impact of open biomass burning on haze pollution during post-harvest seasons has been increasingly significant (Huang et al., 2012b; Zhu et al., 2012; Cheng et al., 2014). Previous studies have investigated the formation mechanism of pollution events by observation of air pollutants (Fu et al., 2008; Fu et al., 2010). Recently, a 3-D model, the Nested Air Quality Prediction Modeling System (NAQPMS), was applied to understand the sources and transport of air pollutants (Wang et al., 2006d; Li et al., 2008; Li et al., 2014). Both monitoring data and modelling results are needed to better understand the formation and evolution of  $\text{PM}_{2.5}$  pollution events.

Most of studies on haze pollution have focused on analyzing the characteristics of chemical compositions and meteorological parameters, sources and evolution mechanisms. However, few studies have investigated the mixture effects and major toxicity drivers of  $\text{PM}_{2.5}$  during haze episode. For example, Yang et al. (2010) found that the concentrations of metal elements in hazy days were higher than that in non-hazy days in autumn and winter, and Cu, Se, Hg and Bi were highly enriched in  $\text{PM}_{2.5}$  in hazy days. It has been hypothesized that airborne PM toxicity might be associated with the bioaccessible transition metals on the particle surface (Molinelli et al., 2002; Merolla and Richards, 2005; Heal et al., 2009). It is important to identify which metal elements and sources dominate in  $\text{PM}_{2.5}$  during hazy days. Due to the various sources and chemical compositions under different types of haze (Huang et al., 2012a), more research is needed to identify the potential toxicity of  $\text{PM}_{2.5}$ , and which kind of air particles dominate the adverse health effects of  $\text{PM}_{2.5}$  and how they affect human health.

### 2.5.5 PM<sub>2.5</sub> Studies in Remote Sites

Observations made at remote sites can provide useful information for the analysis of background PM<sub>2.5</sub> conditions, due to the less influence of local pollutants and the representation of a well-mixed atmosphere over a large area. In China, observations of regional atmospheric background have been made at remote sites for several decades, including Mount Waliguan (the global background station in Qinghai Province), Lin'an (the background of the YRD region), Zhuzhang (the background of southwestern China), Akdala (the background of northwestern China) and Mt. Tai (the background of North China Plain) (Qu et al., 2009; Wang et al., 2012b; Zhou et al., 2012). The long-term observations at background sites mainly targeted gaseous species such as O<sub>3</sub>, CO, CO<sub>2</sub>, CH<sub>4</sub>, SO<sub>2</sub> and NO<sub>x</sub> (Wang et al., 2004; Meng et al., 2009; Meng et al., 2010), while investigations of PM<sub>2.5</sub> in remote sites are limited.

Knowledge of the aerosol background is not only important for studying the changes in atmospheric particles properties caused by humans, but also for assessing the trans-boundary transportation of pollution and for estimating large-scale particles effects on climate and biogeochemical cycles. Gao et al. (2012) revealed the important role of cloud processing in the formation of sulfate in PM<sub>2.5</sub>, based on the observations at Mount Heng in central southern China. The results showed the long-range transport of anthropogenic pollutants from the coastal regions of eastern/northern China and the PRD region to Mount Heng during spring. Wang et al. (2012b) found the formation mechanism of SOM through aqueous-phase reactions in clouds at Mt. Tai, North China. In comparison with the aerosol studies in urban cities, observations of atmospheric particles at background sites were mostly carried out over short term, few studies conducted a long term observation of chemical compositions in PM<sub>2.5</sub> at the regional background sites (Fu et al., 2014; Zhang et al., 2014). The concentrations of PM<sub>2.5</sub> and its major chemical components were detected at a regional background site in the central PRD during fall and winter seasons from 2007 to 2011 (Fu et al., 2014). The results indicated that the reduction of PM<sub>2.5</sub> in the PRD was mainly

attributed to the decrease of OM and  $\text{SO}_4^{2-}$ , while the fast increase of  $\text{NO}_3^-$  was likely due to the increase of power plants and vehicles. A better understanding of the background of  $\text{PM}_{2.5}$  will be helpful for policy makers to control pollution emissions.

During the past decade, researches have been studied the  $\text{PM}_{2.5}$  concentrations and their major chemical components such as water soluble ions (Ma et al., 2003; Che et al., 2009a; Gao et al., 2009) and carbonaceous species (Qu et al., 2008; Qu et al., 2010; Zhang et al., 2012b) at different regional background sites, however, the observations of atmospheric trace metals are limited. Moreover, there are few researches conducted the simultaneous investigation for  $\text{PM}_{2.5}$  and its chemical compositions at different regional background sites in China. Therefore, there is an urgent need for aerosol study in regional background sites in China to evaluate the impact of air pollution on regional climate and human health.

## **2.6 Summary and Outlook**

Atmospheric particulate matters pollution was severe in mega cities and city clusters of China over the past decades, and it will continue to be one of the key concerns for environment and human health. The chemical compositions, sources, formation mechanism and long-range transport of atmospheric particulate matters have been widely studied, and research in these fields has improved in recent years. At the same time, large gaps in the research await further study.

Most studies have focused on the major chemical compositions of  $\text{PM}_{2.5}$  including the secondary inorganic species (sulfate, nitrate and ammonium), carbonaceous species (organic carbon and element carbon) and mineral elements, while relatively few studies have reported trace metals in  $\text{PM}_{2.5}$ . Recently, scientific attention has shifted to the mixture toxic effects and major toxicity drivers of  $\text{PM}_{2.5}$ . Among the chemical compositions in  $\text{PM}_{2.5}$ , bioaccessible transition metals (*e.g.*, Fe, Cu, V, Mn, Ni and Zn) on the particle surface are suspected to cause oxidative damage effects both to the lung and other organs. However, investigations of airborne trace metals in  $\text{PM}_{2.5}$  are insufficient in China. There has a strong

need for more research to investigate airborne trace metals and their impacts on environment and human health on a regional scale, especially in the large city clusters with fast economy development and urbanization, such as the PRD, the YRD and BTH regions. A comprehensive study is needed to simultaneously investigate the temporal-spatial variations, sources and long-range transport of airborne trace metals in large city clusters with typical local emission and meteorological conditions, and to study the possible factors that influence the pollution of  $PM_{2.5}$ . Moreover, little information is available about the bioaccessibility of trace metals in  $PM_{2.5}$ . Consequently, the bioaccessibility of trace metals in  $PM_{2.5}$  in China needs more studies to better understand their potential toxicity and which metal elements and sources dominate the potential toxicity of  $PM_{2.5}$ , which may provide insightful information to policy makers for controlling airborne trace metals pollution.

Regional haze pollution occurred more frequently in recent years (Zhao et al., 2013b; Wang et al., 2015), and is seriously affecting people's quality of life and health, which has attracted extensively public and scientific concern. A series of achievements in chemical compositions, formation mechanisms and meteorological conditions during haze have been gained (Ye et al., 2011; Huang et al., 2012a; Kang et al., 2013), whereas the evolution and regional transport of air pollutants during haze are seldom studied (Wang et al., 2006d). A 3-D model (NAQPMS) is a useful technic to understand the evolution and transport of air pollutants (Wang et al., 2006d; Li et al., 2008; Li et al., 2014). An integrated study of field monitoring and modelling study is needed to investigate the formation, evolution and regional transport of  $PM_{2.5}$  during regional haze event. Moreover, the mixture toxic effects and identification the major toxicity drivers of  $PM_{2.5}$  during haze episodes also required to be further studied.

## **Chapter 3 - Methodology**

### **3.1 Characteristics of the Study Region**

Descriptions of geographical location, population, urbanization and meteorology of the Pearl River Delta (PRD), the Yangtze River Delta (YRD) and North China (NC) are given in this section.

#### **3.1.1 The Pearl River Delta Region**

The Pearl River Delta region, including Guangzhou, Shenzhen, Zhuhai, Dongguan, Zhongshan, Foshan, Huizhou, Jiangmen and Zhaoqing, and the SARs (Special Administrative Region) of Hong Kong and Macau (Fig. 3-1), is actually a city cluster with highly developed industrial operations, and with a population of approximately seventy million in a land area of 56,000 km<sup>2</sup>. This region is located at 21°17'-23°56'N and 115°9'-115°2'E and is close to the South China Sea. In recent decades, the PRD region has been one of the most industrial developed and urbanized regions in China. Due to the developed manufacturing industries such as electric products, garments and textiles, toys and plastic products, the PRD region has become one of the most economical city clusters in China. The region experiences both tropical and sub-tropic monsoon climate, and is a cloud-prone and rainy area with an annual average temperature of 22 °C and annual precipitation of 1,690 mm (Wong et al., 2002). The prevailing wind direction in the PRD region is from the northeast in the winter and from the southeast, south and southwest in the summer. The annual wind speed in the coastal cities (such as Hong Kong, with about 6 m s<sup>-1</sup> in 2014) (Hong Kong Observatory, <http://gb.weather.gov.hk/contentc.htm>) is higher than that in the inland cities (such as Guangzhou and Foshan, with about 2 m s<sup>-1</sup>) (Chan and Yao, 2008).

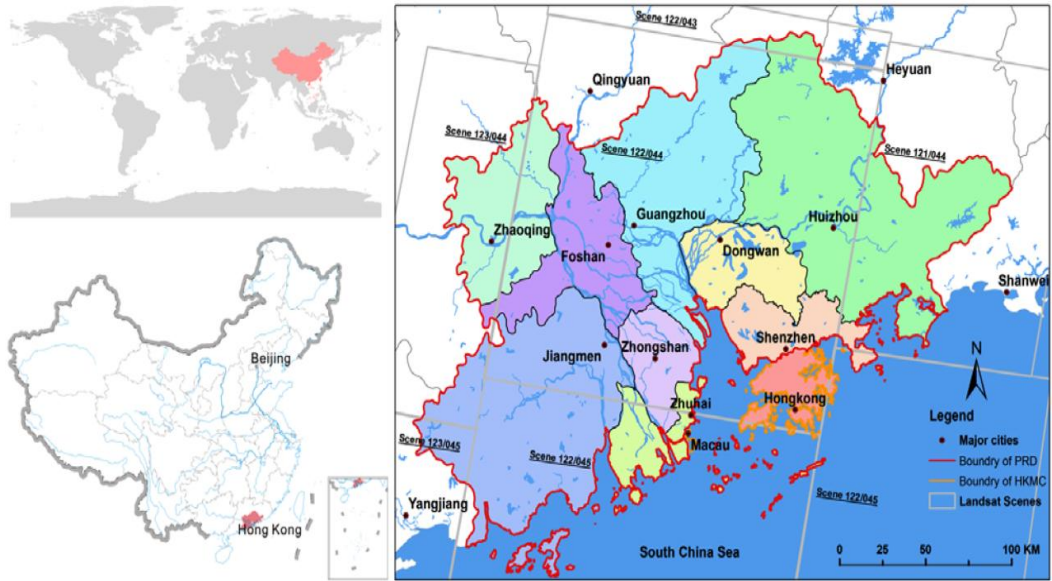


Figure 3-1 City cluster of the Pearl River Delta Region (Du et al., 2013).

### 3.1.2 The Yangtze River Delta Region

The Yangtze River Delta (YRD) is the most economically developed regions of east China, which is characterized by a cluster of 25 cities such as Shanghai, Hangzhou, Nanjing, Suzhou and Ningbo (Fig. 3-2). The YRD region lies in the mid-eastern part of China and covers an area of about 110,600 km<sup>2</sup>, with a population of  $7.54 \times 10^7$  (Huang et al., 2009). The Yangtze River Delta is located on the western coast of the Pacific Ocean and has a subtropical monsoon climate, in which the weather is very hot and humid in summer, cool and dry in winter, and warm in spring and fall. In summer, maritime air masses reach the YRD region by passing through the southern part of China under the influence of the Pacific anticyclone. In winter, it is subjected the regime of the northeastern monsoon. In the YRD region, the annual mean temperature is 18 °C and rainfall is 1,100 mm. Large energy consumption and vehicle population generated a large amount of primary air pollutants in the region. For example, by the end of 2013, the coal consumption in Shanghai reached  $1.17 \times 10^8$  tons SCE (standard coal equivalent). Coal was still the major energy category in Shanghai, which contributed over 49% of the total energy consumed (Shanghai Statistics Yearbook 2014). The automobile population in Shanghai grew to  $2.82 \times 10^8$  in 2013.

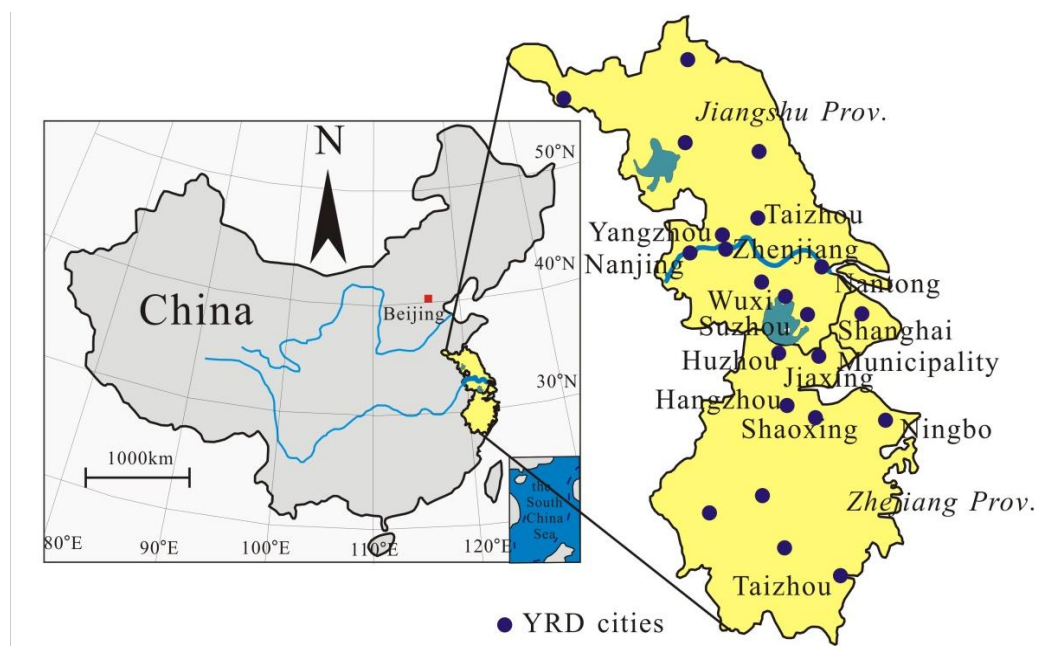


Figure 3-2 City cluster of the Yangtze River Delta Region.

### 3.1.3 North China

The North China Plain (NCP) is the key area of North China, with an area of about 409,500 km<sup>2</sup>. The plain is bordered on the north by the Yanshan Mountains and on the west by the Taihang Mountains edge of the Shanxi plateau. It extends over Beijing, Tianjin, and Hebei, Shandong, Henan, Jiangsu and Anhui provinces (Fig. 3-3). This plain is one of China's most important agricultural regions, producing corn, sorghum, winter wheat, vegetables and cotton. The wind system of this region is controlled by the westerly wind as well as the Asian monsoon which provides warm and humid southern wind in summer and cold and dry northern wind in winter.

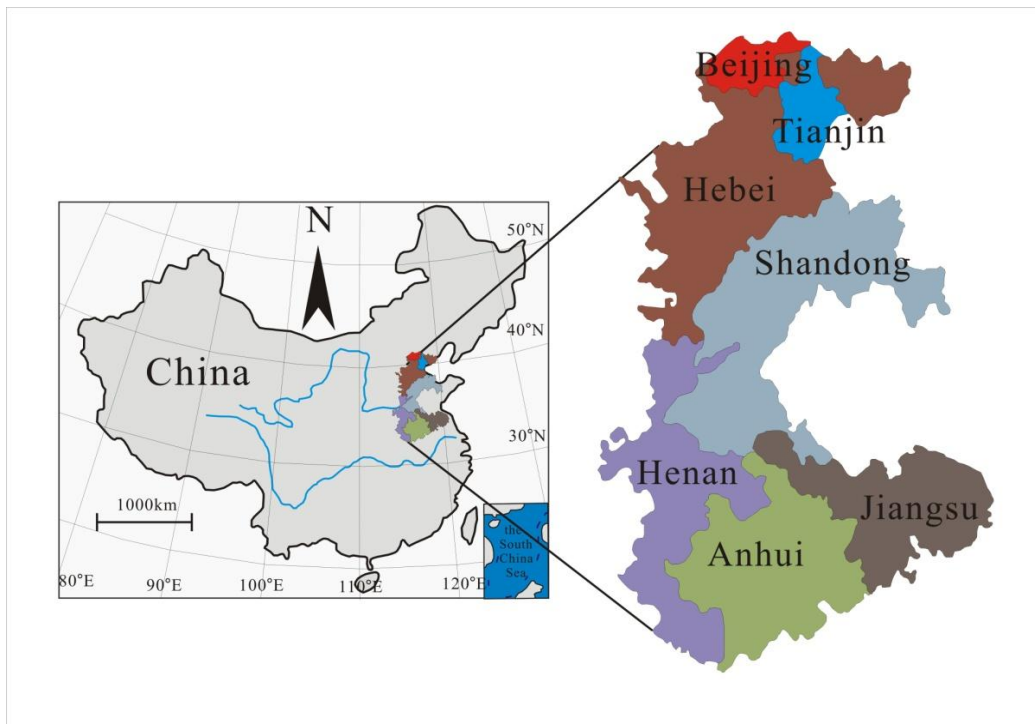


Figure 3-3 City cluster of North China Plain.

### 3.2 Sampling Sites

The sampling sites in the PRD and YRD regions and North China are shown in the Fig. 3-4.

Table 3-1 provides the details of the sampling sites in the present study.

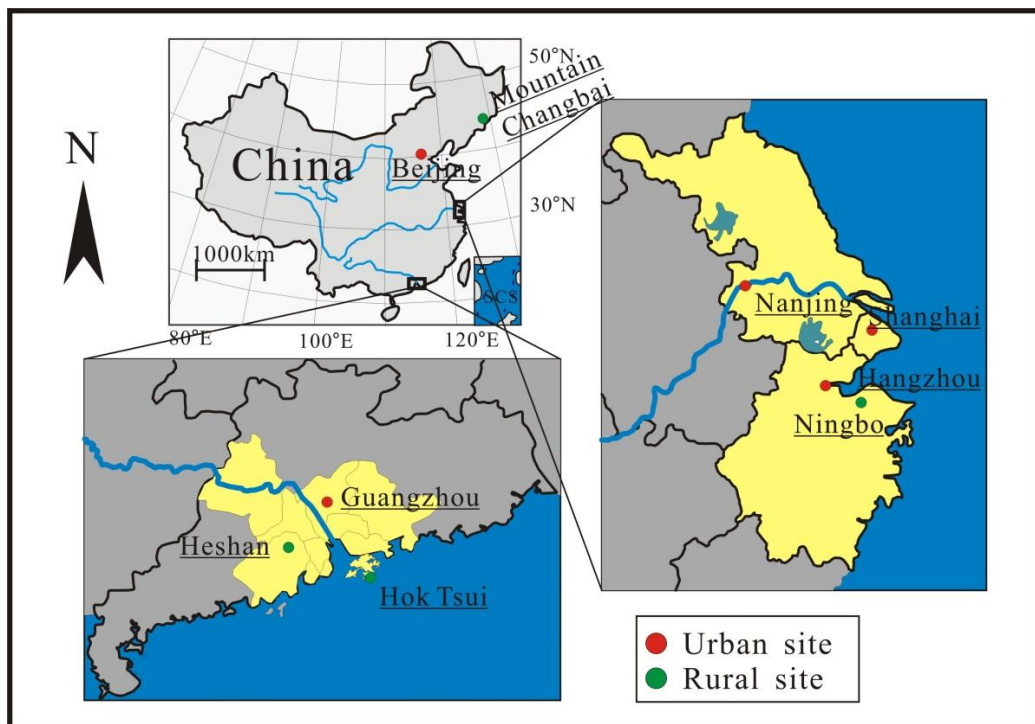


Figure 3-4 The sampling sites in the PRD and YRD regions, and North China.

Table 3-1 Overview of the sampling sites in the present study.

Region	City	Sampling site	Code	Site location	Site characteristics
The PRD	Guangzhou	Guangzhou Institute of Geochemistry	GZ	23°07'N, 113°19'E	Urban site
	Heshan	Huaguo Mountain	HS	22°42'N, 112°55'E	Rural site
	Hong Kong	Hok Tsui	HT	22°12'N, 114°15'E	Coastal rural
The YRD	Shanghai	Handan Campus of Fudan University	SH	31°17.8'N, 121°30'E	Urban site
	Nanjing	Institute of Soil Science	NJ	32°03.5'N, 118°48'E	Urban site
	Hangzhou	Zijin'gang Campus of Zhejiang University	HZ	30°18'N, 120°5.2'E	Urban site
	Ningbo	Ningbo Atmospheric Environment Observatory	NB	29°40.8'N, 121°37'E	Rural site
North China	Beijing	China University of Geosciences, Beijing	BJ	39°56'N, 116°20.4'E	Urban site
	Mount Changbai	Mount Changbai	CBS	42°24'N, 128°06'E	Remote site

### **3.2.1 Description of Sampling Sites in the PRD Region**

In the PRD region, an urban site in Guangzhou, a rural site in Heshan city and a coastal site in Hok Tsui, Hong Kong were selected as the sampling sites.

Guangzhou (GZ): The sampling site is located on the rooftop of a four-story library in Guangzhou Institute of Geochemistry (23°07'N, 113°19'E), about 12 m high and 300 m away from a heavy traffic road. The sampling site is located in Tianhe District (the urban central of Guangzhou city), which represents a mixed residential, traffic, and commercial environments of an urban area in Guangzhou.

Heshan (HS): Heshan station is the first super atmospheric monitoring station in China. It is located in the Huaguo Mountain of the Jiangmen–Heshan city (22°42'N, 112°55'E), the south of the PRD region, China. This sampling site is surrounded by forest, representing a typical rural location. It is seven kilometers away from Heshan city and 4 km east away from the Fokai highway.

Hong Kong (HK), Hok Tsui: The sampling site is located at the southeast coast of Hong Kong Island (22°12'N, 114°15'E, 60 m ASL) with less anthropogenic activities (such as roadways, commercial establishment and industry). It is 15 km away from intense human activities and heavy traffic. Hong Kong is primarily associated with service industries; however it still has some local sources of air pollutants from traffic, shipping and manufacturing.

### 3.2.2 Description of Sampling Sites in the YRD Region

In this study, four representative sites in the YRD were selected for the field sampling. They include three developed cities with a large pollution: Nanjing in Jiangsu Province, Hangzhou in Zhejiang Province and Shanghai, and a background site (Damei Mountain in Ningbo, Zhejiang Province (Fig. 3-3)). With the large primary emissions, Nanjing and Hangzhou had rather poor geographical and meteorological conditions to dilute the aerosol concentration. Nanjing is surrounded by Wuhu, Chuzhou, Yangzhou and Zhenjiang, wherein the aerosol concentrations are rather high. The details of sampling sites were described as below.

Shanghai (SH), Handan Campus of Fudan University: the site is located on the rooftop of a five-story teaching building (about 15 m above the ground) (31°17.8'N, 121°30'E). The site represents a mixed residential, traffic, and commercial environments of the central urban area of Shanghai. Shanghai sits on the eastern coast of China, covering a total area of 6,341 km<sup>2</sup> with a population of over  $2.3 \times 10^7$  in 2010. Shanghai has a humid subtropical climate and experiences four distinct seasons. Winters are chilly and damp, and cold north-westerly winds from Siberia can cause night-time temperatures to drop below freezing, although most years there are only one or two days of snowfall. Summers are hot and humid, with an annually average of 8.7 days exceeding 35 °C. The city is also susceptible to typhoons in summer and the beginning of autumn.

Nanjing (NJ), Institute of Soil Science, Chinese Academy of Sciences: the sampling site is on the rooftop of a five-story laboratory building with in the institute (32°03.5'N, 118°48'E), about 15 m above the ground and 200 m away from a main street. Nanjing Institute of Soil Science is located in Xuanwu District which has the highest population density in Nanjing. The institute is surrounded by residential areas, heavily trafficked roads and commercial centers, representing a typical urban location. Nanjing, with a total land area of 6,598 km<sup>2</sup> and an urban population of over  $7 \times 10^6$  in 2011, is the second-largest commercial centre in the YRD after Shanghai. Nanjing has a humid subtropical climate and is under the influence

of the East Asian monsoon. The four seasons are distinct here, with damp conditions throughout the year, very hot and muggy summers, cold and damp winters, and in between, spring and autumn are of reasonable length. Nanjing is endowed with rich natural resources, which include more than 40 various kinds of minerals. Among them, iron and sulfur reserves make up 40% of those of Jiangsu province.

Hangzhou (HZ), Zijin'gang Campus of Zhejiang University: the sampling site located on the rooftop of a five-story laboratory building in the campus (30°18'N, 120°5.2'E), about 15 m high. The Zijin'gang campus of Zhejiang University is located in the south of Hangzhou City, and nine km away from the downtown of Hangzhou. It is the largest single university campus in Mainland China, which covers 600,000 m<sup>2</sup> land area. The sampling site is in the residential area in Xihu District, which represented a peri-urban site of Hangzhou. Hangzhou is the capital and largest city of Zhejiang Province in Eastern China. Its administrative area (sub-provincial city) extends west to the mountainous parts of Anhui province, and east to the coastal plain near Hangzhou Bay. Within the Hangzhou Metropolitan Area, a population of approximately  $2.1 \times 10^7$  people live in the area with 34,585 km<sup>2</sup>.

Ningbo (NB), Ningbo Atmospheric Environment Observatory (NAEO) (29°40.8'N, 121°37'E, 550 m ASL) is located on a rural mountaintop in Ningbo as a regional background site. It is approximately 15 km to the east of the coast of the East China Sea (ECS), and about 20 km northwest of the city centre of Ningbo. Ningbo is the second largest city in the Zhejiang Province, approximately 150 km west of Hangzhou, and 150 km north of Shanghai. This sampling site is surrounded by forest, and there are several hills around the site with an elevation of less than 600m. In addition to the abovementioned cities around the NAEO, there are a number of smaller pollution sources located in the areas, including villages, small industrial plants, and agriculture-related biomass burning. The site has a subtropical monsoon climate, in which the weather is incredibly hot and humid in summer. In addition, maritime air masses reach the sampling site by passing through the south China under the influence of the Pacific anticyclone in summer. In contrast, the sampling region is

relatively cool and dry in winter. The westerly or north-westerly monsoon winds caused predominantly by the Siberian anticyclone transport the air masses from the northern and the central parts of China to the NAEO.

### **3.2.3 Description of Sampling Sites in North China**

Beijing (BJ): the sampling site (39°56'N, 116°20.4'E) is located on the rooftop of building of national research centre for geoanalysis, China University of Geosciences, Beijing. The site represents a mixture of residential, traffic, and commercial environments of the central urban area of Beijing, and is situated in the north urban areas of Beijing. Beijing is geographically located in northern China, with a permanent resident population of  $2.0 \times 10^7$  in 2010. The main terrain of Beijing is plain, with surrounding mountains (the Yanshan Mountain) in three directions. The special geography favors stagnant atmospheric conditions over the area, where the diffusion ability of air pollutants is poor. Beijing is in the warm temperate zone and has a typical continental monsoon climate with four distinct seasons.

Mountain Changbai (CBS): The sampling site (CBS: 42°24'N, 128°06'E, 741 m ASL) is conducted at a remote site in area, northeastern China and operated by the Chinese Terrestrial Ecosystem Flux Research Network. The site located about 40 km to the north of the major peak of Mount Changbai. This mountain range stretches more than 1,000 km from southwest to northeast. The CBS site is located in a deciduous broad-leaf forest, and the sampling inlet of CBS was 2-3 m above forest canopy.

## **3.3 Sampling Methods**

### **3.3.1 Sampling Instruments**

A high-volume sampler (Fig. 3-5) was applied at each sampling site, equipped with a 2.5  $\mu\text{m}$  inlet at flow rate of  $1 \text{ m}^3 \text{ min}^{-1}$  and quartz microfiber filters (QFFs) of 8  $\times$  10 in. (PALL, USA).



Figure 3-5 The high-volume PM<sub>2.5</sub> sampler.

### 3.3.2 PM<sub>2.5</sub> Sampling

The PM<sub>2.5</sub> samples were collected on quartz microfiber filters (QFFs) of 8 × 10 in. (PALL, USA). The filters were pre-baked for 8 h at 450 °C to remove any contamination caused by carbonaceous material. The filters were weighed twice before and after sampling, using a balance (Sartorius, Analytic) with the sensitivity of ±0.1 mg. Before weighing, the samples were equilibrated in a desiccator at 20-30 °C and a relative humidity of 30-40% for at least 24 hrs. A sampling period of 24 hrs was adopted. After the sampling, the loaded filters were stored in polyethylene bags at -20 °C before analysis. Field blank filters were also collected.

### 3.3.3 Overview of the Sampling

The simultaneously sampling program for PM<sub>2.5</sub> samples has been conducted in the PRD and YRD regions and North China over one-year period from September 2013 to August 2014. The simultaneous weekly sampling (*i.e.*, one 24-h sample per week) was conducted in the PRD and YRD regions over a whole year cycle. In addition, high frequency daily PM<sub>2.5</sub> sampling (*i.e.*, one 24-h sample per day) was conducted simultaneously in Guangzhou, Shanghai, Nanjing and Beijing in the autumn (from 16<sup>th</sup> October 2013 to 14<sup>th</sup> November 2013), winter (from 21<sup>th</sup> December 2013 to 20<sup>th</sup> January 2014), spring (from 21<sup>th</sup> March

2014 to 20<sup>th</sup> April 2014) and summer (from 23<sup>th</sup> June 2014 to 24<sup>th</sup> July 2014). Due to precipitation or occasional sampler instability, some samples were missed at each site. However, at least 20 samples were taken for each period at each site. At the site of Beijing, the sampling period were delayed in the spring and summer season due to the problems of the sampler. The high resolution sampling period at Beijing in the spring and summer was performed from 12<sup>th</sup> April to 12<sup>th</sup> May 2014 and from 30<sup>th</sup> July to 28<sup>th</sup> August 2014, respectively. At CBS, weekly sampling of PM<sub>2.5</sub> was also conducted from 21 Sep 2013 to 21 Jul 2014. Field blank filters were also collected at each site. The details of the sampling program are illustrated in Table 3-2. In this study, same sets of cut-off dates were used to define the four seasons for all the sites in three regions: (a) autumn: September-November 2013; (b) winter: December 2013-February 2014; (c) spring: March-May 2014; and (d) summer: June-August 2014.

Table 3-2 The sampling program for PM<sub>2.5</sub> in the PRD, the YRD and North China.

Region	Site	Sampling frequency	Sampling period	Number
The PRD	GZ	Weekly	Sep 2013 to Aug 2014	136
		Daily	16 <sup>th</sup> Oct~14 <sup>th</sup> Nov 2013; 21 <sup>th</sup> Dec 2013~20 <sup>th</sup> Jan 2014; 21 <sup>th</sup> Mar~20 <sup>th</sup> Apr 2014; 23 <sup>th</sup> Jun~24 <sup>th</sup> Jul	
	HS	Weekly	Sep 2013 to Aug 2014	61
	HT	Biweekly	Nov 2013 to Oct 2014	18
The YRD	SH	Weekly	Sep 2013 to Aug 2014	143
		Daily	16 <sup>th</sup> Oct~14 <sup>th</sup> Nov 2013; 21 <sup>th</sup> Dec 2013~20 <sup>th</sup> Jan 2014; 21 <sup>th</sup> Mar~20 <sup>th</sup> Apr 2014; 23 <sup>th</sup> Jun~24 <sup>th</sup> Jul	
	NJ	Weekly	Sep 2013 to Aug 2014	119
		Daily	16 <sup>th</sup> Oct~14 <sup>th</sup> Nov 2013; 21 <sup>th</sup> Dec 2013~20 <sup>th</sup> Jan 2014; 21 <sup>th</sup> Mar~20 <sup>th</sup> Apr 2014; 23 <sup>th</sup> Jun~24 <sup>th</sup> Jul	
	HZ	Weekly	Sep 2013 to Aug 2014	45
	NB	Weekly	Sep 2013 to Aug 2014	44
North	BJ	Daily	15 <sup>th</sup> Oct~14 <sup>th</sup> Nov 2013; 2 <sup>th</sup> ~21 <sup>th</sup> Jan 2014; 12 <sup>th</sup> Apr~12 <sup>th</sup> May 2014; 30 <sup>th</sup> Jul~28 <sup>th</sup> Aug 2014	101
China	CBS	Weekly	21 Sep 2013 to 21 Jul 2014	42

### 3.4 Chemical Analysis

The chemical analysis of PM<sub>2.5</sub> samples including total metal concentrations, Pb isotopic compositions, bioaccessible fraction of trace metals extracted by simulated lung fluids, water-soluble inorganic ions and carbonaceous species (organic carbon and element carbon). Total concentrations of trace metals were analysed for each filtered PM<sub>2.5</sub> sample collected from all the sampling sites. Pb isotopic compositions were detected for partial samples from all the sampling sites. Concentrations of organic carbon (OC) and element carbon (EC) were analysed for high frequently daily samples from GZ, SH, NJ and BJ. Water-soluble ions (NO<sub>3</sub><sup>-</sup>, Cl<sup>-</sup>, SO<sub>4</sub><sup>2-</sup>, K<sup>+</sup> and NH<sub>4</sub><sup>+</sup>) were measured for samples from SH and NJ. The bioaccessible concentrations of trace metals were analyzed for the samples from GZ, SH and NJ.

#### 3.4.1 Total Metal Concentration

One eighth of the filter was cut using ceramic scissors and placed in acid-cleaned Pyrex test tubes (18 mm ×18mm) for strong inorganic acids (Wong et al., 2003). Twelve mL of 70% high purity nitric acid (HNO<sub>3</sub>) and 3 mL of 65% perchloric acid (HClO<sub>4</sub>) were added to ensure the filters were completely submerged. The mixed solutions were gently shaken using a vortex, and then heated progressively to 190 °C in an aluminium heating block to completely dry. The filter samples were heated according to the temperature settings shown in Table 3-3. After the test tubes cooling, 12 mL of 5% (v/v) HNO<sub>3</sub> were added, in which the samples were fully submerged. The combinations were mixed by a vortex and then heated at 70 °C for 1 h. After cooling, the mixtures were poured into 10 mL plastic tubes for storage at 4 °C until analysis.

All glass and plastic tubes need acid cleaned and rinsed with deionized water before used. Quality control was adopted by reagent blanks, replicated samples and the standard reference materials (NIST 1648a) analysis, representing 10, 20 and 10% of the total number of samples, respectively (Wong et al., 2003). In the present study, the concentrations of major elements (*i.e.*, Al, Fe, K, Ca and Mg) and trace elements (*i.e.*, Cu, Mn, Pb, Zn, Cd, Cr,

V and Ni) in filter samples were determined by using ICP-AES (Inductively Coupled Plasma-Atomic Emission Spectrometry) after calibration using high-purity standard in 5% high-purity HNO<sub>3</sub>. Regent blanks (5% high-purity HNO<sub>3</sub>) and quality control standards were measured at every 10 samples to detect contamination and drift. The metals concentrations in regent blanks were less than 1% of the average analyte concentrations for all the metals, and the precision (RSD) of the control standards and replicates are generally lower than 10%. The recovery rates of the metal elements in the standard reference materials ranged from 96% to 110% (except Al: 54%).

Table 3-3 The temperature setting of aluminium heating block for acid digestion of filter samples.

Temperature ( °C)	Filter (hours)
50	2
75	3
100	3
125	3
145	2
165	2
175	2
190	Until dryness

### 3.4.2 Pb Isotopic Composition Analysis

The Pb isotopic composition analysis was conducted using Inductively Coupled Plasma-Mass Spectrometry (ICP-MS). The solutions were diluted to a Pb concentration of about 30 mg L<sup>-1</sup> using 5% high-purity HNO<sub>3</sub> to optimize the analytical performance of the instrument. The analytical parameters were set as 250 sweeps per reading and 10 readings per sample solution. Procedural blanks and standard reference materials (NIST SRM 981, common lead) were used for quality control. The analysis was repeated when the differences between the measured and certified values of the standard reference materials exceeded 0.5%. The Pb counts of the blanks were less than 0.5% of the samples, and the precision (% RSD) of the Pb isotopic ratios of the 10 replicates was typically lower than 0.5%. The average measured ratios of <sup>204</sup>Pb/<sup>207</sup>Pb, <sup>206</sup>Pb/<sup>207</sup>Pb and <sup>208</sup>Pb/<sup>207</sup>Pb (0.0643 ± 0.0003, 1.0939 ± 0.0006 and 2.3704 ± 0.0017, respectively) were in agreement with the certified standard values (0.0646, 1.0933 and 2.3704, respectively).

### 3.4.3 Bioaccessible Fraction of Trace Metals

In order to evaluate the potential toxicity of airborne metals, simulated lung fluids—Gamble's solution (represents the neutral conditions of the interstitial fluid found deep in the human lung, pH=7.4) were used to extract the bioaccessible fraction of metal in PM<sub>2.5</sub>. Gamble's solution was freshly prepared according to Colombo et al. (2008). The compositions of Gamble's solution were added in the order presented in Table 3-4 to avoid salt precipitation. All chemicals were analytical grades and both solutions were prepared using ultra-pure water. A portion of filter sample was placed in a clean polyethylene tube and 30 mL of extractant was added. The samples were shaken for 24 hrs at 37 °C and 100rpm in a temperate shaker. Extracts were centrifuged for 15 min at 4,000rpm, and then filtered through a polytetrafluoroethylene microporous membrane (0.22 μm pore size and 13 mm diameter). The extraction test was conducted in duplicate, blanks (only contain simulated lung fluids) and standards (a known concentration of metal solution and standard

reference materials–NIST SRM 1648a). A portion of 15 mL of extracts were put into acid-cleaned Pyrex test tubes (18 mm × 18mm) with 2 mL of 70% high purity nitric acid (HNO<sub>3</sub>) to get the soluble metal fractions. The heating block was adjusted to 85°C for a half hour, 120°C for 4 hrs, then to 150°C until the sample reached dryness. When cooled, 10 mL 5% HNO<sub>3</sub> was added. The mixtures were blended by a vortex and then heated at 70 °C for 1 h. After cooling, the mixtures were poured into 15 mL plastic tubes for metal analysis using ICP-MS. The insoluble fraction (filter residue) was acidic digested with 6.0 mL HNO<sub>3</sub> and 1.5 mL HClO<sub>4</sub> in quartz glass tubes. The detailed procedures of insoluble fraction analysis were the same as the metal analysis (see section 3.4.1).

Table 3-4 Composition (g L<sup>-1</sup>) of simulated lung fluids–Gamble’s solution.

Chemicals (g L <sup>-1</sup> )	Gamble’s solution, pH = 7.4
Magnesium chloride, MgCl <sub>2</sub>	0.095
Sodium chloride, NaCl	6.019
Potassium chloride, KCl	0.298
Disodium hydrogen phosphate, Na <sub>2</sub> HPO <sub>4</sub>	0.126
Sodium sulphate, Na <sub>2</sub> SO <sub>4</sub>	0.063
Calcium chloride dihydrate, CaCl <sub>2</sub> • 2H <sub>2</sub> O	0.368
Sodium acetate, C <sub>2</sub> H <sub>3</sub> O <sub>2</sub> Na	0.574
Sodium hydrogen carbonate, NaHCO <sub>3</sub>	2.604
Sodium citrate dihydrate, C <sub>6</sub> H <sub>5</sub> Na <sub>3</sub> O <sub>7</sub> • 2H <sub>2</sub> O	0.097

#### 3.4.4 Water-soluble Ions Analysis

A portion of each sample and blank filter was extracted three times in 10 mL of 18-Ohm MilliQ water and sonicated for each 15 min in an ultrasonic ice-water bath. The total extract was filtered through a polytetrafluoroethylene microporous membrane (0.22 µm pore size and 13 mm diameter). After filtered, the extract was analyzed for anions (*i.e.*, Cl<sup>-</sup>, NO<sub>3</sub><sup>-</sup> and SO<sub>4</sub><sup>2-</sup>) and cations (*i.e.*, NH<sub>4</sub><sup>+</sup> and K<sup>+</sup>) by ion chromatography (Metrohm, 883 Basic IC plus). Cations and anions were measured by a Metrohm Metrosep C4-100 column and a Metrohm

Metrosep A sup5-150 column equipped with a suppressor, respectively. The eluent for cations and anions measurement were  $2 \text{ mmol L}^{-1}$  sulfuric acid and a mixture solution with  $3.2 \text{ mmol L}^{-1} \text{ Na}_2\text{CO}_3$  and  $1.0 \text{ mmol L}^{-1} \text{ NaHCO}_3$ , respectively.

### **3.4.5 Carbonaceous Species**

The OC and EC concentrations were analyzed through thermal optical analysis with a DRI Model 2001 (Atmoslytic, Inc., Calabasas, CA, USA) following the Interagency Monitoring Protected Visual Environment (IMPROVE) thermal optical reflectance (TOR) protocol (Liu et al., 2013). Briefly, a punch ( $0.526 \text{ cm}^2$ ) of each quartz filter was heated to  $120 \text{ }^\circ\text{C}$  (OC1),  $250 \text{ }^\circ\text{C}$  (OC2),  $450 \text{ }^\circ\text{C}$  (OC3), and  $550 \text{ }^\circ\text{C}$  (OC4) in a non-oxidizing helium (He) atmosphere, and  $550 \text{ }^\circ\text{C}$  (EC1),  $700 \text{ }^\circ\text{C}$  (EC2) and  $800 \text{ }^\circ\text{C}$  (EC3) in an oxidizing atmosphere with 2% oxygen in a balance of helium. As the temperature increased in the inert helium, some of the OC was pyrolyzed to yield a darkening of the filter deposit. This darkening was monitored by reflectance and transmittance of light at a wavelength of 633 nm. After the addition of oxygen, the original and pyrolyzed black carbon was combusted, and the reflectance increased. The amount of carbon measured when the reflectance achieved its original value is considered pyrolyzed carbon (PC). The IMPROVE protocol defines OC as  $\text{OC1}+\text{OC2}+\text{OC3}+\text{OC4}+\text{PC}$  and EC as  $\text{EC1}+\text{EC2}+\text{EC3}-\text{PC}$ . Total carbon (TC) is the sum of OC and EC. The quality control was performed by routine measurements of the samples prepared with a standard sucrose solution. A method blank was tested every 10 samples and subtracted from the sample concentrations.

### **3.5 NAQPMS Model Description and Setup**

The Nested Air Quality Prediction Modeling System (NAQPMS) was used in this study to simulate the evolution of  $\text{PM}_{2.5}$  during pollution events. NAQPMS is a multi-scale 3-D Euler chemical transport model developed by the Institute of Atmospheric Physics (IAP), Chinese Academy of Science (Wang et al., 2006d). The Weather Research and Forecasting Model (WRF version 3.5) is used as a meteorological driver to NAQPMS. The nested

chemical transport module includes advection and diffusion processes (Byun and Dennis, 1995; Walcek and Aleksic, 1998), and parameterization of dry and wet deposition of pollutants (Wesely, 1989). The Carbon-Bond mechanism Z (CBM-Z) (Zaveri and Peters, 1999), which contains 133 reactions for 53 species, was used to represent the gas phase chemistry in NAQPMS. The composition and phase state of an ammonia-sulfate-nitrate-chloride-sodium-water inorganic aerosol was calculated by the model ISORROPIA 1.7 (Nenes et al., 1998); and the secondary organic aerosols (SOA) are currently predicted based on a two-product yield scheme (Odum et al., 1997). The detailed description can be found in previous work (Li et al., 2008). The modeling domains consisted of a 27-km horizontal grid covering the East Asia and a 9-km nested grid over eastern China (Fig. 3-6). The vertical structure of the model consisted of 20 layers from the surface to 20 km with the lowest ten layers below two km. The lateral and upper boundary conditions are taken from a global chemical transport model (MOZART-V2.4) with  $2.8^\circ$  resolution. The anthropogenic emission inventory was obtained from the bottom-up Regional Emission inventory in Asia (REAS2.1) data with  $0.25^\circ \times 0.25^\circ$  resolution (Kurokawa et al., 2013). Biomass burning emissions were developed by Cao et al. (2005) and resampled to a daily time step based on MODIS fire hot spots in 2010 with  $1.0^\circ \times 1.0^\circ$  resolution. Monthly biogenic emissions were generated by MEGAN v2.0, a biogenic emission model with  $0.5^\circ \times 0.5^\circ$  resolution provided by NCAR (National Center for Atmospheric Research) ([http://accent.aero.jussieu.fr/database\\_table\\_inventories.php](http://accent.aero.jussieu.fr/database_table_inventories.php)).

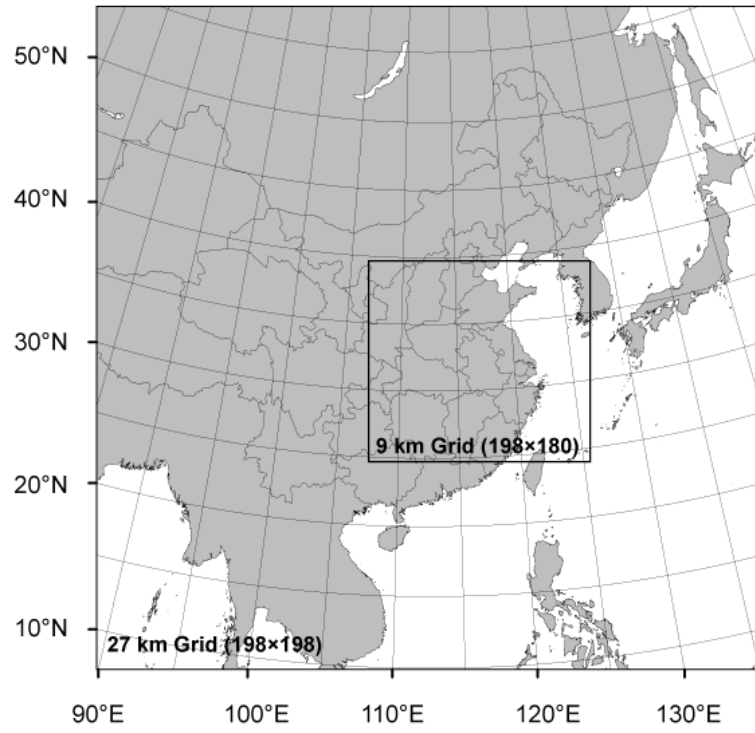


Figure 3-6 The modeling domain.

### 3.6 Enrichment Factor

The enrichment factor can be used to evaluate the potential contribution of crustal and anthropogenic sources for trace metals associated with PM<sub>2.5</sub>. The EFs were calculated using the following equation, in which iron (Fe) was used as a reference element

$$EF = \frac{[C_i/C_{ref}]_{air}}{[C_i/C_{ref}]_{crust}} \dots\dots\dots (Eq. 3-1)$$

where  $C_i$  is the concentration of the metal element considered in the PM<sub>2.5</sub> samples or the crust and  $C_{ref}$  is the concentration of reference element in the PM<sub>2.5</sub> samples or the crust. The elemental concentrations of the crust reference used in the calculation were given by Hans Wedepohl (1995). Generally, EF value close to unity is taken as an indication that a trace element in an aerosol may have a crustal source, while EF value greater than 10 is considered to indicate a significant contribution from non-crustal source (Chen et al., 2008; Waheed et al., 2011).

### 3.7 Meteorological Information

The meteorological parameters including wind speed, wind direction, temperature, precipitation and humidity during the sampling period were obtained from ENVF (Environmental Central Facility) Atmospheric & Environmental Real-time Database (<http://envf.ust.hk/>) and the local statistical yearbook. Since there are no standard meteorological stations at the sampling sites in this study, the meteorological parameters from the standard meteorological station which is close to the sampling site were used. It roughly supposes that the sampling site and its nearby meteorological station had similar meteorological conditions during the study period.

### 3.8 Back Trajectory Analysis

To investigate the possible effects of long-range transportation of trace metals, air mass backward trajectories were calculated using the HYSPLIT model (HYbrid Single-Particle

Lagrangian Integrated Trajectory, Version 4.9), a comprehensive modelling system developed by the National Oceanic and Atmospheric Administration (NOAA) Air Resource Laboratory (<http://www.arl.noaa.gov/HYSPLIT.php>) (Draxler and Rolph, 2003). The FNL archive meteorological datasets from the National Weather Service’s National Centers for Environmental Prediction (NCEP) were used to compute the trajectories. 48-hours air mass backward trajectories were calculated at 6-hour-intervals for sampling days at an elevation of 500 m AGL (above ground level) using the HYSPLIT model. All the air mass backward trajectories were classified into several types by the cluster analysis based on the non-hierarchical clustering algorithm (Dorling et al., 1992).

### 3.9 Potential Source Contribution Function

The Potential Sources Contribution Function (PSCF) model is similar to the framework described by Ashbaugh et al. (1985). The conditional probability of PSCF model is that an air parcel with pollutant concentration higher than a given criterion value arrives at a receptor location after passing through an appointed geographical area. The movement of an air parcel during sampling periods is described using segment endpoints of coordinates in terms of latitude and longitude (Zhang et al., 2014). All the hourly endpoints in the back trajectories generated by the HYSPLIT 4.9 were classified into 1 °latitude by 1 °longitude grid cells to avoid uncertainties in the calculations. The PSCF value for the *ij*-th cell was defined as

$$PSCF_{(i,j)} = m_{(i,j)} / n_{(i,j)} \dots \dots \dots (Eq. 3-2)$$

where  $m_{(i,j)}$  is the number of endpoints corresponding to measured pollutant concentrations higher than a given criterion value, which is set to the mean concentration of each pollutant during the sampling period.  $n_{(i,j)}$  is the total number of endpoints falling in the grid cell. All the values were plotted using mapping software (ArcMap 10.2). Only a given cell including more than 10 total hourly points was plotted.

### 3.10 Health Risk Assessment of Airborne Trace Metals

Generally, human exposure of trace metals in the atmosphere can occur via three pathways: (1) direct inhalation through mouth and nose; (2) ingestion of the deposition of airborne trace metals; and (3) dermal absorption of airborne trace metals adhered to exposed skin. Among the three pathways, inhalation is the most important pathway for human exposure of airborne trace metals (Hu et al., 2012). In this study, the exposure concentration ( $EC_{inh}$ ) was estimated to assess the risks posed by trace metals in  $PM_{2.5}$  by inhalation.  $EC_{inh}$  was estimated by the following equation

$$EC_{inh} = C \times (ET \times EF \times ED) / ATn \quad \text{.....(Eq. 3-3)}$$

where C is bioaccessible concentrations ( $ng\ m^{-3}$ ) of trace metals in  $PM_{2.5}$ ; ET is exposure time (hours/day); EF is exposure frequency ( $EF = 180\ days\ year^{-1}$ ); ED is exposure duration, 6 years for children and 24 years for adults; ATn is average time ( $ATn = ED \times 365\ days\ year^{-1} \times 24\ hours\ day^{-1}$  for non-carcinogens,  $ATn = 70\ years \times 365\ days\ year^{-1} \times 24\ hours\ day^{-1}$  for carcinogens) (US EPA., 2009). Both carcinogenic and non-carcinogenic risks posed by airborne trace metals were quantified in this study. The non- carcinogenic risks (CR) were assessed using the hazard quotient (HQ) (Eq. 3-4). The carcinogenic risks were calculated by Equation 3-5.

$$HQ = EC_{inh} / (RfCi \times 1000\ \mu g\ mg^{-1}) \quad \text{.....(Eq. 3-4)}$$

$$CR = IUR \times EC_{inh} \quad \text{.....(Eq. 3-5)}$$

where RfCi is inhalation reference concentrations ( $mg\ m^{-3}$ ); IUR is inhalation unit risk ( $(\mu g\ m^{-3})^{-1}$ ).

According to the classifications by International Agency for Research on Cancer (IARC) , arsenic (As) and inorganic arsenic compounds, nickel (Ni) compounds, chromium (Cr VI) compounds are Group 1 carcinogenic elements to humans, lead (Pb) inorganic compounds

are Group 2A (probably carcinogenic to humans), vanadium (V) is Groups 2B (possibly carcinogenic to humans), and manganese (Mn) and zinc (Zn) are not found in the list of classifications (WHO, 2015). The values of RfC<sub>i</sub> and IUR for these metal elements can be found from US EPA website (<http://www.epa.gov/region9/superfund/prg/index.html>).

### **3.11 Statistical Analysis**

Statistical analysis was performed using SPSS 16.0 for Windows. All the datasets in this study were statistical analyzed. The student's t test was used to determine whether there was a significant difference in concentrations of PM<sub>2.5</sub> and associated chemical components among different sampling period. Pearson correlation and linear regression were used to identify the relationship.

## **Chapter 4 - Concentrations and Chemical Compositions of PM<sub>2.5</sub> in the Pearl River Delta, the Yangtze River Delta and North China**

In this chapter, investigations of the concentrations and chemical compositions of PM<sub>2.5</sub> were conducted in three representative regions of China: the Pearl River Delta (PRD) including an urban site (Guangzhou) and two rural sites (Heshan and Hok Tsui), the Yangtze River Delta (YRD) including three urban sites (Shanghai, Nanjing and Hangzhou) and one rural site (Ningbo), and North China including one urban site (Beijing) and a background site (Mount Changbai). The previous works of PM<sub>2.5</sub> in the target regions and other areas in the world were compared with the results in this study.

### **4.1 Data Validation-Sum of Chemical Species versus PM<sub>2.5</sub> Mass**

The sum of the individual chemical concentrations determined in this study for PM<sub>2.5</sub> samples should be less than or equal to the corresponding mass concentrations obtained from gravimetric measurements. The chemical species include the measured trace metals, OC and EC that were quantified on quartz microfiber filters from GZ, SH and BJ. The sum of chemical species was plotted against the measured PM<sub>2.5</sub> mass on quartz microfiber filters from GZ, SH and BJ in Fig. 4.1. Linear regression analysis results showed that good correlations ( $R^2=0.68-0.90$ ) were found between the sum of measured species and PM<sub>2.5</sub> mass for the three sampling sites.

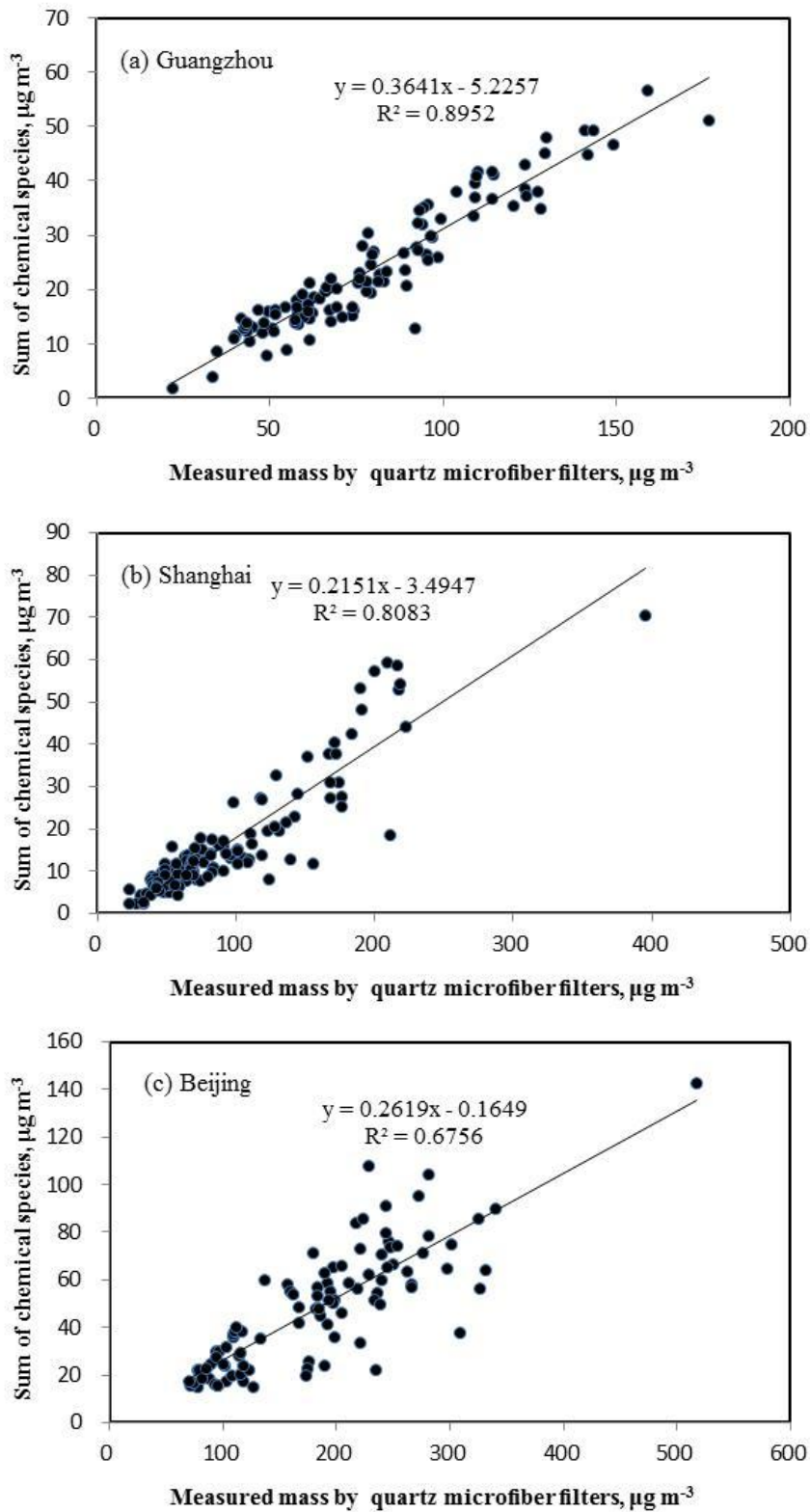


Figure 4-1. Scatter plots of sum of measured chemical species versus measured mass on quartz microfiber filters for  $\text{PM}_{2.5}$  samples collected at (a) Guangzhou, (b) Shanghai and (c) Beijing.

## 4.2 An Overview of PM<sub>2.5</sub> Concentrations

Table 4-1 summarizes the annual mean concentrations and standard deviations of PM<sub>2.5</sub> in the three regions. In the PRD region, PM<sub>2.5</sub> concentrations in Guangzhou (GZ), Heshan (HS) and Hok Tsui (HT) were  $81.9 \pm 30.9$ ,  $86.1 \pm 34.8$  and  $40.1 \pm 18.1 \mu\text{g m}^{-3}$ , respectively. The concentrations of PM<sub>2.5</sub> in GZ and HS far exceeded the Chinese National Ambient Air Quality Standard (NAAQS) Grade II (annual average of  $35 \mu\text{g m}^{-3}$ ), suggesting high pollution of PM<sub>2.5</sub> in GZ and HS. PM<sub>2.5</sub> concentrations in this study were comparable to that in previous studies in the PRD region, such as in Guangzhou ( $106 \pm 71.4 \mu\text{g m}^{-3}$  in the winter of 2001 and  $78.1 \pm 29.7 \mu\text{g m}^{-3}$  in the summer of 2002), Hok Tsui in 2000-2001 ( $32.8 \pm 15.1 \mu\text{g m}^{-3}$  in the winter of 2000 and  $21.8 \pm 10.7 \mu\text{g m}^{-3}$  in the spring of 2001) (Louie et al., 2005) and in 2001-2002 ( $41.3 \pm 20.0 \mu\text{g m}^{-3}$  in the winter of 2001 and  $15.8 \pm 2.4 \mu\text{g m}^{-3}$  in the summer of 2002) (Cao et al., 2003), and Heshan in November 2010 ( $92.02 \pm 43.17 \mu\text{g m}^{-3}$ ) (Ding et al., 2012).

In the YRD region, PM<sub>2.5</sub> concentrations in Shanghai (SH), Nanjing (NJ), Hangzhou (HZ) and Ningbo (NB) were  $94.6 \pm 55.9$ ,  $97.8 \pm 40.5$ ,  $134 \pm 54.3$  and  $94.0 \pm 57.6 \mu\text{g m}^{-3}$ , respectively, which were 9 to 13 times more than the World Health Organization (WHO) standard of  $10 \mu\text{g m}^{-3}$  and 2 to 3 times higher than the NAAQS Grade II standard. In comparison with previous studies in the YRD region, such as  $103 \mu\text{g m}^{-3}$  in Shanghai (annual mean, 2009-2010) (Wang et al., 2013),  $106 \mu\text{g m}^{-3}$  in Nanjing (annual mean, 2011-2012) (Shen et al., 2014),  $86 \mu\text{g m}^{-3}$  in Hangzhou (the three-year average of 2006-2008) (Hong et al., 2013) and  $46 \pm 38 \mu\text{g m}^{-3}$  in Ningbo (annual mean, 2009-2010) (Liu et al., 2013), the concentrations of PM<sub>2.5</sub> in this study showed an increasing trend in HZ and NB, indicating that PM<sub>2.5</sub> pollution in the YRD region became more serious during the sampling period.

The annual PM<sub>2.5</sub> concentration in Beijing (BJ) was  $182 \pm 78.8 \mu\text{g m}^{-3}$ , and approximately 5 times higher than the NAAQS Grade II standard. In comparison with some previous studies in BJ, PM<sub>2.5</sub> concentrations in the present study were higher than that of  $154 \mu\text{g m}^{-3}$  in

2001-2003 (Zhao et al., 2013a) and  $123 \mu\text{g m}^{-3}$  in 2009-2010 (Wang et al., 2005). In Mount Changbai (CBS), annual  $\text{PM}_{2.5}$  concentration was  $34.2 \pm 16.0 \mu\text{g m}^{-3}$ , which was similar to the NAAQS Grade II standard.  $\text{PM}_{2.5}$  concentrations in CBS were lower than that obtained in other background sites in China, such as Jinsha ( $48.7 \pm 26.9 \mu\text{g m}^{-3}$ ) (Zhang et al., 2014), Lin'an ( $58.2 \pm 50.8 \mu\text{g m}^{-3}$ ) (Meng et al., 2012) and Mt. Heng ( $40.7 \pm 30.9 \mu\text{g m}^{-3}$ ) (Zhou et al., 2012), but higher than that in UK ( $8.5 \mu\text{g m}^{-3}$ ) (Heal et al., 2005) and a central Mediterranean coastal site ( $13.9 \mu\text{g m}^{-3}$ ) (Glavas et al., 2008).

As shown in Fig. 4-2, the annual average concentrations and standard deviations of  $\text{PM}_{2.5}$  in the urban/rural/remote sites of the PRD, the YRD and North China were compared. A decreasing trend of  $\text{PM}_{2.5}$  concentrations was observed from urban sites to rural/remote sites, with a decreasing order of  $\text{BJ} > \text{HZ} > \text{NJ} \approx \text{SH} > \text{GZ} > \text{NB} > \text{HS} > \text{HT} > \text{CBS}$ . By comparison,  $\text{PM}_{2.5}$  pollution was more serious in BJ with approximately 2 times greater than that in GZ, SH, HZ and NJ. The rural sites of HS and NB showed similar  $\text{PM}_{2.5}$  concentration to the urban sites in the PRD and YRD regions, respectively. The remote sites of HT and CBS exhibited comparable concentration of NAAQS Grade II standard for  $\text{PM}_{2.5}$ , due to the less anthropogenic pollutions around the sampling sites.  $\text{PM}_{2.5}$  concentrations in the urban sites far exceed the WHO standard and the NAAQS Grade II standard, and were much higher than that in other urban sites in the world (Abu-Allaban et al., 2007; Kendall et al., 2011; Choi et al., 2012; Samara et al., 2014).

Table 4-1 The annual mean concentrations of PM<sub>2.5</sub> (μg m<sup>-3</sup>) in the nine sampling sites.

	Location	PM <sub>2.5</sub> (μg m <sup>-3</sup> )	Number of samples
The PRD	Guangzhou (Urban)	81.9 ± 30.9	136
	Heshan (Rural)	86.1 ± 34.8	61
	Hok Tsui (Coastal rural)	40.1 ± 18.1	18
The YRD	Shanghai (Urban)	94.6 ± 55.9	143
	Nanjing (Urban)	97.8 ± 40.5	119
	Hangzhou (Urban)	134 ± 54.3	45
	Ningbo (Rural)	94.0 ± 57.6	44
North China	Beijing (Urban)	182 ± 78.8	101
	Mount Changbai (Remote)	34.2 ± 16.0	42

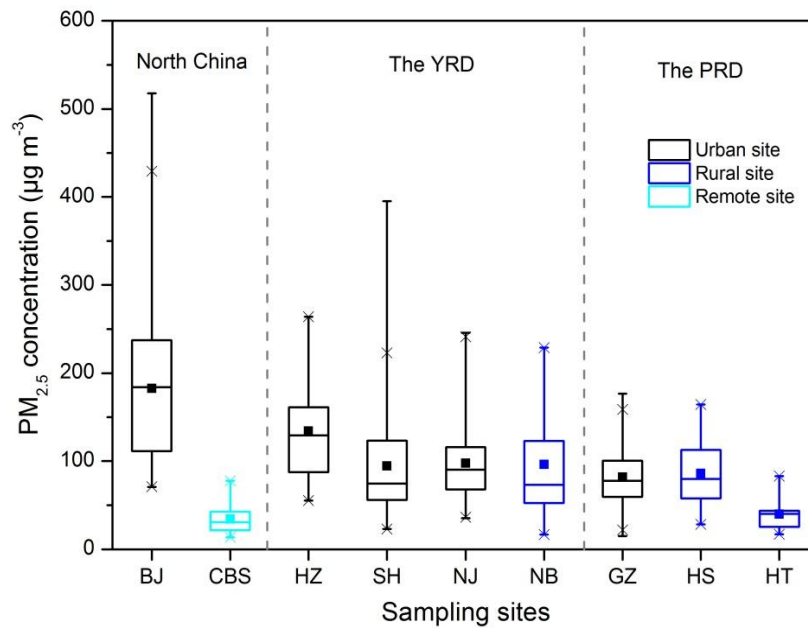


Figure 4-2 The annual averages of PM<sub>2.5</sub> concentrations in the nine sampling sites.

### 4.3 Air Quality in Guangzhou, Shanghai, Nanjing and Beijing

The frequency distributions of PM<sub>2.5</sub> concentrations in GZ, SH, NJ and BJ during the one-month high frequency sampling period in each season (Fig. 4-3) were displayed to evaluate the air quality grade in the four cities, according to Chinese National Ambient Air Quality Standards (NAAQS). The dominant air quality grade in GZ (Fig. 4-3a) was light pollution in autumn (53%) and winter (48%), and fine in spring (47%) and summer (74%). During the winter time in GZ, the daily concentrations for more than 80% of PM<sub>2.5</sub> samples exceeded the NAAQS standard II (daily average limit of 75  $\mu\text{g m}^{-3}$ ), and 6.5% of the samples were severe polluted (daily average PM<sub>2.5</sub>: 150-250  $\mu\text{g m}^{-3}$ ). The data clearly showed that air quality in GZ was fine in spring and summer, light pollution in autumn, and high pollution in winter.

As illustrated in Fig. 4-3b, the air quality grade in SH was dominant in fine (75%), severe pollution (38%), light pollution (55%) and good (68%) in autumn, winter, spring and summer, respectively. In NJ, the air quality grade was light pollution in autumn (48%), winter (36%) and spring (68%), and fine in summer (88%) (Fig. 4-3c). In winter, the daily concentrations for 69% and 100% of PM<sub>2.5</sub> samples in SH and NJ exceeded the NAAQS standard II, respectively, and 38% and 32% of PM<sub>2.5</sub> samples in SH and NJ were severely polluted (daily average PM<sub>2.5</sub>: 150-250  $\mu\text{g m}^{-3}$ ), respectively. The data showed the relatively good air quality in summer, light pollution of PM<sub>2.5</sub> in spring and autumn, and high pollution of PM<sub>2.5</sub> in winter in SH and NJ. Compared to NJ, the air quality was better in SH, but the occurrences of heavy pollution (PM<sub>2.5</sub> > 150  $\mu\text{g m}^{-3}$ ) were more frequent in SH.

In BJ, the dominant air quality was found to be severe pollution in autumn (40.9%), winter (60%) and spring (73.4%), and light pollution in summer (57.2%) (Fig. 4-3d). 22.7%, 25% and 20% of the PM<sub>2.5</sub> samples in BJ were serious polluted (daily average PM<sub>2.5</sub>: 250-500  $\mu\text{g m}^{-3}$ ) in autumn, winter and spring, respectively. Even in summer, the daily concentrations for about 90% of the samples exceeded the NAAQS standard II. The results showed that PM<sub>2.5</sub>

pollution is extremely serious in BJ, followed by NJ, SH and GZ.

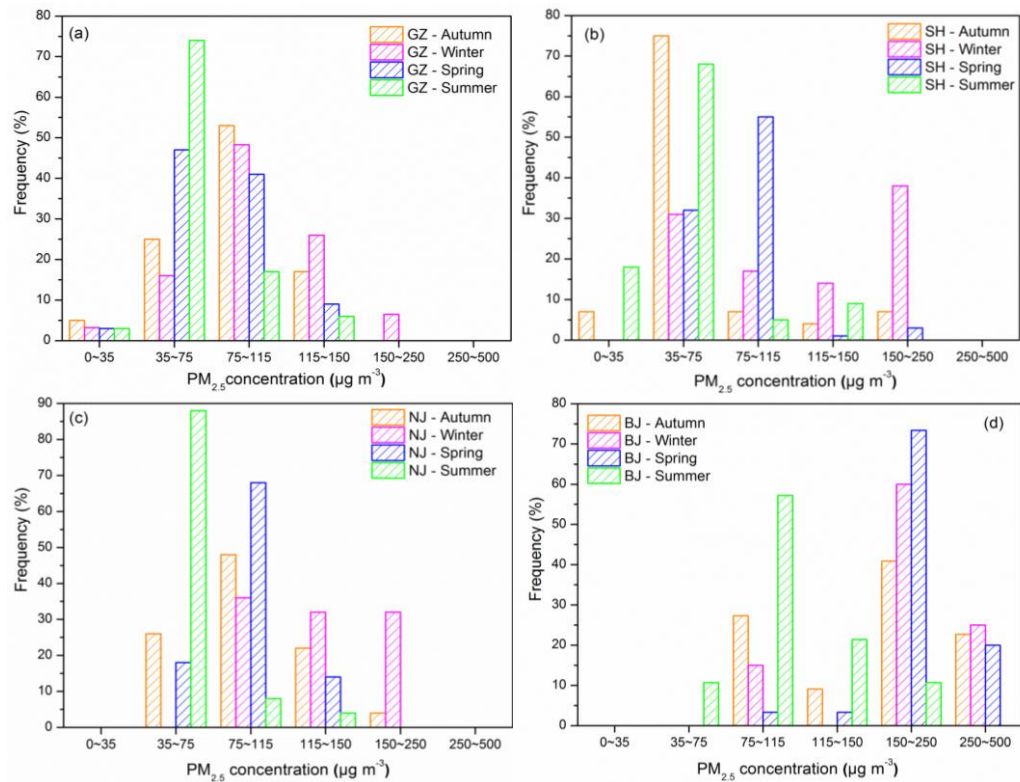


Figure 4-3 The distributions of air quality grades ( $PM_{2.5}$  concentration,  $\mu g m^{-3}$ ) in frequencies in (a) Guangzhou; (b) Shanghai; (c) Nanjing; and (d) Beijing in the autumn, winter, spring and summer (0-35  $\mu g m^{-3}$ : excellent; 35-75  $\mu g m^{-3}$ : fine; 75-115  $\mu g m^{-3}$ : light pollution; 115-150  $\mu g m^{-3}$ : medium pollution; 150-250  $\mu g m^{-3}$ : severe pollution; 250-500  $\mu g m^{-3}$ : serious pollution).

#### 4.4 Concentrations of Airborne Trace Metals in $PM_{2.5}$

The concentrations of airborne trace metals in the three regions are listed in Table 4-2. In the nine sites, the major abundant elements are the crustal elements (*i.e.*, Al, Ca, Fe, K and Mg). The annual mean concentrations of trace elements were generally in the order of  $Zn > Pb > Mn > Cu > Cr > V > Ni$ . Similar to  $PM_{2.5}$  pattern, airborne trace metals concentrations in the three regions generally showed a decreasing trend in the order of urban > rural > remote site. In the urban sites, the concentrations of airborne trace metals were highest in BJ, followed by HZ, and comparable among NJ, SH and GZ. In the rural sites, the crustal elements showed

lower concentrations in HS compared to NB, but the concentrations of Cu, Pb and Zn in HS were much higher than that in NB. High concentrations of airborne trace metals in HS could be attributed to the anthropogenic sources from the PRD region because HS is located at the downwind area of the PRD region. Apparently higher concentrations of airborne trace metals were detected in the rural site from HT compared with the remote site from CBS. At present, there are no regulations for trace metal concentrations in  $PM_{2.5}$ . However, the concentrations of Ni in some samples in SH and BJ exceeded the WHO threshold value of Ni ( $20 \text{ ng m}^{-3}$ ) in  $PM_{10}$  (WHO 2000). As shown in Fig. 4-4, the mass ratios of airborne trace metals to  $PM_{2.5}$  mass varied among the three regions. The crustal elements accounted for 11.8% of the  $PM_{2.5}$  mass in BJ, while they only accounted for 3-5% of the  $PM_{2.5}$  mass in the other sites. In regards to trace elements, similar contributions to  $PM_{2.5}$  mass (0.41-0.68%) were found in the urban and rural sites, and the lowest contributions were found in CBS.

In Guangzhou, the concentrations of Cu, Pb, Zn, V and Ni were lower than those obtained in 2005-2006, while the concentrations of Al, Fe, Cr and Mn were higher (Lee, 2007), reflecting the change in the distribution of source contributions. Compared with the previous studies in the YRD region, such as Shanghai (annual mean, 2009-2010) (Chen et al., 2008), Nanjing (average value from April to September 2010) (Hu et al., 2012) and Hangzhou (annual mean, 2006) (Bao et al., 2010), the concentrations for Zn at SH, Cu and Zn at NJ and HZ showed a decreasing trend, probably attributed to the effectively control in non-ferrous metal industries in the YRD region. However,, trace metal concentrations in the YRD region were still higher than those in some other countries, such as Southern California (Na and Cocker III, 2009) and Turkey (Kendall et al., 2011). In comparison with past monitoring data of airborne metals in BJ (Yang et al., 2005b; Okuda et al., 2008; Zhao et al., 2013a), the results in this study displayed much higher concentrations for crustal elements and similar concentrations for trace elements, suggesting that the contribution of crustal sources to  $PM_{2.5}$  increased in BJ.

Table 4-2 The annual average concentrations (annual  $\pm$ S.D.) of airborne trace metals and the mass ratios of crustal elements (Al, Fe, Ca, K and Mg), trace elements (Cr, Cu, Pb, Mn, Zn, V and Ni) and total metals to PM<sub>2.5</sub> mass (%) at the sampling sites from the PRD and YRD regions, and North China.

	The PRD region			The YRD region				North China	
	Guangzhou	Heshan	Hok Tsui	Shanghai	Nanjing	Hangzhou	Ningbo	Beijing	Mount Changbai
	Urban (n=136)	Rural	Coastal rural	Urban	Urban	Urban (n=45)	Rural (n=44)	Urban	Remote (n=42)
Al ( $\mu\text{g m}^{-3}$ )	0.91 $\pm$ 0.69	0.93 $\pm$ 0.56	0.58 $\pm$ 0.59	0.92 $\pm$ 0.85	0.71 $\pm$ 0.45	1.37 $\pm$ 1.06	1.17 $\pm$ 0.95	4.22 $\pm$ 4.23	0.38 $\pm$ 0.35
Fe ( $\mu\text{g m}^{-3}$ )	0.74 $\pm$ 0.37	0.68 $\pm$ 0.34	0.22 $\pm$ 0.35	1.34 $\pm$ 1.07	0.94 $\pm$ 0.65	1.72 $\pm$ 1.14	1.16 $\pm$ 1.08	4.40 $\pm$ 2.79	0.36 $\pm$ 0.32
Ca ( $\mu\text{g m}^{-3}$ )	0.97 $\pm$ 0.60	0.85 $\pm$ 0.62	0.21 $\pm$ 0.34	1.93 $\pm$ 1.77	1.52 $\pm$ 1.27	3.02 $\pm$ 2.51	1.19 $\pm$ 1.72	8.42 $\pm$ 5.1	0.40 $\pm$ 0.33
K ( $\mu\text{g m}^{-3}$ )	0.88 $\pm$ 0.56	0.78 $\pm$ 0.47	0.45 $\pm$ 0.65	0.81 $\pm$ 0.78	1.03 $\pm$ 0.83	1.54 $\pm$ 1.29	0.62 $\pm$ 0.63	2.35 $\pm$ 1.64	0.30 $\pm$ 0.21
Mg ( $\mu\text{g m}^{-3}$ )	0.15 $\pm$ 0.11	0.13 $\pm$ 0.09	0.23 $\pm$ 0.43	0.30 $\pm$ 0.28	0.21 $\pm$ 0.18	0.45 $\pm$ 0.39	0.22 $\pm$ 0.24	2.07 $\pm$ 1.28	0.11 $\pm$ 0.10
Cr (ng m <sup>-3</sup> )	13.2 $\pm$ 12.6	7.91 $\pm$ 4.54	6.95 $\pm$ 8.85	16.9 $\pm$ 12.1	13.2 $\pm$ 9.51	17.9 $\pm$ 12.7	14.6 $\pm$ 10.5	17.2 $\pm$ 21.3	1.81 $\pm$ 0.81
Cu (ng m <sup>-3</sup> )	43.8 $\pm$ 40.0	28.7 $\pm$ 20.4	31.0 $\pm$ 22.7	24.2 $\pm$ 21.8	24.7 $\pm$ 15.5	38.5 $\pm$ 27.9	16.2 $\pm$ 13.8	58.6 $\pm$ 40.0	4.26 $\pm$ 3.10
Mn (ng m <sup>-3</sup> )	30.8 $\pm$ 15.2	117 $\pm$ 122	9.23 $\pm$ 6.45	49.8 $\pm$ 30.3	47.2 $\pm$ 27.8	66.4 $\pm$ 38.3	264 $\pm$ 188	97.8 $\pm$ 66.8	9.35 $\pm$ 6.52
Pb (ng m <sup>-3</sup> )	78.6 $\pm$ 61.7	75.7 $\pm$ 52.6	28.8 $\pm$ 26.4	69.7 $\pm$ 67.9	90.9 $\pm$ 69.4	122 $\pm$ 86.8	56.3 $\pm$ 52.8	189 $\pm$ 168	14.6 $\pm$ 10.6
Zn (ng m <sup>-3</sup> )	229 $\pm$ 129	297 $\pm$ 131	111 $\pm$ 81.9	215 $\pm$ 186	247 $\pm$ 153	495 $\pm$ 401	190 $\pm$ 156	504 $\pm$ 413	35.8 $\pm$ 18.5
V (ng m <sup>-3</sup> )	9.72 $\pm$ 7.56	6.02 $\pm$ 3.57	18.0 $\pm$ 18.5	16.5 $\pm$ 9.1	9.88 $\pm$ 8.6	15.3 $\pm$ 11.7	7.36 $\pm$ 5.72	6.70 $\pm$ 4.77	1.25 $\pm$ 0.69
Ni (ng m <sup>-3</sup> )	5.91 $\pm$ 3.01	4.59 $\pm$ 2.1	11.1 $\pm$ 9.67	14.9 $\pm$ 8.9	9.25 $\pm$ 5.90	10.4 $\pm$ 7.0	8.25 $\pm$ 5.48	16.4 $\pm$ 22.8	1.18 $\pm$ 0.63
Crustal%	4.32 $\pm$ 1.41	3.81 $\pm$ 1.46	4.16 $\pm$ 3.10	5.42 $\pm$ 2.46	4.29 $\pm$ 2.12	5.82 $\pm$ 2.73	4.92 $\pm$ 2.18	11.8 $\pm$ 5.41	4.05 $\pm$ 1.96
Trace%	0.49 $\pm$ 0.18	0.65 $\pm$ 0.22	0.58 $\pm$ 0.31	0.41 $\pm$ 0.13	0.44 $\pm$ 0.17	0.56 $\pm$ 0.28	0.68 $\pm$ 0.36	0.45 $\pm$ 0.22	0.20 $\pm$ 0.09

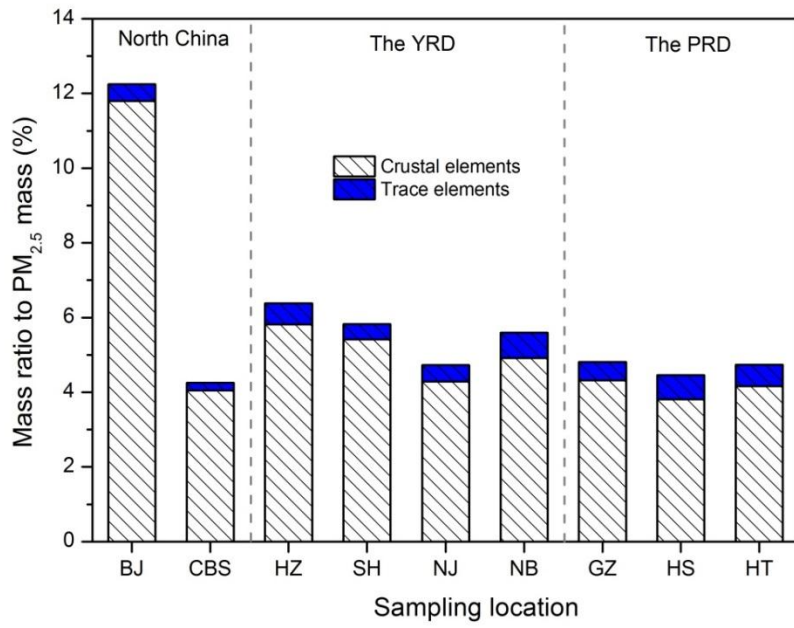


Figure 4-4 The mass ratios of crustal elements and trace elements to PM<sub>2.5</sub> mass in the nine sampling sites.

#### 4.5 Lead Isotopic Compositions in PM<sub>2.5</sub>

The annual average Pb isotopic compositions ( $^{206}\text{Pb}/^{207}\text{Pb}$  and  $^{208}\text{Pb}/^{207}\text{Pb}$  ratios) of PM<sub>2.5</sub> in the sampling sites of the three regions are listed in Table 4-3. In the PRD region, the annual average Pb isotopic compositions ( $^{206}\text{Pb}/^{207}\text{Pb}$  and  $^{208}\text{Pb}/^{207}\text{Pb}$  ratios) of PM<sub>2.5</sub> in GZ ( $1.1675 \pm 0.0040$  and  $2.4491 \pm 0.0066$ ) were found to be slightly higher than those in HS ( $1.1655 \pm 0.0046$  and  $2.4447 \pm 0.0054$ ) and HT ( $1.1662 \pm 0.0030$  and  $2.4462 \pm 0.0065$ ). In GZ, the Pb isotopic ratios of PM<sub>2.5</sub> were similar to the values obtained in 2005-2006 ( $1.1699$  and  $2.4524$ ) (Lee, 2007). Lee et al. (2007) reported that the annual mean ratios of  $^{206}\text{Pb}/^{207}\text{Pb}$  and  $^{208}\text{Pb}/^{207}\text{Pb}$  for TSP samples in HT during the period December 2013 to January 2015 were  $1.161 \pm 0.013$  and  $2.449 \pm 0.015$ , respectively, similar to the result in this study. In the YRD region, the annual average Pb isotopic compositions ( $^{206}\text{Pb}/^{207}\text{Pb}$  and  $^{208}\text{Pb}/^{207}\text{Pb}$  ratios) of PM<sub>2.5</sub> in SH ( $1.1642 \pm 0.0043$  and  $2.4461 \pm 0.0079$ ), NJ ( $1.1672 \pm 0.0037$  and  $2.4496 \pm 0.0073$ ), HZ ( $1.1662 \pm 0.0023$  and  $2.4452 \pm 0.0041$ ) and NB ( $1.1653 \pm 0.0027$  and  $2.4426 \pm 0.0077$ ) showed very slight difference, implying that Pb pollution in the YRD region was more influenced by regional anthropogenic sources rather than local ones (Chen et al., 2008). It was reported that the  $^{206}\text{Pb}/^{207}\text{Pb}$  ratio was increased in SH after phasing out leaded gasoline (Chen et al., 2005; Cheng and Hu, 2010). Compared with their results, the  $^{206}\text{Pb}/^{207}\text{Pb}$  ratios in this study showed an increasing trend in SH, indicating the continued increase of Pb pollution contributed from stationary sources. In North China, the annual average ratio of  $^{206}\text{Pb}/^{207}\text{Pb}$  in BJ ( $1.1593 \pm 0.0068$ ) was lower than that measured in CBS ( $1.1625 \pm 0.0092$ ), while the annual mean ratio of  $^{208}\text{Pb}/^{207}\text{Pb}$  in BJ ( $2.4476 \pm 0.0155$ ) was higher than that in CBS ( $2.4383 \pm 0.0080$ ). In this study, Pb isotope compositions in BJ and CBS were distinctly different from the values observed in the PRD and YRD regions. The differences of Pb isotopic ratios of PM<sub>2.5</sub> among the three regions were related to the mixing of various natural and anthropogenic sources of Pb in the atmosphere, which will be discussed in section 5.2.2 of chapter 5.

Table 4-3 The annual and seasonal averages of Pb isotope compositions (mean  $\pm$  S.D.) in PM<sub>2.5</sub> in the sampling sites from the PRD, the YRD and North China.

Region	Location	$^{206}\text{Pb}/^{207}\text{Pb}$	$^{208}\text{Pb}/^{207}\text{Pb}$
The	Guangzhou (Urban, n=38)	1.1675 $\pm$ 0.0040	2.4491 $\pm$ 0.0066
PRD	Heshan (Rural, n=23)	1.1655 $\pm$ 0.0046	2.4447 $\pm$ 0.0054
	Hok Tsui (Costal rural, n=16)	1.1662 $\pm$ 0.0030	2.4462 $\pm$ 0.0065
The	Shanghai (Urban, n=58)	1.1642 $\pm$ 0.0043	2.4461 $\pm$ 0.0079
YRD	Nanjing (Urban, n=43)	1.1672 $\pm$ 0.0037	2.4496 $\pm$ 0.0073
	Hangzhou (Urban, n=27)	1.1662 $\pm$ 0.0023	2.4452 $\pm$ 0.0041
	Ningbo (Rural, n=23)	1.1653 $\pm$ 0.0027	2.4426 $\pm$ 0.0077
North	Beijing (Urban, n=43)	1.1593 $\pm$ 0.0068	2.4476 $\pm$ 0.0155
China	Mount Changbai (Remote, n=21)	1.1625 $\pm$ 0.0092	2.4383 $\pm$ 0.0080

#### 4.6 Concentrations of Carbonaceous Species in PM<sub>2.5</sub> from Guangzhou, Shanghai and Beijing

Organic carbon (OC) and elemental carbon (EC) were analyzed for the PM<sub>2.5</sub> samples collected in Guangzhou, Shanghai and Beijing during the high frequency sampling periods. As shown in Table 4-4, the annual average concentrations of OC were ranked in the order of BJ ( $20.7 \pm 13.9 \mu\text{g m}^{-3}$ ) > GZ ( $17.3 \pm 9.51 \mu\text{g m}^{-3}$ ) > SH ( $9.89 \pm 8.89 \mu\text{g m}^{-3}$ ). The annual mean concentrations of EC in GZ and BJ were 1.77 and 1.66 times higher than that in SH, respectively. OC and EC were the important components of PM<sub>2.5</sub> in the three cities and contributed 9.85-20.7% and 1.63-2.87% to the total PM<sub>2.5</sub> mass, respectively. The contributions of OC and EC to PM<sub>2.5</sub> mass were more significant in GZ, with fractions of  $20.4 \pm 5.14\%$  and  $3.84 \pm 1.95\%$ , respectively. Although the concentrations of OC and EC in SH were lower than those in BJ, the contributions of OC and EC to PM<sub>2.5</sub> mass were similar between the two cities. In Shanghai, the OC and EC concentrations were lower than the values obtained in 1999-2000 ( $14.3$  and  $6.21 \mu\text{g m}^{-3}$ ) (Ye et al., 2003) and in 2005-2006 ( $14.7 \pm 10.1$  and  $2.8 \pm 1.3 \mu\text{g m}^{-3}$ ) (Feng et al., 2009b), but similar to the levels observed in the same sampling location in Fudan University ( $9.9 \pm 8.4$  and  $2.9 \pm 1.6 \mu\text{g m}^{-3}$ ) (Feng et al., 2009b). The OC and EC concentrations in BJ and GZ were comparable to the values obtained in the previous studies (Cao et al., 2004; Yang et al., 2005a).

The concentrations of primary organic carbon (POC) and secondary organic carbon (SOC) were estimated by using the EC-tracer method (Castro et al., 1999). The concentrations of POC and SOC can be obtained by

$$\text{SOC} = \text{TOC} - \text{POC} \dots\dots\dots(\text{Eq. 4-1})$$

$$\text{POC} = \text{EC} \times (\text{OC/EC})_{\text{pri}} \dots\dots\dots(\text{Eq. 4-2})$$

where SOC is the secondary OC, TOC is the total OC, POC and  $(\text{OC/EC})_{\text{pri}}$  denotes the primary OC and primary OC/EC ratio, respectively.

This method is simple and widely used to estimate the POC and SOC concentrations (Zhou

et al., 2012; Wang et al., 2012b), as it only require the observed concentrations of OC and EC. However, there are also some limitations with this approach. The selection of the primary OC/EC ratio in this method is crucial, which is influenced by the meteorology, diurnal and seasonal fluctuations in emissions. It is therefore important to evaluate whether the adopted  $(OC/EC)_{pri}$  ratios are reasonable in consideration of the main primary combustion sources affecting a sampling site. Some researchers have used the minimum or the lowest 10-20% OC/EC ratios without significant influence from rain and cloud as the primary OC/EC ratio (Zhou et al., 2012). In this study, high frequency data of OC and EC during each season were obtained in GZ, SH and BJ. The minimum OC/EC ratio without significant influence from rain and cloud was selected to be the primary OC/EC ratio during each season at each site. The values of the  $(OC/EC)_{pri}$  were 2.35 (5.32, 2.76 and 1.81), 3.35 (3.29, 2.95 and 2.04) and 1.77 (4.78, 4.19 and 4.85) during autumn (winter, spring and summer) in GZ, SH and BJ, respectively. The calculated annual mean concentrations of SOC were  $8.53 \pm 6.52$ ,  $4.84 \pm 5.67$  and  $11.0 \pm 11.1 \mu\text{g m}^{-3}$  in GZ, SH and BJ, respectively, and contributed  $46.7 \pm 23.2\%$ ,  $49.6 \pm 19.5\%$  and  $49.6 \pm 21.5\%$  of the total OC, respectively. The differences in the contributions of SOC to total OC among the three cities are due to various atmospheric oxidation abilities and the amounts of the gaseous organic pollutants in the atmosphere.

Table 4-4 Statistical description of the concentrations ( $\mu\text{g m}^{-3}$ ) and the mass ratios (%) of carbonaceous species, and the ratio of OC/EC and POC/SOC in Guangzhou, Shanghai and Beijing.

	Guangzhou (n=105)	Shanghai (n=116)	Beijing (n=101)
OC	$17.3 \pm 9.51$	$9.89 \pm 8.89$	$20.7 \pm 13.9$
EC	$2.87 \pm 1.29$	$1.63 \pm 1.53$	$2.71 \pm 2.28$
SOC	$8.53 \pm 6.52$	$4.84 \pm 5.67$	$11.0 \pm 11.1$
OC%	$20.4 \pm 5.14\%$	$9.58 \pm 3.40\%$	$11.1 \pm 3.53\%$
EC%	$3.84 \pm 1.95\%$	$1.62 \pm 0.77\%$	$1.47 \pm 0.92\%$
OC/EC	$6.69 \pm 3.50$	$6.69 \pm 2.64$	$8.65 \pm 3.09$
SOC/OC%	$46.7 \pm 23.2\%$	$49.6 \pm 19.5\%$	$49.6 \pm 21.5\%$

#### 4.7 Concentrations of Water-soluble Ions in PM<sub>2.5</sub> from Shanghai and Nanjing

The concentrations of water-soluble ions ( $\text{NO}_3^-$ ,  $\text{Cl}^-$ ,  $\text{SO}_4^{2-}$ ,  $\text{K}^+$  and  $\text{NH}_4^+$ ) in PM<sub>2.5</sub> from SH and NJ are summarized in Table 4-5. The concentrations of water-soluble ions were comparable between SH and NJ. Secondary ions,  $\text{NO}_3^-$ ,  $\text{SO}_4^{2-}$  and  $\text{NH}_4^+$ , were the dominant water-soluble species. The annual mean concentrations of  $\text{NO}_3^-$ ,  $\text{SO}_4^{2-}$  and  $\text{NH}_4^+$  ranged from 0.39 to 120  $\mu\text{g m}^{-3}$ , 0.87 to 54.5  $\mu\text{g m}^{-3}$  and 0.15 to 40.4  $\mu\text{g m}^{-3}$  in SH, respectively, and ranged from 0.39 to 120  $\mu\text{g m}^{-3}$ , 0.87 to 54.5  $\mu\text{g m}^{-3}$  and 0.15 to 40.4  $\mu\text{g m}^{-3}$  in NJ, respectively. The sum of  $\text{NO}_3^-$ ,  $\text{SO}_4^{2-}$  and  $\text{NH}_4^+$  constituted  $32.0 \pm 14.7\%$  and  $37.7 \pm 15.8\%$  of the total PM<sub>2.5</sub> mass in SH and NJ, respectively. The annual average concentrations of  $\text{Cl}^-$  and  $\text{K}^+$  were  $2.64 \pm 3.06$  and  $1.28 \pm 1.81$   $\mu\text{g m}^{-3}$  in SH, and  $3.41 \pm 3.48$  and  $1.23 \pm 0.84$   $\mu\text{g m}^{-3}$  in NJ. All the measured water-soluble ions accounted for  $35.1 \pm 15.6\%$  and  $41.2 \pm 17.4\%$  of PM<sub>2.5</sub> mass in SH and NJ, respectively. As shown in Table 4-4, the concentrations of water-soluble ions in this study were close to those in Beijing, but lower than those in Tianjin and Shijiazhuang (Zhao et al., 2013a).

Table 4-5 The annual average concentrations of water-soluble ions ( $\mu\text{g m}^{-3}$ ) and their mass contributions to  $\text{PM}_{2.5}$  mass (%), and the ratio of  $\text{NO}_3^-/\text{SO}_4^{2-}$  in Shanghai and Nanjing.

	Shanghai (n=69)	Nanjing (n=63)	Beijing <sup>a</sup>	Tianjin <sup>a</sup>	Shijiazhuang <sup>a</sup>
$\text{Cl}^-$	$2.64 \pm 3.06$	$3.41 \pm 3.48$	$2.92 \pm 3.46$	$8.14 \pm 6.10$	$8.69 \pm 7.88$
$\text{NO}_3^-$	$18.0 \pm 19.1$	$19.5 \pm 16.7$	$20.5 \pm 18.1$	$18.8 \pm 15.8$	$30.1 \pm 28.3$
$\text{SO}_4^{2-}$	$14.5 \pm 9.61$	$15.7 \pm 9.49$	$19.1 \pm 16.4$	$25.0 \pm 22.6$	$35.6 \pm 23.0$
$\text{K}^+$	$1.28 \pm 1.81$	$1.23 \pm 0.84$	$1.68 \pm 1.29$	$2.08 \pm 1.36$	$3.40 \pm 2.14$
$\text{NH}_4^+$	$8.13 \pm 6.99$	$8.57 \pm 6.43$	$6.37 \pm 3.91$	$7.64 \pm 4.27$	$9.33 \pm 4.47$
$\text{NO}_3^-/\text{SO}_4^{2-}$	$1.05 \pm 0.57$	$1.17 \pm 0.60$	1.07	0.75	0.85
$\text{NO}_3^- \%$	$12.7 \pm 7.71$	$16.1 \pm 10.1$	-	-	-
$\text{SO}_4^{2-} \%$	$12.9 \pm 6.20$	$14.1 \pm 6.06$	-	-	-
$\text{NH}_4^+ \%$	$6.39 \pm 3.54$	$7.51 \pm 3.19$	-	-	-

<sup>a</sup>Zhao et al. (2013a)

## 4.8 Summary

In this study, PM<sub>2.5</sub> pollution was serious in the three regions. The annual mean concentrations of PM<sub>2.5</sub> in the nine sampling sites ranged from 34.2 to 182 µg m<sup>-3</sup>, ranking in the order of BJ > HZ > NJ ≈ SH > NB > GZ ≈ HS > HT > CBS. According to the NAAQS, the air quality is extremely deteriorative in BJ, followed by NJ, SH and GZ. Similar to PM<sub>2.5</sub> pattern, airborne trace metal concentrations in the three regions generally showed a decreasing trend in the order of urban > rural > remote site. The annual mean concentrations of airborne trace metals in the urban sites were highest at BJ, followed by HZ and comparable among NJ, SH and GZ. Crustal elements were the dominant metal species, which accounted for 11.8% of the PM<sub>2.5</sub> mass in BJ, while only accounted for 3-5% of the PM<sub>2.5</sub> mass in the other sites. The sum of trace elements constituted 0.20-0.68% of PM<sub>2.5</sub> mass in the nine sampling sites. The Pb isotopic compositions (<sup>206</sup>Pb/<sup>207</sup>Pb and <sup>208</sup>Pb/<sup>207</sup>Pb ratios) in North China were distinctly different from that observed in the PRD and YRD regions. The annual average concentrations of OC and EC were comparable between GZ (17.3 ± 9.51 and 2.87 ± 1.29 µg m<sup>-3</sup>) and BJ (20.7 ± 13.9 and 2.71 ± 2.28 µg m<sup>-3</sup>), which were about two times higher than those in SH (9.89 ± 8.89 and 1.63 ± 1.53 µg m<sup>-3</sup>). The calculated annual mean concentrations for SOC were 12.1 ± 8.55, 6.56 ± 6.68 and 15.9 ± 12.1 µg m<sup>-3</sup> in GZ, SH and BJ, respectively, and contributed 63.4 ± 21.4%, 65.0 ± 13.5% and 76.7 ± 10.4% of the total OC, respectively. NO<sub>3</sub><sup>-</sup>, SO<sub>4</sub><sup>2-</sup> and NH<sub>4</sub><sup>+</sup> were the dominant water-soluble species, accounting for 32.0 ± 14.7% and 37.7 ± 15.8% to the total PM<sub>2.5</sub> mass in SH and NJ, respectively. By comparison, BJ was heavily polluted by PM<sub>2.5</sub>, airborne trace metals and carbonaceous particles, followed by SH and GZ.

## **Chapter 5 -Temporal-Spatial Variations and Source Appointment of PM<sub>2.5</sub> in the PRD, the YRD and North China**

Based on the one-year simultaneous sampling of PM<sub>2.5</sub> in the PRD, the YRD and North China, this chapter aims to: (1) study the temporal and spatial variations of PM<sub>2.5</sub> in the three regions; (2) identify the sources of PM<sub>2.5</sub>; and (3) analyze the differences in pollution characteristics of PM<sub>2.5</sub> among the three regions by studying the local emissions, meteorological conditions and long-range transport pathways.

### **5.1 Temporal and Spatial Variations of PM<sub>2.5</sub>**

#### **5.1.1 The PRD Region**

The temporal variations of PM<sub>2.5</sub> concentrations in GZ, HS and HT over the sampling period are plotted in Fig. 5-1. In general, the time trends of PM<sub>2.5</sub> concentrations exhibited similar pattern, with high concentrations in autumn and winter and low concentrations in spring and summer. The annual and seasonal averages of PM<sub>2.5</sub> and airborne trace metals in the three sites are summarized in Table 5-1. The concentrations of PM<sub>2.5</sub> and airborne trace metals in HS were comparable to that of GZ. High concentrations of airborne trace metals in HS could be attributed to the anthropogenic sources from the PRD region because HS is located at the downwind area of the PRD region. With the exception of Mg, V and Ni, concentrations of the other trace metals and PM<sub>2.5</sub> in HT were lower than that in GZ and HS. Lower air pollution in HT has also been reported by several studies compared to urban site in Hong Kong and other cities in the PRD region (Louie et al., 2005; Hagler et al., 2007). HT is located at the southeast coast of Hong Kong Island with less anthropogenic activities. Lower concentrations of some trace metals and PM<sub>2.5</sub> in HT could be attributed to the less local emission sources (such as industrial activities and coal burning) (Cao et al., 2004; Hagler et al., 2006). The high concentrations of V and Ni in HT were likely due to the fuel oil combustion from the local shipping activity in Hong Kong, and the input of sea salt from the ocean could be the major reason for the high concentration of Mg in HT.

Seasonally, the concentrations of PM<sub>2.5</sub> and airborne trace metals were both higher in autumn and winter than that in spring and summer. During autumn and winter, the concentrations of PM<sub>2.5</sub> and airborne trace metals in HS were comparable to that in GZ, probably due to the transport of atmospheric pollutants from the PRD region under the prevailed northeast winds. As shown in Fig. 5-2, a clear seasonal trend with higher concentrations in winter and lower concentrations in summer was observed for OC, while no significant seasonal variation was found for EC concentrations. The average concentrations of OC in winter ( $26.2 \pm 9.64 \mu\text{g m}^{-3}$ ) were 2.6 times higher than that in summer ( $10.1 \pm 4.72 \mu\text{g m}^{-3}$ ). Similar seasonal variation was found for SOC, with higher concentration in winter ( $20.8 \mu\text{g m}^{-3}$ ) and lower concentration in summer ( $4.83 \mu\text{g m}^{-3}$ ).

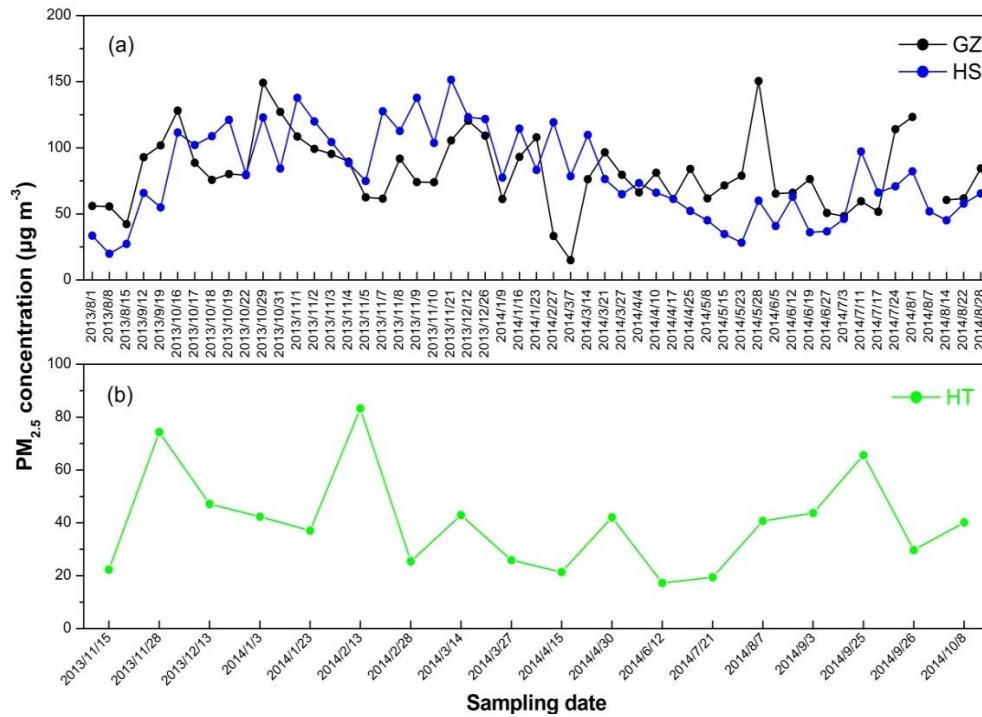


Figure 5-1 Temporal variations of PM<sub>2.5</sub> concentrations (µg m<sup>-3</sup>) over the sampling period in (a) Guangzhou and Heshan and (b) Hok Tsui.

Table 5-1 The annual and seasonal averages of PM<sub>2.5</sub> and airborne trace metal concentrations in PM<sub>2.5</sub> in Guangzhou, Heshan and Hok Tsui.

Locations		µg m <sup>-3</sup>						ng m <sup>-3</sup>						
		PM <sub>2.5</sub>	Al	Ca	Fe	K	Mg	Cr	Cu	Mn	Pb	Zn	V	Ni
Guangzhou	Annual (n=136)	81.9	0.911	0.968	0.743	0.881	0.147	13.2	43.8	30.8	78.6	229	9.70	5.90
	S.D.	30.9	0.694	0.598	0.373	0.558	0.106	12.6	40.0	15.2	61.7	129	7.60	3.00
(Urban)	Autumn (n=36)	87.5	0.831	0.792	0.681	1.13	0.132	17.5	62.9	29.6	101	283	13.9	6.00
	Winter (n=31)	103	1.13	1.27	0.929	1.36	0.207	22.0	59.0	43.1	147	325	7.00	7.00
	Spring (n=34)	77.9	0.972	1.01	0.743	0.623	0.158	9.1	29.7	30.5	45.5	173	11.3	6.70
	Summer (n=35)	61.3	0.743	0.846	0.641	0.454	0.0964	4.6	24.4	21.2	27.4	142	6.70	4.30
Heshan	Annual (n=61)	86.1	0.926	0.848	0.674	0.78	0.127	7.91	28.7	117	75.7	297	6.02	4.59
	S.D.	34.8	0.558	0.621	0.335	0.47	0.0931	4.54	20.4	122	52.6	131	3.57	2.10
(Rural)	Autumn (n=26)	106	1.18	1.13	0.878	1.10	0.161	9.41	41.1	125	104	378	8.14	5.79
	Winter (n=10)	98.2	1.01	1.17	0.692	0.83	0.140	6.51	39.6	60.8	114	300	4.45	3.76
	Spring (n=12)	62.5	0.177	0.293	0.419	0.45	0.0541	6.47	13.3	192	37.9	241	5.38	4.57
	Summer (n=13)	58.4	0.764	0.552	0.489	0.40	0.117	7.31	10.8	76.4	24.6	186	3.61	2.82
Hok Tsui	Annual (n=18)	40.1	0.576	0.209	0.222	0.45	0.256	6.95	31.0	9.23	28.8	111	18.1	11.1
	S.D.	18.1	0.592	0.342	0.350	0.65	0.434	8.85	22.7	6.45	26.4	82.0	18.5	9.67
(Coastal rural)	Autumn (n=6)	46.0	0.608	0.334	0.163	0.65	0.312	7.93	29.4	7.58	25.1	103	16.6	12.6
	Winter (n=5)	47.1	0.464	0.189	0.131	0.62	0.301	9.98	35.4	14.6	53.3	162	19.1	14.0
	Spring (n=4)	33.1	0.446	0.138	0.140	0.21	0.120	5.68	20.8	8.40	20.5	76.8	27.0	10.9
	Summer (n=3)	25.8	0.872	0.0875	0.603	0.10	0.0688	1.64	40.6	4.71	6.76	88.6	7.06	3.47

Autumn: September-November 2013; Winter: December 2013-February 2014; Spring: March-May 2014; Summer: June-August 2014.

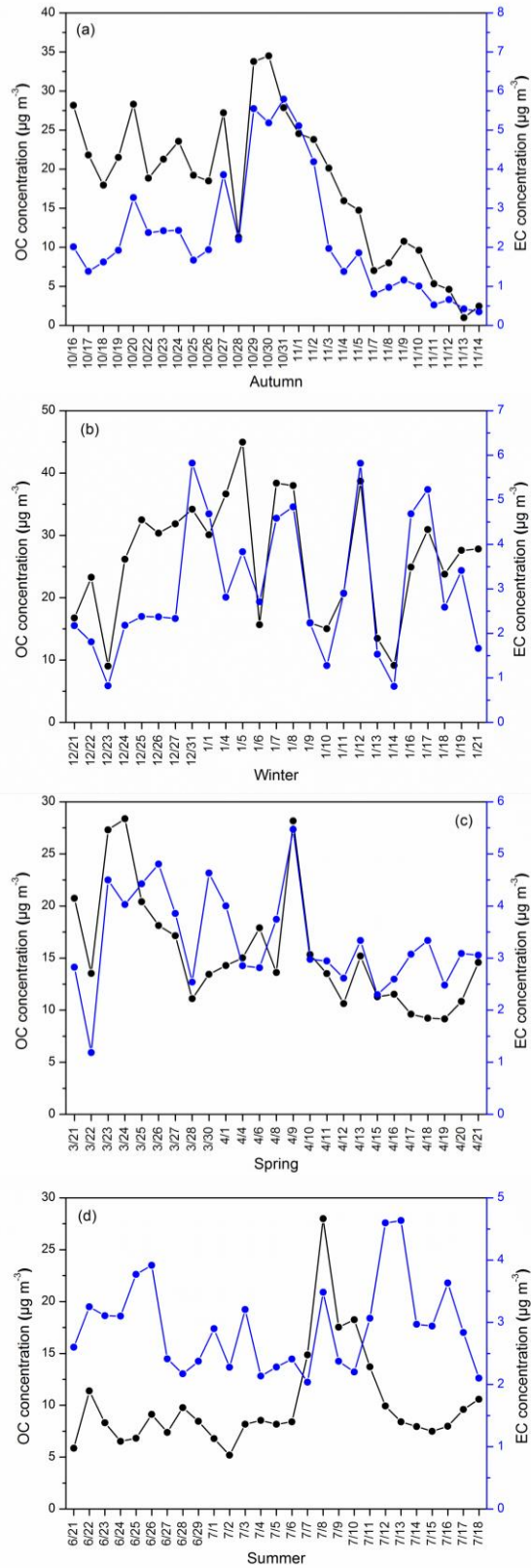


Figure 5-2 Temporal variations of OC and EC ( $\mu\text{g m}^{-3}$ ) in Guangzhou during the high frequency sampling period in each season.

### 5.1.2 The YRD Region

Time series of PM<sub>2.5</sub> concentrations for the spontaneous samples collected from the four cities in the YRD region over the one-year period are displayed in Fig. 5-3. The temporal variations of PM<sub>2.5</sub> in the four sites showed similar fluctuations. The result suggested the regional pollution of PM<sub>2.5</sub> in the YRD region, which similar to that found in North China (Luo et al., 2014) and the North China Plain (Hu et al., 2014). The regional pollution pattern for PM<sub>2.5</sub> indicated that a significant fraction of PM<sub>2.5</sub> in the cities could be secondary particulate particles or fugitive dusts, which have the characteristic of regional distributions (Fu et al., 2008; Fu et al., 2010). Regarding seasonal trends (see Table. 5-2), PM<sub>2.5</sub> concentrations in winter were 2-3 times higher than that in summer, suggesting high PM<sub>2.5</sub> pollution in the YRD region in winter. Similar results were found by previous studies in the YRD region (Ye et al., 2003; Hong et al., 2013; Liu et al., 2013) and the Hebei Province, China (Zhao et al., 2013a). Among the four sites, annual PM<sub>2.5</sub> concentrations were highest in HZ, but no significant differences were observed among SH, NJ and NB. PM<sub>2.5</sub> concentrations were still high in the rural site of NB, mainly due to the transport of air pollutants from the local urban areas in NB and the YRD region.

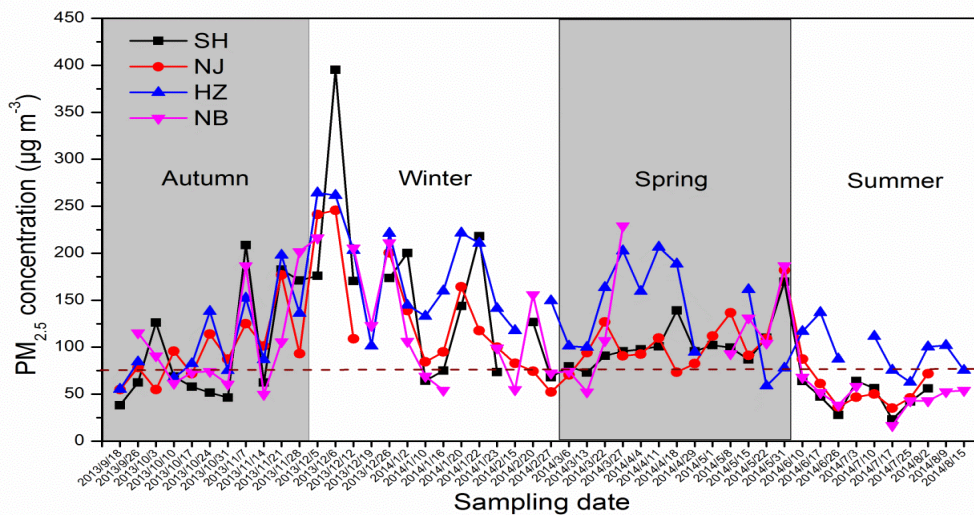


Figure 5-3 Time series of PM<sub>2.5</sub> concentrations for the simultaneous samples in the YRD.

The annual and seasonal averages of trace metal concentrations in PM<sub>2.5</sub> in the YRD region are summarized in Table 5-2. Similar to PM<sub>2.5</sub> mass concentrations, the concentrations of most trace metals were highest in HZ. In general, the concentrations of trace metals in the urban sites were higher in winter and lower in summer, which is similar to other airborne pollutants in the YRD region (Wang et al., 2006c; Cao et al., 2009). In the rural site of NB, the concentrations of trace metals were found to be lowest in summer, but no significant differences were found among autumn, winter and spring. The linear regressions of trace metal and PM<sub>2.5</sub> concentrations in all sites are shown in Fig. 5-4. Generally, strong correlations were found between trace elements (such as Cu, Pb and Zn) and PM<sub>2.5</sub>, while relatively weak correlations were found for crustal elements (such as Al, Ca and Mg). The result suggested that the sources of trace elements were likely to be the major sources of PM<sub>2.5</sub>. This finding was consistent with the fact that crustal elements (such as Si, Ca and Fe) are mainly distributed in coarse particles, while trace elements including Cr, Ni, Cu, Pb and Zn are mainly distributed in the fine particle fraction (Lu et al. 2012). Some previous studies also reported the role of PM mass concentrations on the concentrations of airborne metals (Cheung et al., 2011; Duan et al., 2012).

Table 5-2 The annual and seasonal average concentrations of PM<sub>2.5</sub> and airborne trace metals in the four sites in the YRD region.

Locations		μg m <sup>-3</sup>					ng m <sup>-3</sup>							
		PM <sub>2.5</sub>	Al	Ca	Fe	K	Mg	Cr	Cu	Mn	Pb	Zn	V	Ni
Shanghai (Urban)	Annual (n=143)	94.6	0.92	1.93	1.34	0.81	298	16.9	24.2	49.8	69.7	215	16.5	14.9
	Autumn (n=33)	75.2	0.75	1.62	1.18	0.80	274	18.5	20.0	50.2	65.4	202	13.3	12.4
	Winter (n=40)	138	1.20	2.72	1.85	1.48	415	25.5	45.7	70.9	137	359	23.1	23.6
	Spring (n=41)	95.7	1.08	1.94	1.37	0.59	327	12.3	17.2	44.7	43.2	161	17.5	14.2
	Summer (n=29)	55.5	0.52	1.17	0.75	0.24	124	9.80	9.06	27.6	19.2	104	9.87	6.71
Nanjing (Urban)	Annual (n=119)	97.8	0.71	1.52	0.94	1.03	209	13.2	24.7	47.2	90.9	247	9.88	9.30
	Autumn (n=29)	98.3	0.76	1.52	1.16	1.46	220	16.1	32.5	66.1	111	337	14.2	10.1
	Winter (n=31)	130	0.72	1.67	1.05	1.58	249	24.4	36.8	62.8	149	349	15.9	15.8
	Spring (n=30)	97.6	0.93	2.22	1.18	0.76	278	7.90	20.4	40.5	64.9	193	6.80	7.60
	Summer (n=29)	63.5	0.40	0.65	0.36	0.29	42.2	3.80	8.5	18.3	36.1	106	1.70	3.20
Hangzhou (Urban)	Annual (n=45)	134	1.37	3.02	1.72	1.54	446	17.9	38.5	66.4	122	495	15.3	10.4
	Autumn (n=10)	108	1.25	3.10	1.73	1.60	470	24.5	39.3	74.5	130	604	29.0	13.4
	Winter (n=13)	182	2.05	4.56	2.48	3.18	749	31.8	75.4	106	228	821	19.5	18.8
	Spring (n=11)	138	1.48	3.03	1.73	0.77	419	9.40	19.6	49.3	63.6	313	8.60	5.60
	Summer (n=11)	101	0.71	1.44	0.970	0.55	151	6.00	18.6	35.3	62.3	254	5.50	3.60
Ningbo (Rural)	Annual (n=44)	96.2	1.17	1.19	1.16	0.62	216	14.6	16.2	264	56.3	190	7.36	8.25
	Autumn (n=10)	102	1.58	1.82	1.57	0.84	259	12.8	24.1	130	78.5	281	7.72	10.1
	Winter (n=13)	114	1.28	1.60	1.71	0.84	280	21.3	22.2	206	81.7	246	11.1	11.5
	Spring (n=9)	122	1.43	1.28	1.42	0.82	371	14.1	20.1	385	68.9	229	9.41	9.97
	Summer (n=12)	54.6	0.68	0.47	0.35	0.17	65.1	9.31	4.57	264	14.7	65.3	3.20	4.01

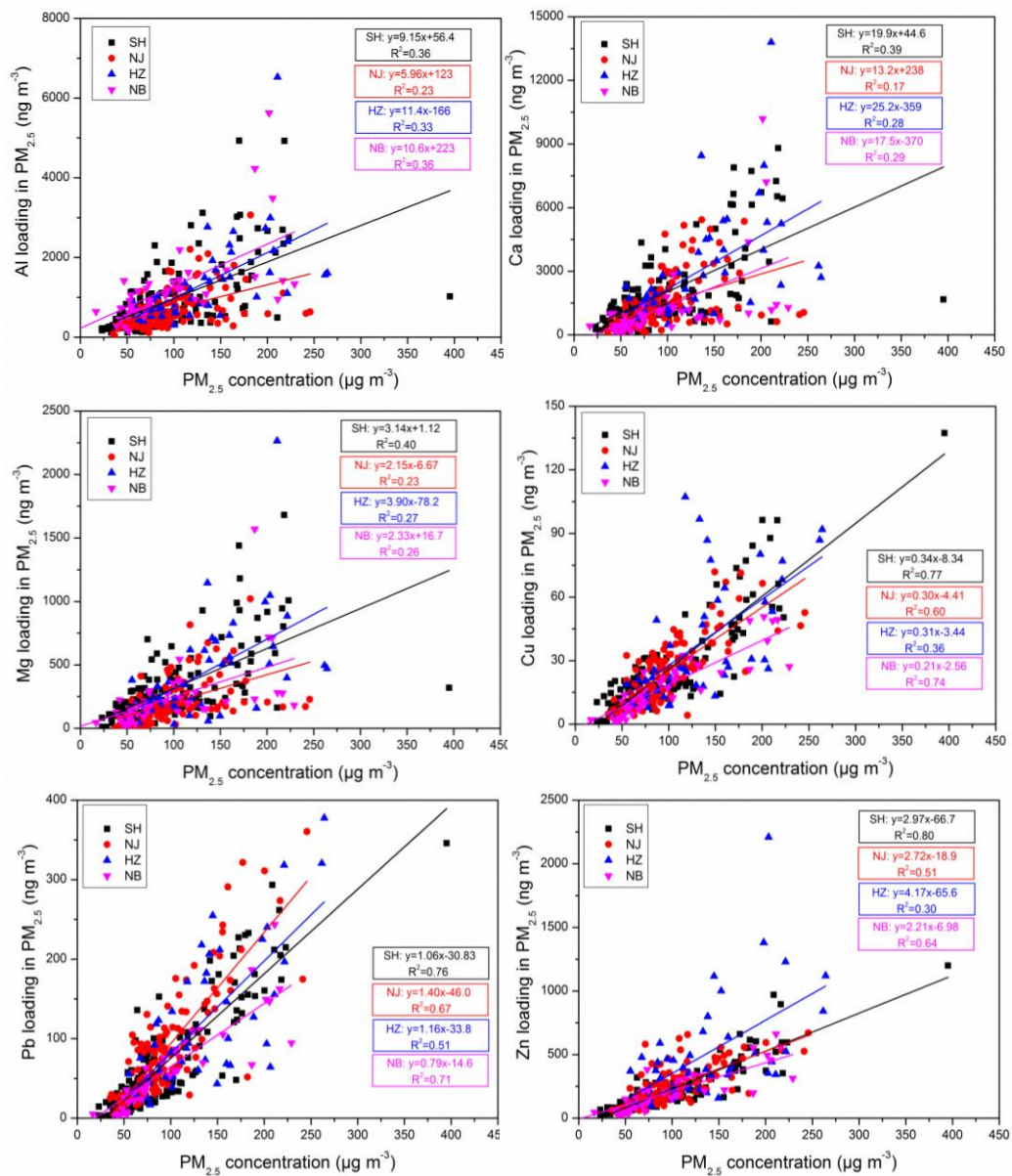


Figure 5-4 The linear regression of trace metal concentrations and  $PM_{2.5}$  in Shanghai, Nanjing, Hangzhou and Ningbo in the YRD region: major elements (Al, Ca and Mg) and trace elements (Cu, Pb and Zn).

As shown in Fig. 5-5, OC and EC concentrations in SH were highest in winter and lowest in summer, similar to the seasonal patterns for PM<sub>2.5</sub> and airborne trace metals. The concentrations of OC and EC in winter were  $17.2 \pm 10.5 \mu\text{g m}^{-3}$  and  $2.88 \pm 2.03 \mu\text{g m}^{-3}$ , respectively, which were 3-4 times higher than those in summer. The contributions of OC and EC to PM<sub>2.5</sub> mass were highest in winter, with  $12.0 \pm 2.63\%$  and  $2.03 \pm 0.82\%$  of the total PM<sub>2.5</sub> mass, respectively. The seasonal variations of secondary inorganic ions (NO<sub>3</sub><sup>-</sup>, SO<sub>4</sub><sup>2-</sup> and NH<sub>4</sub><sup>+</sup>) in SH and NJ showed similar pattern to PM<sub>2.5</sub> mass concentrations, with a decreasing order of winter > autumn > spring > summer. Seasonal variations of secondary inorganic ions were more pronounced for NO<sub>3</sub><sup>-</sup>, with 6-10 times greater in winter than in summer, probably due to more emissions of NO<sub>x</sub> and the high conversion rate of gaseous nitric acid (HNO<sub>3</sub>) to aerosol particles as ammonium nitrate (NH<sub>4</sub>NO<sub>3</sub>) under the low temperature in winter (Zhang et al., 2014). The concentrations of SO<sub>4</sub><sup>2-</sup> were typically higher in winter than summer, probably due to more abundant SO<sub>2</sub> precursor from fuel combustion in winter.

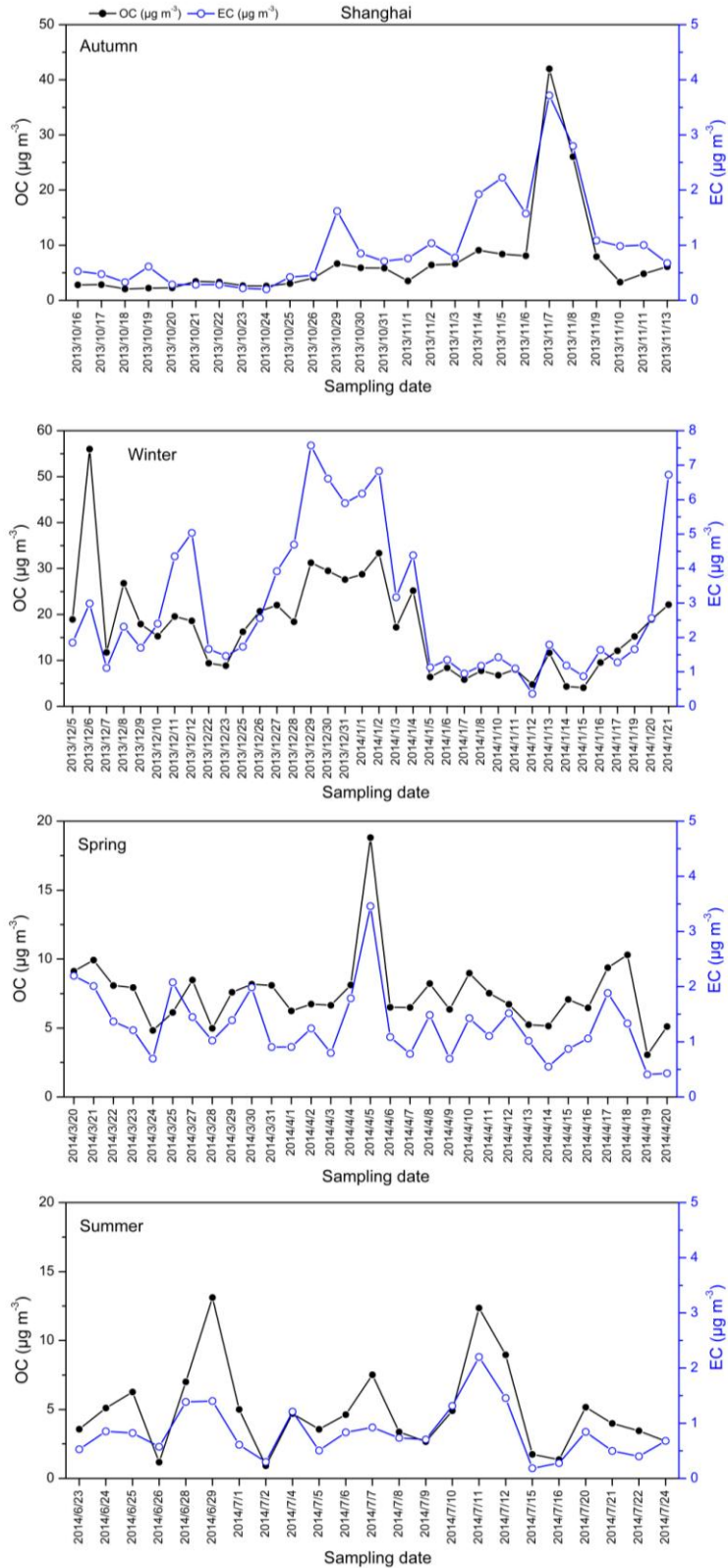


Figure 5-5 Temporal variations of OC and EC ( $\mu\text{g m}^{-3}$ ) in Shanghai during the high frequency sampling period in each season.

### 5.1.3 North China

In Fig. 5-6, obvious temporal variations of  $PM_{2.5}$  concentrations were observed in BJ, with 2-fold higher in winter and spring than that in summer. Although the range of  $PM_{2.5}$  concentrations in winter was larger compared to spring, the average means between winter and spring were comparable. Similar seasonal pattern of  $PM_{2.5}$  was observed by Wang et al. (2005), with a decline order as winter > spring > autumn > summer. In Beijing, obvious seasonal patterns for trace metal concentrations were found from the data in Table 5-3. Cr, Cu Pb and Zn showed the highest concentrations in autumn and winter, probably attributed to the heating activities and poor diffusion under the low wind speed in BJ. However, Al, Fe, Ca, K, Mg, V and Ni exhibited the highest concentrations in spring, mainly due to the occurrence of dust storms in spring (Zhang et al., 2003; Sun et al., 2005).

The temporal and seasonal variations of OC and EC in BJ are illustrated in Fig. 5-7. The average OC concentrations were  $26.9 \pm 11.7$ ,  $30.7 \pm 21.3$ ,  $19.2 \pm 6.31$  and  $10.4 \pm 2.51 \mu\text{g m}^{-3}$  in autumn, winter, spring and summer, respectively. The average EC concentrations were  $4.22 \pm 3.68$ ,  $3.35 \pm 1.56$ ,  $2.69 \pm 1.08$  and  $1.10 \pm 0.44 \mu\text{g m}^{-3}$  in autumn, winter, spring and summer, respectively. OC and EC exhibited higher concentrations in autumn and winter and lower concentrations in summer. Similar with the seasonal patterns of OC and EC, the concentrations for the calculated SOC in winter ( $24.8 \mu\text{g m}^{-3}$ ) was 3 times higher than that in summer ( $8.23 \mu\text{g m}^{-3}$ ). In BJ, more emissions of  $SO_2$  and  $NO_x$  from the coal consumptions during winter heating period could increase the amount of SOC in the atmosphere.

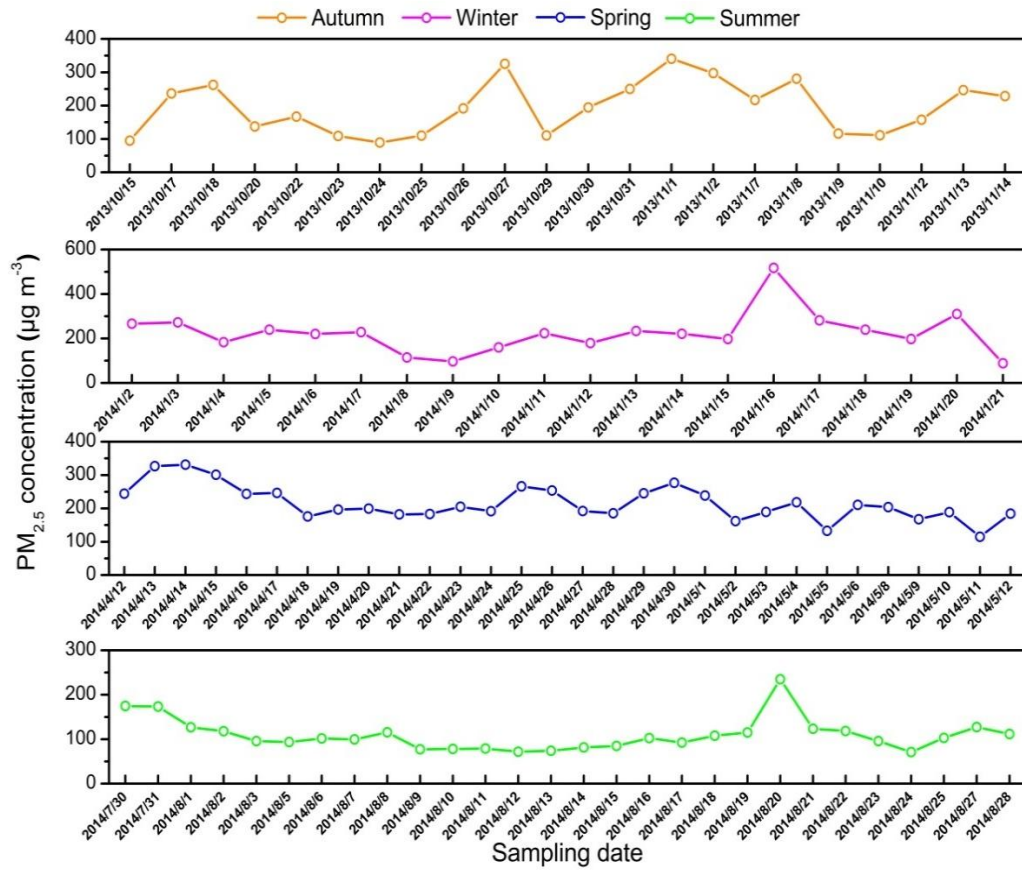


Figure 5-6 Temporal variations of PM<sub>2.5</sub> concentrations in Beijing in autumn (from 15<sup>th</sup> October to 14<sup>th</sup> November 2013), winter (from 2 to 21 January 2014), spring (from 12<sup>th</sup> April to 12<sup>th</sup> May 2014) and summer (30<sup>th</sup> July to 28<sup>th</sup> August 2014).

Table 5-3 The annual and seasonal averages of PM<sub>2.5</sub> and airborne trace metals in Beijing and Mount Changbai.

Location		$\mu\text{g m}^{-3}$						$\text{ng m}^{-3}$						
		PM <sub>2.5</sub>	Al	Ca	Fe	K	Mg	Cr	Cu	Mn	Pb	Zn	V	Ni
Beijing (Urban)	Annual (n=101)	183	4.22	8.42	4.40	2.35	2.07	17.2	58.6	97.8	189	504	6.70	16.4
	S.D.	78.8	4.23	5.10	2.79	1.64	1.28	21.3	40.0	66.8	168	413	4.77	22.8
	Autumn (n=22)	194	4.59	10.5	5.34	3.20	2.42	22.5	87.6	138	229	692	5.05	9.81
	Winter (n=20)	224	3.82	8.87	5.40	3.27	2.24	17.3	78.1	121	348	795	4.77	10.2
	Spring (n=30)	215	7.08	11.3	5.91	2.66	2.97	18.0	53.8	116	156	424	8.47	17.2
	Summer (n=29)	109	1.36	3.52	1.45	0.76	0.76	6.16	28.2	32.5	81.6	245	4.39	3.71
Mount Changbai (Remote)	Annual (n=42)	34.2	0.39	0.40	0.36	0.30	0.11	1.81	4.26	9.35	14.6	35.8	1.25	1.18
	S.D.	16.0	0.35	0.33	0.32	0.21	0.103	0.81	3.10	6.52	10.6	18.5	0.69	0.63
	Autumn (n=10)	27.4	0.21	0.25	0.21	0.16	0.060	2.33	6.17	7.58	11.1	31.6	1.48	1.54
	Winter (n=13)	35.3	0.31	0.31	0.27	0.35	0.087	1.72	4.90	8.49	21.9	43.6	1.11	1.19
	Spring (n=11)	49.0	0.78	0.77	0.71	0.50	0.22	2.03	3.69	15.6	17.3	43.7	1.43	1.09
	Summer (n=8)	20.4	0.18	0.214	0.18	0.11	0.045	0.99	1.78	4.06	5.38	19.8	0.55	0.20

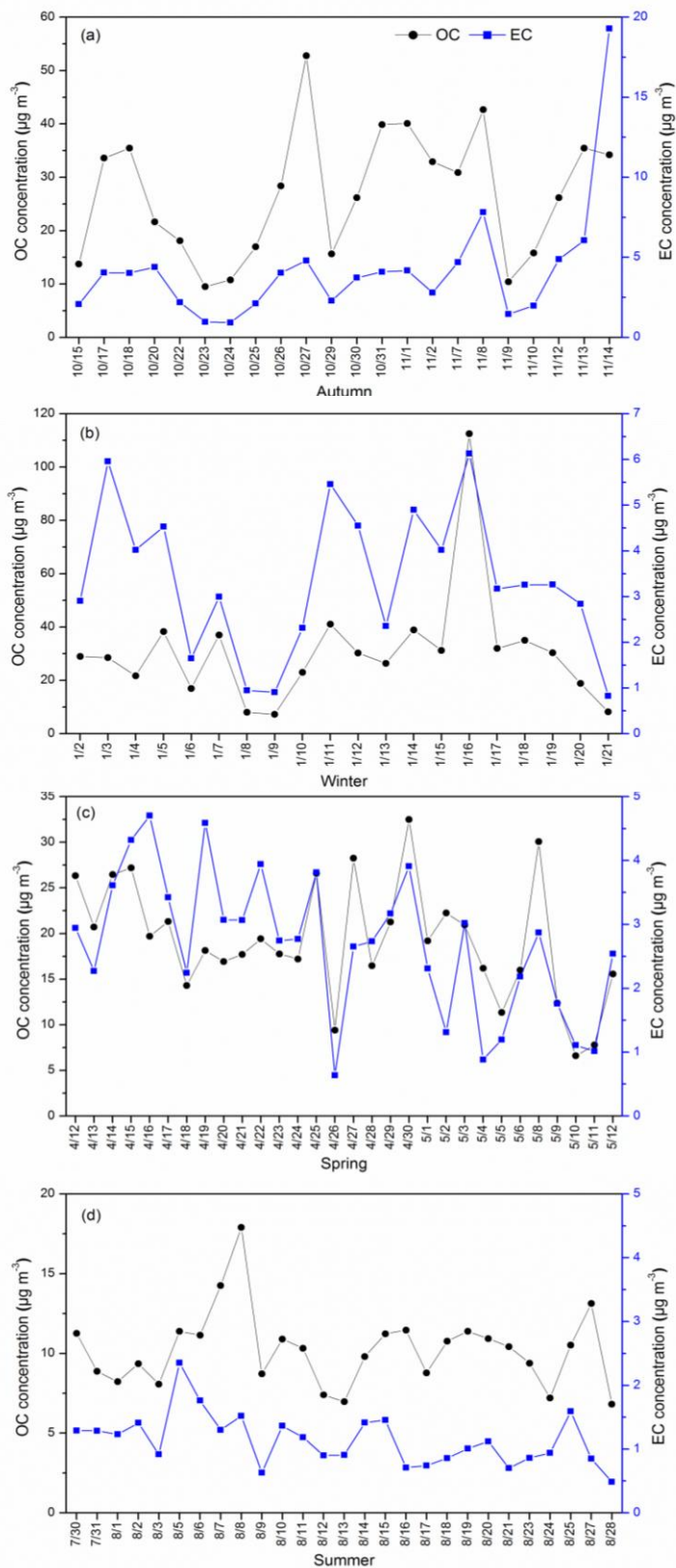


Figure 5-7 Temporal variations of OC and EC ( $\mu\text{g m}^{-3}$ ) in Beijing during the high frequency sampling period in each season.

The temporal variations of PM<sub>2.5</sub> mass concentrations in CBS are shown in Fig. 5-8. Clear seasonal pattern in PM<sub>2.5</sub> mass concentrations was observed, with a decreasing order of spring (49.0 μg m<sup>-3</sup>) > winter (35.3 μg m<sup>-3</sup>) > autumn (27.4 μg m<sup>-3</sup>) > summer (20.4 μg m<sup>-3</sup>). Only two samples were found to be polluted during the entire sampling period, in which PM<sub>2.5</sub> concentration slightly exceeded the daily average limit of 75 μg m<sup>-3</sup>. The two samples were collected on 18 April 2014 and 3 May 2014, with PM<sub>2.5</sub> concentrations of 76.7 and 77.7 μg m<sup>-3</sup>, respectively. The results indicated that PM<sub>2.5</sub> pollution was more serious in spring. As summarized in Table 5-3, the concentrations of major elements, including Al, Fe, Ca, K and Mg, were 2-4 times higher in spring than those in other seasons. The lowest concentrations of all the trace elements were observed in summer. The concentrations of Mn, Pb and Zn were highest in winter and spring, while Cr, Cu, Ni and V showed less temporal variations from autumn to spring.

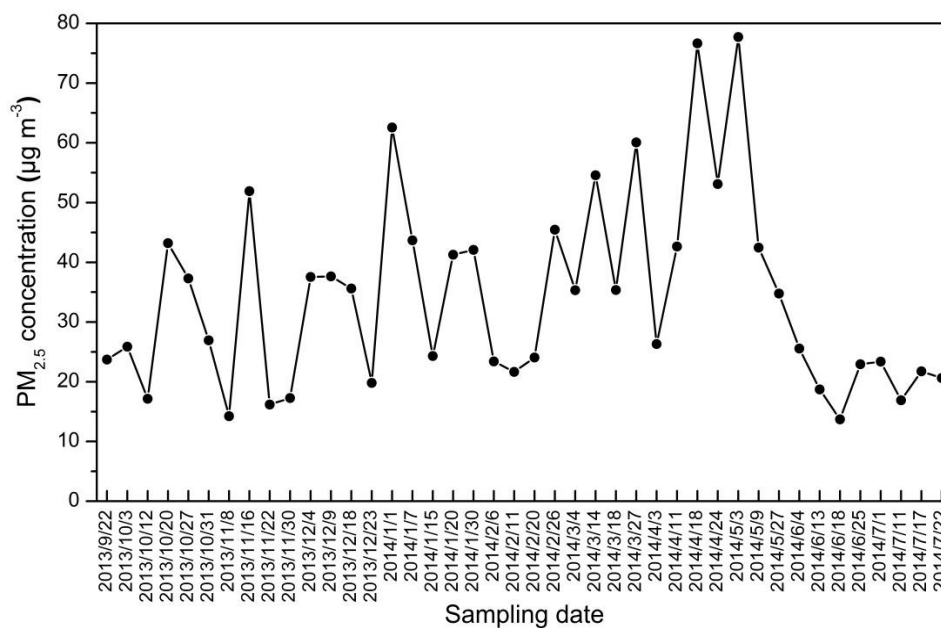


Figure 5-8 Temporal variations of PM<sub>2.5</sub> concentrations in Mount Changbai.

#### 5.1.4 Comparison among the Three Regions

Guangzhou, Shanghai and Beijing are the typical large city in the PRD, the YRD and North China, respectively. Generally,  $PM_{2.5}$  mass concentrations were ranked in the order of BJ > SH > GZ, while the concentrations of the measured chemical components (trace metals, POC, SOC and EC) were decreased in the order of BJ > GZ > SH. Similar seasonal patterns for  $PM_{2.5}$ , SOC and trace elements were found in the three cities, with higher concentrations in autumn and winter and lower concentrations in spring and summer. In contrast with GZ and SH, the concentrations of airborne crustal elements increased from summer to spring in BJ. Regarding EC and POC, no significant seasonal variation was observed in GZ, while the pattern of higher concentrations in winter and lower concentrations in summer was found in SH and BJ.

The contributions of POC, EC, SOC, crustal elements and trace elements to  $PM_{2.5}$  mass in GZ, SH and BJ are shown in Fig. 5-9. All the measured chemical components constituted 27.8%, 24.8% and 16.9% of the total  $PM_{2.5}$  mass in GZ, BJ and SH, respectively. By comparison, the contributions of POC, SOC and EC were relatively higher in GZ, and crustal elements exhibited larger fraction to  $PM_{2.5}$  mass in BJ. The results indicated that the carbonaceous aerosol was more important in GZ, and crustal source to  $PM_{2.5}$  was more significant in BJ. In the three cities, SOC and trace elements showed higher fractions in winter, consistent with the seasonal patterns for their concentrations. In GZ, although the concentrations of EC and POC have no seasonal variation, their contributions to  $PM_{2.5}$  increased from autumn to summer.

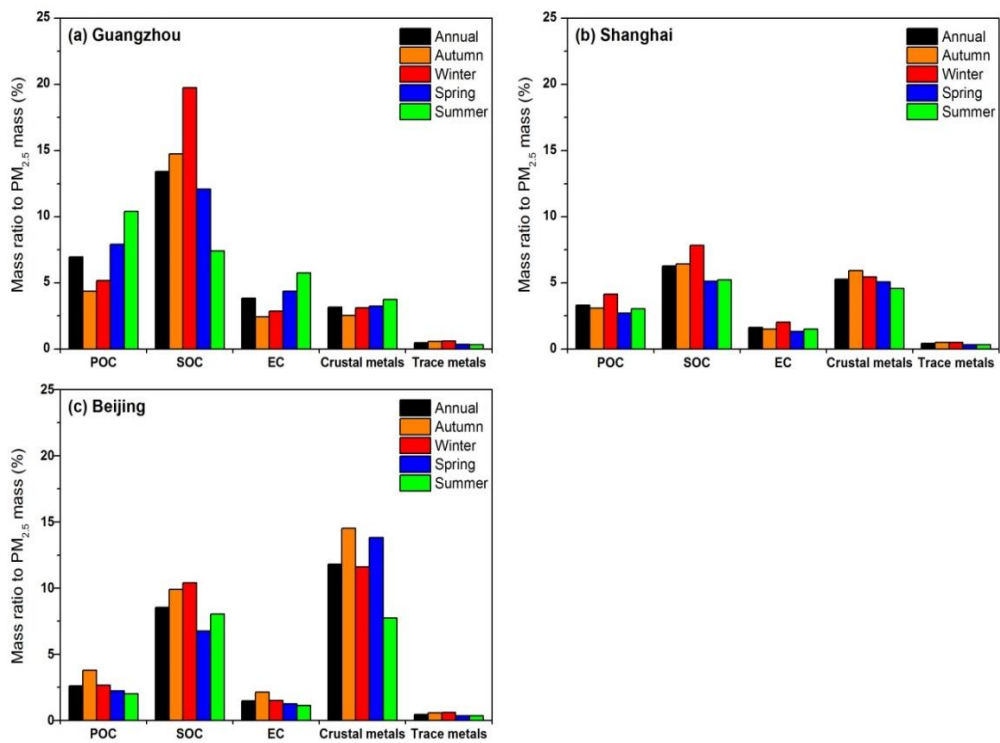


Figure 5-9 Mass contributions of POC, EC, SOC, crustal elements and trace elements to  $PM_{2.5}$  in (a) Guangzhou; (b) Shanghai; and (c) Beijing.

## 5.2 Source Appointment of PM<sub>2.5</sub>

### 5.2.1 Enrichment Factor of Trace Metals

The seasonal averages of enrichment factors (EF) for metal elements in PM<sub>2.5</sub> in the PRD, the YRD and North China are plotted in Fig. 5-10, 5-11 and 5-12, respectively. The EF values for Al, Fe, Ca and Mg were around unity, suggesting a major contribution from natural sources, such as the crustal materials. A similar pattern was observed for EF values of trace elements in the three regions, with the order of Zn > Pb > Cu ≥ Ni > Cr > V. The significantly high EF values of Cu, Pb, Zn and Ni indicated the anthropogenic sources for these metals, while less proportion of Cr and V originated from anthropogenic sources. The average EF values of most trace elements were higher in autumn and winter in GZ, HT, SH, NJ, HZ and CBS, mainly due to their intensive anthropogenic inputs from coal combustion, traffic emissions and heavy industries. In contrast with the urban sites in the PRD and YRD regions, the average EF values of most trace elements in BJ were lower in spring (see Fig. 5-12a), probably due to the influence of dust storms in northern China. The seasonal patterns of EFs for most trace elements were not significant in the rural site of NB (see Fig. 5-11d), implying that the sampling site is more prone to be influenced by anthropogenic pollution.

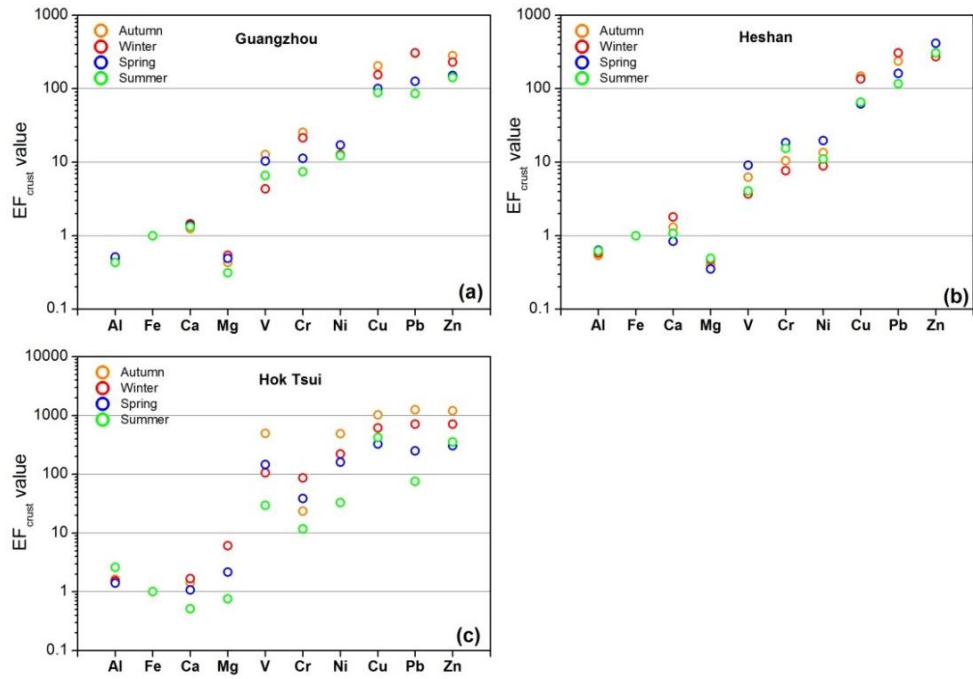


Figure 5-10 The seasonal averages of enrichment factors (EF) for metal elements in PM<sub>2.5</sub> in the PRD region: (a) Guangzhou; (b) Heshan; and (c) Hok Tsui.

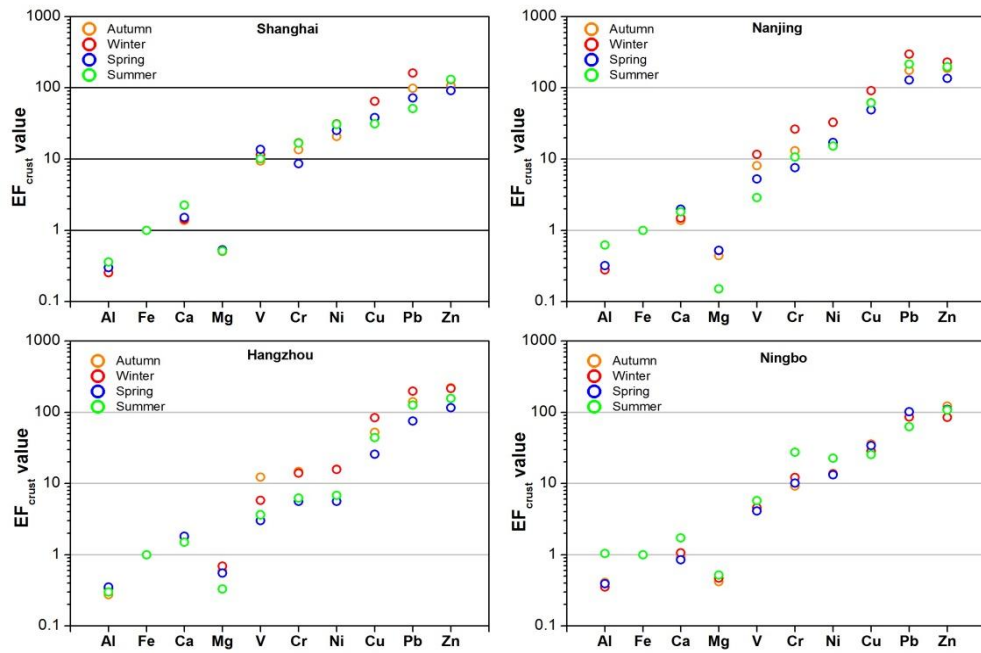


Figure 5-11 The seasonal averages of enrichment factors (EF) for metal elements in PM<sub>2.5</sub> in the YRD region: (a) Shanghai; (b) Nanjing; (c) Hangzhou; and (d) Ningbo.

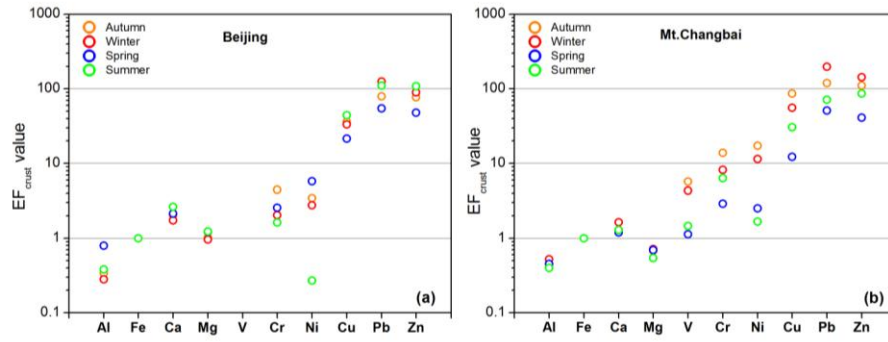


Figure 5-12 The seasonal averages of enrichment factors (EF) for metal elements in PM<sub>2.5</sub> in North China: (a) Beijing and (b) Mount Changbai.

### 5.2.2 Sources of Pb in PM<sub>2.5</sub>

Lead isotopic fingerprinting is a useful technique in establishing the sources of lead in the environment, which is based on the differences of Pb isotopic compositions among the various emission sources. Coal combustion, industry emissions and vehicle exhausts are considered the three major sources of atmospheric Pb in China. In the past decade, more research reported the Pb isotopic compositions in atmospheric particulate matters (Widory et al., 2010; Zhao et al., 2015). However, few Pb isotope data for Chinese coal, coal combustion ash and industrial activities have been published. Base on previous studies of Pb isotopic fingerprinting in the three regions, Pb isotopic compositions in some known natural and anthropogenic sources and other environmental samples in the PRD, the YRD and North China are summarized in Table 5-4, 5-5 and 5-6, respectively.

In the PRD region, the scatter plots of  $^{206}\text{Pb}/^{207}\text{Pb}$  versus  $^{208}\text{Pb}/^{207}\text{Pb}$  of PM<sub>2.5</sub> from the three sites were compared with known natural and anthropogenic sources from this region (Fig. 5-13a). The  $^{206}\text{Pb}/^{207}\text{Pb}$  ratios of coals used in GZ were reported to be 1.184-1.287 (Bi, unpublished), and of coal combustion were 1.1716 and 1.1732 from FanKou Pb-Zn deposit and power station in GZ, respectively (Zhu et al., 2001). The ratios of  $^{206}\text{Pb}/^{207}\text{Pb}$  observed in hardware factory and plastic factory in Foshan were 1.1651 and 1.1669, respectively (Zhu et al., 2001). The Pb isotopic ratios of PM<sub>2.5</sub> in GZ and HS were close to the industrial and coal combustion sources, but distinct from the data observed in vehicle exhausts. The result indicated that the major sources of atmospheric Pb in GZ and HS are coal combustion and industrial activities rather than vehicle exhausts. Before the banning of leaded gasoline, Pb isotopic compositions in aerosols in Hong Kong were different with that in GZ due to the different origin of leaded gasoline (Australian Pb ore) and less industrial activities in Hong Kong (Lee et al., 2007). After that, the local sources of airborne Pb in Hong Kong are fossil fuel combustion (vehicle exhausts and power stations) and the suspended of soil dust and road dust. As shown in Fig. 5-13a, the ratios of  $^{206}\text{Pb}/^{207}\text{Pb}$  and  $^{208}\text{Pb}/^{207}\text{Pb}$  in PM<sub>2.5</sub> at HT ( $1.1662 \pm 0.0030$  and  $2.4462 \pm 0.0065$ ) were close to those in road dust of Hong Kong and the vehicle

emissions in the PRD, suggesting the contribution of traffic emissions on atmospheric Pb in Hong Kong. Local sources such as coal combustion were also the possible contributors of airborne Pb in Hong Kong, but no Pb isotopic composition data for those were reported. Lee et al. (2007) found that higher Pb isotopic ratios in winter than that in summer in HT were likely due to the long-range transport of Pb from the PRD region. In this study, the ratios of  $^{206}\text{Pb}/^{207}\text{Pb}$  of  $\text{PM}_{2.5}$  in HT showed slightly higher in winter than that in summer. Moreover, high concentrations of Pb ( $\text{mg kg}^{-1}$ ) mainly in the range of coal combustion level were observed in winter in HT (Fig. 5-14), reflecting the influence of long-range transport of coal combustion from the PRD to Hong Kong. In this study, Pb isotopic ratios in  $\text{PM}_{2.5}$  were lower than those of TSP samples in the PRD reported by Lee et al. (2007), indicating the preferential enrichment of anthropogenic Pb in fine atmospheric particles (Li et al., 2009).

In the YRD region, the Pb isotope ratios of  $\text{PM}_{2.5}$  in the four cities were similar and distinctly different from the values observed in leaded and lead free vehicle exhausts and iron ore sinter dust, but close to the ratios that were found in coal and coal combustion dust, metallurgic dust and cement (Fig. 5-13b). The result suggested that the major sources of Pb in  $\text{PM}_{2.5}$  were the stationary sources, similar to the reports from previous studies in the YRD region (Zheng et al., 2004; Tan et al., 2006). The  $^{206}\text{Pb}/^{207}\text{Pb}$  ratios increased in SH after the banning of leaded gasoline (Chen et al., 2005; Cheng and Hu, 2010). In the present study, the  $^{206}\text{Pb}/^{207}\text{Pb}$  ratios showed a continuous increasing trend, reflecting the continued increase of Pb contribution from the stationary sources. As shown in Fig. 5-15, relatively high concentrations of airborne Pb ( $> 1788 \text{ mg kg}^{-1}$ ) and high  $^{206}\text{Pb}/^{207}\text{Pb}$  ratios in  $\text{PM}_{2.5}$  were obtained in winter in SH, HZ and NJ compared to other seasons, suggesting the possible changes in Pb sources in winter. In NB, higher ratios of  $^{208}\text{Pb}/^{207}\text{Pb}$  and lower concentrations of Pb ( $49\text{-}290 \text{ mg kg}^{-1}$ ) were observed in summer, indicating more contribution of Pb from natural sources. In addition, relatively lower concentrations of Pb in NB suggested less local sources of Pb in the rural site.

In BJ, the isotopic ratios ( $^{204}\text{Pb}/^{207}\text{Pb}$  and  $^{206}\text{Pb}/^{207}\text{Pb}$ ) in  $\text{PM}_{2.5}$  samples were close to the

ratios that found in industrial sources (*e.g.*, cement factories and lead refining plants) and coal combustion from BJ (Fig. 5-13c). The characteristics of Pb isotopic compositions from traffic emissions in BJ were obtained from the literature. The banning of leaded gasoline was first started in BJ, and then in other cities, such as Shanghai, Guangzhou and Tianjin. The contribution of vehicle exhausts to Pb in the atmosphere declined in China after the phase-out of leaded gasoline (Tan et al., 2006; Cheng and Hu, 2010). Pb isotopic ratios in CBS were distinctly different from the values observed in anthropogenic sources from BJ and aerosol samples in major cities of North China, such as Changchun, Dalian and Harbin, suggesting the less influence of anthropogenic Pb sources at CBS. As displayed in Fig. 5-16, the  $^{206}\text{Pb}/^{207}\text{Pb}$  ratios in BJ and CBS exhibited relatively lower values in winter compared to other seasons. During winter, when coal is frequently used in BJ and North China for heating, lower ratios of  $^{206}\text{Pb}/^{207}\text{Pb}$  in BJ and CBS confirmed the result that higher Pb concentration (Fig. 5-16) in winter are mainly due to coal combustion. Although high ratios of  $^{206}\text{Pb}/^{207}\text{Pb}$  were also measured in spring and summer, the Pb concentrations ( $\text{mg kg}^{-1}$ ) were much lower, implying the contribution of sources other than coal combustion in BJ and CBS.

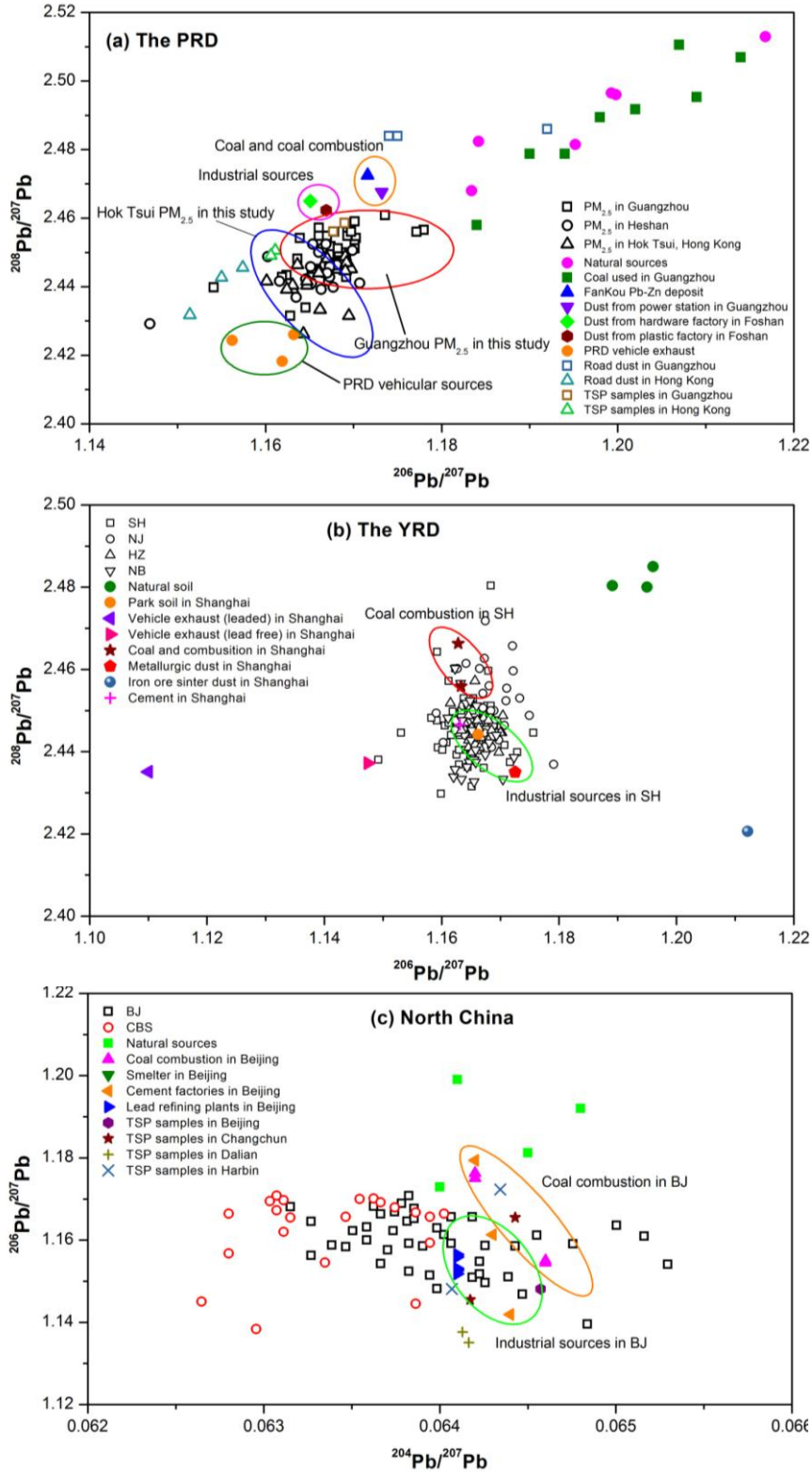


Figure 5-13 Comparison of  $^{206}\text{Pb}/^{207}\text{Pb}$  and  $^{208}\text{Pb}/^{207}\text{Pb}$  of  $\text{PM}_{2.5}$  samples in this study and some known natural/anthropogenic sources and other environmental samples in (a) the PRD; (b) the YRD; and (c) North China.

Table 5-4 The Pb isotopic compositions of some known natural/anthropogenic sources and other environmental samples in the PRD region.

Location and materials	$^{206}\text{Pb}/^{207}\text{Pb}$	$^{208}\text{Pb}/^{207}\text{Pb}$	References
<b>Natural sources</b>			
Granite in eastern Cathaysia	1.1834	2.4680	Zhu et al. (1998)
Granite in the PRD	1.1842	2.4824	Zhu et al. (1998)
Volcanic rocks in Foshan	1.1993	2.4965	Zhu et al. (1998)
Natural bedrock in HT	1.2168	2.5129	Lee et al. (2006)
Country park soils in Hong Kong	1.1998	2.4960	Lee et al. (2006)
Uncontaminated soils in the PRD	1.1952	2.4815	Zhu et al. (2001)
<b>Anthropogenic sources</b>			
FanKou Pb-Zn deposit	1.1716	2.4725	Zhu et al. (1998)
Automobile exhausts in the PRD	1.1562-1.1632	2.4182-2.426	Zhu et al. (2001)
Power station in Guangzhou	1.1732	2.4676	Zhu et al. (2001)
Hardware factory in Foshan	1.1651	2.4650	Zhu et al. (2001)
Plastic factory in Foshan	1.1669	2.4623	Zhu et al. (2001)
Coal used in Guangzhou	1.184-1.287	2.458-2.511	Bi, unpublished
<b>Road dust in Hong Kong</b>			Duzgoren-Aydin
HKU car park	1.1514	2.4318	(2004)
High Street	1.1574	2.4456	
Mongkok	1.1550	2.4427	
<b>Road dust in Guangzhou (&lt; 50 <math>\mu\text{m}</math>)</b>			Bi et al. (2013)
Street site-1	1.1750	2.4840	
Urban park site-1	1.1740	2.4840	
Street site-4	1.1920	2.4860	
<b>TSP samples in Guangzhou</b>			(Lee et al., 2007)
Urban site	1.1677	2.4561	
Suburban site	1.1690	2.4586	
<b>TSP samples in Hong Kong</b>			(Lee et al., 2007)
Urban site	1.1611	2.4506	
Suburban site	1.1606	2.4491	

Table 5-5 The Pb isotopic compositions of some known natural/anthropogenic sources and other environmental samples in Shanghai.

Location and materials	Pb (mg kg <sup>-1</sup> )	<sup>206</sup> Pb/ <sup>207</sup> Pb	<sup>208</sup> Pb/ <sup>207</sup> Pb	References
<b>Natural sources</b>				
Urban soil	11.7 ± 0.3	1.1891	2.4804	Tan et al. (2006)
Park soil	64.9 ± 65.6	1.1662	2.4442	Zhang et al. (2008b)
<b>Anthropogenic sources</b>				
Vehicle exhaust (leaded)	7804 ± 160	1.1100	2.4351	Tan et al. (2006)
Vehicle exhaust (Pb free)	235 ± 5	1.1474	2.4372	Tan et al. (2006)
Metallurgic dust	6140 ± 130	1.1725	2.4350	Tan et al. (2006)
Coal combustion dust	1788 ± 37	1.1633	2.4559	Tan et al. (2006)
Cement	103 ± 2	1.1631	2.4466	Tan et al. (2006)
Coal	13 ± 5	1.1628	2.4663	Chen et al. (2005)
Iron ore sinter dust	750	1.2121	2.4206	Chen et al. (2005)

Table 5-6 The Pb isotopic compositions of some known natural/anthropogenic sources and other environmental samples in North China.

Location and materials	Pb (mg kg <sup>-1</sup> )	<sup>206</sup> Pb/ <sup>207</sup> Pb	<sup>204</sup> Pb/ <sup>207</sup> Pb	References
<b>Natural sources</b>				Widory et al.
Chinese loess	29	1.1990	0.0641	(2010)
Simulated Chinese loess	40	1.1920	0.0648	
Soil collected in BJ	41	1.1812	0.0645	
	24	1.1729	0.0640	
<b>Anthropogenic sources in BJ (Aerosol samples)</b>				Widory et al.
Power plants	112	1.1545	0.0646	(2010)
	103	1.1550	0.0646	
	118	1.1763	0.0642	
	104	1.1751	0.0642	
Cement factories	14	1.1794	0.0642	
	20	1.1613	0.0643	
	30	1.1419	0.0644	
Lead refining plants	997700	1.1565	0.0641	
	940600	1.1518	0.0641	
	994300	1.1531	0.0641	
	900700	1.1559	0.0641	
	921100	1.1526	0.0641	
	771400	1.1518	0.0641	
<b>Aerosol samples in North China</b>				Mukai et al.(2001)
Beijing	Winter	1.1481	2.4443	
Changchun	Winter	1.1655	2.4627	
	Summer	1.1455	2.4410	
Dalian	Winter	1.1351	2.4415	
	Summer	1.1377	2.4414	
Harbin	Winter	1.1723	2.4596	
	Summer	1.1481	2.4363	

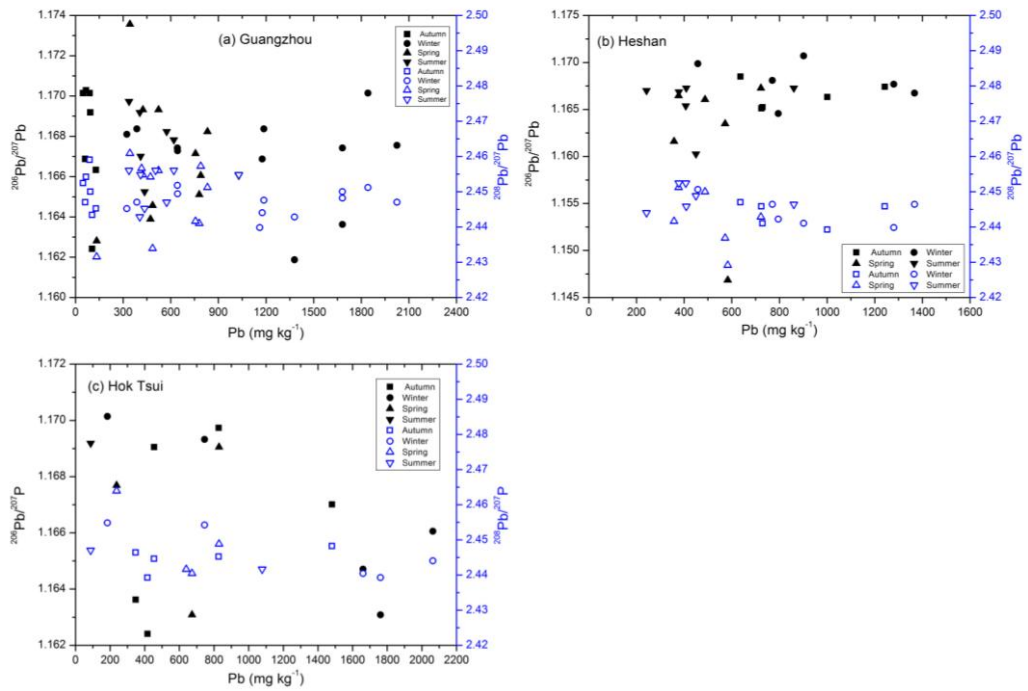


Figure 5-14 Seasonal variations of Pb isotopic ratios (<sup>206</sup>Pb/<sup>207</sup>Pb and <sup>208</sup>Pb/<sup>207</sup>Pb) and Pb concentrations (mg kg<sup>-1</sup>) for PM<sub>2.5</sub> samples in (a) Guangzhou; (b) Heshan; and (c) Hok Tsui.

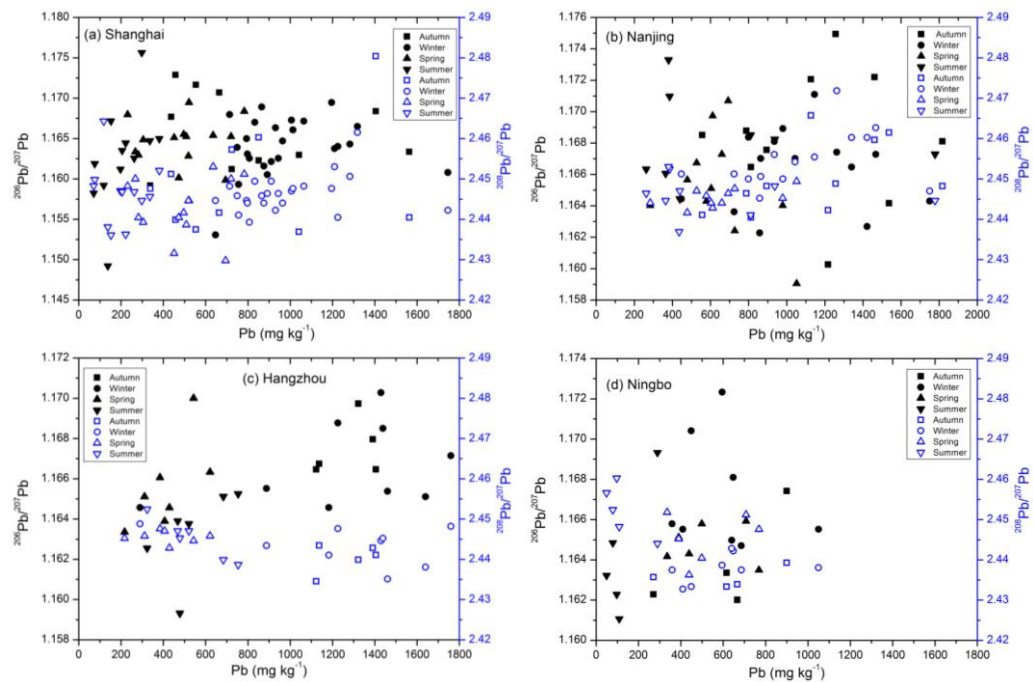


Figure 5-15 Seasonal variations of Pb isotopic ratios (<sup>206</sup>Pb/<sup>207</sup>Pb and <sup>208</sup>Pb/<sup>207</sup>Pb) and Pb concentrations (mg kg<sup>-1</sup>) for PM<sub>2.5</sub> samples in (a) Shanghai; (b) Nanjing; (c) Hangzhou; and (d) Ningbo.

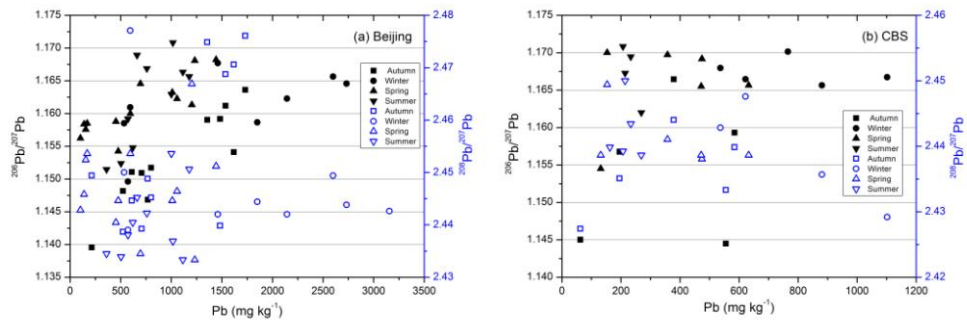


Figure 5-16 Seasonal variations of Pb isotopic ratios ( $^{206}\text{Pb}/^{207}\text{Pb}$  and  $^{208}\text{Pb}/^{207}\text{Pb}$ ) and Pb concentrations ( $\text{mg kg}^{-1}$ ) for  $\text{PM}_{2.5}$  samples in (a) Beijing and (b) Mount Changbai.

### 5.2.3 The Relationship between OC and EC

The relationship between OC and EC concentrations can be used to estimate the origin of carbonaceous aerosols (Duan et al., 2007; Zhou et al., 2012). Strong correlations between OC and EC suggest that the major fractions of OC and EC in the atmosphere are emitted by primary sources. The scatter plots of OC and EC during the four seasons in GZ, SH and BJ are displayed in Fig. 5-17. OC and EC were highly correlated in all the season with  $r = 0.68-0.89$  and  $r = 0.48-0.70$  in SH and BJ, respectively, while they were only strongly correlated from autumn to spring with  $r = 0.62-0.8$  in GZ. The result indicated that OC and EC at SH and BJ were likely to be derived from their common dominant sources, such as coal combustion and vehicle exhausts. Similar results were also observed in previous studies (Yang et al., 2005a; Feng et al., 2009b).

The ratios of OC/EC provide information about the emission and transformation characteristics of carbonaceous aerosol. The ratios of OC/EC have been detected in some typical emission sources, such as wood kitchen emissions (32.9-81.6), combustion (16.8-40.0), residential coal smoke (2.5-10.5), biomass burning (7.7) and vehicular exhaust (1.0-4.2) (Feng et al., 2009b). The annual means of OC/EC were 6.69, 6.69 and 8.65 at GZ, SH and BJ, respectively. Relative high ratios of OC/EC were found in BJ due to the high concentrations of SOC. The OC/EC ratios exhibited no seasonal variations in SH and BJ, while clear seasonal pattern was found in GZ with high values in autumn and winter and low values in spring and summer. The similar seasonal patterns for OC (POC and SOC) and EC were likely to result in the stable values of OC/EC in SH and BJ. However, the seasonal pattern in OC/EC was probably due to the less seasonal variations for EC concentrations in GZ. Additionally, no correlation between OC and EC in the summer at GZ indicated their different sources. Since carbonaceous aerosols originate from various sources that are temporal and spatial dependent, it is difficult to identify and quantify their sources. Other techniques, such as radiocarbon ( $^{14}\text{C}$ ) analysis (Liu et al., 2013), are needed to better investigate the emission sources and their contributions in future work.

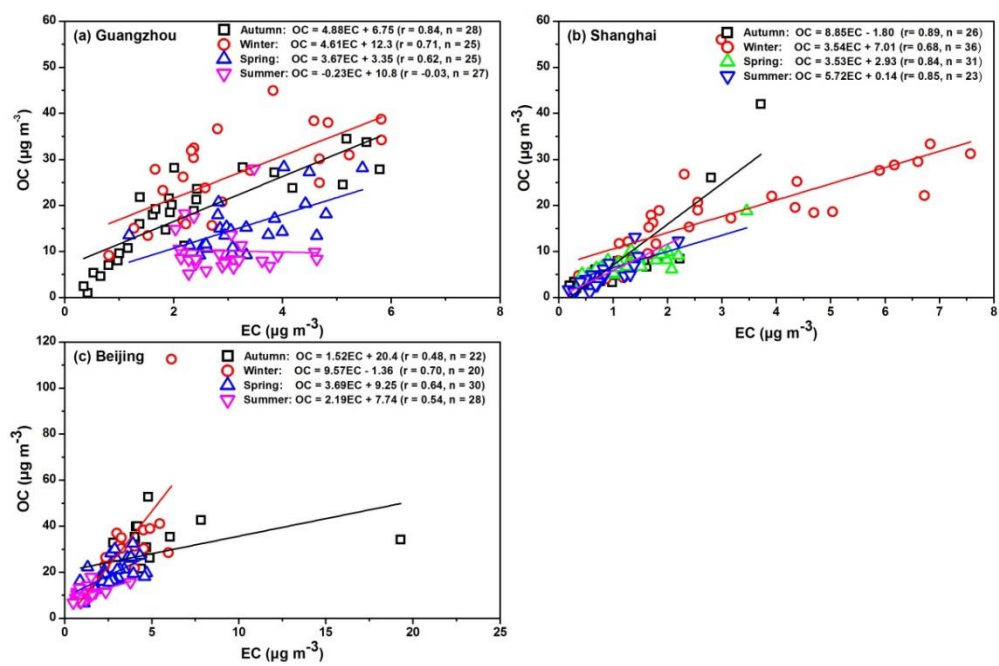


Figure 5-17 Correlation between OC and EC concentrations in PM<sub>2.5</sub> in (a) Guangzhou; (b) Shanghai; and (c) Beijing during the four seasons.

#### 5.2.4 The Ratio of $\text{NO}_3^-/\text{SO}_4^{2-}$

$\text{NO}_3^-$  and  $\text{SO}_4^{2-}$  are formed by gas-particle conversion processes from nitrogen oxides ( $\text{NO}_x$ ) and sulfur dioxide ( $\text{SO}_2$ ) in the atmosphere into particulate phase, respectively. In urban environment, the major emission sources of  $\text{NO}_x$  are fossil fuels combustion and traffic emissions, while the emission of  $\text{SO}_2$  is mainly from the industrial activities (Chan 2008). The ratio of  $\text{NO}_3^-$  to  $\text{SO}_4^{2-}$  has been used as an indicator to identify the relative contributions of the particles from mobile vs stationary sources of N and S (Wang et al., 2006c; Cao et al., 2009). The annual average values of  $\text{NO}_3^-/\text{SO}_4^{2-}$  were  $1.05 \pm 0.57$  and  $1.17 \pm 0.60$  in SH and NJ, respectively, which were higher than that in previous studies in the YRD region, such as 0.43 in Shanghai (Yao et al., 2002) and 0.36 in Hangzhou (Cao et al., 2009), suggesting that the contribution of mobile sources may become more important. As displayed in Fig. 5-18,  $\text{NO}_3^-/\text{SO}_4^{2-}$  ratios were highest in winter, followed by autumn and spring, and lowest in summer. An important factor responsible for the higher ratio of  $\text{NO}_3^-/\text{SO}_4^{2-}$  in winter was the high conversion rate of gaseous nitric acid ( $\text{HNO}_3$ ) to aerosol particles as ammonium nitrate ( $\text{NH}_4\text{NO}_3$ ) under the low temperature in winter. Relatively low  $\text{NO}_3^-/\text{SO}_4^{2-}$  ratios in summer may be due to the higher conversion rate of  $\text{SO}_2$  to  $\text{SO}_4^{2-}$  in summer caused by higher photochemical oxidation ability (Zhao et al., 2013a).

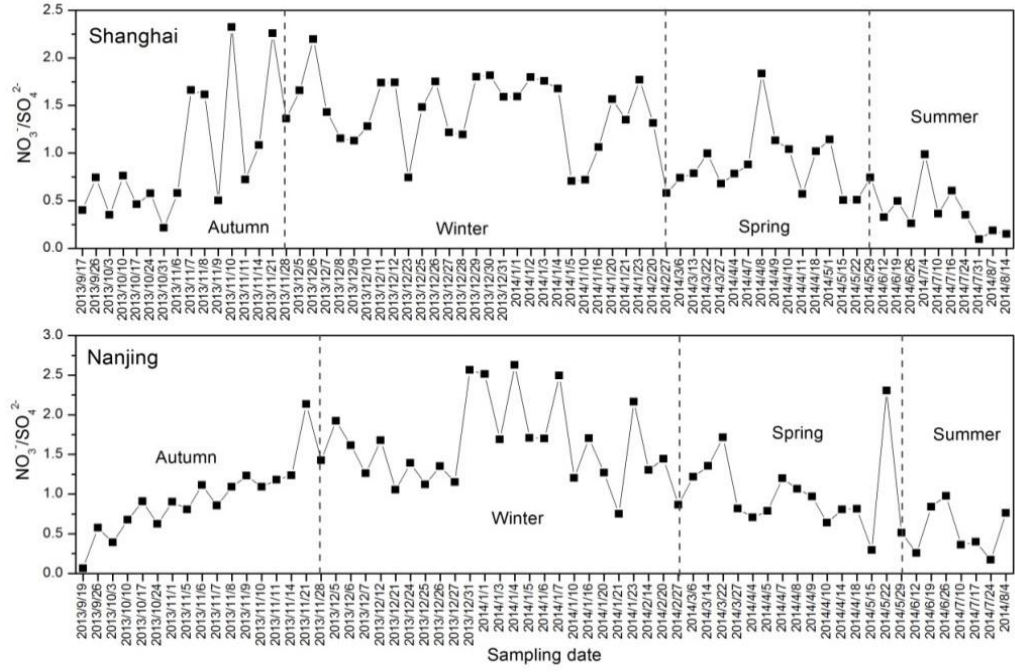


Figure 5-18 Time series of  $\text{NO}_3^-/\text{SO}_4^{2-}$  ratio in Shanghai and Nanjing.

### 5.3 Influent Factors for PM<sub>2.5</sub> Pollution

As discussed above, the three regions are distinguished by the characteristics of PM<sub>2.5</sub>. In this section, three major factors including emission inventories and source contributions for primary atmospheric pollutants, meteorological conditions and long-range transport pathways were investigated to analyze the differences in pollution characteristics of PM<sub>2.5</sub> among Guangzhou, Shanghai and Beijing.

#### 5.3.1 Emission Inventories and Source Contributions for Primary Atmospheric Pollutants

Primary emissions, secondary formation and regional transports are important PM<sub>2.5</sub> sources in the atmosphere. The quantification of primary air pollutant emissions provides strong information on the characteristics of air pollutants. The emission inventories of primary air pollutants from the PRD, the YRD and Beijing were obtained from literature review (Zheng et al., 2009; Huang et al., 2011; Zhao et al., 2012). As shown in Table 5-7, the emissions of SO<sub>2</sub>, NO<sub>x</sub>, VOCs (Volatile Organic Compounds), PM<sub>10</sub> and PM<sub>2.5</sub> in the YRD region in 2007 were 3-7 times greater than those in the PRD region in 2006. In the present study, higher concentrations of PM<sub>2.5</sub> in the YRD than that in the PRD were likely due to the higher emissions of primary PM<sub>2.5</sub> and gaseous pollutants in the YRD. In the YRD region, the highest emission intensities of those air pollutants are located along the banks of the Yangtze River and Hangzhou Bay, such as Nanjing, Shanghai, Ningbo and Hangzhou (Huang et al., 2011). The primary emissions of PM<sub>2.5</sub> ranked in the order of HZ ≈ NJ > SH > NB in 2007 (Table 5-7), which is consistent with the results in this study. Table 5-8 shows that the total emissions of primary atmospheric pollutants (*i.e.*, industrial waste gas, smoke, dust and SO<sub>2</sub>) and the energy consumption and electricity power consumption in 2013 were highest in SH, followed by BJ and GZ. However, other factors such as secondary formation and regional transports of PM<sub>2.5</sub> could influence the pollution status of PM<sub>2.5</sub> in the three cities.

The major emission sources of PM<sub>2.5</sub> and primary air pollutants among the three regions are

different. The expansion of economy in the PRD causes higher demands for energy, mobility, and communications. As a consequence, both coal combustion and traffic exhausts cause serious PM pollution from the urban to regional scale. In the PRD, industrial activities, vehicle exhausts and power plants are the major contributors to local PM<sub>2.5</sub> emissions, accounting for 43.1%, 35.5% and 18.7% of the total PM<sub>2.5</sub> emissions in 2006, respectively (Zheng et al., 2009). In addition, about 91.4% of SO<sub>2</sub> was emitted from power plants and industrial sources, and 87.2% of NO<sub>x</sub> was generated by power plants and mobile sources (Zheng et al., 2009). In contrast with the PRD region, heavy industries including petrochemical industry, automobile manufacturing, and iron and steel production drive the YRD economy. In the YRD, the major sources of local primary air pollutants are from anthropogenic activities including power plants and other fuel combustion facilities, and non-combustion processes, which contribute about 97%, 86%, 89%, 91% and 69% of the total SO<sub>2</sub>, NO<sub>x</sub>, PM<sub>10</sub>, PM<sub>2.5</sub> and VOCs emissions, respectively (Huang et al., 2011). Furthermore, vehicle exhaust contributed 12.3% and 12.4% of the total NO<sub>x</sub> and VOCs emission in the YRD region, respectively (Huang et al., 2011). In Beijing, power plants, domestic heating and industrial sources contributed 49%, 26% and 24% of the total SO<sub>2</sub> emissions; the vehicle exhausts contributed 74% of NO<sub>x</sub> concentrations (Hao et al., 2005). Yu et al. (2013) reported that the sources of PM<sub>2.5</sub> in the urban environment of Beijing were secondary sulfate (26.5%), vehicle exhaust (17.1%), fossil fuel combustion (16%), road dust (12.7%), biomass burning (11.2%), soil dust (10.4%) and metal processing (6.0%). Heavy industries and vehicle exhausts contribute the most of PM<sub>2.5</sub> emissions in the three regions. Fugitive dust including soil and road dust contributed a large fraction of PM<sub>2.5</sub> in BJ, particularly in spring season, which was different from SH and GZ. In this study, the relatively high ratios of crustal elements to PM<sub>2.5</sub> mass, and the distinct seasonal variation with higher concentrations of PM<sub>2.5</sub> and crustal elements in spring in BJ confirmed the large contribution of fugitive dust in PM<sub>2.5</sub> in BJ.

Due to the rapid growth of automobile ownership in China, the contribution of vehicle exhausts to air pollution is more serious in some mega cities. Liu et al. (2007) established a

detailed mobile emission inventory in BJ and SH. They estimated that the daily emissions of particulate matters, NO<sub>x</sub>, VOCs and CO from vehicle exhaust were 3 t, 199 t, 192 t and 2403 t in BJ, respectively, while were 4 t, 189 t, 113 t and 1009 t in SH, respectively. Based on the data from the National Bureau of Statistics of China in 2013 (<http://data.stats.gov.cn/>), the number of civil motor vehicles and private car ownership in BJ (5,170 and 4,241 thousand, respectively) was much higher than those in SH (2,341 and 1,630 thousand, respectively). In GZ, the number of vehicle ownership was 2,146 in 2010 (Guangzhou Environmental Protection, <http://www.gzepb.gov.cn/>). The number of vehicle ownership displayed an increasing trend in the order of GZ < SH < BJ, which can possibly reflect the order of atmospheric pollutants emission from vehicle exhaust because of the different local policy and pollution control performance regarding vehicles.

Table 5-7 Emission inventory (kt) of primary atmospheric pollutants in the PRD, the YRD and Beijing.

Region	Year	SO <sub>2</sub>	NO <sub>x</sub>	PM <sub>10</sub>	PM <sub>2.5</sub>	VOC <sub>s</sub>	Reference
The PRD	2006	711	892	418	205	1180	Zheng et al. (2009)
The YRD	2007	2392	2293	3116	1511	2767	Huang et al. (2011)
	2010	2147	2776	1006	643	3822 <sup>a</sup>	Fu et al. (2013)
Shanghai	2007	399	380	266	119	587	Huang et al. (2011)
Nanjing	2007	221	144	256	130	153	
Hangzhou	2007	126	134	282	129	392	
Ningbo	2007	255	211	212	112	150	
Beijing	2003	187	309	168	90	346 <sup>a</sup>	Zhao et al. (2012)

<sup>a</sup>NMVOCs: Non-methane Volatile Organic Compounds

Table 5-8 Emission of primary atmospheric pollutants and energy consumption in Guangzhou, Shanghai and Beijing during the year of 2013.

2013	Industrial waste gas emission (100 million cu.m)	Total emission of smoke and dust (10000 tons)	Total emission of NO <sub>x</sub> (10000 tons)	Total emission of SO <sub>2</sub> (10000 tons)	Energy consumption (10000 tons SCE)	Electricity power consumption (100 million kwh)
Guangzhou <sup>a</sup>	3754	1.10	5.74	6.33	7083	711
Shanghai <sup>b</sup>	13344	8.09	38.0	21.6	11704	1411
Beijing	-	5.93 <sup>c</sup>	16.6 <sup>c</sup>	8.70 <sup>c</sup>	7354 <sup>d</sup>	913 <sup>d</sup>

<sup>a</sup>Guangzhou Statistical Yearbook 2014, Guangzhou Statistical Bureau ([www.gzstats.gov.cn](http://www.gzstats.gov.cn))

<sup>b</sup>Shanghai Statistical Yearbook 2014, Shanghai Statistical ([www.stats-sh.gov.cn](http://www.stats-sh.gov.cn))

<sup>c</sup>National data, National Bureau of Statistics of China (<http://data.stats.gov.cn/>)

<sup>d</sup>Beijing Statistical Information Net ([www.bjstats.gov.cn](http://www.bjstats.gov.cn))

### 5.3.2 Meteorological Conditions

Generally, the meteorological conditions among the three regions are distinctly different. The PRD region features the subtropical monsoon climate. The prevailing wind direction in the PRD region is from the northeast in winter and from the southeast, south and southwest in summer. The annual wind speed in the coastal cities (such as Hong Kong, with about  $6 \text{ m s}^{-1}$  in 2014) (Hong Kong Observatory, <http://gb.weather.gov.hk/contentc.htm>) was higher than that in the inland cities (such as Guangzhou and Foshan, with about  $2 \text{ m s}^{-1}$ ) (Chan and Yao, 2008). Thus, the inland cities in the PRD region favor the accumulation of air pollutants due to the lower wind speed. The YRD is located on the western coast of the Pacific Ocean and has a subtropical monsoon climate. The movement of East Asia monsoon plays an important role in the transport of pollutants in the YRD (Wang et al., 2008). In winter, the long-range transport of aerosols along with the prevailing northeastern winds could mix with local aerosols in the YRD and make the aerosols more complexed. The winter monsoon is also a main mechanism which moves air pollutants from the YRD to south China and West Pacific ocean. In summer, marine air masses reach the YRD region by passing through the southern part of China under the influence of the Pacific anticyclone. Beijing, located in north China, has a typical continental monsoon climate with four distinct seasons. The prevailing wind in BJ is from the north and northwest in winter and spring, respectively. In spring, BJ is often influenced by Asian dust under the northwest winds (Zhang et al., 2003; Sun et al., 2005).

The meteorological parameters including temperature, precipitation and relative humidity at GZ, SH and BJ during the year of 2013 are summarized in Table 5-9. The annual mean temperature was highest in GZ, followed by SH and BJ. Due to the low temperature in winter, the domestic heating period in BJ usually lasts from the mid-November to the end of the following March by coal combustion. In Beijing, high concentrations of  $\text{PM}_{2.5}$  and chemical compositions in autumn and winter probably attributed to the much increased coal combustion for domestic heating. Although no domestic heating activities in the PRD and YRD, the prevailing northwest winds during the late autumn and winter could bring air

pollutants from North China. Atmospheric wet deposition is one of the important ways to remove particle pollutants from the atmosphere (Sakata et al., 2008; Cong et al., 2010). The removal of atmospheric pollutants by wet deposition depends on particle size, rain duration, rain intensity and their concentrations in the atmosphere (Andronache, 2003; Kulshrestha et al., 2009). In 2013, the annual precipitation was highest in GZ, followed by SH and lowest in BJ. In summer, the dominant southerly wind brings clean marine air masses and abundant precipitation, causing rapid diffusion of air pollution in GZ and SH. Thus, high rainfall capacity and diffusion ability of air pollutants in Guangzhou resulted in the large reduction of atmospheric contaminants.

Table 5-9 Meteorological parameters in the year of 2013 in Guangzhou, Shanghai and Beijing.

Location	Temperature ( °C)			Precipitation <sup>d</sup> (mm)	Annual mean humidity <sup>d</sup> (%)
	Annual mean	Extreme max	Extreme min		
Guangzhou <sup>a</sup>	21.5	37.7	3.3	2095	81.0
Shanghai <sup>b</sup>	17.6	39.9	-4.2	1173	68.0
Beijing <sup>c</sup>	12.8	38.2	-14.1	579	55.0

<sup>a</sup> Guangzhou Statistical Yearbook 2014, Guangzhou Statistical Bureau ([www.gzstats.gov.cn](http://www.gzstats.gov.cn))

<sup>b</sup> Shanghai Statistical Yearbook 2014, Shanghai Statistical ([www.stats-sh.gov.cn](http://www.stats-sh.gov.cn))

<sup>c</sup> Beijing Statistical Information Net ([www.bjstats.gov.cn](http://www.bjstats.gov.cn))

<sup>d</sup> National Bureau of Statistical of the People's Republic of China (<http://www.stats.gov.cn/tjsj/ndsj/2014/indexch.htm>)

### 5.3.3 Impact of Long-range Transport

#### 5.3.3.1. Potential Source Regions

In order to investigate the effects of possible long-range transport of air pollutants, the two-day backward air mass trajectories and clustering analysis in Guangzhou, Shanghai and Beijing were conducted using the HYSPLIT model. The Potential Sources Contribution Function (PSCF) model was further used to identify the potential source regions of  $PM_{2.5}$ .

The clustering results of backward air mass trajectories arriving at GZ during the four seasons are displayed in Fig. 5-19. A total of 144, 124, 136 and 140 two-day backward air mass trajectories during the four seasons were calculated using the HYSPLIT model, respectively, and then classified into several clusters by clustering analysis, respectively. The air masses were mainly come from the northeast that originated from the continental inland areas of central China in winter, while the major air masses were originated from the east of South China Sea in summer. Based on the backward trajectory analysis, maps of potential sources of  $PM_{2.5}$  in GZ during the four seasons are illustrated in Fig. 5-22. The darkness of red cells represents PSCF values. Maps of potential sources of  $PM_{2.5}$  in GZ showed seasonal variations. The central China and the coastal areas of eastern China contributed high  $PM_{2.5}$  to GZ in winter (Fig. 5-22b), while the major potential source regions of  $PM_{2.5}$  were from the coastal areas of southern China and the South China Sea in summer (Fig. 5-22d). A modelling study reported that the annual contributions of  $PM_{10}$  from other regions in China reached 30% in South China, and this transport from external regions was most significant in winter (with contribution of 30-40%) (Li et al., 2014), which confirmed our PSCF results during the winter. In summer, the less external regional transport in South China (Li et al., 2014) and the prevailed southerly wind from the ocean could weaken the air pollution in GZ.

In Shanghai, the results of the long-range transport pattern of backward air mass trajectories exhibited a clear seasonal pattern (see Fig. 5-20). In winter, the air masses arriving in Shanghai were mainly from the northwest that originated from the continental inland areas

of northern China and travelled along the east coastal area of China. In contrast, the air masses arriving in Shanghai were mainly from the sea including the South China Sea and the East China Sea and the eastern coastal area of China during summer. PSCF results identified that the areas of central China including Henan, Hubei and Anhui Province, and North China were the important potential source regions of  $PM_{2.5}$  during winter (Fig. 5-23b). Li et al. (2014) also denoted that central China, the North China Plain and northeast China contributed 16.0%, 9.4% and 6.5% of  $PM_{10}$  mass concentrations in eastern China in winter, respectively. The intensive emission of air pollutants from coal combustion for heating in North China (Zhao et al., 2013a) and high  $PM_{2.5}$  pollution in central China during winter (Cao et al., 2012) could contribute to the increase of  $PM_{2.5}$  and other air pollutants in SH. In summer, the dominant source regions of  $PM_{2.5}$  were from the East China Sea and the east coastal area of China (Fig. 5-23d), which brought clean marine air masses and abundant precipitation to dilute the air pollution. As a consequence, relatively lower concentrations of chemical components for  $PM_{2.5}$  were observed in summer in the YRD.

In Beijing, the seasonal variations of clustering analysis of backward air masses were displayed in Fig. 5-21. In winter and spring, the long-range transport of air masses was mainly come from the northern China and the Inner Mongolia. In summer, the long-range transport of air masses was dominated from the south that originated from the continental inland areas of Tianjin, Hebei and Shandong Province. Clear seasonal variations were found in the distribution of potential source regions. PSCF results illustrated that the northern China and Mongolia were the important potential source regions of  $PM_{2.5}$  during winter (Fig. 5-24b). The occurrence of northwest winds in spring brought dust and air pollutants from the Gobi desert and the Junggar Basin to BJ (Fig. 5-24c). In summer,  $PM_{2.5}$  in north central China including Tianjin, Hebei Province, Shandong Province and the north part of east China transported northward into BJ (Fig. 5-24d). The regional transport of  $PM_{10}$  in north central China was studied using a model by Li et al. (2014). They found that north central China is the major receptor of trans-boundary transport within China, with 27.5% of annual contributions from other regions in China. They also estimated that the contribution of  $PM_{10}$

from east China to north central China reached 9.4% and 11.6% in winter and summer, respectively.

Results of cluster analysis of backward air mass trajectory and PSCF analysis showed that the potential source regions of PM<sub>2.5</sub> in the three cities were seasonally dependent, due to the specific monsoon climate over the three cities. The contributions of PM<sub>2.5</sub> via the long-range transport were more significantly in winter, confirming the high concentrations of PM<sub>2.5</sub> in winter. The results also indicated the trans-boundary transport of PM<sub>2.5</sub> among the three regions. In winter, the PRD region was the receptor of transport from the coastal areas of the YRD region, while the YRD region was the receptor of transport from North China. In summer, the transport occurred from the YRD region to North China. It was reported that East China was the most influential source, due to its largest emission and its location where northwest/northeast winds in winter are capable of transporting air pollutants to South China and southeast winds in summer favor the transport of air pollutants to North China (Li et al., 2014).

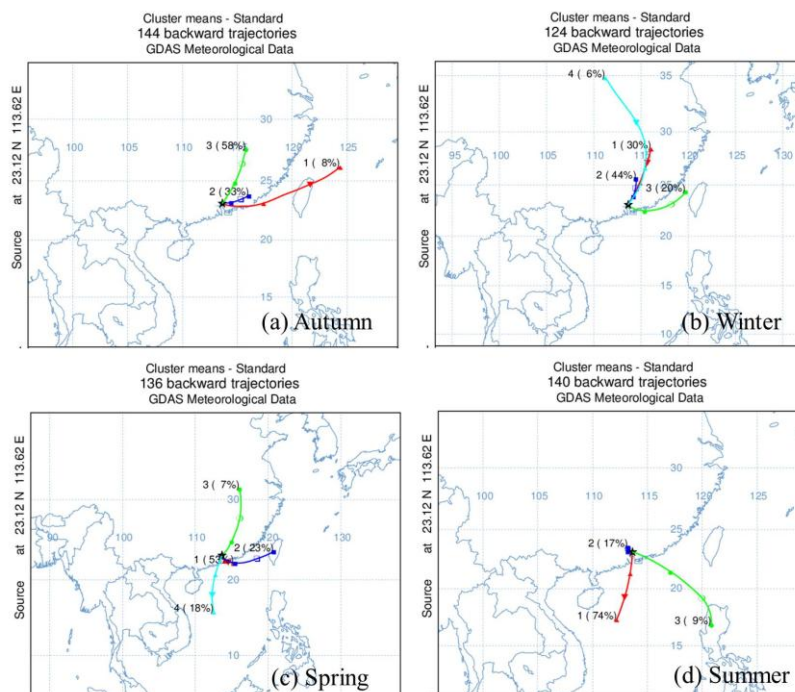


Figure 5-19 Cluster analysis of two-day backward trajectories of air masses during the four seasons in Guangzhou.

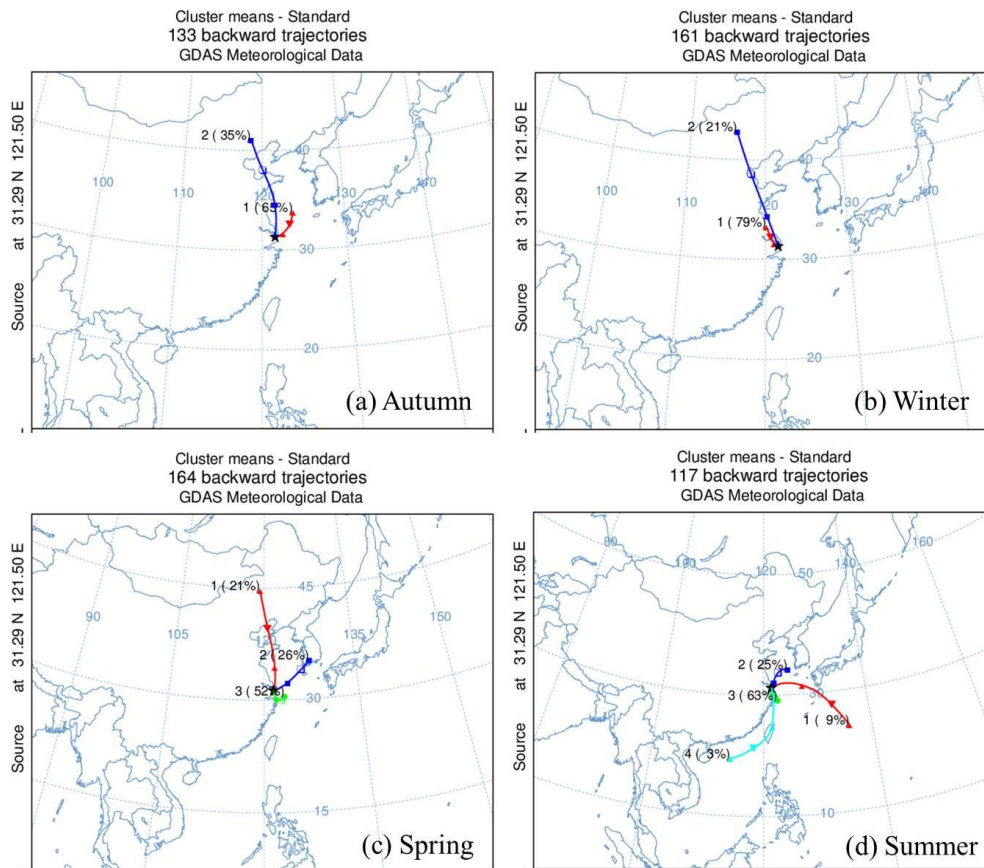


Figure 5-20 Cluster analysis of two-day backward trajectories of air masses during the four seasons in Shanghai.

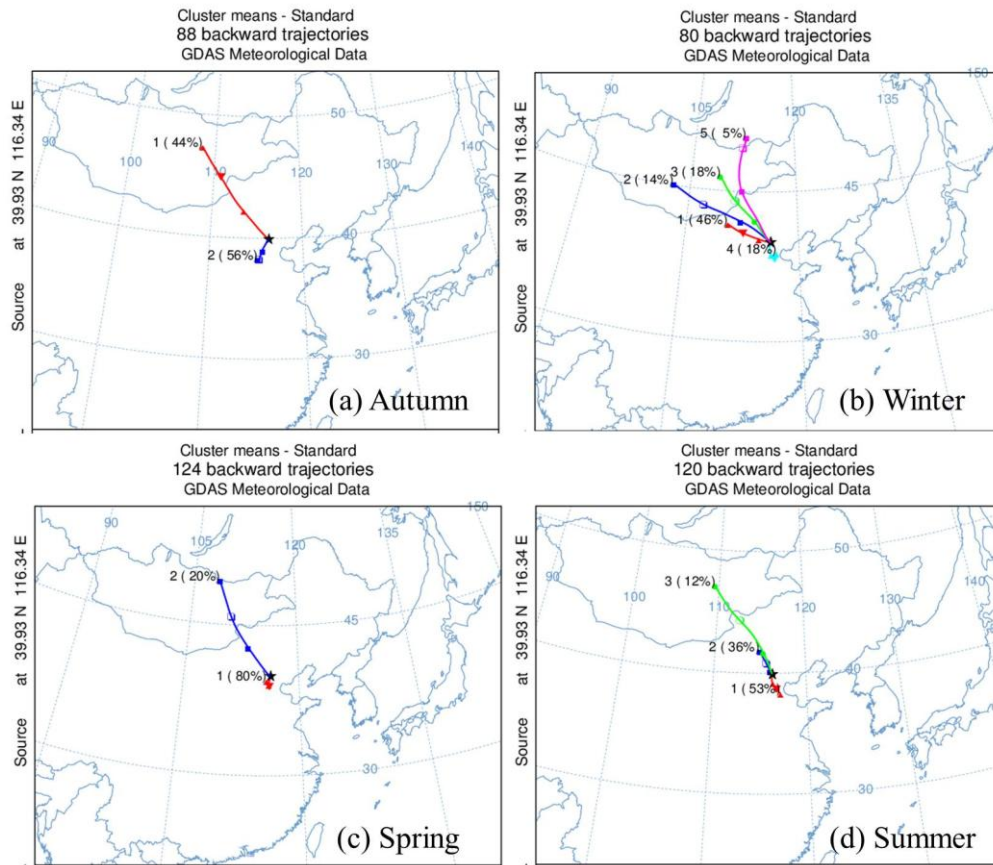


Figure 5-21 Cluster analysis of two-day backward trajectories of air masses during the four seasons in Beijing.

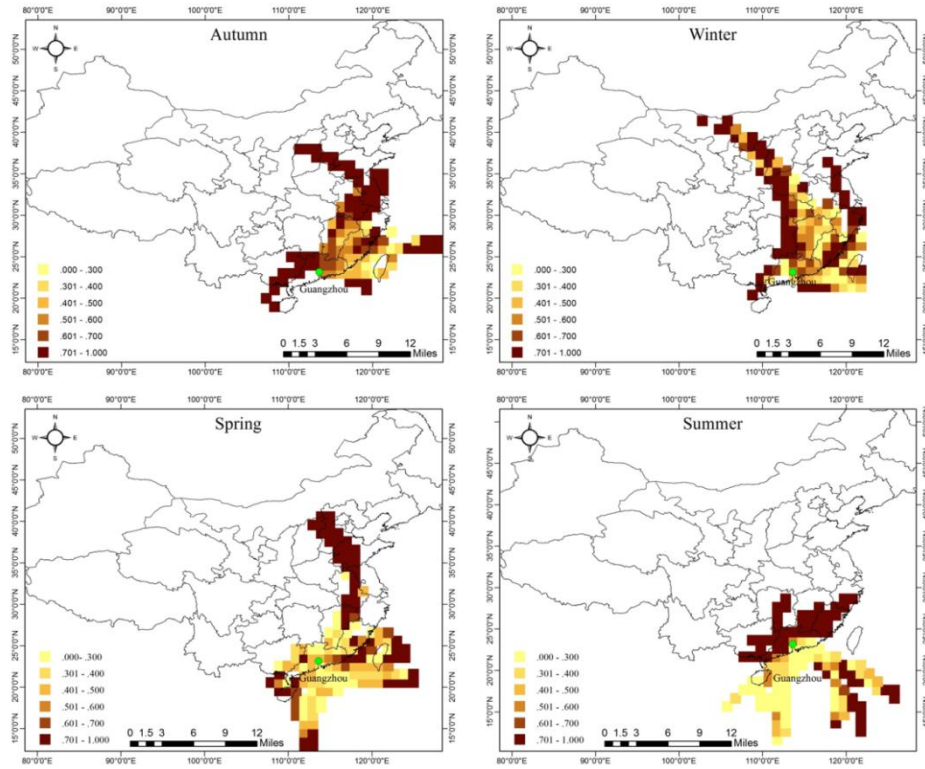


Figure 5-22 Maps of potential sources of PM<sub>2.5</sub> in Guangzhou during the four seasons. The darkness of red cells represents PSCF values.

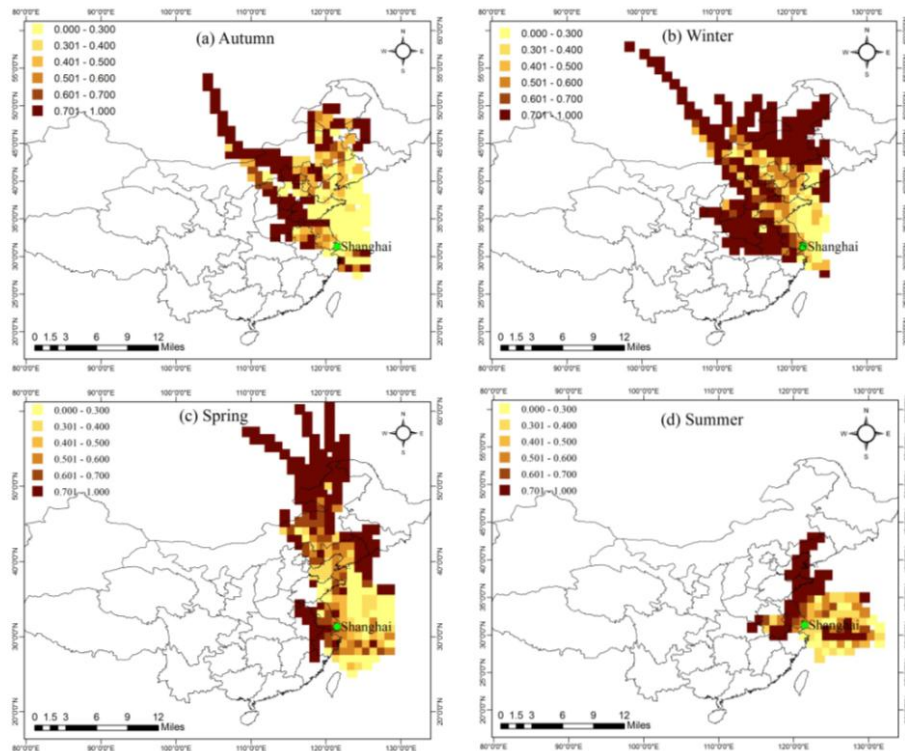


Figure 5-23 Maps of potential sources of PM<sub>2.5</sub> in Shanghai during the four seasons.

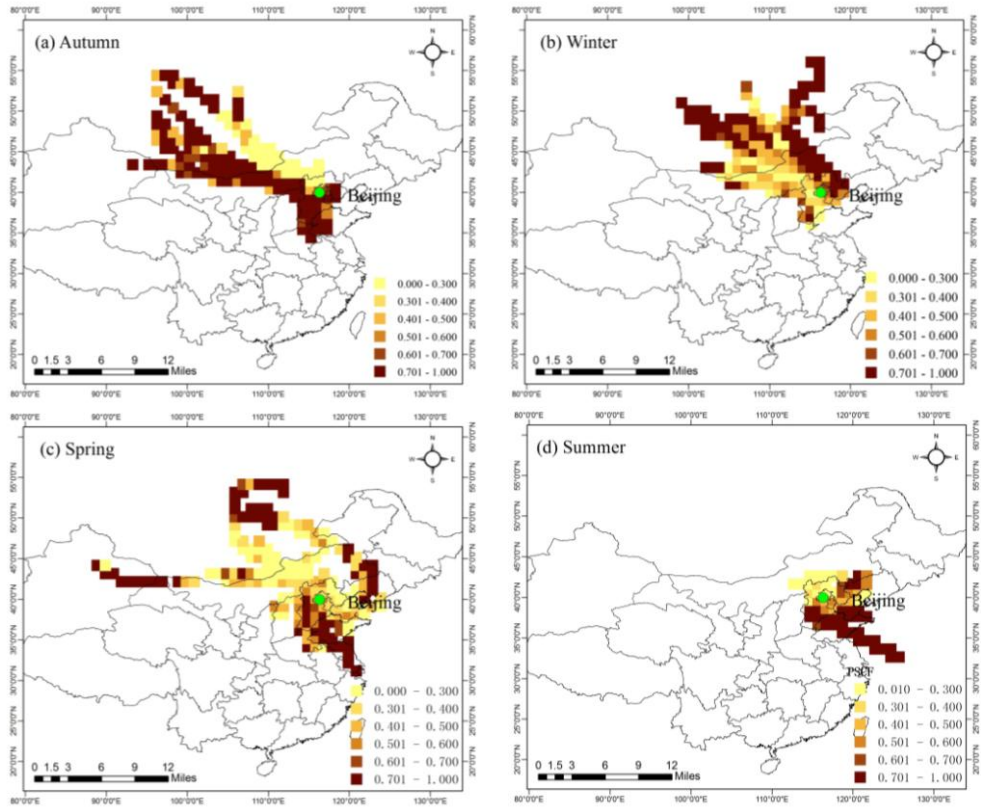


Figure 5-24 Maps of potential sources of PM<sub>2.5</sub> in Beijing during the four seasons.

### 5.3.3.2. Long-range Transport of Pb

As discussed above, long-range transport probably contributed the trans-boundary transport of  $PM_{2.5}$  in the three regions. Lead isotopic ratios have been used in assessing the long-range transport of anthropogenic Pb (Hsu et al., 2006; Lee et al., 2007). Thus, Pb isotopic fingerprinting was analyzed to investigate the possible long-range transport of  $PM_{2.5}$  in the three regions in this section.

The annual means of Pb isotopic ratios from the nine sampling sites are plotted in Fig. 5-25. The ratios of  $^{206}Pb/^{207}Pb$  in BJ and CBS were lower than that in the PRD and YRD regions, while no significant differences were found between the PRD and the YRD regions. The differences of lead isotope fingerprinting in the atmosphere among the three regions are related to the sources of Pb and the contribution of each source. Results in section 5.2.2 demonstrated that the major sources of atmospheric Pb were coal combustion and industrial activities in the three regions. Chinese coal has been reported to have wide variations in  $^{206}Pb/^{207}Pb$  ratios (1.14-1.22) (Mukai et al., 2001). The ratios of  $^{206}Pb/^{207}Pb$  for coal combustion ash were 1.1732 and 1.1633 in GZ and SH, respectively (Zhu et al., 2001; Tan et al., 2006), and were reported to have large variations ( $^{206}Pb/^{207}Pb$ : 1.1545-1.1763) in BJ (Widory et al., 2010). As plotted in Fig. 5-26, Pb isotopic ratios of coal combustion ash varied in China, with higher values in Guizhou Province of southwest China and lower values in Hebei Province of North China. The results showed that Pb isotopic compositions of coal combustion ash in North China were clearly different from Guangzhou, Shanghai, Hubei Province and Guizhou Province. Data from GZ and SH was closer to that in Hubei Province of central China and North China, respectively.

In this study, lower ratios of  $^{206}Pb/^{207}Pb$  and concentration of Pb in BJ and CBS during winter (Fig. 5-16) reflected that the contribution of coal combustion to atmospheric Pb was increased, which were likely due to the long-range transport from the potential source regions in North China. In Fig. 5-14, relatively higher concentrations of airborne Pb ( $> 1788 \text{ mg kg}^{-1}$ , in the

range of coal combustion level) and higher  $^{206}\text{Pb}/^{207}\text{Pb}$  ratios were observed in winter in the PRD region. Higher  $^{206}\text{Pb}/^{207}\text{Pb}$  ratios in winter in the PRD region confirmed the long-range transport of Pb from the central China and the coastal areas of eastern China where the  $^{206}\text{Pb}/^{207}\text{Pb}$  ratios were relatively high in coal combustion ash. In Fig. 5-15, relatively higher concentrations of airborne Pb ( $> 1788 \text{ mg kg}^{-1}$ , in the range of coal combustion level) and higher  $^{206}\text{Pb}/^{207}\text{Pb}$  ratios were observed in winter in the YRD region, which indicated the inputs of atmospheric Pb from coal combustion from the potential source regions of central China. The results implied large inputs of atmospheric Pb from coal combustion in the PRD and YRD regions during winter. Pb isotope signatures in  $\text{PM}_{2.5}$  showed strong evidence of inputs of atmospheric Pb from coal combustion via long-range transport in winter in the three regions.

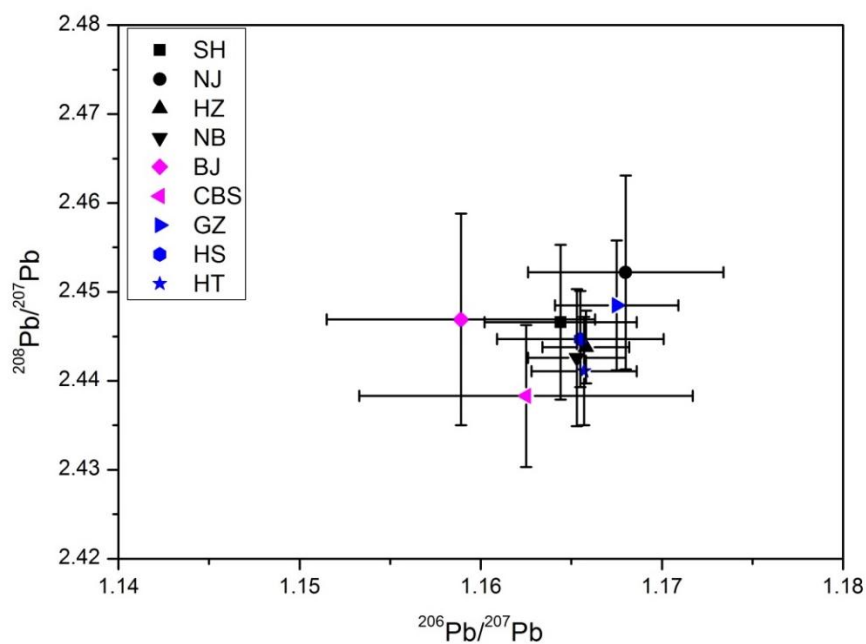


Figure 5-25 Comparison of annual means of Pb isotopic ratios in PM<sub>2.5</sub> from the nine sampling sites.

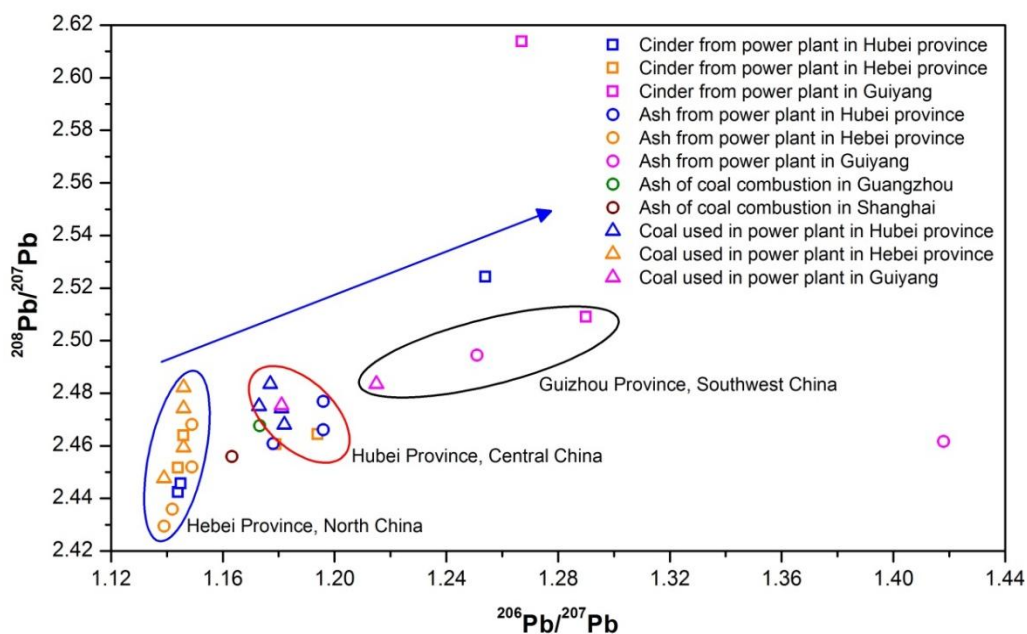


Figure 5-26 Lead isotopic compositions of coal samples, cinder samples and ash samples from power plants in China (the dataset were provided by Dr. Xiangyang Bi from the State Key Laboratory of Biogeology and Environmental Geology, China University of Geosciences, Wuhan).

## 5.4 Summary

Clear seasonal variations in the mass concentrations and chemical compositions of  $PM_{2.5}$  were observed in the nine sampling sites over the three regions. In the PRD region, the concentrations of  $PM_{2.5}$  and airborne trace metals were highest in winter and lowest in summer. In Guangzhou, higher concentrations of OC and SOC were found in winter, while no significant seasonal variation was found for EC concentrations. In the YRD region,  $PM_{2.5}$  and ambient trace metals showed higher concentrations in winter and lower concentrations in summer. Similar seasonal pattern was found for OC, EC, and water-soluble inorganic ions in Shanghai. In Beijing and Mount Changbai from North China,  $PM_{2.5}$  and airborne crustal elements were higher in spring, while the concentrations of most trace elements were higher in winter. Obvious temporal variations in the concentrations of OC, EC and SOC were observed in Beijing, with highest in winter and spring and lowest in summer.

Enrichment factors indicated the large inputs of atmospheric sources of airborne trace metals in the three regions during winter. Pb isotopic analysis suggested that the major sources of atmospheric Pb in the three regions are coal combustion and industrial activities, and large inputs of atmospheric Pb from coal combustion in winter in the three regions. High ratios of OC/EC in GZ, SH and BJ showed the relatively high concentrations of SOC. High  $NO_3^-/SO_4^{2-}$  ratios in SH and NJ indicated that more  $NO_x$  were released mainly due to vehicular emissions. Source appointment of chemical compositions of  $PM_{2.5}$  demonstrated that anthropogenic sources including coal combustion, heavy industries and traffic emissions are the major contributors to  $PM_{2.5}$  in the three regions.

Different characteristics in the concentrations and temporal-spatial variations of  $PM_{2.5}$  were driven by their local emissions, seasonal meteorological conditions and long-range transport pathways, which were distinctly different in the three regions. The total emissions of primary atmospheric pollutants and the energy consumption and electricity power consumption in 2013 were highest in SH, followed by BJ and GZ. Heavy industries and vehicle exhausts

were the major emission sources of  $PM_{2.5}$  in the three regions; and the contribution of fugitive dust to  $PM_{2.5}$  was more significant in BJ. Furthermore, the number of vehicle ownership showed an increasing trend in the order of GZ < SH < BJ. These results provide important basis for the temporal and spatial variations of  $PM_{2.5}$  in the three regions. In BJ, high concentrations of  $PM_{2.5}$  in autumn and winter were likely due to the much increased coal combustion for domestic heating to resist the low temperature. High rainfall capacity and diffusion ability of air pollutants in GZ benefit the elimination of contaminants in the atmosphere, which are important contributors to the relatively low concentrations of  $PM_{2.5}$  in GZ. Results of backward trajectory analysis and the PSCF model showed that the long-range transport of  $PM_{2.5}$  from other source regions was seasonally dependent due to the specific energy consumption and monsoon climate in GZ, SH and BJ. Moreover, Pb isotope signatures in  $PM_{2.5}$  further confirmed the inputs of atmospheric Pb from coal combustion via long-range transport in the three regions.

## **Chapter 6 - Regional Transport of PM<sub>2.5</sub> in China: Analysis of Pollution Events**

To further investigate the trans-boundary transport of PM<sub>2.5</sub> among the PRD, the YRD and North China, both simultaneous field observations and NAQPMS model were used during a typical regional pollution event that occurred over most areas of East and South China, and the North China Plain. The formation mechanism, evolution and regional transport of PM<sub>2.5</sub> in three pollution events in Shanghai were discussed by studying the characteristics of chemical compositions and sources of PM<sub>2.5</sub>, meteorological conditions, and trans-boundary transport of PM<sub>2.5</sub>.

### **6.1 A Modeling Study of Regional Transport of PM<sub>2.5</sub> during a Severe and Long-lasting Pollution Event**

A severe and long-lasting pollution event occurred over most areas of East and South China, and the North China Plain from 2 to 14 December 2013. Observation results showed high PM<sub>2.5</sub> pollution in the PRD and YRD regions, and Beijing during this period. In this study, a 3-D chemical transport model, NAQPMS (Nested Air Quality Prediction Modeling System), was applied to simulate the evolution and regional transport of PM<sub>2.5</sub> over China, typically in the three regions.

#### **6.1.1 Air Quality during the Pollution Event**

Although PM<sub>2.5</sub> samples were only collected daily in Shanghai during the pollution period, the daily PM<sub>2.5</sub> concentrations were obtained from the network of air quality monitoring stations from Beijing and the cities in the PRD and YRD regions (<http://www.cnpm25.cn/>). Daily average PM<sub>2.5</sub> concentrations in Guangzhou, Jiangmen (Heshan), Shanghai, Nanjing, Hangzhou, Ningbo and Beijing during the pollution event are displayed in Fig. 6-1. In the PRD region, PM<sub>2.5</sub> concentrations reached to more than 100  $\mu\text{g m}^{-3}$  from 3 to 13 December 2013 in Guangzhou and Jiangmen. In the YRD region (Shanghai, Nanjing, Hangzhou and

Ningbo),  $PM_{2.5}$  concentrations were more than  $200 \mu\text{g m}^{-3}$  during 2-8 December, and then dramatically declined and remained at more than  $100 \mu\text{g m}^{-3}$  after 9 December 2013. Our field observations also showed that  $PM_{2.5}$  daily concentrations reached their peak value on 6 December, with 395, 246, 264 and  $216 \mu\text{g m}^{-3}$  in Shanghai, Nanjing, Hangzhou and Ningbo, respectively, both far exceeded the limit of the NAAQS standard II (daily limit of  $75 \mu\text{g m}^{-3}$ ). In Beijing, an increasing period for  $PM_{2.5}$  concentration occurred from 6 to 8 December.  $PM_{2.5}$  concentration in Beijing reached to the peak value of  $241 \mu\text{g m}^{-3}$  on 7 December. Compared with the PRD region and Beijing,  $PM_{2.5}$  pollution was more serious in the YRD region during this pollution event.

The satellite image confirmed the severity of visibility on 7 December 2013 in Eastern China (Fig. 6-2). For example, as shown in Fig. 6-3, the daily average visibility in Shanghai was less than 5 km from 5 to 10 December. After that, it was still less than 10 km during most of the sampling time. The visibility decreased with the increase of  $PM_{2.5}$ , and the visibility dropped to  $< 1$  km on 6 December when the  $PM_{2.5}$  increased to the peak value. This severe pollution event displayed the typical characteristics of high concentrations of  $PM_{2.5}$  and low visibility in the three regions.

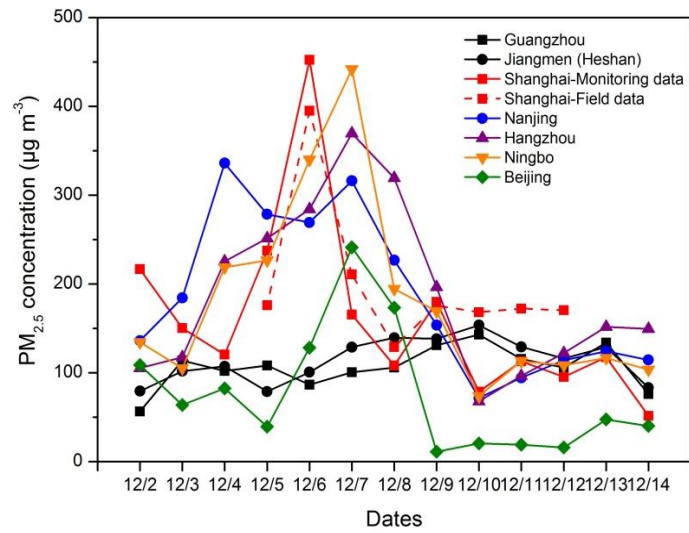


Figure 6-1 Daily average PM<sub>2.5</sub> concentrations ( $\mu\text{g m}^{-3}$ ) in Guangzhou, Jiangmen (Heshan), Shanghai, Nanjing, Hangzhou, Ningbo and Beijing during the pollution event.

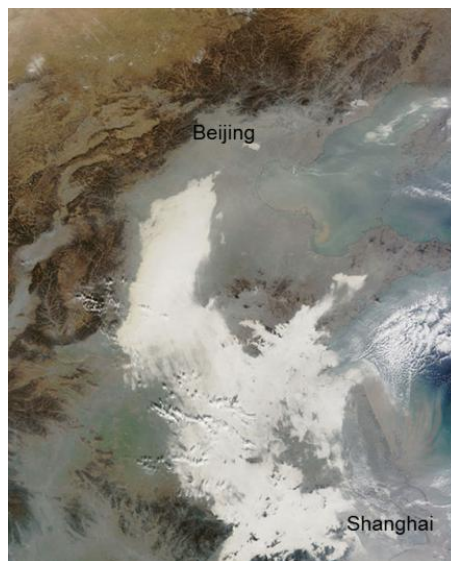


Figure 6-2 Satellite image on 7 December 2013 in Eastern China (<http://earthobservatory.nasa.gov/NaturalHazards/view.php?id=82535>).

### 6.1.2 Meteorological Conditions

Meteorological conditions often play a key role on the formation of pollution episode (Fu et al., 2008; Kang et al., 2013). Since  $PM_{2.5}$  pollution was severe in the YRD region, the meteorological conditions in Shanghai were typically analyzed to evaluate the relationship between the meteorological conditions and the formation of pollution event. The surface meteorological parameters including wind speed, wind direction, relative humidity and temperature in Shanghai during the pollution episode are plotted in Fig. 6-3. During the heavily polluted period (from 5 to 8 December), the surface winds were from various directions and the wind speeds were relatively low (less than  $2 \text{ m s}^{-1}$ ) and even stagnant sometimes, which were limited the dispersion of air pollutants. Meanwhile, the relative humidity (RH) and temperature was high. Moreover, both surface and upper-level (from 750 to 650 hPa) temperature inversion were evident in the sounding data in SH on 6 December (Fig. 6-4), decreasing the vertical mixing of air. The stable meteorological conditions with low wind speed, high RH, temperature inversion and no precipitation enhanced the accumulation of air pollutants during the episode. After 9 December, due to a cold front affecting the YRD region (Wang et al., 2015), the wind speeds increased while RH and temperature decreased, contributing the decline of  $PM_{2.5}$  concentration and the increase of visibility in Shanghai. When the cold air ended on 12 December,  $PM_{2.5}$  concentrations obviously increased over the YRD region until 14 December. After 15 December, the air pollution was alleviated by the heavy rainfall in the PRD and YRD regions.

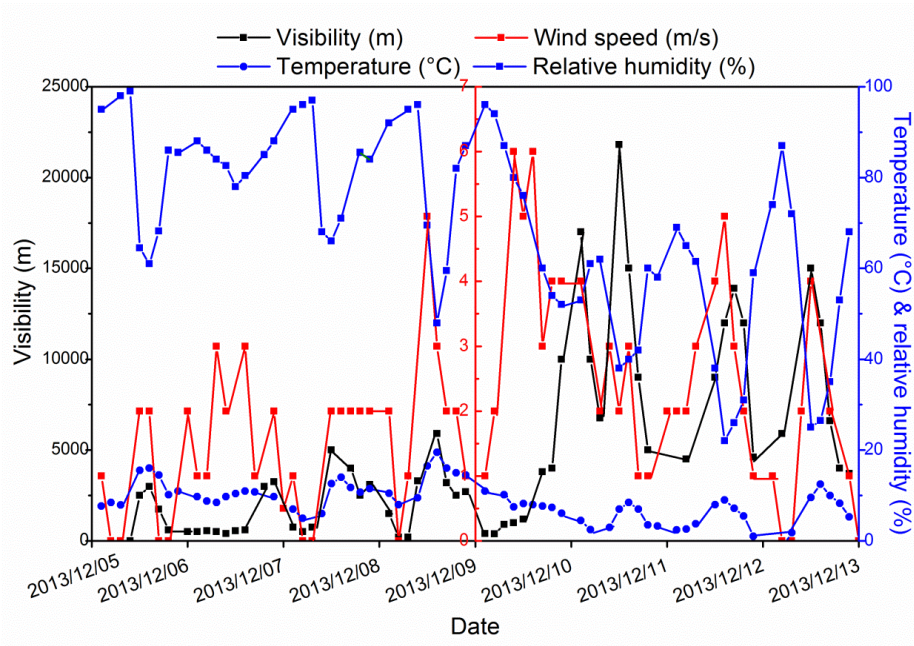


Figure 6-3 Surface meteorological conditions from 5 to 12 December 2013 in Shanghai from the monitoring station (31.4N, 121.47E) (Real-time data display from ENVF Atmospheric & Environmental Real-time Database: <http://envf.ust.hk/>).

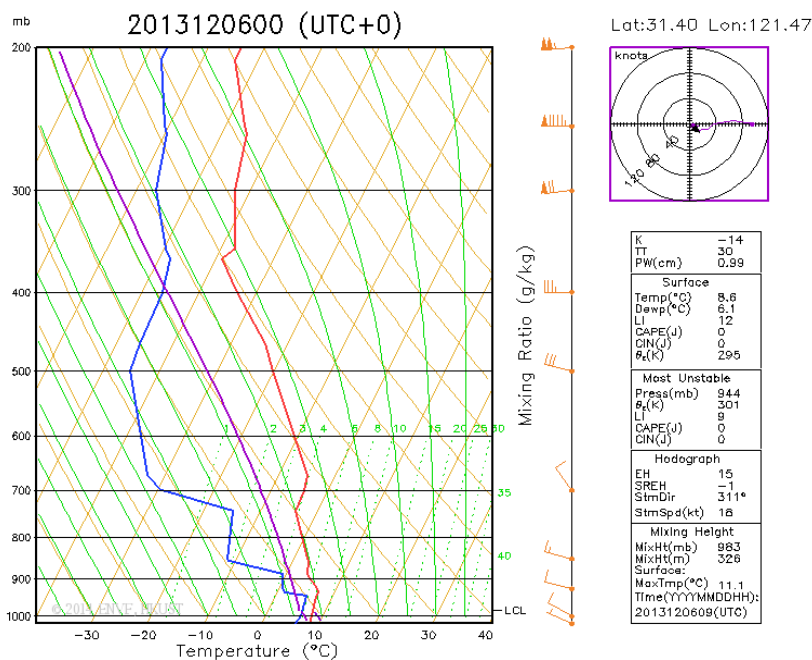


Figure 6-4 Vertical sounding plots on 6 December 2013 in Shanghai from the monitoring station (31.4N, 121.47E) (Real-time data display from ENVF Atmospheric & Environmental Real-time Database: <http://envf.ust.hk/>) (the blue line represents dew point and the red line represents temperature).

### 6.1.3 The Evolution and Regional Transport of PM<sub>2.5</sub>-Modeling Results

The simulated daily average of surface PM<sub>2.5</sub> concentration and wind field over China during the processes of pollution event are displayed in Fig. 6-5. On 5 December, heavy PM<sub>2.5</sub> region with more than 300  $\mu\text{g m}^{-3}$  located over the YRD region and eastern China (Fig. 6-5a). At the same time, high PM<sub>2.5</sub> region with more than 100  $\mu\text{g m}^{-3}$  occurred in the PRD region and South China, while the simulated PM<sub>2.5</sub> concentration was low in Beijing. The simulated surface PM<sub>2.5</sub> concentrations were consistent with the observation results over the PRD and YRD regions and Beijing. On 7 December, PM<sub>2.5</sub> concentrations were still high over the YRD region due to the stable wind field. However, the strong south wind prevails over Northeast China, driving the movement of polluted air masses from the north part of Eastern China to Beijing (Fig. 6-5b). The prevailing northeast winds in the PRD region contributed the transport of high PM<sub>2.5</sub> from the central China and coastal areas of the YRD region to the PRD region. The modelling results showed the transport of PM<sub>2.5</sub> from the YRD region to the PRD region and Beijing during 7-8 December.

On 9 December, the strong north wind prevailed over North, East and South China, driving the movement of high PM<sub>2.5</sub> region from North China to South China (Fig. 6-5c). Thus, the YRD region was the receptor of movement from North China, and the PRD region was the receptor of transport from the YRD region. On 11 December, PM<sub>2.5</sub> pollution over the YRD and Beijing has gradually weakened due to the effect of cold air, while high PM<sub>2.5</sub> region still located over the PRD (Fig. 6-5d). When the cold air ended on 12 December, PM<sub>2.5</sub> concentrations obviously increased over the YRD region until 14 December (Fig. 6-5e and f). After the pollution event, PM<sub>2.5</sub> pollution decreased over the PRD and YRD regions due to the effect of rainfall. The modelling results clearly illustrated the trans-boundary transport of PM<sub>2.5</sub> among the PRD and YRD regions and Beijing during this pollution event.

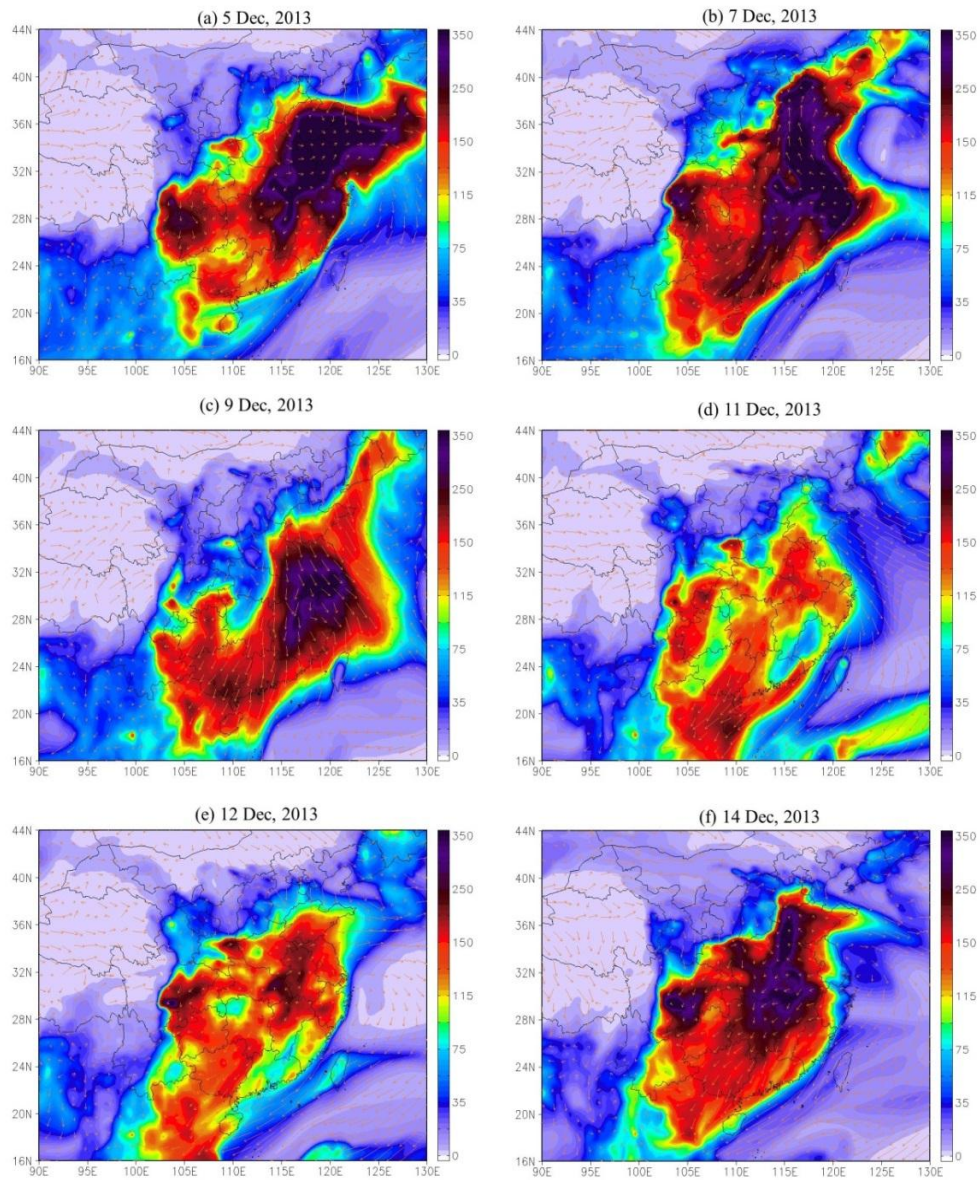


Figure 6-5 The simulated daily average of surface PM<sub>2.5</sub> concentration ( $\mu\text{g m}^{-3}$ ) and wind vector ( $\text{m s}^{-1}$ ) in China during the severe pollution event: (a) on 5 December 2013; (b) on 7 December 2013; (c) on 9 December 2013; (d) on 11 December 2013; (e) on 12 December 2013; and (f) on 14 December 2013.

## 6.2 Formation Mechanisms of Pollution Events in the YRD Region

Based on the field observation in the YRD region, pollution days with high  $PM_{2.5}$  concentrations were occurred more frequently during the autumn and winter. As shown in Fig. 6-6, three periods with high  $PM_{2.5}$  concentrations were simultaneously observed in SH and NJ. In this section, the evolution and transport of  $PM_{2.5}$  and formation mechanisms of pollution events in Shanghai will be studied using the observations and model results.

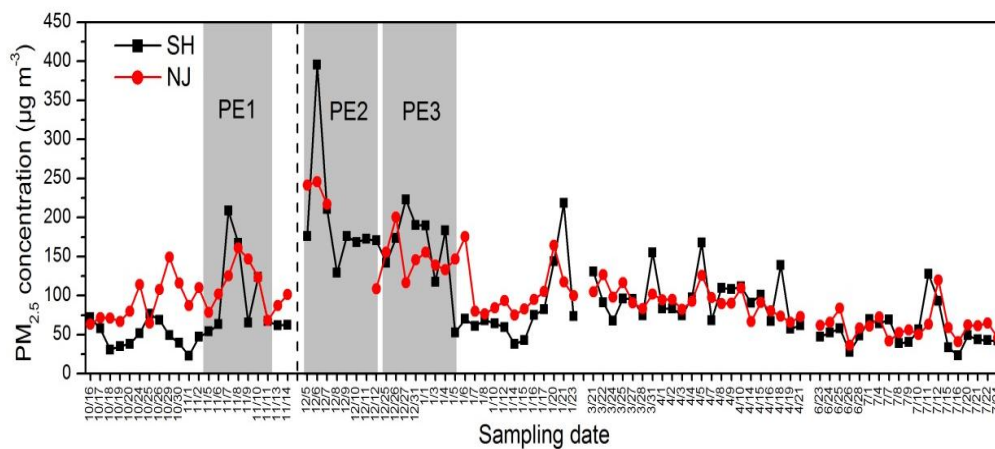


Figure 6-6 Temporal variations of  $PM_{2.5}$  concentrations for the samples collected in Shanghai and Nanjing during high frequency sampling period. PE 1 = pollution event 1; PE 2 = pollution event 2 and PE 3 = pollution event 3.

### 6.2.1 Identification of Three Pollution Events in the YRD Region

Based on the  $PM_{2.5}$  concentration (Fig. 6-7), visibility (Fig. 6-8) and relative humidity (Fig. 6-9), three pollution events were identified. During most of the sampling time over the three pollution events, the visibility were less than 10 km and the relative humidity were lower than 80%. **Pollution Event 1:** The process of first pollution event occurred from 5 to 11 November 2013, which can be divided into before pollution event period (BPE1 period: 5-6 November), pollution event period (PE1 period: 7-8 November) and after pollution event (APE1 period: 9-11 November) (Fig. 6-7). During PE1, the daily  $PM_{2.5}$  concentrations on 7 November were 209, 125, 152 and 187  $\mu g m^{-3}$  in Shanghai, Nanjing, Hangzhou and Ningbo,

respectively, which were 2-3 times higher than those during BPE1 and APE1 periods. As shown in Fig. 6-8a, there was an obvious decrease of visibility during PE1, and the minimum visibilities in PE1 were less than 6 km. **Pollution Event 2:** A severe and long-lasting pollution event (PE2) occurred in the YRD region from 5 to 12 December 2013. In Shanghai, PM<sub>2.5</sub> concentrations increased from 176 µg m<sup>-3</sup> on 5 December to the peak value of 395 µg m<sup>-3</sup> on 6 December, and then decreased at 129 µg m<sup>-3</sup> on 8 December. After that, the concentrations of PM<sub>2.5</sub> kept at about 170 µg m<sup>-3</sup>. The visibility in Shanghai was less than 5 km from 5 to 10 December, and less than 10 km after 10 December. **Pollution Event 3:** The process of third pollution event can be divided into before pollution event period (BPE3 period: 22-24 December 2013), pollution event period (PE3 period: 25 December 2013-4 January 2014) and after pollution event period (APE3 period: 5-7 January 2014). The average concentrations of PM<sub>2.5</sub> during PE3 were 182 µg m<sup>-3</sup> in Shanghai, and 2-3 times greater than that during BPE3 and APE3 periods. The visibility in SH were less than 10 km during PE3. The three pollution events in Shanghai displayed high concentrations of PM<sub>2.5</sub> and low visibility. The PE1 lasted a short period for 2 days, and the peak value of PM<sub>2.5</sub> concentrations were relatively low compared with the other two events. A fast accumulation of PM<sub>2.5</sub> and low visibility were observed in PE2. The PE 3 had a long duration with 10 days.

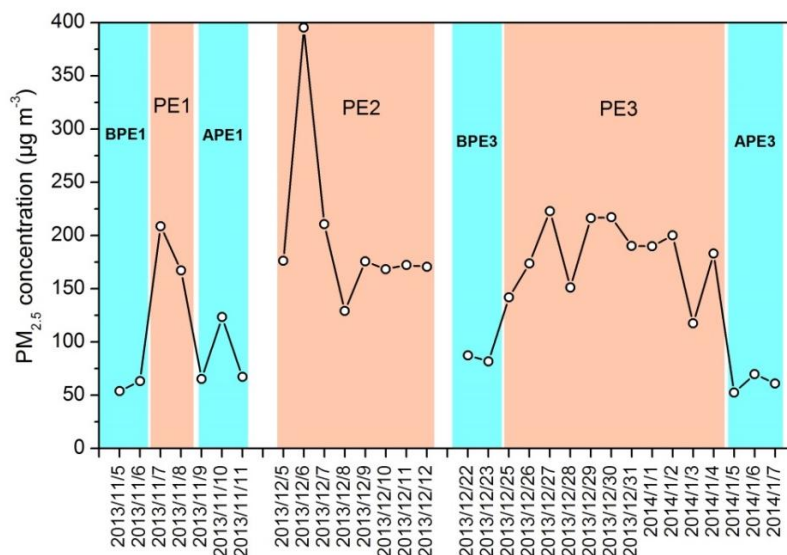


Figure 6-7 Time series of PM<sub>2.5</sub> concentrations in Shanghai during the processes of the three pollution events.

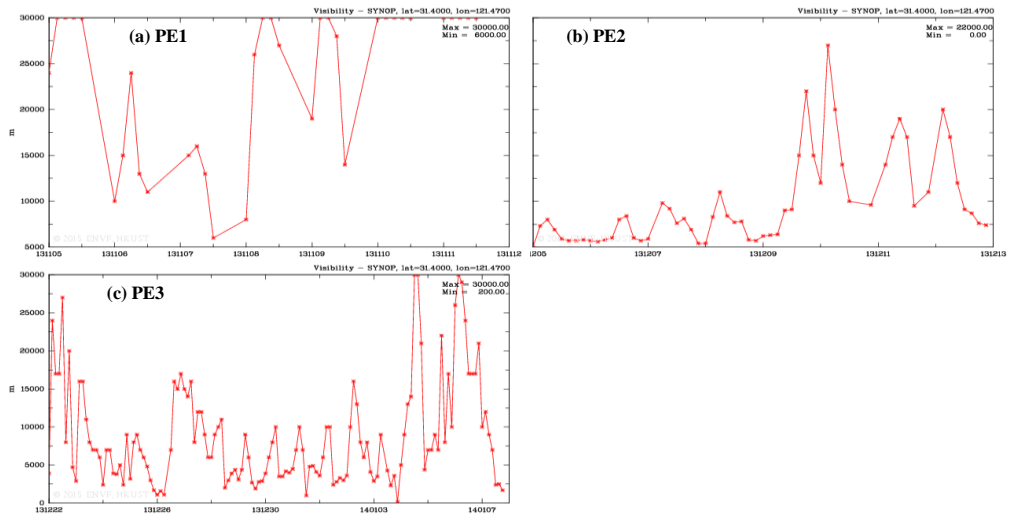


Figure 6-8 Time series of visibility in the monitoring station (31.4N, 121.47E) during the three pollution events (Real-time data display from ENVF Atmospheric & Environmental Real-time Database: <http://envf.ust.hk/>).

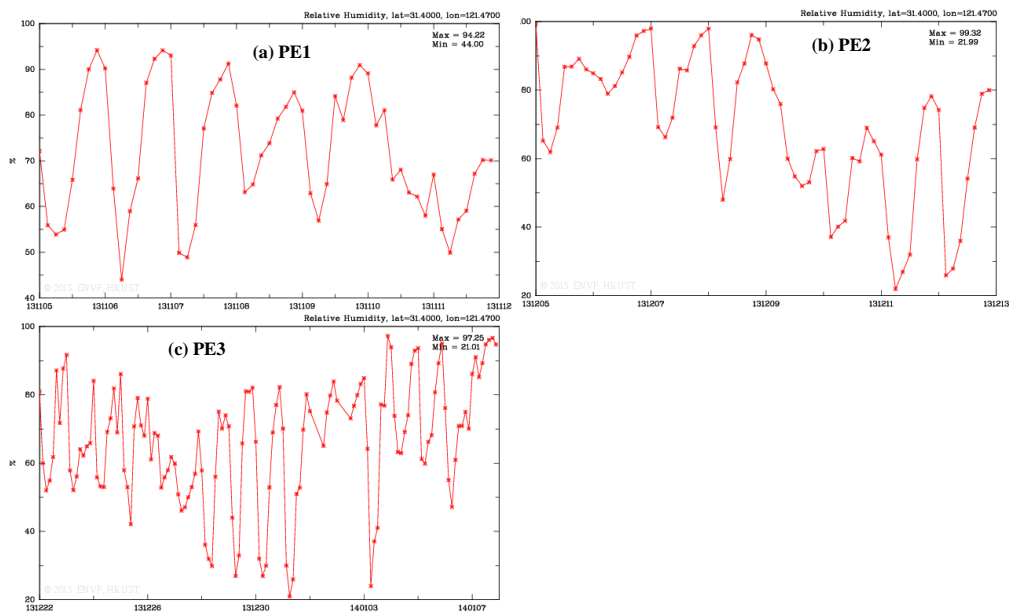


Figure 6-9 Time series of relative humidity in the monitoring station (31.4N, 121.47E) during the three pollution events (Real-time data display from ENVF Atmospheric & Environmental Real-time Database: <http://envf.ust.hk/>).

### 6.2.2 Meteorological Conditions during Three Pollution Events

The surface meteorological parameters including wind speed, wind direction and temperature in Shanghai during the three pollution events are plotted in Fig. 6-10. During PE1, the unstable wind directions and relatively low wind speeds were not beneficial the dispersion of air pollutants. Air mass backward trajectories were used to study the air mass transport characteristics. As shown in Fig. 6-11a, one-day backward trajectories of air masses arrived at SH during PE1 from the inland areas of Jiangsu and Anhui Province, which different from BPE1 and APE1 periods when clean air masses were from the eastern coastal region. The air masses from the inland areas of Jiangsu and Anhui Province may contribute to PE1. During the heavily polluted period of PE2 (from 5 to 8 December 2013), the surface winds were from various directions and the wind speeds were relatively low and even stagnant sometimes, which were limited the dispersion of air pollutants. After 9 December, winds blew from the northwest and the wind speeds increased. An obvious decrease of temperature indicated a cold front affecting the YRD region (Wang et al., 2015). Backward trajectories analysis showed that short-range air masses from the YRD region were observed from 5 to 9 December, while long-range air masses occurred from 10 to 12 December (Fig. 6-11b), consistent with the surface meteorological conditions. During PE3, the wind directions showed a dominant northwest wind (Fig. 6-10c) and air masses arrived at SH from the northwest that originated from northern China and travelled over central China (Fig. 6-11c), which were different from that during BPE3 and APE3 periods when clean air masses originated from the ocean. Thus, the influence of air masses from northern China and central China may contribute to high PM<sub>2.5</sub> pollution in PE 3. The results suggested that the meteorological conditions are important in the formation of pollution events.

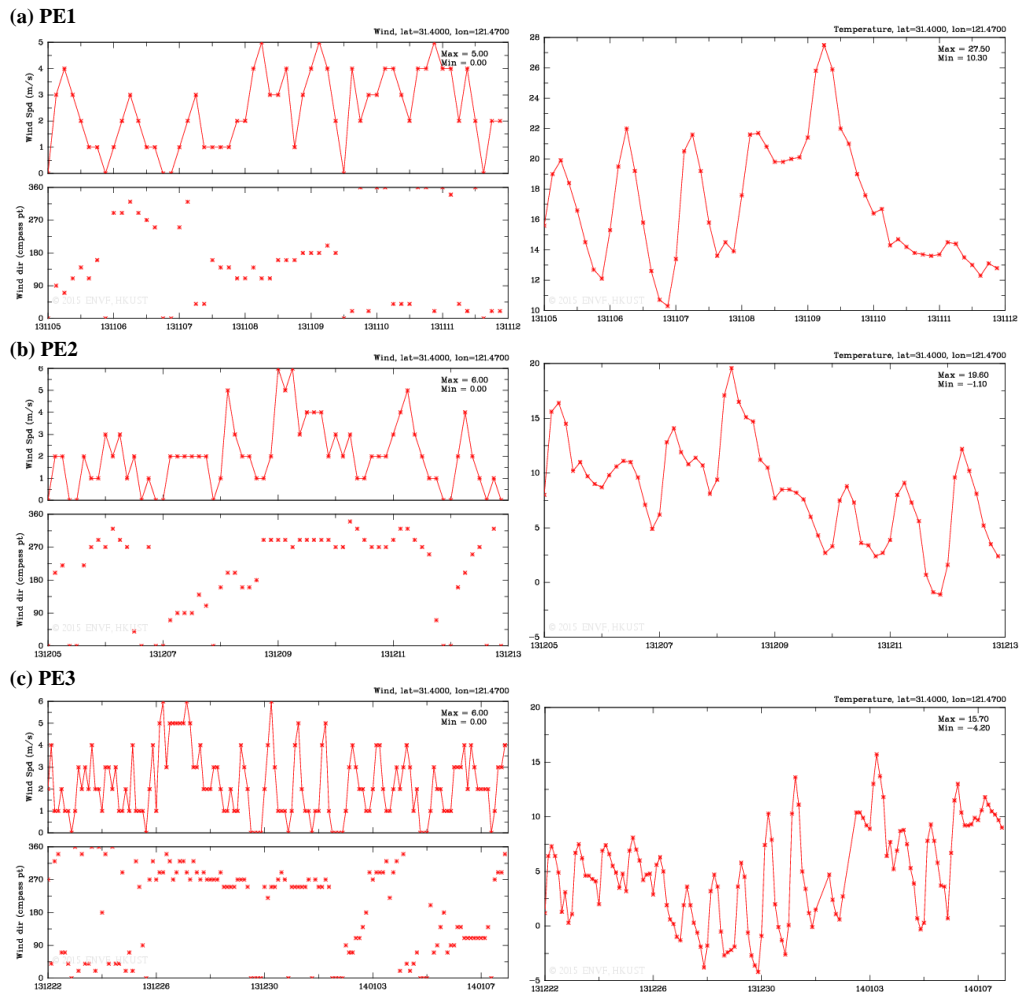


Figure 6-10 Surface meteorological conditions during the three pollution events in Shanghai from the monitoring station (31.4N, 121.47E) (Real-time data display from ENVF Atmospheric & Environmental Real-time Database: <http://envf.ust.hk/>).

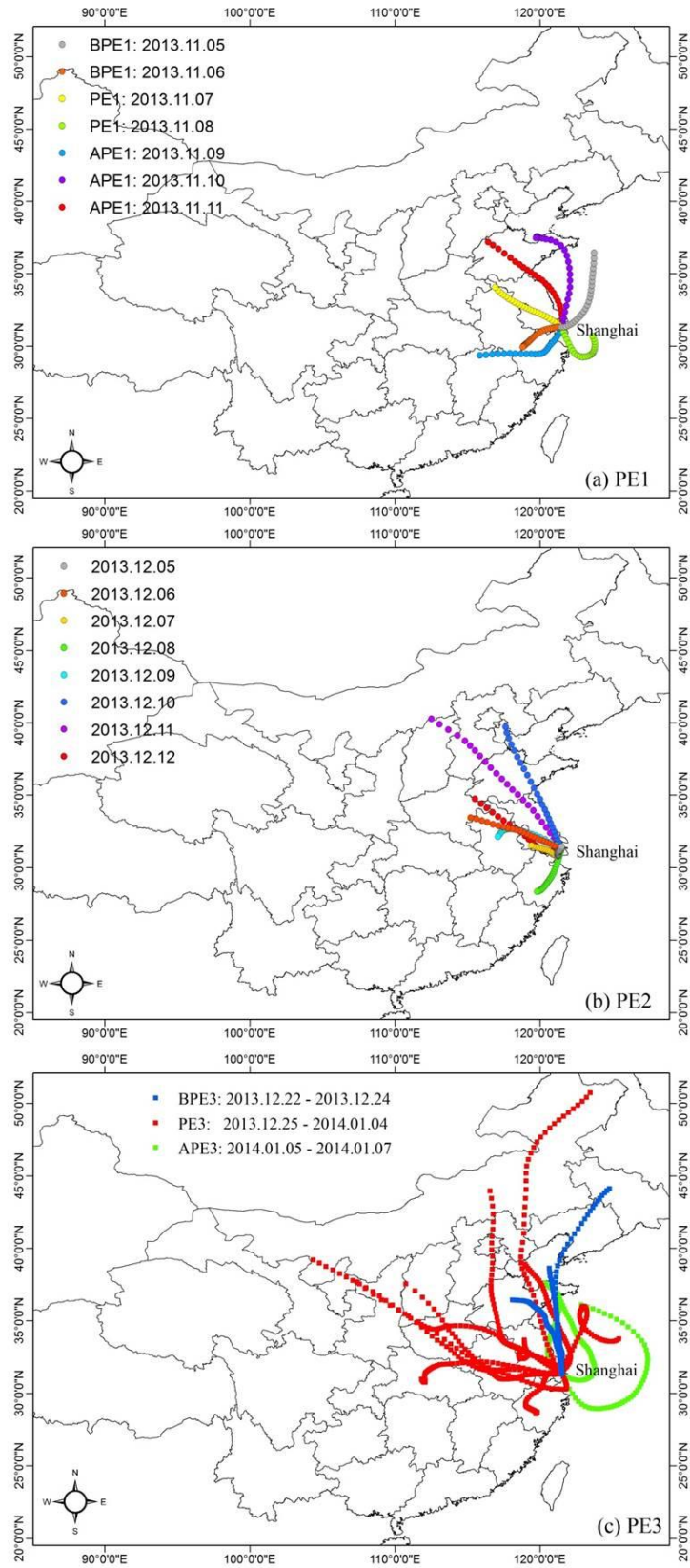


Figure 6-11 One-day backward trajectories of air masses arriving at Shanghai at an altitude 1000 m during the process of the three pollution events (PE1, 2 and 3).

### 6.2.3 Regional Transport of PM<sub>2.5</sub> during Three Pollution Events–Modeling Results

The daily average of surface PM<sub>2.5</sub> concentration and wind field during the processes of pollution events were simulated to display the evolution and transport of PM<sub>2.5</sub> over the YRD region using the NAQPMS model.

**Pollution Event 1:** Prior to PE1, on 5 November (Fig. 6-12a), the prevailed easterly wind from the ocean with high wind speed favoured the low PM<sub>2.5</sub> concentration with less than 75  $\mu\text{g m}^{-3}$  in the YRD region. On 6 November (Fig. 6-12b), the dominant west winds drove the movement of high PM<sub>2.5</sub> over Anhui, Henan and Shandong Province from the west to the east in the YRD region. After that, high PM<sub>2.5</sub> region occurred in the YRD with stable wind field on 7 November, and was more serious in the east part of the YRD region (Fig. 6-12c). The field observation also confirmed that PM<sub>2.5</sub> concentration was highest in SH during PE1 compared with the other three sampling sites in the YRD. From 8 November, PM<sub>2.5</sub> was transported from the southeast to the northwest in the YRD due to the strong sea winds from the southeast (Fig. 6-12d), which resulted in the alleviation of PE1.

**Pollution Event 2:** During the early stage of PE2 (Fig. 6-13a and b), stable meteorological conditions and high PM<sub>2.5</sub> region with more than 300  $\mu\text{g m}^{-3}$  (duck blue shade) were observed in the YRD and eastern China. On 9 December, the strong north wind prevailed over eastern China due to cold front, driving the movement of air masses fast over the heavy PM<sub>2.5</sub> elevated region of the YRD (Fig. 6-13c). High PM<sub>2.5</sub> zone over the YRD moved from the north to south under the prevailed north winds. Due to the influence of north wind, PM<sub>2.5</sub> pollution over the YRD region has litter weakened on 11 December (Fig. 6-13d). After the cold air ended on 12 December (Fig. 6-13e), PM<sub>2.5</sub> concentrations increased over the YRD region until 14 December (Fig. 6-13f).

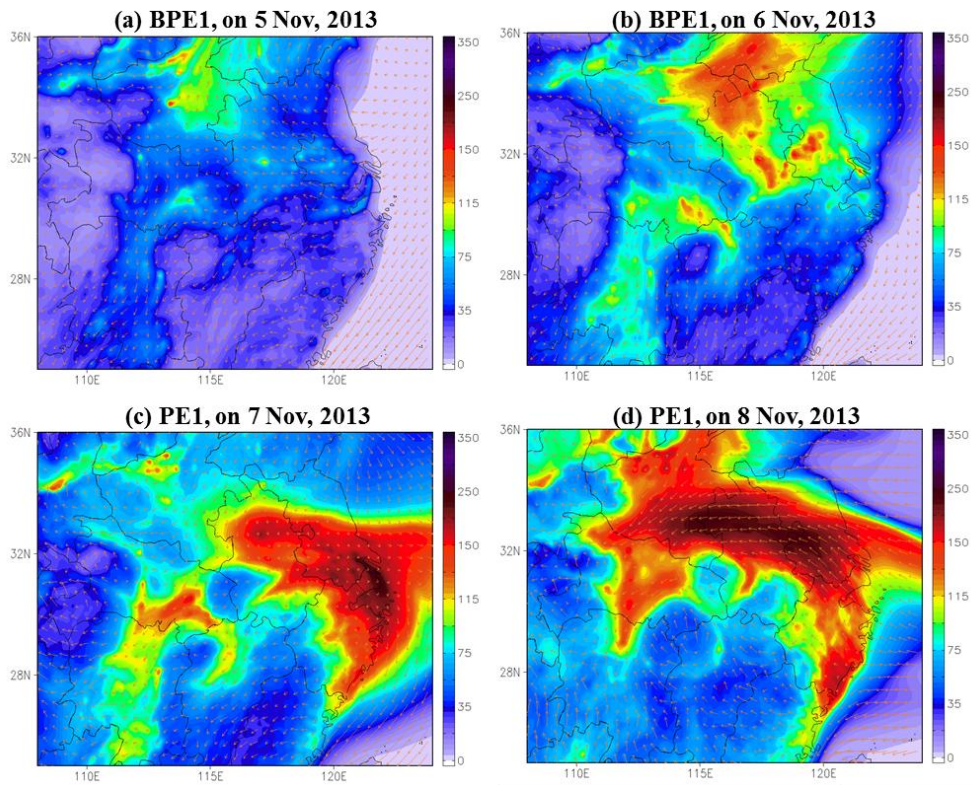


Figure 6-12 The simulated daily average of surface PM<sub>2.5</sub> concentration ( $\mu\text{g m}^{-3}$ ) and wind vector ( $\text{m s}^{-1}$ ) in eastern China during the first pollution event (PE1): (a) on 5 November 2013; (b) on 6 November 2013; (c) on 7 November 2013; and (d) on 8 November 2013.

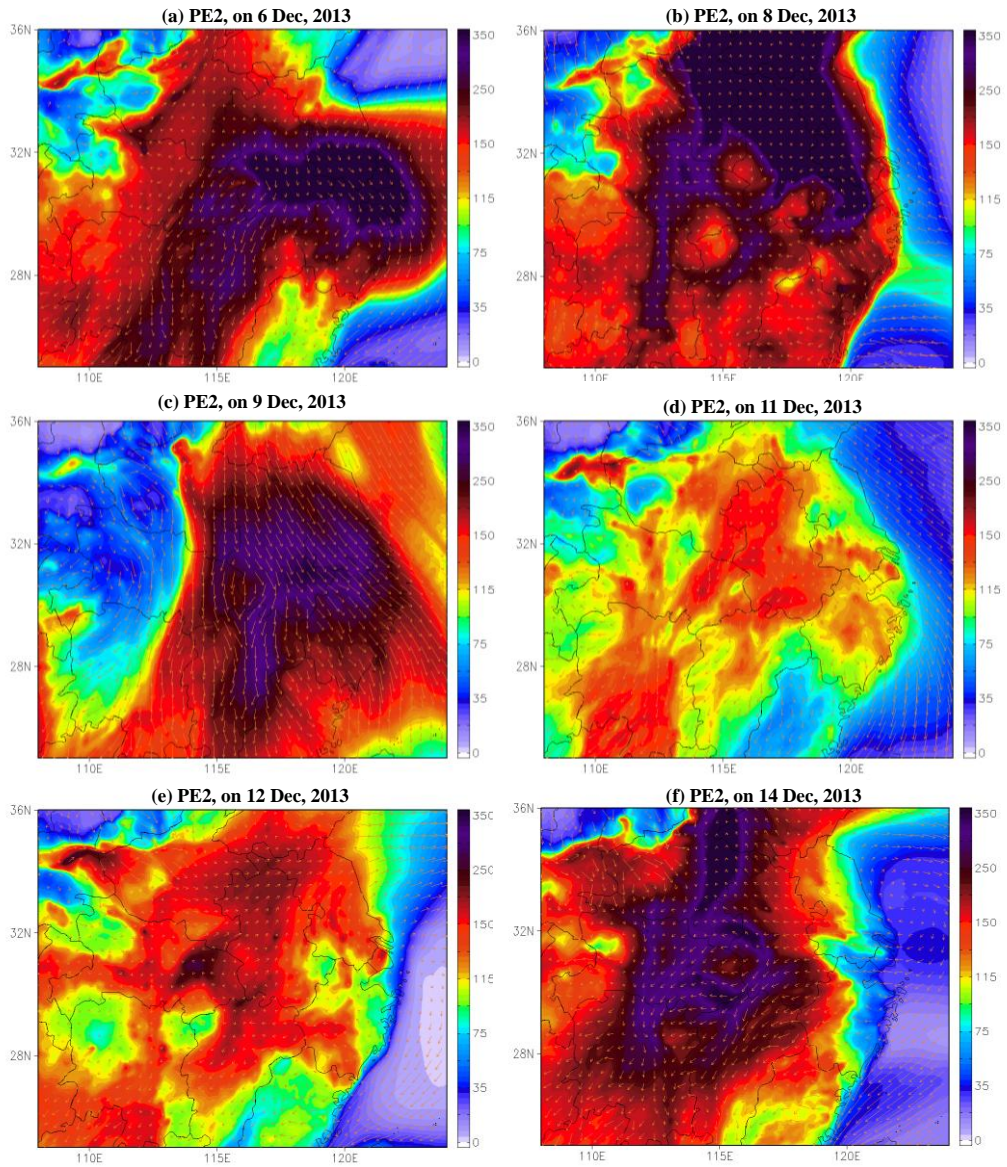


Figure 6-13 The simulated daily average of surface PM<sub>2.5</sub> concentration ( $\mu\text{g m}^{-3}$ ) and wind vector ( $\text{m s}^{-1}$ ) in eastern China during the secondary pollution event (PE2): (a) on 6 December 2013; (b) on 8 December 2013; (c) on 9 December 2013; (d) on 11 December 2013; (e) on 12 December 2013; and (f) on 14 December 2013.

**Pollution Event 3:** At the beginning of PE3, on 26 December, high PM<sub>2.5</sub> region occurred in the YRD, but the strong north wind prevailed over eastern China, bringing clean air from northern China (Fig. 6-14a). From 31 December, the wind field changed and forced the high PM<sub>2.5</sub> air over central China from west to the YRD (Fig. 6-14b). On 2 January 2014, high PM<sub>2.5</sub> zone over the YRD was transported from the southeast to the northwest due to the prevailing southeast winds (Fig. 6-14c). As shown in Fig. 6-14d, the strong northeast winds from the East China Sea dominated in the YRD region on 4 January 2014, driving the movement of high PM<sub>2.5</sub> from the north part of the YRD to the East China Sea. After that, the high PM<sub>2.5</sub> region in the YRD weakened. Compared with field observations, the modelling results clearly showed the observed patterns of PM<sub>2.5</sub> and backward trajectory of air mass during the processes of the three pollution events.

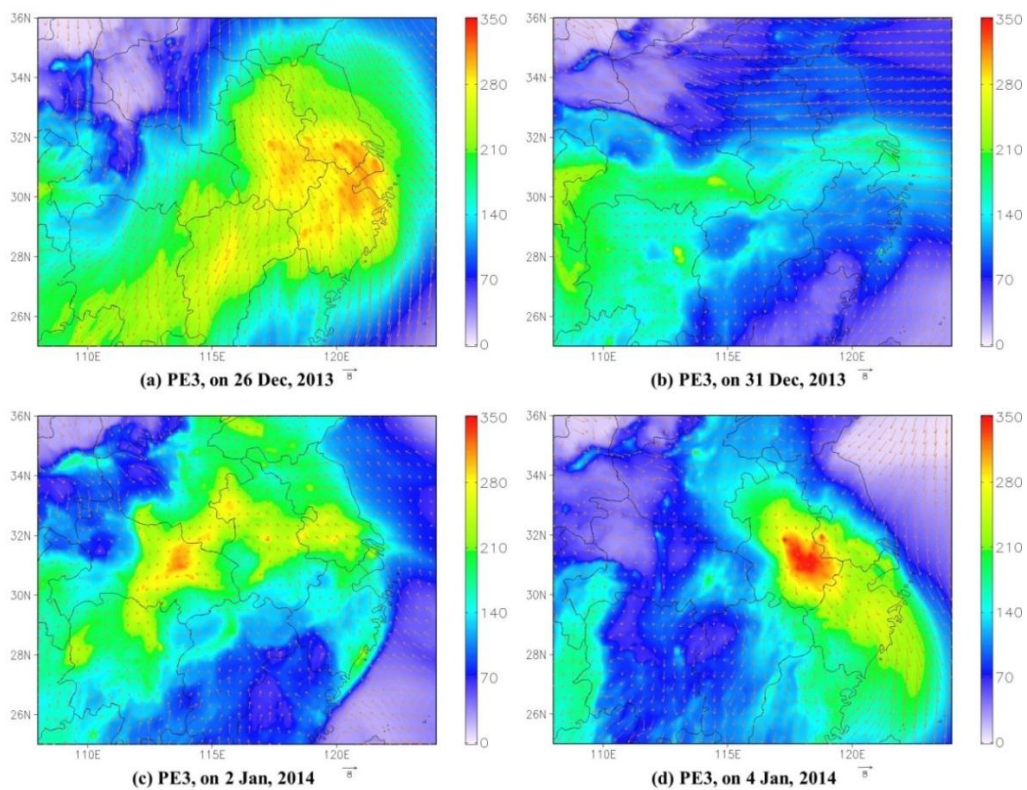


Figure 6-14 The simulated daily average of surface PM<sub>2.5</sub> concentration ( $\mu\text{g m}^{-3}$ ) and wind vector ( $\text{m s}^{-1}$ ) in eastern China during the third pollution event (PE3): (a) on 26 December 2013; (b) on 31 December 2013; (c) on 2 January 2014; and (d) on 4 January 2014.

## 6.2.4 Chemical Compositions during Three Pollution Events

Time series of the measured chemical composition concentrations and the relative abundance of POC and SOC during the three pollution processes are plotted in Fig. 6-15.

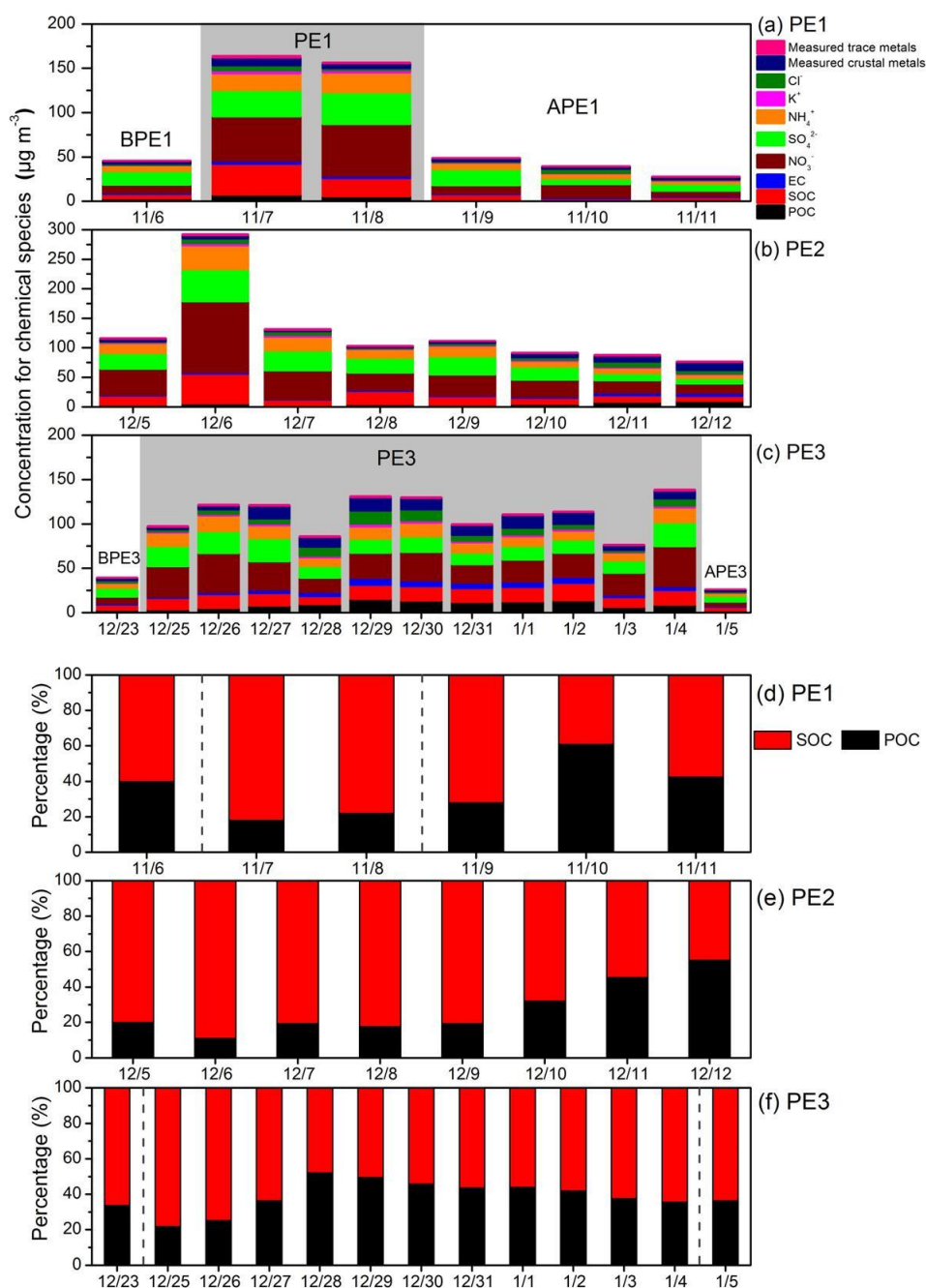


Figure 6-15 Concentrations of the measured chemical compositions and the relative abundance of POC and SOC in PM<sub>2.5</sub> samples in Shanghai during PE1, 2 and 3.

#### 6.2.4.1 Pollution Event 1

As shown in Fig. 6-15a, the concentrations of all the measured chemical components in PE1 were sharply increased compared to BPE1 and APE1 periods. The concentrations of SOC,  $\text{NO}_3^-$ ,  $\text{SO}_4^{2-}$  and  $\text{NH}_4^+$  during PE1 were 3-6 times higher than those in BPE1 and APE1 periods.  $\text{NO}_3^-$ ,  $\text{SO}_4^{2-}$  and  $\text{NH}_4^+$  were the dominant components, accounting for 29.3%, 18.0% and 11.2% of  $\text{PM}_{2.5}$  mass in PE1, respectively (Fig. 6-16). The ratio of  $\text{NO}_3^-$  to  $\text{SO}_4^{2-}$  has been used as an indicator of the relative contributions to the aerosol particles from mobile vs stationary sources of S and N in the particulate matters (Wang et al., 2006c; Cao et al., 2009). The average value of  $\text{NO}_3^-/\text{SO}_4^{2-}$  during PE1 (1.64) were higher than that in BPE1 (0.58) and APE1 (1.18), revealing that more  $\text{NO}_x$  were released mainly due to vehicular emissions. During APE1, when the southeast sea winds prevail,  $\text{SO}_4^{2-}$  instead of  $\text{NO}_3^-$  became the dominant secondary ions (Fig. 6-16), reflecting the influence of marine aerosol with high  $\text{SO}_4^{2-}/\text{NO}_3^-$ .  $\text{K}^+$  has been used as tracer element for biomass burning (Urban et al., 2012), although it have some other sources, such as crustal dust, sea salt and the dust from smelting activities. The concentration of  $\text{K}^+$  in  $\text{PM}_{2.5}$  during PE1 was 4 times higher than that in BPE1 and APE1 periods, different with other crustal metals, such as Al, Fe, Ca and Mg, which increased only 2-fold when compared to the non-pollution days. The relatively high increase of  $\text{K}^+$  suggested the contribution of biomass burning to PE1. In addition, high ratios of OC/EC in PE1 (with an average value of 10.3) also confirmed the presence of emissions from biomass burning. The results showed that the vehicular emissions and biomass burning are the key contributors for PE1 at Shanghai. Compared with BPE1 and APE1 periods, the contributions of SOC and  $\text{NO}_3^-$  to  $\text{PM}_{2.5}$  were increased by two folds in PE1, while the fractions of POC, EC and measured crustal metals in  $\text{PM}_{2.5}$  obviously decreased in PE1 (Fig. 6-16), indicating the large contribution of secondary aerosol and less contribution of primary aerosol in PE1. Furthermore, the contributions of SOC to the total organic carbon reached to 80% during PE1 (Fig. 6-15d). These results suggested the importance of secondary organic aerosol formation in driving  $\text{PM}_{2.5}$  pollution (Huang et al., 2014).

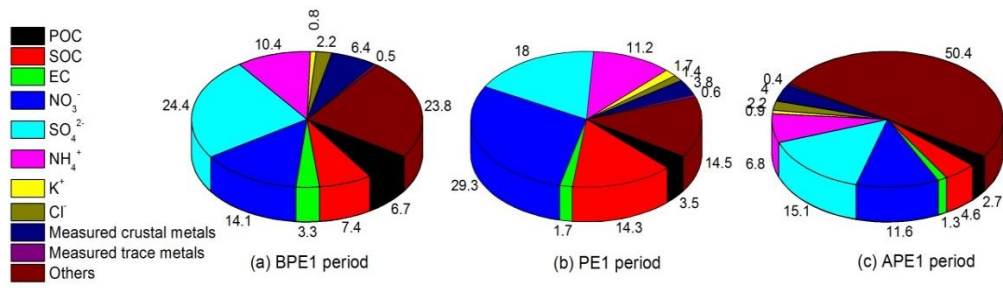


Figure 6-16 Chemical composition of PM<sub>2.5</sub> samples collected before pollution event 1 (BPE 1), in pollution event (PE 1) and after pollution event (APE 1) in Shanghai.

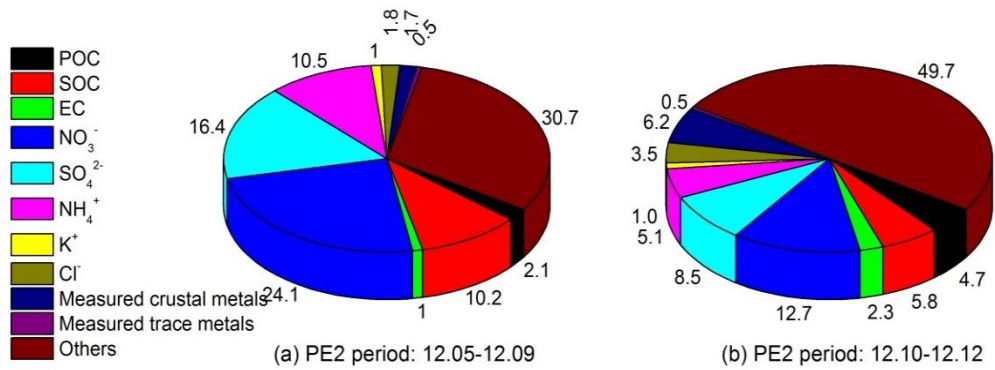


Figure 6-17 Chemical composition of PM<sub>2.5</sub> during pollution event 2 (PE2) in Shanghai.

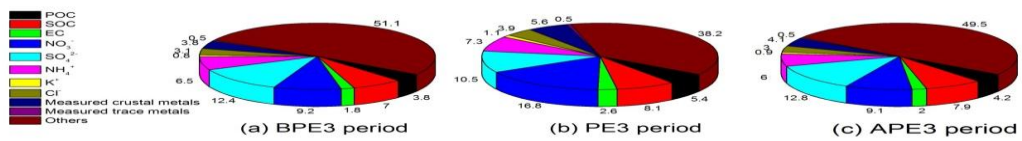


Figure 6-18 Chemical composition of PM<sub>2.5</sub> samples collected before pollution event 3 (BPE 3), in pollution event (PE 3) and after pollution event (APE 3) in Shanghai.

#### 6.2.4.2 Pollution Event 2

During PE2, the concentrations of chemical components reached to a high level, especially on 6 December (Fig. 6-15b). It is interesting that the concentrations of chemical components displayed different variation tendency in PE2. During 5-9 December, the concentrations of SOC,  $\text{NO}_3^-$ ,  $\text{SO}_4^{2-}$ ,  $\text{NH}_4^+$  and trace metals were extremely high, while the concentrations of POC, EC and crustal metals were as low as those on the normal days. After December 9, the concentrations of SOC, secondary inorganic ions and trace metals declined, while the concentrations of POC, EC and crustal metals sharply increased. The relative abundance of SOC was strongly enhanced during 5-9 December, while the relative abundance of POC increased during 10-12 December (Fig. 6-15e). Moreover, as shown in Fig. 6-17, the contributions of secondary components (SOC,  $\text{NO}_3^-$ ,  $\text{SO}_4^{2-}$  and  $\text{NH}_4^+$ ) to  $\text{PM}_{2.5}$  during 5-9 December were two times higher than those in the period from 10 to 12 December. In contrast, the contributions of primary components (POC, EC and crustal metals) to  $\text{PM}_{2.5}$  during 10-12 December were two times higher than those in the period from 5 to 9 December.

During 5-9 December, the low wind speed, short-range backward air mass and the dominance of CO and  $\text{NO}_2$  (Wang et al., 2015) could facilitate the formation of SOC and secondary inorganic ions, while reduce the re-suspended of surface soil and road dust which can contribute to crustal metals associated with  $\text{PM}_{2.5}$  (Tanner et al., 2008). During 10-12 December, when the long-range air mass appeared due to the cold front, the presence of coarse particles and the dominant of  $\text{SO}_2$  and CO were observed (Wang et al., 2015), corroborating the results of the increase in POC and crustal metals and the decline in secondary components in this study. Our observations on chemical components and simulated modeling results during PE2 were confirmed the results. The stable meteorological conditions during 5-9 December accelerated the accumulation of local or regional air pollutants and the formation of secondary aerosols, and the occurrence of cold air during 10-12 December resulted in more inputs of primary aerosols via long range transport. Similar with PE1, high ratios of  $\text{NO}_3^-/\text{SO}_4^{2-}$  (with an average value of 1.54) in PE2 also indicated the serious pollution of vehicle exhaust in Shanghai.

### 6.2.4.3 Pollution Event 3

Similar with PE1 and PE2, elevated concentrations for all chemical components were observed during PE3 (Fig. 6-15c). Among the measured chemical components,  $\text{NO}_3^-$ ,  $\text{SO}_4^{2-}$  and  $\text{NH}_4^+$  were the dominant components. Compared with BPE3 and APE3 periods, the contributions of POC, EC,  $\text{NO}_3^-$  and crustal metals to  $\text{PM}_{2.5}$  were increased during PE3, while the fractions of the other components in  $\text{PM}_{2.5}$  have no obvious changes during PE3 (Fig. 6-18). As indicated in Fig. 6-15f, an increase trend in the relative abundance of POC and a declining trend in the abundance of SOC were measured during PE3, comparing with BPE3 and APE3 periods. The ratios of OC/EC kept a stable low value (with an average value of 5.54) during the pollution process, confirming the low presence of SOC in PE3. In addition, the average value of  $\text{NO}_3^-/\text{SO}_4^{2-}$  during PE3 (1.61) were higher than that in BPE3 (1.14) and APE3 (0.71). These results indicated more contribution of primary aerosol and  $\text{NO}_3^-$  in PE3 during the long range transport.

### 6.2.4.4 Comparison the Three Pollution Events

The results of chemical compositions in  $\text{PM}_{2.5}$  during the three pollution events were further compared to investigate the difference in formation mechanisms among pollution events. Fig. 6-19 shows the relative abundances of chemical components for  $\text{PM}_{2.5}$  in Shanghai during the three events. The dominance of secondary components (SOC and secondary inorganic ions) suggested the importance of secondary aerosol formation during the three pollution events. By comparison, the dominances of secondary components were more significant in PE1 and PE2, while the abundances of primary components (POC, EC and crustal metals) were highest in PE3. Based on the backward trajectory and modelling analysis above, the occurrence of PE1 and PE2 was related to the accumulation of air contaminants in the YRD under stable meteorological conditions, while the formation of PE3 was attributed to the regional transport of air pollutants under different wind directions. The results suggested that the characteristics of chemical components in  $\text{PM}_{2.5}$  are related to the emission sources, meteorological conditions and long-range transport of air pollutants (Huang et al., 2012a;

Kang et al., 2013). The input of primary aerosols were more significant under the regional transport of air pollutants during PE3, comparing with PE1 and PE2.

Mineral particles in the atmosphere participate in various atmospheric processes, such as radiative forcing, cloud condensation and ice nuclei, biogeochemical cycles, and heterogeneous reactions with secondary aerosol precursor gases (Li and Shao, 2009; McNaughton et al., 2009). The heterogeneous reactions of mineral particles with  $\text{HNO}_3$  and  $\text{NO}_2$  have received significant interest because they can affect the hygroscopic properties of aerosols. Li and Shao (2009) have demonstrated that mineral particles were mainly covered with coating including  $\text{Ca}(\text{NO}_3)_2$ ,  $\text{Mg}(\text{NO}_3)_2$  and  $\text{NaNO}_3$ , and the coatings increased the size of mineral particles. They also reported that about 90% of the collected mineral particles were coated in haze samples, and most of the coatings were possibly nitrates. In this study, the ratios of  $\text{NO}_3^-/\text{Al}$  during pollution events (33.9 in PE1, 56.8 in PE2 and 22.9 in PE3) were found to be much higher than those during non-pollution periods (11.8-19.4), probably attributed to the heterogeneous reactions of crustal elements with  $\text{HNO}_3$  and  $\text{NO}_2$  in pollution events. The coatings of nitrate on mineral particles can be transported over longer distances along with mineral particles, comparing with pure secondary nitrate (McNaughton et al., 2009; Li et al., 2012). During PE3, more contributions of crustal elements together with  $\text{NO}_3^-$  were observed during the long range transport, probably due to the capture of nitrate by mineral particles during the long-range transport.

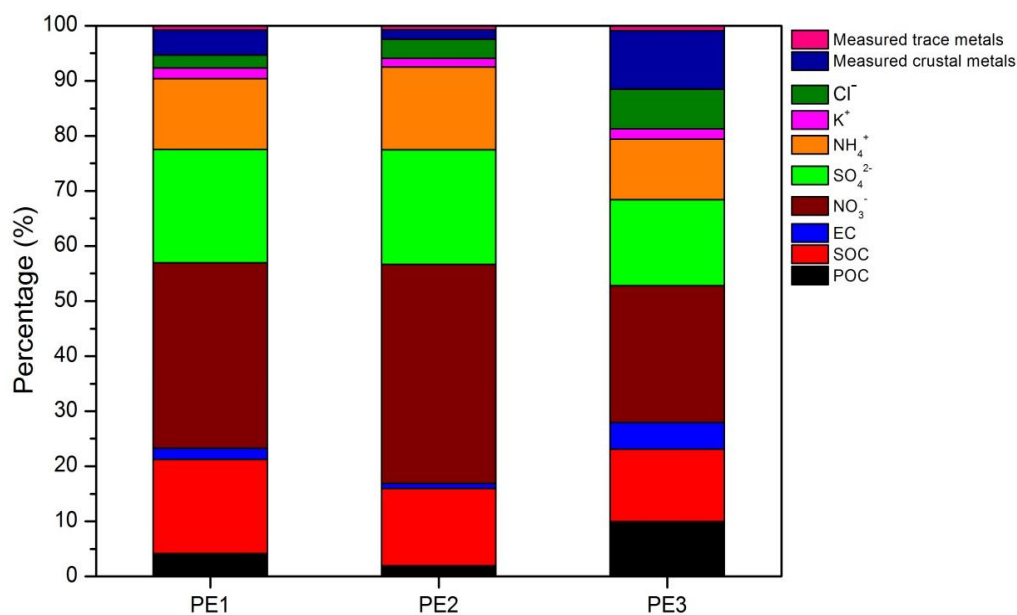


Figure 6-19 Relative abundances of the measured chemical compositions in PM<sub>2.5</sub> samples in Shanghai during the three pollution events: PE1, 7-8 November 2013; PE2, 5-12 December 2013; and PE3, 25 December 2013-5 January 2014.

### 6.3 Summary

The NAQPMS modelling results clearly showed the trans-boundary transport of PM<sub>2.5</sub> among the PRD and YRD regions and Beijing during a severe and long-lasting pollution event occurred from 2 to 14 December 2013. The results showed the transport of PM<sub>2.5</sub> from the YRD region to the PRD region and Beijing during 7-8 December. After 9 December, the YRD region was the receptor of transport from North China, and the PRD region became the receptor of transport from the YRD region. Three pollution events were identified in Shanghai during the autumn and winter. Analysis of air mass backward trajectories and meteorological parameters suggested that the meteorological condition was one of the key factors in the formation of pollution events. By using the NAQPMS model, the evolution and transport of PM<sub>2.5</sub> over the YRD region during the three pollution events indicated that regional transport play an important role in the formation of pollution events. The dominance of secondary components (SOC and secondary inorganic ions) during the three pollution events suggested the importance of secondary aerosol formation in driving PM<sub>2.5</sub> pollution.

More contributions of crustal elements together with  $\text{NO}_3^-$  were observed in PE3, probably attributed to the heterogeneous reactions of crustal particles with  $\text{HNO}_3$  and  $\text{NO}_2$  during the long-range transport.

## **Chapter 7 - Bioaccessibility and Health Risks of Trace Metals in PM<sub>2.5</sub> in Large Cities of China using Simulated Lung Fluids**

Investigation of bioaccessibility and health risks of airborne trace metals provide information regarding the health risks of PM<sub>2.5</sub> in urban environment. The purposes of this chapter are: (1) to investigate the bioaccessibility of trace metals in PM<sub>2.5</sub> in Guangzhou (GZ), Shanghai (SH) and Nanjing (NJ) using simulated lung fluids–Gamble’s solution; (2) to study the variations of bioaccessibility of trace metals as a function of time (*e.g.*, seasonal, and pollution days vs non-pollution days); and (3) to evaluate the health risks of airborne trace metals via inhalation exposure. A total of 40, 61 and 42 samples from Guangzhou, Shanghai and Nanjing cover the period from October 2013 to 17 July 2014 were analyzed for bioaccessibility investigation and risk assessment, respectively.

### **7.1 Total and Bioaccessible Concentrations of Trace Metals in PM<sub>2.5</sub>**

Total and bioaccessible concentrations of Cr, As, Mn, Ni, Pb, V and Zn in PM<sub>2.5</sub> in Guangzhou, Shanghai and Nanjing are listed in Table 7-1. Total metal concentrations in the three cities were found to be variable in a large range, between 7.63 ng m<sup>-3</sup> (for Ni in GZ) and 273 ng m<sup>-3</sup> (for Zn in SH). Generally, total concentrations of trace metals were in the order of Ni < V < As < Cr < Mn < Pb < Zn. Spatially, the total concentrations of trace metals in PM<sub>2.5</sub> were highest in Shanghai, followed by Nanjing and Guangzhou.

Bioaccessible concentrations of airborne trace metals obtained in the three cities showed less variability. Relatively high bioaccessible concentrations of Mn (5.10-10.0 ng m<sup>-3</sup>), V (2.05-6.30 ng m<sup>-3</sup>) and Zn (3.80-14.4 ng m<sup>-3</sup>) were obtained. Similar with total concentrations, the bioaccessible concentrations of Mn, Ni, Pb, V and Zn were highest in SH, followed by NJ and GZ. Although the total concentration of Cr was lowest in Guangzhou, the highest bioaccessible concentration of Cr was found in GZ. Overall, the bioaccessible concentrations of trace metals in this study were lower than to those measured in PM<sub>2.5</sub> from Frankfurt,

Germany using Gamble's solution as the extractant for 24 h (Wiseman and Zereini, 2014).

Table 7-1 Total and Bioaccessible concentrations ( $\text{ng m}^{-3}$ , annual mean  $\pm$  S.D.), and bioaccessible fraction (%) of trace metals in  $\text{PM}_{2.5}$  from Guangzhou, Shanghai and Nanjing.

Location		Cr	As	Mn	Ni	Pb	V	Zn
Guangzhou (n=40)	Total ( $\text{ng m}^{-3}$ )	13.4 $\pm$ 12.1	12.3 $\pm$ 10.3	32.6 $\pm$ 18.5	7.63 $\pm$ 3.97	42.5 $\pm$ 30.0	10.5 $\pm$ 7.01	175 $\pm$ 112
	Bioaccessible ( $\text{ng m}^{-3}$ )	3.11 $\pm$ 6.52	2.99 $\pm$ 2.35	5.10 $\pm$ 3.58	0.57 $\pm$ 0.38	1.18 $\pm$ 1.21	3.61 $\pm$ 2.32	3.80 $\pm$ 3.72
	Bioaccessible fraction (%)	22.9 $\pm$ 19.6	30.6 $\pm$ 13.7	20.6 $\pm$ 18.1	6.19 $\pm$ 7.10	4.42 $\pm$ 4.83	55.0 $\pm$ 65.5	3.15 $\pm$ 4.51
Shanghai (n=61)	Total ( $\text{ng m}^{-3}$ )	21.0 $\pm$ 11.8	-	60.0 $\pm$ 36.2	18.1 $\pm$ 8.07	95.2 $\pm$ 76.8	18.3 $\pm$ 9.28	273 $\pm$ 234
	Bioaccessible ( $\text{ng m}^{-3}$ )	1.33 $\pm$ 0.64	2.75 $\pm$ 3.65	10.0 $\pm$ 10.3	1.34 $\pm$ 1.08	3.93 $\pm$ 6.71	6.30 $\pm$ 4.09	9.28 $\pm$ 17.8
	Bioaccessible fraction (%)	8.25 $\pm$ 5.80	-	15.7 $\pm$ 9.17	8.96 $\pm$ 10.6	2.90 $\pm$ 3.31	38.1 $\pm$ 18.3	2.05 $\pm$ 2.98
Nanjing (n=42)	Total ( $\text{ng m}^{-3}$ )	14.1 $\pm$ 9.67	-	48.8 $\pm$ 32.1	9.02 $\pm$ 5.66	110 $\pm$ 93.3	9.58 $\pm$ 9.02	251 $\pm$ 180
	Bioaccessible ( $\text{ng m}^{-3}$ )	1.31 $\pm$ 0.49	2.83 $\pm$ 2.50	6.99 $\pm$ 5.77	0.81 $\pm$ 0.41	1.72 $\pm$ 1.94	2.05 $\pm$ 1.07	5.56 $\pm$ 8.33
	Bioaccessible fraction (%)	15.2 $\pm$ 13.9	-	14.3 $\pm$ 5.62	17.7 $\pm$ 25.3	1.41 $\pm$ 0.50	40.4 $\pm$ 32.2	1.63 $\pm$ 1.36

## **7.2 Bioaccessibility of Airborne Trace Metals**

The bioaccessible fraction of each trace metals was calculated by dividing the bioaccessible concentration by the total concentration of the metal in the sample. As shown in Table 7-1, bioaccessible fractions in  $PM_{2.5}$  in the three cities varied among trace metals, with high fractions for V (38.1-55.0%), intermediate fractions for Mn (14.3-20.6%), Cr (8.25-22.9%) and Ni (6.19-17.7%), and low fractions for Pb (1.41-4.42%) and Zn (1.63-3.15%). In the three cities, V presented high bioaccessibility in  $PM_{2.5}$ ; Mn, Cr and Ni showed intermediate bioaccessibility; and Pb and Zn exhibited low bioaccessibility. The bioaccessible fractions of trace metals were lower than those reported in  $PM_{2.5}$  from Frankfurt, Germany using the Gamble's solution as the extractant for 24 h (Wiseman and Zereini, 2014) and from Beijing, China using water for extraction test (Schleicher et al., 2011). The use of simulated lung fluid does provide more real bioavailability of airborne metals compared to using water as leaching agents, as it is more likely to reflect real human body conditions (Mukhtar and Limbeck, 2013). Compared with Shanghai and Nanjing, the total and bioaccessible concentrations of trace metals in Guangzhou were lower, while the bioaccessibility of trace metals in Guangzhou were higher, with the exception of Ni. The bioaccessibility of airborne trace metals is influenced by particle sources (Desboeufs et al., 2005; Heal et al., 2005), metal speciation in particles (Chester et al., 1989) and chemical properties of particles, such as water soluble organic matter (Wozniak et al., 2013) and particle acidity (Desboeufs et al., 2005). Further study is needed to investigate the factors that affect the bioaccessibility of trace metals in  $PM_{2.5}$ .

## **7.3 Seasonal Variations of Airborne Trace Metals Bioaccessibility**

The seasonal variations of bioaccessible trace metal concentrations in  $PM_{2.5}$  in Guangzhou, Shanghai and Nanjing are displayed in Fig. 7-1. In the three cities, clear seasonal variations with higher concentrations in winter and lower concentrations in summer were both observed for bioaccessible Cr, As, Mn, Pb and Zn. In Guangzhou, high bioaccessible

concentrations of V were observed in spring, whereas no significant differences of Ni were found among the four seasons. Ni and V exhibited less variation in Shanghai and Nanjing. In general, the seasonal patterns of bioaccessible trace metal concentrations were similar to PM<sub>2.5</sub> and total trace metal concentrations. Good correlations between PM<sub>2.5</sub> concentrations and bioaccessible concentrations were found for Cr, As, Mn, Pb and Zn, while no correlations were observed for Ni and V (Table 7-2). The result suggested the significant role of PM<sub>2.5</sub> mass concentrations on the bioaccessible concentrations of Cr, As, Mn, Pb and Zn. In winter, both high concentrations of PM<sub>2.5</sub> and bioaccessible trace metals may cause a high potential toxicity to human health in the three cities.

As shown in Fig 7-2, high levels of bioaccessibility for Mn, Pb and Zn were observed in winter in all the cities, while the bioaccessibilities of Cr, Ni and V exhibited a high level in summer. Seasonal variations of bioaccessibility in airborne trace metals reflected the variations of the sources of trace metals in the atmosphere and the chemical properties of aerosols. In the three cities, positive correlations between PM<sub>2.5</sub> concentrations and trace metal bioaccessibility were found for Mn, Pb and Zn, while negative correlations were observed for Cr, Ni and V (Table 7-3). In winter, more anthropogenic inputs of PM<sub>2.5</sub> and trace metals have been investigated by previous results in Chapter 5. High bioaccessibility of Mn, Pb and Zn in winter probably due to the more input of anthropogenic PM<sub>2.5</sub> and these trace metals in the atmosphere. Although the bioaccessible concentrations of Cr, Ni and V were relatively low in summer, their high bioaccessibility in summer needs to be paid more attention regarding the health risk.

Table 7-2 Correlation coefficients between PM<sub>2.5</sub> and bioaccessible trace metal concentrations in Guangzhou, Shanghai and Nanjing.

Location	<i>r</i>	Cr	As	Mn	Ni	Pb	V	Zn
Guangzhou	PM <sub>2.5</sub>	0.295	0.567**	0.899**	0.193	0.614**	0.244	0.701**
Shanghai	PM <sub>2.5</sub>	0.749**	0.821**	0.809**	0.142	0.695**	0.216	0.724**
Nanjing	PM <sub>2.5</sub>	0.693**	0.831**	0.884**	0.053	0.847**	0.613**	0.852**

\*\* stand for statistical significance at the 0.01 level.

\* stand for statistical significance at the 0.05 level.

Table 7-3 Correlation coefficients between PM<sub>2.5</sub> concentration and trace metal bioaccessibility in Guangzhou, Shanghai and Nanjing.

Location	<i>r</i>	Cr	As	Mn	Ni	Pb	V	Zn
Guangzhou	PM <sub>2.5</sub>	-0.240	-0.446**	0.618**	0.351*	0.439**	0.157	0.431**
Shanghai	PM <sub>2.5</sub>	-0.251		0.372**	-0.240	0.358**	-0.281*	0.717**
Nanjing	PM <sub>2.5</sub>	-0.463**		0.140	-0.466**	0.355*	-0.311*	0.682**

\*\* stand for statistical significance at the 0.01 level.

\* stand for statistical significance at the 0.05 level.

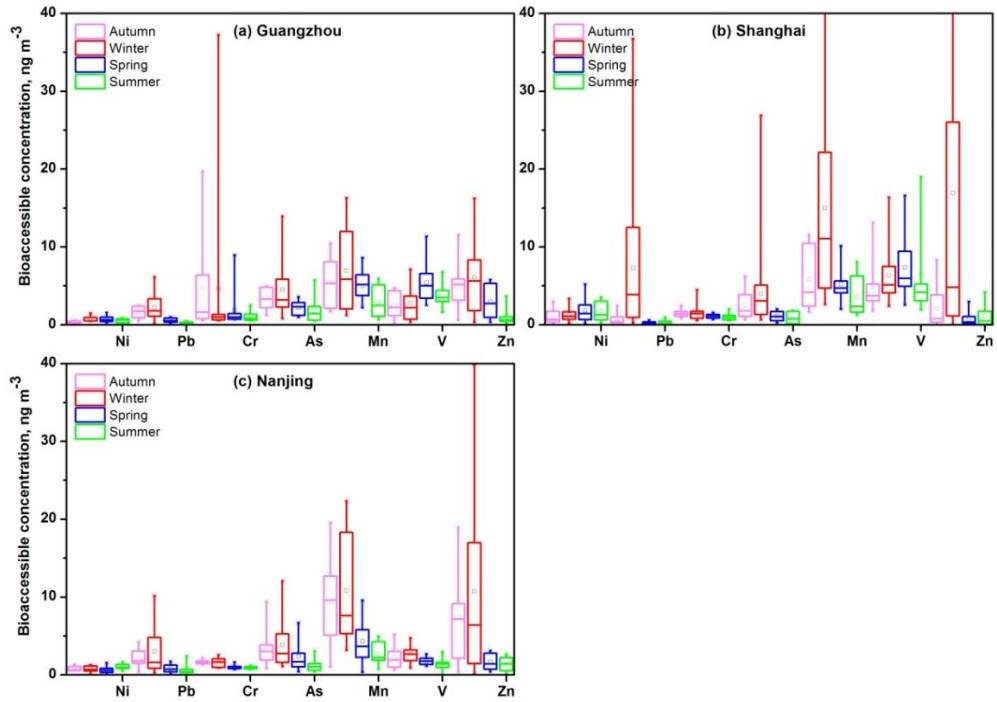


Figure 7-1 Seasonal variations of bioaccessible concentrations for trace metals in PM<sub>2.5</sub> in (a) Guangzhou; (b) Shanghai; and (c) Nanjing. The boxes and whiskers denote the minimums, 25, 50, 75 percentiles and maximums; the dots denote the mean values.

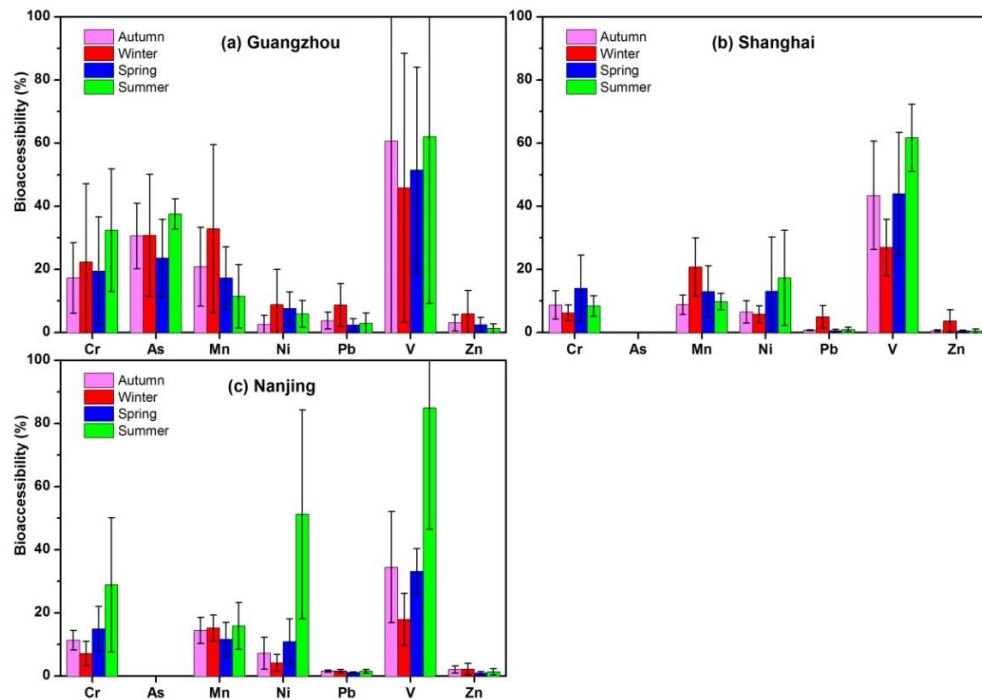


Figure 7-2 Bioaccessibility (mean  $\pm$  S.D.) of trace metals in PM<sub>2.5</sub> in four seasons in (a) Guangzhou; (b) Shanghai; and (c) Nanjing.

## **7.4 Bioaccessibility of Airborne Trace Metals on Pollution Days and Non-pollution Days**

The bioaccessible concentrations of trace metals during pollution (daily  $PM_{2.5}$  higher than the average values) and non-pollution days (daily  $PM_{2.5}$  less than the average values) in GZ, SH and NJ in four seasons are displayed in Fig. 7-3, 7-4 and 7-5, respectively. Compared with non-pollution days, the bioaccessible concentrations of As, Mn, Pb and Zn were found to be high on pollution days in each season, implying high potential toxicity of these metals during the pollution days. In contrast, the bioaccessible concentrations of Ni and V were higher on non-pollution days than those on pollution days in spring. The bioaccessible concentrations of Cr were found no significant differences between pollution days and non-pollution days in SH and NJ, while were higher on pollution days in autumn, winter and summer seasons in GZ. High bioaccessible concentrations of As, Mn, Pb and Zn on pollution days were likely due to the high  $PM_{2.5}$  concentrations.

The bioaccessibilities of Mn, Pb and Zn on pollution days were higher than those on non-pollution days in winter in GZ (see Fig. 7-6). Compared with non-pollution days, higher bioaccessibilities of Zn on pollution days were investigated in winter in SH (see Fig. 7-7) and NJ (see Fig. 7-8). High bioaccessibilities of these trace metals were found on pollution days, probably due to the differences of emission sources and chemical components between pollution and non-pollution days. The toxic effect posed by Mn during the pollution days may be worthy of further study because of their high bioaccessible concentration and bioaccessibility in  $PM_{2.5}$ . Although the bioaccessibility of Pb and Zn were small, their high bioaccessible concentrations during the pollution days remain potential toxic risk in comparison with the non-pollution days.

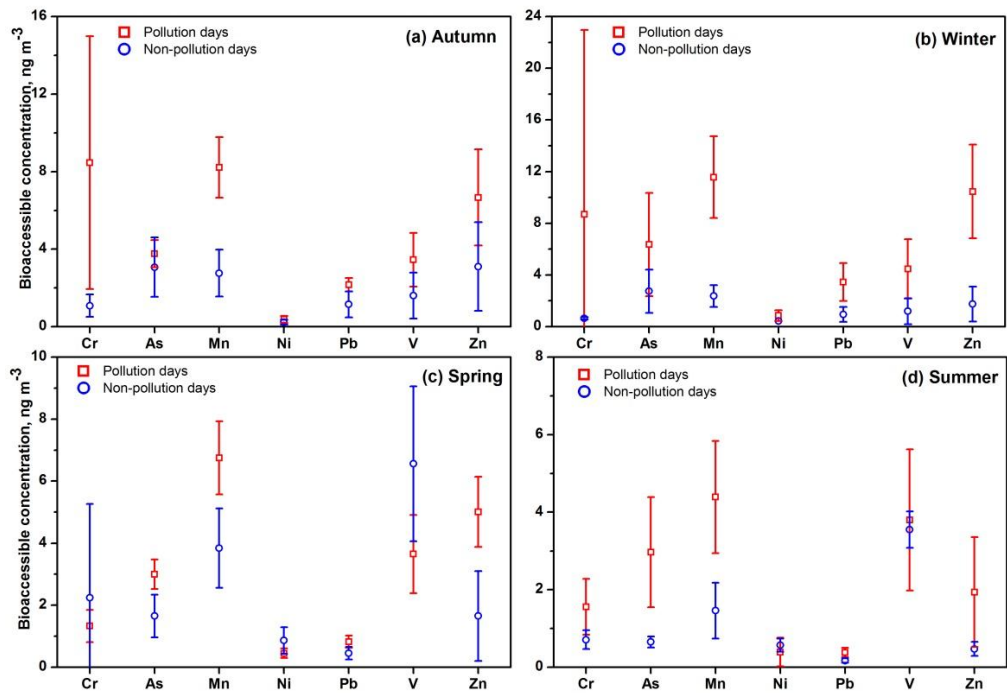


Figure 7-3 Bioaccessible concentrations of trace metals during pollution and non-pollution days in Guangzhou in four seasons.

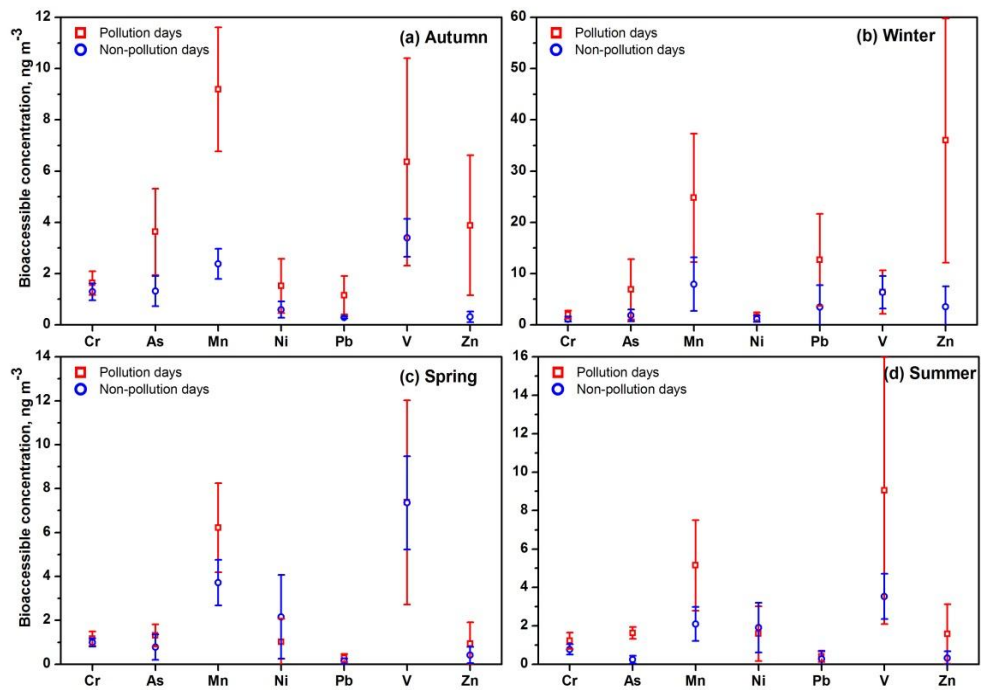


Figure 7-4 Bioaccessible concentrations of trace metals during pollution during pollution and non-pollution days in Shanghai in four seasons.

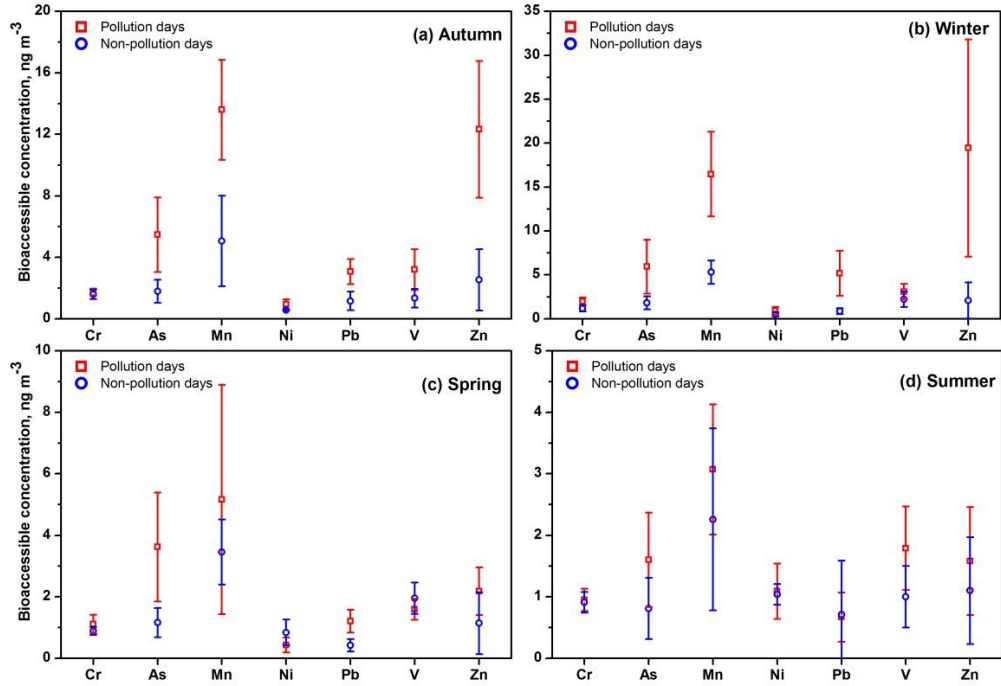


Figure 7-5 Bioaccessible concentrations of trace metals during pollution during pollution and non-pollution days in Nanjing in four seasons.

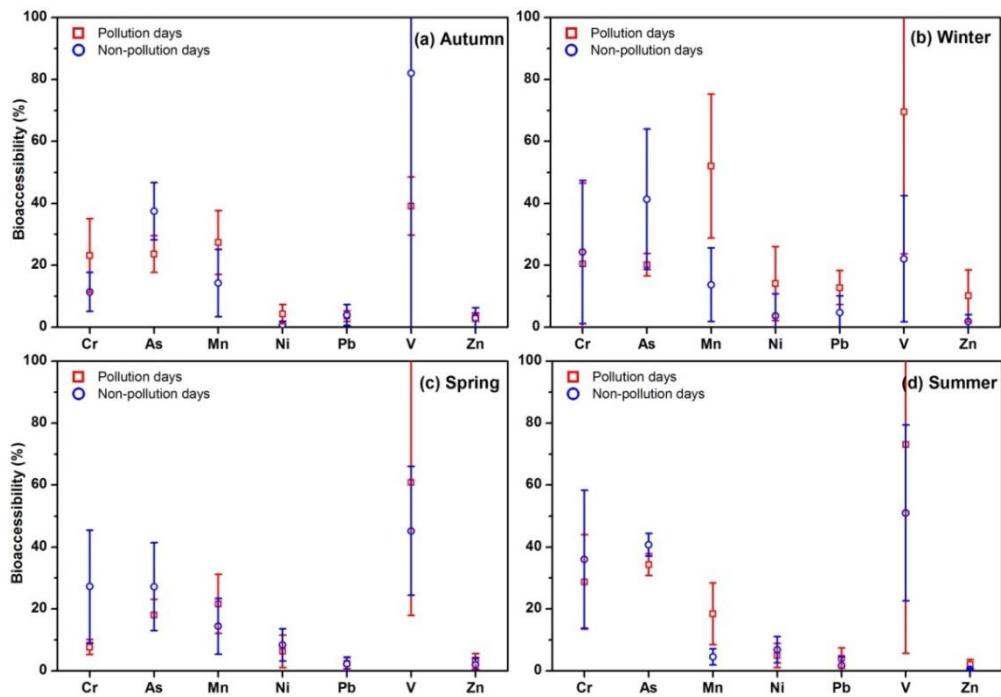


Figure 7-6 Bioaccessibility of trace metals during pollution and non-pollution days in Guangzhou in four seasons.

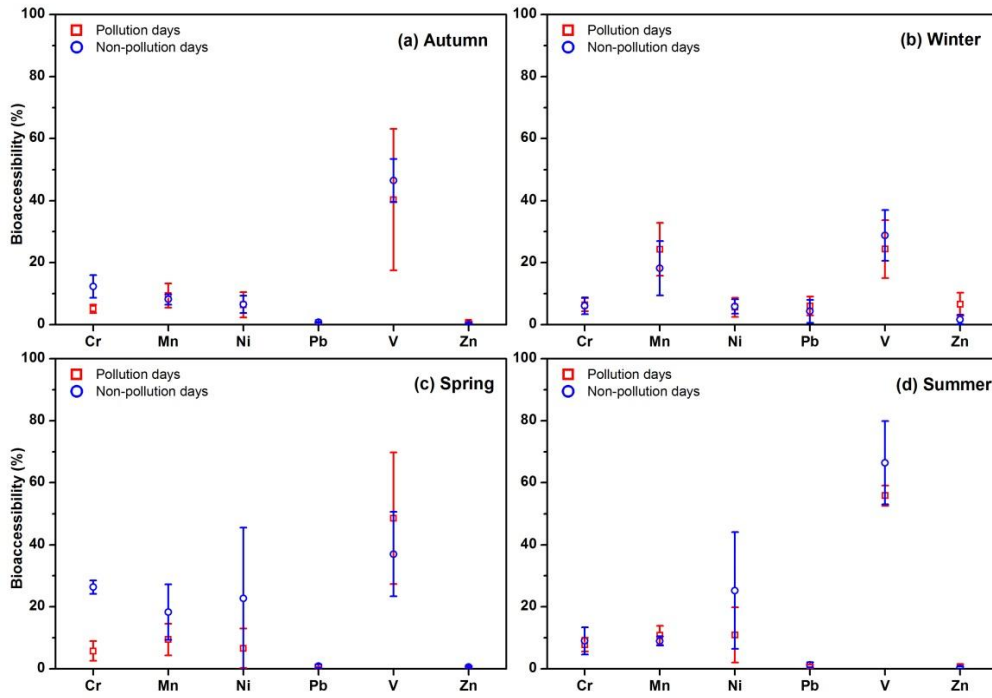


Figure 7-7 Bioaccessibility of trace metals during pollution and non-pollution days in Shanghai in four seasons.

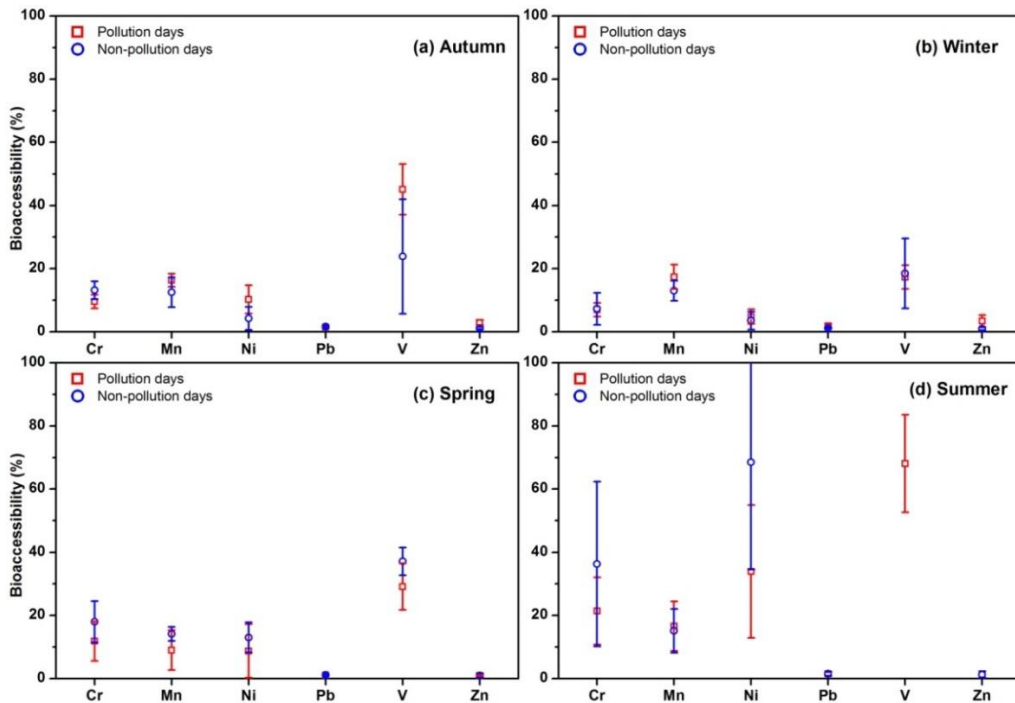


Figure 7-8 Bioaccessibility of trace metals during pollution and non-pollution days in Nanjing in four seasons.

## 7.5 Health Risks Assessment of Airborne Trace Metals

It is now widely recognized that the bioaccessible concentrations of trace metals in atmospheric PM is important for risk assessment of metal toxicity instead of total metal concentrations. Inhalation is the most important pathway for human exposure of airborne trace metals. In this study, both carcinogenic (Cr, As, Ni and Pb) and non-carcinogenic (Cr, As, Ni and Mn) risks posed by airborne trace metals via inhalation to children and adults were calculated by using the method (see Section 3.11) and related parameters from US EPA. Table 7-4 shows the related parameters for risk assessment calculation of airborne trace metals via inhalation exposure. As shown in Table 7-5, the annual mean, and mean in pollution days and non-pollution days during winter of bioaccessible concentrations for trace metals were used to calculate the carcinogenic and non-carcinogenic risks.

The calculated carcinogenic and non-carcinogenic risks to children and adults in the three cities using the annual mean of bioaccessible concentrations for trace metals are shown in Table 7-6. Generally, the US EPA considers that carcinogenic risks lower than  $1 \times 10^{-6}$  can be negligible, and risks higher than  $1 \times 10^{-4}$  can be sufficiently large that some sort of remediation is desirable. Therefore, the carcinogenic risks for lower than  $1 \times 10^{-4}$  are generally considered to be acceptable. In the three cities, the carcinogenic risks via inhalation to children and adults were in the order of Cr > As > Ni > Pb. The carcinogenic risks of Cr and As were higher in GZ than those in SH and NJ, while Ni and Pb exhibited higher carcinogenic risks in SH compared to NJ and GZ. The carcinogenic risks of As, Ni and Pb via inhalation exposure were less than the threshold level of  $1 \times 10^{-6}$  for children and adults at all the cities, indicating that the carcinogenic risks posed by those toxic metals are negligible during the period. Cr toxicity is directly dependent on its valence state (Cr (III) and Cr (VI)); Cr (VI) is more toxicity than Cr (III). In this study, only total bioaccessible concentrations of Cr instead of bioaccessible concentrations of Cr (VI) were determined. The IUR and RfCi of Cr (VI) represented that of total Cr for risk assessment. The calculated carcinogenic risks for Cr presented higher risk than that of Cr (VI). Table 7-6 showed that

the carcinogenic risks of Cr were less than the negligible level of  $1 \times 10^{-6}$  for children and adults in SH and NJ. However, the carcinogenic risk of Cr was slightly higher than  $1 \times 10^{-6}$  for adults in GZ, suggesting that the carcinogenic risk of Cr due to inhalation exposure by  $PM_{2.5}$  can be acceptable in GZ.

The hazard quotient (HQ) for Cr, As, Mn and Ni via inhalation exposure at the three cities were both lower than the safe value of 1, suggesting no non-carcinogenic risks to children and adults. Similar to carcinogenic risks, HQ for Cr and As were higher in GZ than those in SH and NJ, while Ni and Pb exhibited higher HQ in SH compared to NJ and GZ. In the three cities, the element of Cr showed the highest carcinogenic risk to children and adults; and As and Mn exhibited the highest non-carcinogenic risks (HQ).

In winter, the ratios of CR on pollution days to CR on non-pollution days and the ratios of HQ on pollution days to HQ on non-pollution days posed by airborne trace metals are displayed in Fig. 7-9 (a) and (b), respectively. At the three cities, both CR and HQ to children and adults showed higher values on pollution days than those on non-pollution days. In Guangzhou, the health risks of Cr, Mn, Pb, As and Ni for one pollution day exposure equal those for 13.4, 4.89, 3.68, 2.33 and 1.93 non-pollution days exposure, respectively. In Shanghai, the health risks of As, Pb, Mn, Cr and Ni on pollution days were 3.76, 3.67, 3.13, 1.77 and 1.32 times higher than that on non-pollution days, respectively. In Nanjing, the health risks of Pb, As, Mn, Ni and Cr on pollution days were 6.01, 3.28, 3.10, 1.85 and 1.68 times higher than that on non-pollution days, respectively. The results indicated that carcinogenic and non-carcinogenic risks posed by airborne trace metals via inhalation exposure to children and adults were significantly higher on pollution days than those on non-pollution days during winter.

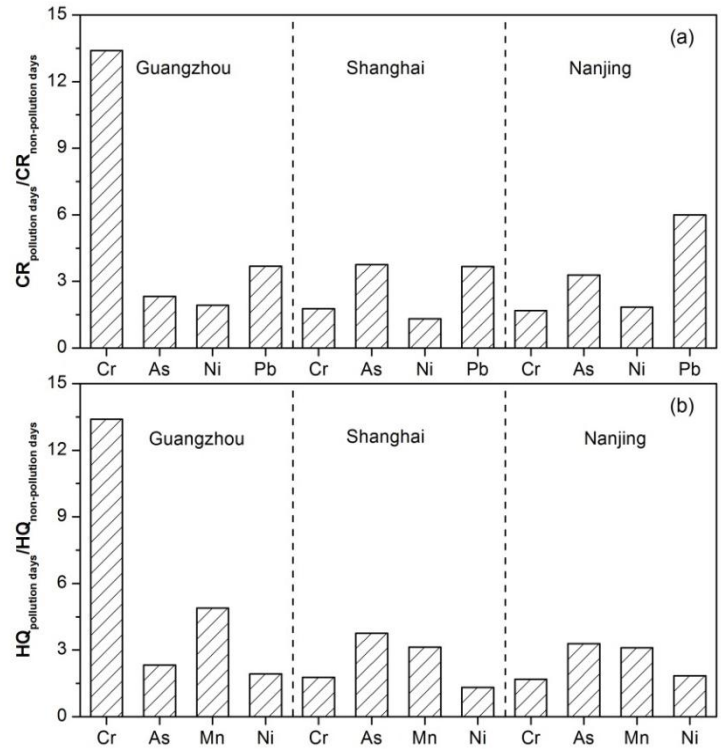


Figure 7-9 The ratios of (a) CR on pollution days to CR on non-pollution days and (b) HQ on pollution days to HQ on non-pollution days posed by airborne trace metals during winter in Guangzhou, Shanghai and Nanjing.

Table 7-4 Related parameters for risk assessment calculation of airborne trace metals via inhalation exposure.

Element	IUR <sup>a</sup>	RfCi <sup>a</sup>	ET (hours day <sup>-1</sup> )	EF (days year <sup>-1</sup> )		
	(µg/m <sup>3</sup> ) <sup>-1</sup>	(mg m <sup>-3</sup> )		Annual	Pollution days	Non-pollution days
Cr <sup>b</sup>	1.20E-02	1.00E-04	8	180	45	45
As	4.30E-03	1.50E-05	8	180	45	45
Ni	2.40E-04	5.00E-05	8	180	45	45
Pb <sup>b,C</sup>	8.00E-05		8	180	45	45
V <sup>c</sup>			8	180	45	45
Mn		5.00E-05	8	180	45	45
Zn			8	180	45	45

<sup>a</sup> IUR and RfCi were obtained from US EPA website (<http://www.epa.gov/region9/superfund/prg/index.html>).

<sup>b</sup> Cr for Cr (VI), Pb for inorganic Pb.

<sup>c</sup> No IUR for V; no RfCi for Pb, V and Zn.

Table 7-5 Mean concentrations (ng m<sup>-3</sup>) of bioaccessible trace metals in PM<sub>2.5</sub> in Guangzhou, Shanghai and Nanjing.

Metals	Guangzhou			Shanghai			Nanjing		
	Annual	Pollution	Non-pollution	Annual	Pollution	Non-pollution	Annual	Pollution	Non-pollution
Cr	3.11	8.69	0.65	1.33	1.97	1.11	1.31	1.97	1.18
As	2.99	6.36	2.74	2.75	6.90	1.84	2.83	5.94	1.81
Mn	5.10	11.57	2.37	10.01	24.79	7.93	6.99	16.46	5.31
Ni	0.57	0.85	0.44	1.34	1.52	1.15	0.81	0.92	0.50
Pb	1.18	3.46	0.94	3.93	12.68	3.46	1.72	5.18	0.86
V	3.61	4.46	1.19	6.30	6.39	6.36	2.05	3.08	2.22
Zn	3.80	10.46	1.74	9.28	36.0	3.53	5.56	19.44	2.09

Annual = annual mean concentration; Pollution = mean concentration in pollution days during winter; Non-pollution = mean concentration in non-pollution days during winter.

Table 7-6 Carcinogenic risk (CR) and non-carcinogenic risk (HQ) of airborne trace metals (annual mean concentrations) via inhalation exposure to children and adults in Guangzhou, Shanghai and Nanjing.

	Guangzhou				Shanghai				Nanjing			
	CR		HQ		CR		HQ		CR		HQ	
	Children	Adults	Children	Adults	Children	Adults	Children	Adults	Children	Adults	Children	Adults
Cr	5.26E-07	2.10E-06	5.12E-03	5.12E-03	2.25E-07	8.99E-07	2.18E-03	2.18E-03	2.21E-07	8.84E-07	2.15E-03	2.15E-03
As	1.81E-07	7.25E-07	3.28E-02	3.28E-02	1.67E-07	6.66E-07	3.01E-02	3.01E-02	1.71E-07	6.85E-07	3.10E-02	3.10E-02
Mn			1.68E-02	1.68E-02			3.29E-02	3.29E-02			2.30E-02	2.30E-02
Ni	1.93E-09	7.71E-09	1.87E-03	1.87E-03	4.54E-09	1.82E-08	4.42E-03	4.42E-03	2.72E-09	1.09E-08	2.65E-03	2.65E-03
Pb	1.33E-09	5.33E-09			4.43E-09	1.77E-08			1.94E-09	7.77E-09		

## 7.6 Summary

Relatively high bioaccessible concentrations for Mn, V and Zn were obtained in GZ, SH and NJ. The bioaccessible concentrations of Mn, Ni, Pb, V and Zn were highest in SH, followed by NJ and GZ. In the three cities, V presented high bioaccessibility in PM<sub>2.5</sub>; Mn, Cr and Ni showed intermediate bioaccessibility; and Pb and Zn exhibited low bioaccessibility. Both high bioaccessible concentrations and bioaccessibilities were observed in winter for Mn, Pb and Zn, probably due to the more input of anthropogenic PM<sub>2.5</sub> and these trace metals in the atmosphere. Compared with non-pollution days, the bioaccessible concentrations of trace metals were higher on pollution days; the bioaccessibility of Mn, Pb, V and Zn in GZ, and Zn in SH and NJ were higher on pollution days. The carcinogenic risks of As, Ni and Pb via inhalation exposure were lower than the acceptable level of  $1 \times 10^{-6}$  for children and adults in the three cities, whereas the carcinogenic risk of Cr was higher than  $1 \times 10^{-6}$  for adults in GZ. The non-carcinogenic risks for Cr, As, Mn and Ni via inhalation exposure to children and adults were lower than the safe value of 1. The element of Cr showed the highest carcinogenic risk to children and adults; and As and Mn exhibited the highest non-carcinogenic risks (HQ). Among the three cities, both carcinogenic risks and HQ showed relatively higher values for Cr and As in GZ, and were higher in SH for Ni and Pb. Carcinogenic and non-carcinogenic risks posed by airborne trace metals via inhalation exposure to children and adults were significantly higher on pollution days than those on non-pollution days during winter. The inhalation of PM<sub>2.5</sub> on pollution days in winter season should be attached more attention in the three cities.

## Chapter 8 - Conclusions and Recommendations

### 8.1 Summary of Major Results

The major findings in the PM<sub>2.5</sub> study in the PRD, the YRD and North China are as follows:

1. Heavy PM<sub>2.5</sub> pollution was observed in the three regions and showed a decreasing trend among the urban sites in the order of North China (Beijing) > the YRD (Shanghai, Nanjing and Hangzhou) > the PRD (Guangzhou). Airborne trace metal pollution was both significant in the three regions, and most serious in Beijing due to the highest contribution of crustal elements. Carbonaceous species (OC and EC) and secondary inorganic species (NO<sub>3</sub><sup>-</sup>, SO<sub>4</sub><sup>2-</sup> and NH<sub>4</sub><sup>+</sup>) were the important components of PM<sub>2.5</sub>. Among Guangzhou (GZ), Shanghai (SH) and Beijing (BJ), PM<sub>2.5</sub> concentrations were ranked in the order of BJ > SH > GZ, while the concentrations for trace elements, OC and EC were decreased in the order of BJ > GZ > SH.
2. The concentrations and chemical compositions of PM<sub>2.5</sub> showed clear temporal-spatial and seasonal variability in all the sampling sites. However, the seasonal patterns of PM<sub>2.5</sub> showed regional differences among the three regions. Similar seasonal patterns for PM<sub>2.5</sub>, SOC and trace elements were found in GZ, SH and BJ, with higher concentrations in winter and lower concentrations in summer. In contrast with other two cities, the concentrations of airborne crustal elements increased from summer to spring in BJ, while no significant seasonal variations of EC and POC were found in GZ.
3. Source appointment of chemical compositions of PM<sub>2.5</sub> demonstrated that anthropogenic sources including coal combustion, heavy industries and traffic emissions were the major contributors to PM<sub>2.5</sub> in the three regions. Enrichment factor and Pb isotopic analysis indicated the large inputs of atmospheric Pb from coal combustion in the three regions during winter.
4. Results of backward trajectory analysis and PSCF model showed that the long-range transport pathways and potential source regions of PM<sub>2.5</sub> in GZ, SH and BJ were

seasonally dependent. Pb isotope signatures in  $PM_{2.5}$  confirmed the inputs of atmospheric Pb from coal combustion via long-range transport in winter in the three regions.

5. Different characteristics in the temporal-spatial and seasonal variations of  $PM_{2.5}$  among the three regions were driven by their local emissions, meteorological conditions and long-range transport pathways.
6. Seasonal trans-boundary transport of  $PM_{2.5}$  over the three regions was found by the PSCF modelling results. In winter, the PRD region was the receptor of transport from the coastal areas of the YRD region, while the YRD region was the receptor of transport from North China. In summer, the transport occurred from the YRD region to North China. Trans-boundary transport of  $PM_{2.5}$  among the three regions was further demonstrated in a severe and long-lasting pollution event that occurred from 2 to 14 December 2013 by the NAQPMS model.
7. Three pollution events (PE1-PE3) were identified in Shanghai during the autumn and winter. Analysis of air mass backward trajectories and meteorological parameters suggested that the meteorological condition was one of the key factors in the formation of pollution events. By using the NAQPMS model, the evolution and transport of  $PM_{2.5}$  over the YRD region during the three pollution events indicated that regional transport play an important role in the formation of pollution events. Secondary aerosols were the dominant components of  $PM_{2.5}$  during the three pollution events. More contributions of crustal elements together with  $NO_3^-$  were observed in PE3, probably attributed to the heterogeneous reactions of  $HNO_3$  and  $NO_2$  on the surface of crustal particles during the long-range transport. The results suggested that the formation of pollution events are related to emission sources, meteorological conditions and long-range transport of air pollutants.
8. High bioaccessibility for V (38.1-55.0%), intermediate bioaccessibility for Mn (14.3-20.6%), Cr (8.25-22.9%) and Ni (6.19-17.7%), and low bioaccessibility for Pb (1.41-4.42%) and Zn (1.63-3.15%) were investigated in  $PM_{2.5}$  in GZ, SH and NJ. Seasonally, the bioaccessibility of Mn, Pb and Zn were highest in winter. Compared

with non-pollution days, the bioaccessibility of Mn, Pb, V and Zn at GZ, and Zn in SH and NJ were higher on pollution days. Carcinogenic and non-carcinogenic risks posed by airborne trace metals via inhalation exposure to children and adults were significantly higher on pollution days than those on non-pollution days during winter.

## **8.2 Recommendations**

Based on the present study, several recommendations are proposed:

- (1) Air quality policy and strategy on the control of PM<sub>2.5</sub> pollution should be adopted to improve air quality in the PRD, the YRD and North China.
- (2) Strategic emission standard and environmental regulations on the emissions of atmospheric particulate matters from various anthropogenic sources, especially from vehicular emissions and coal combustions, should be implemented to control PM<sub>2.5</sub> pollution in the three regions.
- (3) Urban air quality forecasting system and regional haze weather forecasting system should be applied to foster urban and regional air quality management and realize operational prediction and early warning of air pollution and haze weather episode.
- (4) Effective countermeasures, such as reducing outdoor activities, wearing masks and eating more run lung's food, should be adopted to reduce the harm of haze weather to human body.

## **8.3 Limitations and Future Research**

The Pb isotope technique was used to assess the sources and the long-range transport of anthropogenic Pb. However, the method has its limitations. More precise analytical instruments, such as MC-ICP-MS, are required to increase the accuracy of Pb isotopic signature in environmental materials. The lead isotope fingerprinting of Pb emission sources from the literatures is not available to identify the exactly major sources and their contribution of Pb in the air. The differences in Pb isotopic compositions among the various anthropogenic pollution sources may be smaller than what was observed previously.

Moreover, the current regional characteristics of Pb isotopic fingerprint in the air are expected to bring further changes to Pb isotopic compositions due to the free trading of Pb ore and refined products in China, which will make Pb isotope technology for source identification and tracing long-range transport of air pollutants more difficult in the future. Further studies are needed to investigate the Pb isotope signatures in the major sources of atmospheric Pb.

Carbonaceous matter is one of the most abundant components of  $PM_{2.5}$  in China. Investigation of the concentrations and sources of carbonaceous species in  $PM_{2.5}$  requires further research in the city clusters of China. However, it is difficult to identify and quantify their sources due to the various sources. Moreover, the limitations of the widely used methods are lack of the knowledge of the contribution of fossil fuel emissions vs biomass and the differences between primary and secondary sources for carbonaceous species in  $PM_{2.5}$ . The technique of radiocarbon ( $^{14}C$ ) analysis provides unambiguous differentiation among the fossil fuel, biomass burning and biogenic sources on carbonaceous matters in  $PM_{2.5}$ , and is also helpful to understand the formation mechanisms of SOC. Hence, the application of  $^{14}C$  analysis technique is required to better investigate the emission sources and their contributions of carbonaceous matters in  $PM_{2.5}$  in the future work.

Investigation of the bioaccessibility of trace metals in  $PM_{2.5}$  is the first step to understand their potential toxicity. The bioaccessibility of airborne trace metals are related to the emission sources and chemical characteristics of aerosols and meteorological conditions. The factors that possible influence the bioaccessibility of trace metals in  $PM_{2.5}$  should be further studied. In addition, more researches are needed to study the in vitro effects of  $PM_{2.5}$  and to determine the contribution of trace metals in the toxic effect of  $PM_{2.5}$ . Moreover, the toxic effect of  $PM_{2.5}$  was not only due to a direct action of fine particles on the respiratory tissue or lung tissues, but also attributed to the toxicological effects of chemical compounds associated with particles. It is critical to understand the mixture toxic effects and identification of which components and sources dominate the toxicity of  $PM_{2.5}$ .

## References

- Abu-Allaban, M., Gillies, J.A., Gertler, A.W., Clayton, R. and Proffitt, D., 2007. Motor vehicle contributions to ambient PM<sub>10</sub> and PM<sub>2.5</sub> at selected urban areas in the USA. *Environ. Monit. Assess.* 132 (1-3), 155-163.
- Adamson, I., Frieditis, H., Hedgecock, C. and Vincent, R., 2000. Zinc is the toxic factor in the lung response to an atmospheric particulate sample. *Toxicol. Appl. Pharmacol.* 166 (2), 111-119.
- Al-Masri, M.S., Al-Kharfan, K. and Al-Shamali, K., 2006. Speciation of Pb, Cu and Zn determined by sequential extraction for identification of air pollution sources in Syria. *Atmos. Environ.* 40 (4), 753-761.
- Al-Momani, I., 2003. Trace elements in atmospheric precipitation at Northern Jordan measured by ICP-MS: acidity and possible sources. *Atmos. Environ.* 37 (32), 4507-4515.
- Alexander, B., Allman, D., Amos, H., Fairlie, T., Dachs, J., Hegg, D.A. and Sletten, R.S., 2012. Isotopic constraints on the formation pathways of sulfate aerosol in the marine boundary layer of the subtropical northeast Atlantic Ocean. *J. Geophys. Res.* 117 (D6).
- Andronache, C., 2003. Estimated variability of below-cloud aerosol removal by rainfall for observed aerosol size distributions. *Atmos. Chem. Phys.* 3 (1), 131-143.
- Ashbaugh, L.L., Malm, W.C. and Sadeh, W.Z., 1985. A residence time probability analysis of sulfur concentrations at Grand Canyon National Park. *Atmos. Environ.* 19 (8), 1263-1270.
- Bao, Z., Fen, Y.C., Jiao, L., Hong, S.M. and Liu, W.G., 2010. Characterization and source apportionment of PM<sub>2.5</sub> and PM<sub>10</sub> in Hangzhou. *Environ. Monit. in China* 26 (2), 44-48 (in Chinese).
- Basta, N. and Tabatabai, M., 1992. Effect of cropping systems on adsorption of metals by soils: II. Effect of pH. *Soil Science* 153 (3), 195.
- Bi, X.Y., Liang, S.Y. and Li, X.D., 2013. A novel in situ method for sampling urban soil dust: Particle size distribution, trace metal concentrations, and stable lead isotopes. *Environ. Pollut.* 177, 48-57.
- Birmili, W., Allen, A.G., Bary, F. and Harrison, R.M., 2006. Trace metal concentrations and water solubility in size-fractionated atmospheric particles and influence of road traffic. *Environ. Sci. Technol.* 40 (4), 1144-1153.
- Burling, I.R., Yokelson, R.J., Griffith, D.W.T., Johnson, T.J., Veres, P., Roberts, J.M., Warneke,

- C., Urbanski, S.P., Reardon, J. and Weise, D.R., 2010. Laboratory measurements of trace gas emissions from biomass burning of fuel types from the southeastern and southwestern United States. *Atmos. Chem. Phys.* 10 (22), 11115-11130.
- Byun, D.W. and Dennis, R., 1995. Design artifacts in Eulerian air quality models: evaluation of the effects of layer thickness and vertical profile correction on surface ozone concentrations. *Atmos. Environ.* 29 (1), 105-126.
- Calvo, A.I., Alves, C., Castro, A., Pont, V., Vicente, A.M. and Fraile, R., 2013. Research on aerosol sources and chemical composition: past, current and emerging issues. *Atmos. Res.* 120, 1-28.
- Cao, G.L., Zhang, X.Y., Wang, D. and Zheng, F.C., 2005. Inventory of atmospheric pollutants discharged from biomass burning in China continent. *China Environ. Sci.* 25 (4), 389-393 (in Chinese).
- Cao, J.J., Lee, S.C., Ho, K.F., Zou, S.C., Fung, K., Li, Y., Watson, J.G. and Chow, J.C., 2004. Spatial and seasonal variations of atmospheric organic carbon and elemental carbon in Pearl River Delta Region, China. *Atmos. Environ.* 38 (27), 4447-4456.
- Cao, J.J., Lee, S.C., Ho, K.F., Zou, S.C., Zhang, X.Y. and Pan, J.G., 2003. Spatial and seasonal distributions of atmospheric carbonaceous aerosols in Pearl River Delta Region, China. *China Particology* 1 (1), 33-37.
- Cao, J.J., Shen, Z.X., Chow, J.C., Qi, G.W. and Watson, J.G., 2009. Seasonal variations and sources of mass and chemical composition for PM<sub>10</sub> aerosol in Hangzhou, China. *Particology* 7 (3), 161-168.
- Cao, J.J., Shen, Z.X., Chow, J.C., Watson, J.G., Lee, S.C., Tie, X.X., Ho, K.F., Wang, G.H. and Han, Y.M., 2012. Winter and summer PM<sub>2.5</sub> chemical compositions in fourteen Chinese cities. *J. Air Waste Manage. Assoc.* 62 (10), 1214-1226.
- Carslaw, K.S., Boucher, O., Spracklen, D.V., Mann, G.W., Rae, J.G.L., Woodward, S. and Kulmala, M., 2010. A review of natural aerosol interactions and feedbacks within the Earth system. *Atmos. Chem. Phys.* 10 (4), 1701-1737.
- Castro, L.M., Pio, C.A., Harrison, R.M. and Smith, D.J.T., 1999. Carbonaceous aerosol in urban and rural European atmospheres: estimation of secondary organic carbon concentrations. *Atmos. Environ.* 33 (17), 2771-2781.
- Chan, C.K. and Yao, X., 2008. Air pollution in mega cities in China. *Atmos. Environ.* 42 (1), 1-42.
- Charrier, J., McFall, A., Richards-Henderson, N. and Anastasio, C., 2014. Hydrogen peroxide

- formation in a surrogate lung fluid by transition metals and quinones present in particulate matter. *Environ. Sci. Technol.* 48, 7010-7017.
- Che, H.Z., Yang, Z.F., Zhang, X.Y., Zhu, C.Z., Ma, Q.L., Zhou, H.G. and Wang, P., 2009a. Study on the aerosol optical properties and their relationship with aerosol chemical compositions over three regional background stations in China. *Atmos. Environ.* 43 (5), 1093-1099.
- Che, H.Z., Zhang, X.Y., Li, Y., Zhou, Z.J., Qu, J.J. and Hao, X.J., 2009b. Haze trends over the capital cities of 31 provinces in China, 1981–2005. *Theor. Appl. Climatol* 97 (3-4), 235-242.
- Chen, J.M., Tan, M.G., Li, Y.L., Zhang, Y.M., Lu, W.W., Tong, Y.P., Zhang, G.L. and Li, Y., 2005. A lead isotope record of Shanghai atmospheric lead emissions in total suspended particles during the period of phasing out of leaded gasoline. *Atmos. Environ.* 39 (7), 1245-1253.
- Chen, J.M., Tan, M.G., Li, Y.L., Zheng, J., Zhang, Y.M., Shan, Z.C., Zhang, G.L. and Li, Y., 2008. Characteristics of trace elements and lead isotope ratios in PM<sub>2.5</sub> from four sites in Shanghai. *J. Hazard. Mater.* 156 (1), 36-43.
- Chen, J.M., Tong, Y.P., Xu, J.Z., Liu, X.L., Li, Y.L., Tan, M.G. and Li, Y., 2012. Environmental lead pollution threatens the children living in the Pearl River Delta region, China. *Environ. Sci. Pollut. Res.* 19 (8), 3268-3275.
- Cheng, H.F. and Hu, Y.A., 2010. Lead (Pb) isotopic fingerprinting and its applications in lead pollution studies in China: a review. *Environ. Pollut.* 158 (5), 1134-1146.
- Cheng, M.C., You, C.F., Cao, J.J. and Jin, Z.D., 2012. Spatial and seasonal variability of water-soluble ions in PM<sub>2.5</sub> aerosols in 14 major cities in China. *Atmos. Environ.* 60, 182-192.
- Cheng, Y., Brook, J.R., Li, S.M. and Leithead, A., 2011. Seasonal variation in the biogenic secondary organic aerosol tracer *cis*-pinonic acid: Enhancement due to emissions from regional and local biomass burning. *Atmos. Environ.* 45 (39), 7105-7112.
- Cheng, Y., Engling, G., He, K.B., Duan, F.K., Ma, Y.L., Du, Z.Y., Liu, J.M., Zheng, M. and Weber, R.J., 2013. Biomass burning contribution to Beijing aerosol. *Atmos. Chem. Phys. Discuss* 13 (3), 8387-8434.
- Cheng, Z., Wang, S., Fu, X., Watson, J.G., Jiang, J., Fu, Q., Chen, C., Xu, B., Yu, J. and Chow, J.C., 2014. Impact of biomass burning on haze pollution in the Yangtze River delta, China: a case study in summer 2011. *Atmos. Chem. Phys.* 14 (9), 4573-4585.
- Chester, R., Lin, F.J. and Murphy, K.J.T., 1989. A three stage sequential leaching scheme for the characterisation of the sources and environmental mobility of trace metals in the marine

- aerosol. Environ. Technol. 10 (10), 887-900.
- Cheung, K., Daher, N., Kam, W., Shafer, M.M., Ning, Z., Schauer, J.J. and Sioutas, C., 2011. Spatial and temporal variation of chemical composition and mass closure of ambient coarse particulate matter (PM<sub>10-2.5</sub>) in the Los Angeles area. Atmos. Environ. 45 (16), 2651-2662.
- Choi, J.K., Heo, J.B., Ban, S.J., Yi, S.M. and Zoh, K.D., 2012. Chemical characteristics of PM<sub>2.5</sub> aerosol in Incheon, Korea. Atmos. Environ. 60, 583-592.
- Claeys, M., Kourtchev, I., Pashynska, V., Vas, G., Vermeylen, R., Wang, W., Cafmeyer, J., Chi, X.G., Artaxo, P. and Andreae, M.O., 2010. Polar organic marker compounds in atmospheric aerosols during the LBA-SMOCC 2002 biomass burning experiment in Rondônia, Brazil: sources and source processes, time series, diel variations and size distributions. Atmos. Chem. Phys 10, 9319-9331.
- Clements, A.L., Buzcu-Guven, B., Fraser, M.P., Kulkarni, P. and Chellam, S., 2013. Role of particulate metals in heterogenous secondary sulfate formation. Atmos. Environ. 75, 233-240.
- Colin, J.L., Jaffrezo, J.L. and Gros, J.M., 1990. Solubility of major species in precipitation: factors of variation. Atmos. Environ. Part A. General Topics 24 (3), 537-544.
- Colombo, C., Monhemius, A.J. and Plant, J.A., 2008. Platinum, palladium and rhodium release from vehicle exhaust catalysts and road dust exposed to simulated lung fluids. Ecotoxicol. Environ. Saf. 71 (3), 722-730.
- Cong, Z.Y., Kang, S.C., Zhang, Y.L. and Li, X.D., 2010. Atmospheric wet deposition of trace elements to central Tibetan Plateau. Appl. Geochem. 25 (9), 1415-1421.
- Corbett, J.J., Winebrake, J.J., Green, E.H., Kasibhatla, P., Eyring, V. and Lauer, A., 2007. Mortality from ship emissions: a global assessment. Environ. Sci. Technol. 41 (24), 8512-8518.
- Deng, X.J., Tie, X.X., Wu, D., Zhou, X.J., Bi, X.Y., Tan, H.B., Li, F. and Jiang, C.L., 2008. Long-term trend of visibility and its characterizations in the Pearl River Delta (PRD) region, China. Atmos. Environ. 42 (7), 1424-1435.
- Desboeufs, K.V., Sofikitis, A., Losno, R., Colin, J.L. and Auset, P., 2005. Dissolution and solubility of trace metals from natural and anthropogenic aerosol particulate matter. Chemosphere 58 (2), 195-203.
- Ding, Q., Liu, J.G., Lu, Y.H., Lu, F., Wang, Y.P., Shi, J.G. and Shen, Y., 2012. Measurement and analysis of particulate matter and carbonaceous aerosol in Heshan during Guangzhou Asian Games. Environ. Sci. Technol. 35 (7), 43-49.

- Ding, Y.H., 1994. *Monsoons over China*. Kluwer Academic Publishers.
- Dorling, S.R., Davies, T.D. and Pierce, C.E., 1992. Cluster analysis: a technique for estimating the synoptic meteorological controls on air and precipitation chemistry—method and applications. *Atmospheric Environment. Part A. General Topics* 26 (14), 2575-2581.
- Draxler, R. and Rolph, G., 2003. HYSPLIT (HYbrid Single-Particle Lagrangian Integrated Trajectory) Model, NOAA Air Resour. Lab., Silver Spring, Md.
- Du, H.H., Kong, L.D., Cheng, T.T., Chen, J.M., Du, J.F., Li, L., Xia, X.G., Leng, C.P. and Huang, G.H., 2011. Insights into summertime haze pollution events over Shanghai based on online water-soluble ionic composition of aerosols. *Atmos. Environ.* 45 (29), 5131-5137.
- Du, S.Q., Shi, P.J. and Van Rompaey, A., 2013. The Relationship between Urban Sprawl and Farmland Displacement in the Pearl River Delta, China. *Land* 3 (1), 34-51.
- Duan, F.K., Liu, X.D., Yu, T. and Cachier, H., 2004. Identification and estimate of biomass burning contribution to the urban aerosol organic carbon concentrations in Beijing. *Atmos. Environ.* 38 (9), 1275-1282.
- Duan, J.C., Tan, J.H., Cheng, D.X., Bi, X.H., Deng, W.J., Sheng, G.Y., Fu, J.M. and Wong, M.H., 2007. Sources and characteristics of carbonaceous aerosol in two largest cities in Pearl River Delta Region, China. *Atmos. Environ.* 41 (14), 2895-2903.
- Duan, J.C., Tan, J.H., Hao, J.M. and Chai, F.H., 2014. Size distribution, characteristics and sources of heavy metals in haze episod in Beijing. *J. Environ. Sci. (China)* 26 (1), 189-196.
- Duan, J.C., Tan, J.H., Wang, S.L., Hao, J.M. and Chai, F.H., 2012. Size distributions and sources of elements in particulate matter at curbside, urban and rural sites in Beijing. *J. Environ. Sci* 24 (1), 87-94.
- Duzgoren-Aydin, N.S., Li, X.D. and Wong, S.C., 2004. Lead contamination and isotope signatures in the urban environment of Hong Kong. *Environ. Int.* 30 (2), 209-217.
- Elias, V.O., Simoneit, B.R., Cordeiro, R.C. and Turcq, B., 2001. Evaluating levoglucosan as an indicator of biomass burning in Carajas, Amazonia: A comparison to the charcoal record. *Geochim. Cosmochim. Acta* 65 (2), 267-272.
- Engling, G., Carrico, C.M., Kreidenweis, S.M., Collett, J.L., Day, D.E., Malm, W.C., Lincoln, E., Hao, W.M., Iinuma, Y. and Herrmann, H., 2006. Determination of levoglucosan in biomass combustion aerosol by high-performance anion-exchange chromatography with pulsed amperometric detection. *Atmos. Environ.* 40, 299-311.
- Falta, T., Limbeck, A., Koellensperger, G. and Hann, S., 2008. Bioaccessibility of selected trace

- metals in urban PM<sub>2.5</sub> and PM<sub>10</sub> samples: a model study. *Anal. Bioanal. Chem.* 390 (4), 1149-1157.
- Feng, J.L., Guo, Z.G., Zhang, T.R., Yao, X.H., Chan, C.K. and Fang, M., 2012. Source and formation of secondary particulate matter in PM<sub>2.5</sub> in Asian continental outflow. *J. Geophys. Res.* 117 (D3).
- Feng, X.D., Dang, Z., Huang, W.L. and Yang, C., 2009a. Chemical speciation of fine particle bound trace metals. *Int. J. Environ. Sci. Tech* 6 (3), 337-346.
- Feng, Y.L., Chen, Y.J., Guo, H., Zhi, G.R., Xiong, S.C., Li, J., Sheng, G.Y. and Fu, J.M., 2009b. Characteristics of organic and elemental carbon in PM<sub>2.5</sub> samples in Shanghai, China. *Atmos. Res.* 92 (4), 434-442.
- Fu, Q.Y., Zhuang, G.S., Li, J., Huang, K., Wang, Q.Z., Zhang, R., Fu, J., Lu, T., Chen, M. and Wang, Q., 2010. Source, long-range transport, and characteristics of a heavy dust pollution event in Shanghai. *J. Geophys. Res.* 115 (D7).
- Fu, Q.Y., Zhuang, G.S., Wang, J., Xu, C., Huang, K., Li, J., Hou, B., Lu, T. and Streets, D.G., 2008. Mechanism of formation of the heaviest pollution episode ever recorded in the Yangtze River Delta, China. *Atmos. Environ.* 42 (9), 2023-2036.
- Fu, T.M., Cao, J.J., Zhang, X.Y., Lee, S.C., Zhang, Q., Han, Y.M., Qu, W.J., Han, Z.W., Zhang, R.J. and Wang, Y.X., 2012. Carbonaceous aerosols in China: top-down constraints on primary sources and estimation of secondary contribution. *Atmos. Chem. Phys.* 12 (5), 2725-2746.
- Fu, X., Wang, S.X., Zhao, B., Xing, J., Cheng, Z., Liu, H. and Hao, J.M., 2013. Emission inventory of primary pollutants and chemical speciation in 2010 for the Yangtze River Delta region, China. *Atmos. Environ.* 70, 39-50.
- Fu, X.X., Wang, X.M., Guo, H., Cheung, K., Ding, X., Zhao, X.Y., He, Q.F., Gao, B., Zhang, Z. and Liu, T.Y., 2014. Trends of ambient fine particles and major chemical components in the Pearl River Delta region: Observation at a regional background site in fall and winter. *Sci. Total. Environ.* 497, 274-281.
- Gao, J., Wang, T., Zhou, X.H., Wu, W.S. and Wang, W.X., 2009. Measurement of aerosol number size distributions in the Yangtze River delta in China: Formation and growth of particles under polluted conditions. *Atmos. Environ.* 43 (4), 829-836.
- Gao, J.J., Tian, H.Z., Cheng, K., Lu, L., Zheng, M., Wang, S.X., Hao, J.M., Wang, K., Hua, S.B. and Zhu, C.Y., 2015. The variation of chemical characteristics of PM<sub>2.5</sub> and PM<sub>10</sub> and formation causes during two haze pollution events in urban Beijing, China. *Atmos. Environ.* 107, 1-8.

- Gao, X.M., Xue, L.K., Wang, X.F., Wang, T., Yuan, C., Gao, R., Zhou, Y., Nie, W., Zhang, Q.Z. and Wang, W.X., 2012. Aerosol ionic components at Mt. Heng in central southern China: Abundances, size distribution, and impacts of long-range transport. *Sci. Total. Environ.* 433, 498-506.
- Gelencs, A., May, B., Simpson, D., Sanchez-Ochoa, A., Kasper-Giebl, A., Puxbaum, H., Caseiro, A., Pio, C. and Legrand, M., 2007. Source apportionment of PM<sub>2.5</sub> organic aerosol over Europe: Primary/secondary, natural/anthropogenic, and fossil/biogenic origin. *J. Geophys. Res.* 112 (D23).
- Gerlofs-Nijland, M.E., Rummelhard, M., Boere, A.J.F., Leseman, D.L., Duffin, R., Schins, R.P., Borm, P.J., Sillanpa, M., Salonen, R.O. and Cassee, F.R., 2009. Particle induced toxicity in relation to transition metal and polycyclic aromatic hydrocarbon contents. *Environ. Sci. Technol.* 43 (13), 4729-4736.
- Ghio, A.J., 1999. Metals associated with both the water-soluble and insoluble fractions of an ambient air pollution particle catalyze an oxidative stress. *Inhal. Toxicol.* 11 (1), 37-49.
- Gioda, A., Reyes-Rodriguez, G.J., Santos-Figueroa, G., Collett, J.L., Decesari, S., Ramos, M.d.C.K., Bezerra Netto, H.J., de Aquino Neto, F.R. and Mayol-Bracero, O.L., 2011. Speciation of water-soluble inorganic, organic, and total nitrogen in a background marine environment: Cloud water, rainwater, and aerosol particles. *J. Geophys. Res.* 116 (D5).
- Glavas, S.D., Nikolakis, P., Ambatzoglou, D. and Mihalopoulos, N., 2008. Factors affecting the seasonal variation of mass and ionic composition of PM<sub>2.5</sub> at a central Mediterranean coastal site. *Atmos. Environ.* 42 (21), 5365-5373.
- Guerreiro, C., de Leeuw, F. and Foltescu, V., 2013. European Environmental Agency. Air Quality in Europe: 2013 Report. Denmark. Rosendahls-Schultz Grafisk.
- Guo, S., Hu, M., Wang, Z.B., Slanina, J. and Zhao, Y.L., 2010. Size-resolved aerosol water-soluble ionic compositions in the summer of Beijing: implication of regional secondary formation. *Atmos. Chem. Phys.* 10 (3), 947-959.
- Hagler, G.S.W., Bergin, M.H., Salmon, L.G., Yu, J.Z., Wan, E.C.H., Zheng, M., Zeng, L.M., Kiang, C.S., Zhang, Y.H. and Lau, A.K.H., 2006. Source areas and chemical composition of fine particulate matter in the Pearl River Delta region of China. *Atmos. Environ.* 40 (20), 3802-3815.
- Hagler, G.S.W., Bergin, M.H., Salmon, L.G., Yu, J.Z., Wan, E.C.H., Zheng, M., Zeng, L.M., Kiang, C.S., Zhang, Y.H. and Schauer, J.J., 2007. Local and regional anthropogenic influence on PM<sub>2.5</sub> elements in Hong Kong. *Atmos. Environ.* 41 (28), 5994-6004.
- Hallquist, M., Wenger, J.C., Baltensperger, U., Rudich, Y., Simpson, D., Claeys, M., Dommen, J.,

- Donahue, N.M., George, C. and Goldstein, A.H., 2009. The formation, properties and impact of secondary organic aerosol: current and emerging issues. *Atmos. Chem. Phys.* 9 (14), 5155-5236.
- Hans Wedepohl, K., 1995. The composition of the continental crust. *Geochim. Cosmochim. Acta* 59 (7), 1217-1232.
- Hao, J.M., Wang, L.T., Li, L., Hu, J.N. and Yu, X.C., 2005. Air pollutants contribution and control strategies of energy-use related sources in Beijing. *Science in China Series D* 48 (Suppl. II), 138-146.
- He, K., Zhao, Q., Ma, Y., Duan, F., Yang, F., Shi, Z., Chen, G. and Tie, X., 2012. Spatial and seasonal variability of PM<sub>2.5</sub> acidity at two Chinese megacities: insights into the formation of secondary inorganic aerosols. *Atmos. Chem. Phys.* 12 (3).
- Heal, M.R., Elton, R.A., Hibbs, L.R., Agius, R.M. and Beverland, I.J., 2009. A time-series study of the health effects of water-soluble and total-extractable metal content of airborne particulate matter. *Occup. Environ. Med.* 66 (9), 636-638.
- Heal, M.R., Hibbs, L.R., Agius, R.M. and Beverland, I.J., 2005. Total and water-soluble trace metal content of urban background PM<sub>10</sub>, PM<sub>2.5</sub> and black smoke in Edinburgh, UK. *Atmos. Environ.* 39 (8), 1417-1430.
- Hillamo, R., Allegrini, I., Sparapani, R. and Kerminen, V.-M., 1998. Mass Size Distributions and Precursor Gas Concentrations of Major Inorganic Ions in Antarctic Aerosol. *Int. J. Environ. Anal. Chem.* 71 (3-4), 353-372.
- Hong, S.M., Jiao, L. and Ma, W.L., 2013. Variation of PM<sub>2.5</sub> concentration in Hangzhou, China. *Particuology* 11 (1), 55-62.
- Hsu, S.C., Chen Liu, S., Jeng, W.L., K Chou, C.C., Hsu, R.T., Huang, Y.T. and Chen, Y.W., 2006. Lead isotope ratios in ambient aerosols from Taipei, Taiwan: Identifying long-range transport of airborne Pb from the Yangtze Delta. *Atmos. Environ.* 40 (28), 5393-5404.
- Hsu, S.C., Liu, S.C., Arimoto, R., Shiah, F.K., Gong, G.C., Huang, Y.T., Kao, S.J., Chen, J.P., Lin, F.J. and Lin, C.Y., 2010a. Effects of acidic processing, transport history, and dust and sea salt loadings on the dissolution of iron from Asian dust. *J. Geophys. Res.* 115 (D19).
- Hsu, S.C., Liu, S.C., Jeng, W.L., Lin, F.J., Huang, Y.T., Candice Lung, S.C., Liu, T.H. and Tu, J.Y., 2005. Variations of Cd/Pb and Zn/Pb ratios in Taipei aerosols reflecting long-range transport or local pollution emissions. *Sci. Total. Environ.* 347 (1), 111-121.
- Hsu, S.C., Wong, G.T., Gong, G.C., Shiah, F.K., Huang, Y.T., Kao, S.J., Tsai, F.J., Candice Lung, S.C., Lin, F.J. and Lin, I., 2010b. Sources, solubility, and dry deposition of aerosol trace

elements over the East China Sea. *Mar. Chem.* 120 (1), 116-127.

- Hu, J.L., Wang, Y.G., Ying, Q. and Zhang, H.L., 2014. Spatial and temporal variability of PM<sub>2.5</sub> and PM<sub>10</sub> over the North China Plain and the Yangtze River Delta, China. *Atmos. Environ.* 95, 598-609.
- Hu, X., Zhang, Y., Ding, Z.H., Wang, T.J., Lian, H.Z., Sun, Y.Y. and Wu, J.C., 2012. Bioaccessibility and health risk of arsenic and heavy metals (Cd, Co, Cr, Cu, Ni, Pb, Zn and Mn) in TSP and PM<sub>2.5</sub> in Nanjing, China. *Atmos. Environ.* 57, 146-152.
- Hua, Y., Cheng, Z., Wang, S.X., Jiang, J.K., Chen, D., Cai, S.Y., Fu, X., Fu, Q., Chen, C.H. and Xu, B.Y., 2015. Characteristics and source apportionment of PM<sub>2.5</sub> during a fall heavy haze episode in the Yangtze River Delta of China. *Atmos. Environ.* 123, 380-391.
- Huang, C., Chen, C.H., Li, L., Cheng, Z., Wang, H.L., Huang, H.Y., Streets, D.G., Wang, Y.J., Zhang, G.F. and Chen, Y.R., 2011. Emission inventory of anthropogenic air pollutants and VOC species in the Yangtze River Delta region, China. *Atmos. Chem. Phys.* 11 (9), 4105-4120.
- Huang, H., Lee, S.C., Cao, J.J., Zou, C.W., Chen, X.G. and Fan, S.J., 2007. Characteristics of indoor/outdoor PM<sub>2.5</sub> and elemental components in generic urban, roadside and industrial plant areas of Guangzhou City, China. *J. Environ. Sci-China* 19 (1), 35-43.
- Huang, K., Zhuang, G., Lin, Y., Fu, J.S., Wang, Q., Liu, T., Zhang, R., Jiang, Y., Deng, C., Fu, Q., Hsu, N.C. and Cao, B., 2012a. Typical types and formation mechanisms of haze in an Eastern Asia megacity, Shanghai. *Atmos. Chem. Phys.* 12 (1), 105-124.
- Huang, R.J., Zhang, Y.I., Bozzetti, C., Ho, K.F., Cao, J.J., Han, Y.M., Daellenbach, K.R., Slowik, J.G., Platt, S.M. and Canonaco, F., 2014. High secondary aerosol contribution to particulate pollution during haze events in China. *Nature* 514 (7521), 218-222.
- Huang, S.S., Tu, J., Liu, H.Y., Hua, M., Liao, Q.L., Feng, J.S., Weng, Z.H. and Huang, G.M., 2009. Multivariate analysis of trace element concentrations in atmospheric deposition in the Yangtze River Delta, East China. *Atmos. Environ.* 43 (36), 5781-5790.
- Huang, X.F., Sun, T.L., Zeng, L.W., Yu, G.H. and Luan, S.J., 2012b. Black carbon aerosol characterization in a coastal city in South China using a single particle soot photometer. *Atmos. Environ.* 51, 21-28.
- Huang, X.F., Xue, L., Tian, X.D., Shao, W.W., Sun, T.L., Gong, Z.H., Ju, W.W., Jiang, B., Hu, M. and He, L.Y., 2013. Highly time-resolved carbonaceous aerosol characterization in Yangtze River Delta of China: Composition, mixing state and secondary formation. *Atmos. Environ.* 64, 200-207.

- Huang, X.F. and Yu, J.Z., 2008. Size distributions of elemental carbon in the atmosphere of a coastal urban area in South China: characteristics, evolution processes, and implications for the mixing state. *Atmos. Chem. Phys.* 8 (19), 5843-5853.
- Ip, C.C., Li, X.D., Zhang, G., Wai, O.W. and Li, Y.S., 2007. Trace metal distribution in sediments of the Pearl River Estuary and the surrounding coastal area, South China. *Environ. Pollut.* 147 (2), 311-323.
- Kang, H.Q., Zhu, B., Su, J.F., Wang, H.L., Zhang, Q.C. and Wang, F., 2013. Analysis of a long-lasting haze episode in Nanjing, China. *Atmos. Res.* 120, 78-87.
- Kendall, M., Pala, K., Ucakli, S. and Gucer, S., 2011. Airborne particulate matter (PM<sub>2.5</sub> and PM<sub>10</sub>) and associated metals in urban Turkey. *Air Qual. Atmos. Health* 4 (3-4), 235-242.
- Kolb, C.E. and Worsnop, D.R., 2012. Chemistry and Composition of Atmospheric Aerosol Particles. *Annu. Rev. Phys. Chem.* 63, 471-491.
- Kulmala, M., Vehkamäki, H., Petäjä, T., Dal Maso, M., Lauri, A., Kerminen, V.M., Birmili, W. and McMurry, P.H., 2004. Formation and growth rates of ultrafine atmospheric particles: a review of observations. *J. Aerosol Sci* 35 (2), 143-176.
- Kulshrestha, A., Satsangi, P.G., Masih, J. and Taneja, A., 2009. Metal concentration of PM<sub>2.5</sub> and PM<sub>10</sub> particles and seasonal variations in urban and rural environment of Agra, India. *Sci. Total. Environ.* 407 (24), 6196-6204.
- Kumagai, K., Iijima, A., Shimoda, M., Saitoh, Y., Kozawa, K., Hagino, H. and Sakamoto, K., 2010. Determination of dicarboxylic acids and levoglucosan in fine particles in the Kanto Plain, Japan, for source apportionment of organic aerosols. *Aerosol. Air. Qual. Res* 10 (3), 282-291.
- Kurokawa, J., Ohara, T., Morikawa, T., Hanayama, S., Janssens-Maenhout, G., Fukui, T., Kawashima, K. and Akimoto, H., 2013. Emissions of air pollutants and greenhouse gases over Asian regions during 2000–2008: Regional Emission inventory in ASia (REAS) version 2. *Atmos. Chem. Phys.* 13 (21), 11019-11058.
- Lanki, T., de Hartog, J.J., Heinrich, J., Hoek, G., Janssen, N.A., Peters, A., Stözel, M., Timonen, K.L., Vallius, M. and Vanninen, E., 2006. Can we identify sources of fine particles responsible for exercise-induced ischemia on days with elevated air pollution? The ULTRA study. *Environ. Health Perspect.* 114, 655-660.
- Lee, C.S.L. 2007. Study of atmospheric trace metals in particulate matter, dry and wet depositions, and mosses in the Pearl River Delta region. Doctor of Philosophy, The Hong Kong Polytechnic University.

- Lee, C.S.L., Li, X.D., Shi, W.Z., Cheung, S.C.N. and Thornton, I., 2006. Metal contamination in urban, suburban, and country park soils of Hong Kong: a study based on GIS and multivariate statistics. *Sci. Total. Environ.* 356 (1), 45-61.
- Lee, C.S.L., Li, X.D., Zhang, G., Li, J., Ding, A.J. and Wang, T., 2007. Heavy metals and Pb isotopic composition of aerosols in urban and suburban areas of Hong Kong and Guangzhou, South China—evidence of the long-range transport of air contaminants. *Atmos. Environ.* 41 (2), 432-447.
- Li, J., Wang, Z., Akimoto, H., Yamaji, K., Takigawa, M., Pochanart, P., Liu, Y., Tanimoto, H. and Kanaya, Y., 2008. Near-ground ozone source attributions and outflow in central eastern China during MTX2006. *Atmos. Chem. Phys.* 8 (24), 7335-7351.
- Li, J., Wang, Z., Zhuang, G., Luo, G., Sun, Y. and Wang, Q., 2012. Mixing of Asian mineral dust with anthropogenic pollutants over East Asia: a model case study of a super-duststorm in March 2010. *Atmos. Chem. Phys.* 12 (16), 7591-7607.
- Li, J., Yang, W.Y., Wang, Z.F., Chen, H.S., Hu, B., Li, J.J., Sun, Y.L. and Huang, Y., 2014. A modeling study of source–receptor relationships in atmospheric particulate matter over Northeast Asia. *Atmos. Environ.* 91, 40-51.
- Li, N., Sioutas, C., Cho, A., Schmitz, D., Misra, C., Sempf, J., Wang, M., Oberley, T., Froines, J. and Nel, A., 2003. Ultrafine particulate pollutants induce oxidative stress and mitochondrial damage. *Environ. Health Perspect.* 111 (4), 455.
- Li, W.J. and Shao, L.Y., 2009. Observation of nitrate coatings on atmospheric mineral dust particles. *Atmos. Chem. Phys.* 9 (6), 1863-1871.
- Li, X.L., Zhang, Y.X., Tan, M.G., Liu, J.F., Bao, L.M., Zhang, G.L., Li, Y. and IIDA, A., 2009. Atmospheric lead pollution in fine particulate matter in Shanghai, China. *J. Environ. Sci* 21 (8), 1118-1124.
- Liang, F., Zhang, G.L., Tan, M.G., Yan, C.H., Li, X.L., Li, Y.L., Li, Y., Zhang, Y.M. and Shan, Z.C., 2010. Lead in children's blood is mainly caused by coal-fired ash after phasing out of leaded gasoline in Shanghai. *Environ. Sci. Technol.* 44 (12), 4760-4765.
- Lin, W.S., Xu, Y., Huang, C.C., Ma, Y.F., Shannon, K.B., Chen, D.R. and Huang, Y.W., 2009. Toxicity of nano- and micro-sized ZnO particles in human lung epithelial cells. *J. Nanopart. Res.* 11 (1), 25-39.
- Liu, D., Li, J., Zhang, Y.L., Xu, Y., Liu, X., Ding, P., Shen, C.D., Chen, Y.J., Tian, C.G. and Zhang, G., 2013. The use of levoglucosan and radiocarbon for source apportionment of PM<sub>2.5</sub> carbonaceous aerosols at a background site in East China. *Environ. Sci. Technol.* 47 (18), 10454-10461.

- Liu, H., He, K.B., Wang, Q.D., Huo, H., Lents, J., Davis, N., Nikkila, N., Chen, C.H., Osses, M. and He, C.Y., 2007. Comparison of vehicle activity and emission inventory between Beijing and Shanghai. *J. Air Waste Manage. Assoc.* 57 (10), 1172-1177.
- Liu, J.W., Li, J., Zhang, Y.L., Liu, D., Ding, P., Shen, C.D., Shen, K.J., He, Q.F., Ding, X., Wang, X.M., Chen, D.H., Szidat, S. and Zhang, G., 2014. Source apportionment using radiocarbon and organic tracers for PM<sub>2.5</sub> carbonaceous aerosols in Guangzhou, South China: contrasting local-and regional-scale haze events. *Environ. Sci. Technol.* 48 (20), 12002-12011.
- Louie, P.K., Watson, J.G., Chow, J.C., Chen, A., Sin, D.W. and Lau, A.K., 2005. Seasonal characteristics and regional transport of PM<sub>2.5</sub> in Hong Kong. *Atmos. Environ.* 39 (9), 1695-1710.
- Lu, S.L., Zhang, R., Yao, Z.K., Yi, F., Ren, J.J., Wu, M.H., Feng, M. and Wang, Q.Y., 2012. Size distribution of chemical elements and their source apportionment in ambient coarse, fine, and ultrafine particles in Shanghai urban summer atmosphere. *J. Environ. Sci-China* 24 (5), 882-890.
- Lu, Z.F., Zhang, Q. and Streets, D.G., 2011. Sulfur dioxide and primary carbonaceous aerosol emissions in China and India, 1996–2010. *Atmos. Chem. Phys.* 11 (18), 9839-9864.
- Luo, X.S., Ip, C.C.M., Li, W., Tao, S. and Li, X.D., 2014. Spatial–temporal variations, sources, and transport of airborne inhalable metals (PM<sub>10</sub>) in urban and rural areas of northern China. *Atmos. Chem. Phys. Discuss* 14 (9), 13133-13165.
- Ma, J.Z., Tang, J., Li, S.M. and Jacobson, M.Z., 2003. Size distributions of ionic aerosols measured at Waliguan Observatory: Implication for nitrate gas-to-particle transfer processes in the free troposphere. *J. Geophys. Res.* 108 (D17).
- McLean, J.E. and Bledsoe, B.E., 1996. Behavior of Metals in Soils<sup>1</sup>. EPA Environmental Assessment Sourcebook, 19.
- McNaughton, C.S., Clarke, A.D., Kapustin, V., Shinozuka, Y., Howell, S.G., Anderson, B., Winstead, E., Dibb, J., Scheuer, E. and Cohen, R.C., 2009. Observations of heterogeneous reactions between Asian pollution and mineral dust over the Eastern North Pacific during INTEX-B. *Atmos. Chem. Phys.* 9 (21), 8283-8308.
- Meng, Z.Y., Jia, X.F., Zhang, R.J., Yu, X.M. and Ma, Q.L., 2012. Characteristics of PM<sub>2.5</sub> at Lin'an regional background station in the Yangtze River Delta Region. *Journal of Applied Meteorological Science* 23 (4), 424-432.
- Meng, Z.Y., Xu, X.B., Wang, T., Zhang, X.Y., Yu, X.L., Wang, S.F., Lin, W.L., Chen, Y.Z., Jiang, Y.A. and An, X.Q., 2010. Ambient sulfur dioxide, nitrogen dioxide, and ammonia at ten

- background and rural sites in China during 2007–2008. *Atmos. Environ.* 44 (21), 2625-2631.
- Meng, Z.Y., Xu, X.B., Yan, P., Ding, G.A., Tang, J., Lin, W.L., Xu, X.D. and Wang, S.F., 2009. Characteristics of trace gaseous pollutants at a regional background station in Northern China. *Atmos. Chem. Phys.* 9 (3), 927-936.
- Merolla, L. and Richards, R.J., 2005. In vitro effects of water-soluble metals present in UK particulate matter. *Exp. Lung Res.* 31 (7), 671-683.
- Milford, J.B. and Davidson, C.I., 1985. The size of particulate trace elements in the atmosphere—a review. *J. Air Pollut. Control Assoc.* 35 (12), 1249-1260.
- Molinelli, A.R., Madden, M.C., McGee, J.K., Stonehuerter, J.G. and Ghio, A.J., 2002. Effect of metal removal on the toxicity of airborne particulate matter from the Utah Valley. *Inhal. Toxicol.* 14 (10), 1069-1086.
- Moloi, K., Viksna, A., Selin Lindgren, E. and Standzenieks, P., 2002. Sequential leaching of trace elements in fine-particle aerosol samples on Teflon filters. *X-Ray Spectrom.* 31 (1), 27-34.
- Mukai, H., Tanaka, A., Fujii, T., Zeng, Y.Q., Hong, Y.T., Tang, J., Guo, S., Xue, H.S., Sun, Z.L. and Zhou, J.T., 2001. Regional characteristics of sulfur and lead isotope ratios in the atmosphere at several Chinese urban sites. *Environ. Sci. Technol.* 35 (6), 1064-1071.
- Mukhtar, A. and Limbeck, A., 2011. Development of an ETV-ICP-OES procedure for assessment of bio-accessible trace metal fractions in airborne particulate matter. *J. Anal. At. Spectrom.* 26 (10), 2081-2088.
- Mukhtar, A. and Limbeck, A., 2013. Recent developments in assessment of bio-accessible trace metal fractions in airborne particulate matter: a review. *Anal. Chim. Acta* 774, 11-25.
- Na, K. and Cocker III, D.R., 2009. Characterization and source identification of trace elements in PM<sub>2.5</sub> from Mira Loma, Southern California. *Atmos. Res.* 93 (4), 793-800.
- Nakano, T., Morohashi, S., Yasuda, H., Sakai, M., Aizawa, S., Shichi, K., Morisawa, T., Takahashi, M., Sanada, M. and Matsuura, Y., 2006. Determination of seasonal and regional variation in the provenance of dissolved cations in rain in Japan based on Sr and Pb isotopes. *Atmos. Environ.* 40 (38), 7409-7420.
- Nel, A., 2005. Air pollution-related illness: effects of particles. *Science* 308 (5723), 804-806.
- Nemmar, A., Hoet, P.M., Vanquickenborne, B., Dinsdale, D., Thomeer, M., Hoylaerts, M., Vanbilloen, H., Mortelmans, L. and Nemery, B., 2002. Passage of inhaled particles into the

- blood circulation in humans. *Circulation* 105 (4), 411-414.
- Nenes, A., Pandis, S.N. and Pilinis, C., 1998. ISORROPIA: A new thermodynamic equilibrium model for multiphase multicomponent inorganic aerosols. *Aquat. Geochem.* 4 (1), 123-152.
- Niemi, J., Saarikoski, S., Tervahattu, H., Mäkelä T., Hillamo, R., Vehkamäki, H., Sogacheva, L. and Kulmala, M., 2006. Changes in background aerosol composition in Finland during polluted and clean periods studied by TEM/EDX individual particle analysis. *Atmos. Chem. Phys.* 6, 5049-5066.
- Nriagu, J.O., 1979. Global inventory of natural and anthropogenic emissions of trace metals to the atmosphere. *Nature* 279, 409-411.
- Odum, J.R., Jungkamp, T., Griffin, R., Flagan, R.C. and Seinfeld, J.H., 1997. The atmospheric aerosol-forming potential of whole gasoline vapor. *Science* 276 (5309), 96-99.
- Okubo, A., Takeda, S. and Obata, H., 2013. Atmospheric deposition of trace metals to the western North Pacific Ocean observed at coastal station in Japan. *Atmos. Res.* 129-130, 20-32.
- Okuda, T., Katsuno, M., Naoi, D., Nakao, S., Tanaka, S., He, K., Ma, Y., Lei, Y. and Jia, Y., 2008. Trends in hazardous trace metal concentrations in aerosols collected in Beijing, China from 2001 to 2006. *Chemosphere* 72 (6), 917-924.
- Pöschl, U., 2005. Atmospheric aerosols: Composition, transformation, climate and health effects. *Angew. Chem. Int. Ed.* 44 (46), 7520-7540.
- Pakkanen, T.A., Kerminen, V.-M., Korhonen, C.H., Hillamo, R.E., Aarnio, P., Koskentalo, T. and Maenhaut, W., 2001. Urban and rural ultrafine (PM<sub>0.1</sub>) particles in the Helsinki area. *Atmos. Environ.* 35 (27), 4593-4607.
- Pathak, R., Wu, W. and Wang, T., 2009. Summertime PM<sub>2.5</sub> ionic species in four major cities of China: nitrate formation in an ammonia-deficient atmosphere. *Atmos. Chem. Phys.* 9 (5), 1711-1722.
- Pathak, R.K., Yao, X.H. and Chan, C.K., 2004. Sampling artifacts of acidity and ionic species in PM<sub>2.5</sub>. *Environ. Sci. Technol.* 38 (1), 254-259.
- Phillips, J.I., Green, F.Y., Davies, J.C. and Murray, J., 2010. Pulmonary and systemic toxicity following exposure to nickel nanoparticles. *Am. J. Ind. Med.* 53 (8), 763-767.
- Qu, W., Wang, D., Wang, Y., Sheng, L. and Fu, G., 2010. Seasonal variation, source, and regional representativeness of the background aerosol from two remote sites in western China. *Environ. Monit. Assess.* 167 (1-4), 265-288.

- Qu, W., Zhang, X.Y., Arimoto, R., Wang, Y.Q., Wang, D., Sheng, L.F. and Fu, G., 2009. Aerosol background at two remote CAWNET sites in western China. *Sci. Total. Environ.* 407 (11), 3518-3529.
- Qu, W.J., Zhang, X.Y., Arimoto, R., Wang, D., Wang, Y.Q., Yan, L.W. and Li, Y., 2008. Chemical composition of the background aerosol at two sites in southwestern and northwestern China: potential influences of regional transport. *Tellus B* 60 (4), 657-673.
- Ramanathan, V. and Carmichael, G., 2008. Global and regional climate changes due to black carbon. *Nature Geoscience* 1 (4), 221-227.
- Ramanathan, V., Crutzen, P., Kiehl, J. and Rosenfeld, D., 2001. Aerosols, climate, and the hydrological cycle. *Science* 294 (5549), 2119-2124.
- Reche, C., Viana, M., Amato, F., Alastuey, A., Moreno, T., Hillamo, R., Teinilä K., Saarnio, K., Seco, R. and Peñuelas, J., 2012. Biomass burning contributions to urban aerosols in a coastal Mediterranean city. *Sci. Total. Environ.* 427-428, 175-190.
- Reiss, R., Anderson, E.L., Cross, C.E., Hidy, G., Hoel, D., McClellan, R. and Moolgavkar, S., 2007. Evidence of health impacts of sulfate-and nitrate-containing particles in ambient air. *Inhal. Toxicol.* 19 (5), 419-449.
- Riley, M.R., Boesewetter, D.E., Kim, A.M. and Sirvent, F.P., 2003. Effects of metals Cu, Fe, Ni, V, and Zn on rat lung epithelial cells. *Toxicology* 190 (3), 171-184.
- Rizzo, M.J. and Scheff, P.A., 2007. Utilizing the chemical mass balance and positive matrix factorization models to determine influential species and examine possible rotations in receptor modeling results. *Atmos. Environ.* 41 (33), 6986-6998.
- Rosenfeld, D., 2006. Aerosols, clouds, and climate. *Science* 312 (5778), 1323-1324.
- Sakata, M., Ishikawa, T. and Mitsunobu, S., 2012. Effectiveness of sulfur and boron isotopes in aerosols as tracers of emissions from coal burning in Asian continent. *Atmos. Environ.* 67, 296-303.
- Sakata, M., Tani, Y. and Takagi, T., 2008. Wet and dry deposition fluxes of trace elements in Tokyo Bay. *Atmos. Environ.* 42 (23), 5913-5922.
- Samara, C., Voutsas, D., Kouras, A., Eleftheriadis, K., Maggos, T., Saraga, D. and Petrakakis, M., 2014. Organic and elemental carbon associated to PM<sub>10</sub> and PM<sub>2.5</sub> at urban sites of northern Greece. *Environ. Sci. Pollut. Res.* 21 (3), 1769-1785.
- Sang, X.F., Chan, C.Y., Engling, G., Chan, L.Y., Wang, X.M., Zhang, Y.N., Shi, S., Zhang, Z.S., Zhang, T. and Hu, M., 2011. Levoglucosan enhancement in ambient aerosol during

- springtime transport events of biomass burning smoke to Southeast China. *Tellus B* 63 (1), 129-139.
- Schkolnik, G., Falkovich, A.H., Rudich, Y., Maenhaut, W. and Artaxo, P., 2005. New analytical method for the determination of levoglucosan, polyhydroxy compounds, and 2-methylerythritol and its application to smoke and rainwater samples. *Environ. Sci. Technol.* 39 (8), 2744-2752.
- Schleicher, N.J., Norra, S., Chai, F.H., Chen, Y.Z., Wang, S.L., Cen, K., Yu, Y. and Stüben, D., 2011. Temporal variability of trace metal mobility of urban particulate matter from Beijing—A contribution to health impact assessments of aerosols. *Atmos. Environ.* 45 (39), 7248-7265.
- Schroeder, W.H., Dobson, M., Kane, D.M. and Johnson, N.D., 1987. Toxic trace elements associated with airborne particulate matter: a review. *JAPCA* 37 (11), 1267-1285.
- Schroth, A.W., Crusius, J., Sholkovitz, E.R. and Bostick, B.C., 2009. Iron solubility driven by speciation in dust sources to the ocean. *Nature Geoscience* 2 (5), 337-340.
- Schuetzle, D., 1983. Sampling of vehicle emissions for chemical analysis and biological testing. *Environ. Health Perspect.* 47, 65.
- Seinfeld, J.H. and Pandis, S.N., 2012. *Atmospheric chemistry and physics: from air pollution to climate change*. Second edition. Hoboken, New Jersey. John Wiley & Sons.
- Shao, L., Shi, Z., Jones, T., Li, J., Whittaker, A. and B ́r ́B ́ K., 2006. Bioreactivity of particulate matter in Beijing air: results from plasmid DNA assay. *Sci. Total. Environ.* 367 (1), 261-272.
- Shen, G.F., Yuan, S.Y., Xie, Y.N., Xia, S.J., Li, L., Yao, Y.K., Qiao, Y.Z., Zhang, J., Zhao, Q.Y. and Ding, A.J., 2014. Ambient levels and temporal variations of PM<sub>2.5</sub> and PM<sub>10</sub> at a residential site in the mega-city, Nanjing, in the western Yangtze River Delta, China. *J. Environ. Sci. Heal. A.* 49 (2), 171-178.
- Shi, Z., Bonneville, S., Krom, M., Carslaw, K., Jickells, T., Baker, A. and Benning, L.G., 2011. Iron dissolution kinetics of mineral dust at low pH during simulated atmospheric processing. *Atmos. Chem. Phys.* 11 (3), 995-1007.
- Simoneit, B.R., Schauer, J.J., Nolte, C., Oros, D.R., Elias, V.O., Fraser, M., Rogge, W. and Cass, G.R., 1999. Levoglucosan, a tracer for cellulose in biomass burning and atmospheric particles. *Atmos. Environ.* 33 (2), 173-182.
- Smichowski, P., Polla, G. and G ́omez, D., 2005. Metal fractionation of atmospheric aerosols via sequential chemical extraction: a review. *Anal. Bioanal. Chem.* 381 (2), 302-316.

- Spurný, K., 2000. *Aerosol chemical processes in the environment*. CRC Press.
- Streets, D.G., Bond, T., Carmichael, G., Fernandes, S., Fu, Q., He, D., Klimont, Z., Nelson, S., Tsai, N. and Wang, M.Q., 2003. An inventory of gaseous and primary aerosol emissions in Asia in the year 2000. *J. Geophys. Res.* 108 (D21).
- Sun, G., Crissman, K., Norwood, J., Richards, J., Slade, R. and Hatch, G.E., 2001. Oxidative interactions of synthetic lung epithelial lining fluid with metal-containing particulate matter. *American Journal of Physiology-Lung Cellular and Molecular Physiology* 281 (4), L807-L815.
- Sun, Y.L., Zhuang, G.S., Wang, Y., Zhao, X.J., Li, J., Wang, Z.F. and An, Z.S., 2005. Chemical composition of dust storms in Beijing and implications for the mixing of mineral aerosol with pollution aerosol on the pathway. *J. Geophys. Res.* 110 (D24).
- Surratt, J.D., Lewandowski, M., Offenberg, J.H., Jaoui, M., Kleindienst, T.E., Edney, E.O. and Seinfeld, J.H., 2007. Effect of acidity on secondary organic aerosol formation from isoprene. *Environ. Sci. Technol.* 41 (15), 5363-5369.
- Tan, J.H., Duan, J.C., Chen, D.H., Wang, X.H., Guo, S.J., Bi, X.H., Sheng, G.Y., He, K.B. and Fu, J.M., 2009. Chemical characteristics of haze during summer and winter in Guangzhou. *Atmos. Res.* 94 (2), 238-245.
- Tan, M.G., Zhang, G.L., Li, X.L., Zhang, Y.X., Yue, W.S., Chen, J.M., Wang, Y.S., Li, A.G., Li, Y. and Zhang, Y.M., 2006. Comprehensive study of lead pollution in Shanghai by multiple techniques. *Anal. Chem.* 78 (23), 8044-8050.
- Tanner, P.A., Ma, H.L. and Yu, P.K.N., 2008. Fingerprinting metals in urban street dust of Beijing, Shanghai, and Hong Kong. *Environ. Sci. Technol.* 42 (19), 7111-7117.
- Tao, F., Gonzalez-Flecha, B. and Kobzik, L., 2003. Reactive oxygen species in pulmonary inflammation by ambient particulates. *Free Radic. Biol. Med.* 35 (4), 327.
- Tessier, A., Campbell, P.G.C. and Bisson, M., 1979. Sequential extraction procedure for the speciation of particulate trace metals. *Anal. Chem.* 51 (7), 844-851.
- Twining, J., McGlenn, P., Loi, E., Smith, K. and Gieré R., 2005. Risk ranking of bioaccessible metals from fly ash dissolved in simulated lung and gut fluids. *Environ. Sci. Technol.* 39 (19), 7749-7756.
- Urban, R.C., Lima-Souza, M., Caetano-Silva, L., Queiroz, M.E.C., Nogueira, R.F.P., Allen, A.G., Cardoso, A.A., Held, G. and Campos, M.L.A.M., 2012. Use of levoglucosan, potassium, and water-soluble organic carbon to characterize the origins of biomass-burning aerosols. *Atmos. Environ.* 61, 562-569.

- US EPA., 2009. Risk Assessment Guidance for Superfund. Part F, Supplemental Guidance for Inhalation Risk Assessment, vol, I. <http://www2.epa.gov/sites/production/files/2015-09/documents/partf>.
- Uzu, G., Sauvain, J.J., Baeza-Squiban, A., Riediker, M., Sánchez Sandoval Hohl, M., Val, S., Tack, K., Denys, S., Pradère, P. and Dumat, C., 2011. In vitro assessment of the pulmonary toxicity and gastric availability of lead-rich particles from a lead recycling plant. *Environ. Sci. Technol.* 45 (18), 7888-7895.
- Viana, M., Querol, X., Alastuey, A., Ballester, F., Llop, S., Esplugues, A., Fernández-Patier, R., García dos Santos, S. and Herce, M.D., 2008. Characterising exposure to PM aerosols for an epidemiological study. *Atmos. Environ.* 42 (7), 1552-1568.
- Voutsas, D. and Samara, C., 2002. Labile and bioaccessible fractions of heavy metals in the airborne particulate matter from urban and industrial areas. *Atmos. Environ.* 36 (22), 3583-3590.
- Waheed, A., Li, X.L., Tan, M.G., Bao, L.M., Liu, J.F., Zhang, Y.X., Zhang, G.L. and Li, Y., 2011. Size distribution and sources of trace metals in ultrafine/fine/coarse airborne particles in the atmosphere of Shanghai. *Aerosol Sci. Technol.* 45 (2), 163-171.
- Walcek, C.J. and Aleksic, N.M., 1998. A simple but accurate mass conservative, peak-preserving, mixing ratio bounded advection algorithm with FORTRAN code. *Atmos. Environ.* 32 (22), 3863-3880.
- Wang, G.H., Huang, L.M., Gao, S.X., Gao, S.T. and Wang, L.S., 2002. Characterization of water-soluble species of PM<sub>10</sub> and PM<sub>2.5</sub> aerosols in urban area in Nanjing, China. *Atmos. Environ.* 36 (8), 1299-1307.
- Wang, G.H., Wang, H., Yu, Y.J., Gao, S.X., Feng, J.F., Gao, S.T. and Wang, L.S., 2003. Chemical characterization of water-soluble components of PM<sub>10</sub> and PM<sub>2.5</sub> atmospheric aerosols in five locations of Nanjing, China. *Atmos. Environ.* 37 (21), 2893-2902.
- Wang, J., Hu, Z.M., Chen, Y.Y., Chen, Z.L. and Xu, S.Y., 2013. Contamination characteristics and possible sources of PM<sub>10</sub> and PM<sub>2.5</sub> in different functional areas of Shanghai, China. *Atmos. Environ.* 68, 221-229.
- Wang, M.Y., Cao, C.X., Li, G.S. and Singh, R.P., 2015. Analysis of a severe prolonged regional haze episode in the Yangtze River Delta, China. *Atmos. Environ.* 102, 112-121.
- Wang, P., Bi, S.P., Zhou, Y.P., Tao, Q.S., Gan, W.X., Xu, Y., Hong, Z. and Cai, W.S., 2007a. Study of aluminium distribution and speciation in atmospheric particles of different diameters in Nanjing, China. *Atmos. Environ.* 41 (27), 5788-5796.

- Wang, Q.Q., Shao, M., Liu, Y., William, K., Paul, G., Li, X.H., Liu, Y. and Lu, S.H., 2007b. Impact of biomass burning on urban air quality estimated by organic tracers: Guangzhou and Beijing as cases. *Atmos. Environ.* 41 (37), 8380-8390.
- Wang, T., Wong, C.H., Cheung, T.F., Blake, D.R., Arimoto, R., Baumann, K., Tang, J., Ding, G.A., Yu, X.M. and Li, Y.S., 2004. Relationships of trace gases and aerosols and the emission characteristics at Lin'an, a rural site in eastern China, during spring 2001. *J. Geophys. Res.* 109 (D19).
- Wang, W., Liu, X.D., Zhao, L.W., Guo, D.F., Tian, X.D. and Adams, F., 2006a. Effectiveness of leaded petrol phase-out in Tianjin, China based on the aerosol lead concentration and isotope abundance ratio. *Sci. Total. Environ.* 364 (1), 175-187.
- Wang, X.F., Wang, W.X., Yang, L.X., Gao, X.M., Nie, W., Yu, Y.C., Xu, P.J., Zhou, Y. and Wang, Z., 2012a. The secondary formation of inorganic aerosols in the droplet mode through heterogeneous aqueous reactions under haze conditions. *Atmos. Environ.* 63, 68-76.
- Wang, X.H., Bi, X.H., Sheng, G.Y. and Fu, J.M., 2006b. Chemical composition and sources of PM<sub>10</sub> and PM<sub>2.5</sub> aerosols in Guangzhou, China. *Environ. Monit. Assess.* 119 (1-3), 425-439.
- Wang, Y., Chai, F.H., Liu, H.F. and Wang, Y.H., 2008. Analysis on the characteristics of horizontal transport of the atmospheric pollutant over the Yangtze Delta. *Res. Environ. Sci.* 21 (1), 22-29 (in Chinese).
- Wang, Y., Zhuang, G.S., Tang, A.H., Yuan, H., Sun, Y.L., Chen, S. and Zheng, A.H., 2005. The ion chemistry and the source of PM<sub>2.5</sub> aerosol in Beijing. *Atmos. Environ.* 39 (21), 3771-3784.
- Wang, Y., Zhuang, G.S., Zhang, X.Y., Huang, K., Xu, C., Tang, A.H., Chen, J.M. and An, Z.S., 2006c. The ion chemistry, seasonal cycle, and sources of PM<sub>2.5</sub> and TSP aerosol in Shanghai. *Atmos. Environ.* 40 (16), 2935-2952.
- Wang, Z., Wang, T., Guo, J., Gao, R., Xue, L.K., Zhang, J.M., Zhou, Y., Zhou, X.H., Zhang, Q.Z. and Wang, W.X., 2012b. Formation of secondary organic carbon and cloud impact on carbonaceous aerosols at Mount Tai, North China. *Atmos. Environ.* 46, 516-527.
- Wang, Z.F., Li, J., Wang, X.Q., Pochanart, P. and Akimoto, H., 2006d. Modeling of regional high ozone episode observed at two mountain sites (Mt. Tai and Huang) in East China. *J. Atmos. Chem.* 55 (3), 253-272.
- Wesely, M., 1989. Parameterization of surface resistances to gaseous dry deposition in regional-scale numerical models. *Atmos. Environ.* 23 (6), 1293-1304.
- Wessels, A., Birmili, W., Albrecht, C., Hellack, B., Jermann, E., Wick, G., Harrison, R.M. and

- Schins, R.P., 2010. Oxidant generation and toxicity of size-fractionated ambient particles in human lung epithelial cells. *Environ. Sci. Technol.* 44 (9), 3539-3545.
- WHO. 2000. Air Quality Guidelines for Europe, 2nd edn. World Health Organization, Regional Office for Europe, Copenhagen.
- WHO. 2015. Agents Classified by the IARC Monographs. World Health Organization, International Agency for Research on Cancer.
- Wichmann, H.E. and Peters, A., 2000. Epidemiological evidence of the effects of ultrafine particle exposure. *Philosophical Transactions of the Royal Society of London. Series A: Mathematical, Physical and Engineering Sciences* 358 (1775), 2751-2769.
- Widory, D., Liu, X.D. and Dong, S.P., 2010. Isotopes as tracers of sources of lead and strontium in aerosols (TSP & PM<sub>2.5</sub>) in Beijing. *Atmos. Environ.* 44 (30), 3679-3687.
- Wiseman, C.L. and Zereini, F., 2014. Characterizing metal (loid) solubility in airborne PM<sub>10</sub>, PM<sub>2.5</sub> and PM<sub>1</sub> in Frankfurt, Germany using simulated lung fluids. *Atmos. Environ.* 89, 282-289.
- Wong, C.S.C., Li, X.D., Zhang, G., Qi, S.H. and Peng, X.Z., 2003. Atmospheric deposition of heavy metals in the Pearl River Delta, China. *Atmos. Environ.* 37 (6), 767-776.
- Wong, S.C., Li, X.D., Zhang, G., Qi, S.H. and Min, Y.S., 2002. Heavy metals in agricultural soils of the Pearl River Delta, South China. *Environ. Pollut.* 119 (1), 33-44.
- Wozniak, A.S., Shelley, R.U., Sleighter, R.L., Abdulla, H.A., Morton, P.L., Landing, W.M. and Hatcher, P.G., 2013. Relationships among aerosol water soluble organic matter, iron and aluminum in European, North African, and Marine air masses from the 2010 US GEOTRACES cruise. *Mar. Chem.* 154 (24-33).
- Wu, F., Zhang, D.Z., Cao, J.J., Xu, H.M. and An, Z.S., 2012. Soil-derived sulfate in atmospheric dust particles at Taklimakan desert. *Geophys. Res. Lett.* 39 (24).
- Xiao, S., Wang, Q.Y., Cao, J.J., Huang, R.J., Chen, W.D., Han, Y.M., Xu, H.M., Liu, S.X., Zhou, Y.Q. and Wang, P., 2014. Long-term trends in visibility and impacts of aerosol composition on visibility impairment in Baoji, China. *Atmos. Res.* 149, 88-95.
- Xiao, Z.H., Shao, L.Y., Zhang, N., Wang, J. and Wang, J.Y., 2013. Heavy Metal Compositions and Bioreactivity of Airborne PM<sub>10</sub> in a Valley-Shaped City in Northwestern China. *Aerosol. Air. Qual. Res* 13 (3), 1116-1125.
- Xiu, G.L., Zhang, D.N., Chen, J.Z., Huang, X.J., Chen, Z.X., Guo, H.L. and Pan, J.F., 2004. Characterization of major water-soluble inorganic ions in size-fractionated particulate

- matters in Shanghai campus ambient air. *Atmos. Environ.* 38 (2), 227-236.
- Yadav, A.K., Kumar, K., Kasim, M.H.A., Singh, M.P., Parida, S.K. and Sharan, M., 2003. Visibility and incidence of respiratory diseases during the 1998 haze episode in Brunei Darussalam. *Air Quality*, Springer
- Yang, F., He, K., Ye, B., Chen, X., Cha, L., Cadle, S.H., Chan, T. and Mulawa, P.A., 2005a. One-year record of organic and elemental carbon in fine particles in downtown Beijing and Shanghai. *Atmos. Chem. Phys.* 5 (6), 1449-1457.
- Yang, F.M., Ye, B.M., He, K.B., Ma, Y.L., Cadle, S.H., Chan, T. and Mulawa, P.A., 2005b. Characterization of Atmospheric Mineral Components of PM<sub>2.5</sub> in Beijing and Shanghai, China. *Sci. Total. Environ.* 343 (1), 221-230.
- Yang, H., Yu, J.Z., Ho, S.S.H., Xu, J.H., Wu, W.S., Wan, C.H., Wang, X.D., Wang, X.R. and Wang, L.S., 2005c. The chemical composition of inorganic and carbonaceous materials in PM<sub>2.5</sub> in Nanjing, China. *Atmos. Environ.* 39 (20), 3735-3749.
- Yang, W.F., Yin, Y., Wei, Y.X. and Chen, K., 2010. Characteristics and sources of metal elements in PM<sub>2.5</sub> during hazy days in Nanjing. *China Environ. Sci.* 1, 003 (in Chinese).
- Yao, X.H., Chan, C.K., Fang, M., Cadle, S., Chan, T., Mulawa, P., He, K. and Ye, B., 2002. The water-soluble ionic composition of PM<sub>2.5</sub> in Shanghai and Beijing, China. *Atmos. Environ.* 36 (26), 4223-4234.
- Ye, B.M., Ji, X.L., Yang, H.Z., Yao, X.H., Chan, C.K., Cadle, S.H., Chan, T. and Mulawa, P.A., 2003. Concentration and chemical composition of PM<sub>2.5</sub> in Shanghai for a 1-year period. *Atmos. Environ.* 37 (4), 499-510.
- Ye, X.N., Ma, Z., Zhang, J.C., Du, H.H., Chen, J.M., Chen, H., Yang, X., Gao, W. and Geng, F.H., 2011. Important role of ammonia on haze formation in Shanghai. *Environmental Research Letters* 6 (2), 024019.
- Yttri, K.E., Dye, C. and Kiss, G., 2007. Ambient aerosol concentrations of sugars and sugar-alcohols at four different sites in Norway. *Atmos. Chem. Phys.* 7 (16), 4267-4279.
- Yu, L.D., Wang, G.F., Zhang, R.J., Zhang, L.M., Song, Y., Wu, B.B., Li, X.F., An, K. and Chu, J.H., 2013. Characterization and source apportionment of PM<sub>2.5</sub> in an urban environment in Beijing. *Aerosol. Air. Qual. Res.* 13 (2), 574-583.
- Zaveri, R.A. and Peters, L.K., 1999. A new lumped structure photochemical mechanism for large-scale applications. *J. Geophys. Res.* 104 (D23), 30387-30415.
- Zereini, F., Wiseman, C.L.S. and Püttmann, W., 2012. In Vitro Investigations of Platinum,

Palladium, and Rhodium Mobility in Urban Airborne Particulate Matter (PM<sub>10</sub>, PM<sub>2.5</sub>, and PM<sub>1</sub>) Using Simulated Lung Fluids. *Environ. Sci. Technol.* 46 (18), 10326-10333.

Zhang, F., Cheng, H.R., Wang, Z.W., Lv, X.P., Zhu, Z.M., Zhang, G. and Wang, X.M., 2014. Fine particles (PM<sub>2.5</sub>) at a CAWNET background site in Central China: Chemical compositions, seasonal variations and regional pollution events. *Atmos. Environ.* 86, 193-202.

Zhang, G., Li, J., Li, X.D., Xu, Y., Guo, L.L., Tang, J.H., Lee, C.S.L., Liu, X. and Chen, Y.J., 2010. Impact of anthropogenic emissions and open biomass burning on regional carbonaceous aerosols in South China. *Environ. Pollut.* 158 (11), 3392-3400.

Zhang, Q., Jimenez, J.L., Worsnop, D.R. and Canagaratna, M., 2007. A case study of urban particle acidity and its influence on secondary organic aerosol. *Environ. Sci. Technol.* 41 (9), 3213-3219.

Zhang, Q., Quan, J.N., Tie, X.X., Li, X., Liu, Q., Gao, Y. and Zhao, D.L., 2015. Effects of meteorology and secondary particle formation on visibility during heavy haze events in Beijing, China. *Sci. Total. Environ.* 502, 578-584.

Zhang, Q., Streets, D.G., Carmichael, G.R., He, K.B., Huo, H., Kannari, A., Klimont, Z., Park, I.S., Reddy, S. and Fu, J.S., 2009a. Asian emissions in 2006 for the NASA INTEX-B mission. *Atmos. Chem. Phys.* 9 (14), 5131-5153.

Zhang, R.J., Wang, M.X., Zhang, X.Y. and Zhu, G.H., 2003. Analysis on the chemical and physical properties of particles in a dust storm in spring in Beijing. *Powder Technol.* 137 (1), 77-82.

Zhang, S.M., Dai, Y.H., Xie, X.H., Fan, Z.Y., Tan, Z.W. and Zhang, Y.F., 2009b. Surveillance of childhood blood lead levels in 14 cities of China in 2004-2006. *Biomed. Environ. Sci.* 22 (4), 288-296.

Zhang, T., Claeys, M., Cachier, H., Dong, S., Wang, W., Maenhaut, W. and Liu, X., 2008a. Identification and estimation of the biomass burning contribution to Beijing aerosol using levoglucosan as a molecular marker. *Atmos. Environ.* 42 (29), 7013-7021.

Zhang, W., Sun, Y., Zhuang, G. and Xu, D., 2006. Characteristics and seasonal variations of PM<sub>2.5</sub>, PM<sub>10</sub>, and TSP aerosol in Beijing. *Biomed. Environ. Sci.* 19 (6), 461.

Zhang, W.G., Feng, H., Chang, J.N., Qu, J.G. and Yu, L.Z., 2008b. Lead (Pb) isotopes as a tracer of Pb origin in Yangtze River intertidal zone. *Chem. Geol.* 257 (3), 257-263.

Zhang, X.Y., Wang, Y.Q., Niu, T., Zhang, X.C., Gong, S.L., Zhang, Y.M. and Sun, J.Y., 2012a. Atmospheric aerosol compositions in China: spatial/temporal variability, chemical signature,

- regional haze distribution and comparisons with global aerosols. *Atmos. Chem. Phys.* 12 (2), 779-799.
- Zhang, Y.L. and Cao, F., 2015. Fine particulate matter (PM<sub>2.5</sub>) in China at a city level. *Scientific Reports* 5:14884.
- Zhang, Y.N., Zhang, Z.S., Chan, C.Y., Engling, G., Sang, X.F., Shi, S. and Wang, X.M., 2012b. Levoglucosan and carbonaceous species in the background aerosol of coastal southeast China: case study on transport of biomass burning smoke from the Philippines. *Environ. Sci. Pollut. Res.* 19 (1), 244-255.
- Zhang, Y.Y., Obrist, D., Zielinska, B. and Gertler, A., 2013. Particulate emissions from different types of biomass burning. *Atmos. Environ.* 72, 27-35.
- Zhao, B., Wang, P., Ma, J.Z., Zhu, S., Pozzer, A. and Li, W., 2012. A high-resolution emission inventory of primary pollutants for the Huabei region, China. *Atmos. Chem. Phys.* 12 (1), 481-501.
- Zhao, P.S., Dong, F., He, D., Zhao, X.J., Zhang, X.L., Zhang, W.Z., Yao, Q. and Liu, H.Y., 2013a. Characteristics of concentrations and chemical compositions for PM<sub>2.5</sub> in the region of Beijing, Tianjin, and Hebei, China. *Atmos. Chem. Phys.* 13 (9), 4631-4644.
- Zhao, X.J., Zhao, P.S., Xu, J., Meng, W., Pu, W.W., Dong, F., He, D. and Shi, Q.F., 2013b. Analysis of a winter regional haze event and its formation mechanism in the North China Plain. *Atmos. Chem. Phys.* 13 (11), 5685-5696.
- Zhao, Z.Q., Zhang, W., Li, X.D., Yang, Z., Zheng, H.Y., Ding, H., Wang, Q.L., Xiao, J. and Fu, P.Q., 2015. Atmospheric lead in urban Guiyang, Southwest China: isotopic sources signatures. *Atmos. Environ.* 115, 163-169.
- Zheng, J., Tan, M.G., Shibata, Y., Tanaka, A., Li, Y., Zhang, G.L., Zhang, Y.M. and Shan, Z.C., 2004. Characteristics of lead isotope ratios and elemental concentrations in PM<sub>10</sub> fraction of airborne particulate matter in Shanghai after the phase-out of leaded gasoline. *Atmos. Environ.* 38 (8), 1191-1200.
- Zheng, J.Y., Zhang, L.J., Che, W.W., Zheng, Z.Y. and Yin, S.S., 2009. A highly resolved temporal and spatial air pollutant emission inventory for the Pearl River Delta region, China and its uncertainty assessment. *Atmos. Environ.* 43 (32), 5112-5122.
- Zheng, M., Wang, F., Hagler, G., Hou, X., Bergin, M., Cheng, Y., Salmon, L., Schauer, J.J., Louie, P.K. and Zeng, L., 2011. Sources of excess urban carbonaceous aerosol in the Pearl River Delta Region, China. *Atmos. Environ.* 45 (5), 1175-1182.
- Zhou, S.Z., Wang, Z., Gao, R., Xue, L.K., Yuan, C., Wang, T., Gao, X.M., Wang, X.F., Nie, W.

and Xu, Z., 2012. Formation of secondary organic carbon and long-range transport of carbonaceous aerosols at Mount Heng in South China. *Atmos. Environ.* 63, 203-212.

Zhu, B., Su, J.F., Kang, H.Q. and Cai, Y., 2012. The impact of crop residue burning on air quality over Yangtze River delta, China: Observation and simulation. *Geoscience and Remote Sensing Symposium (IGARSS), 2012 IEEE International*, 3642-3645.

Zhu, B.Q., 1998. *Theory and application of isotopic systematic in Earth Science*. Science Press, Beijing (in Chinese).

Zhu, B.Q., Chen, Y.W. and Peng, J.H., 2001. Lead isotope geochemistry of the urban environment in the Pearl River Delta. *Appl. Geochem.* 16 (4), 409-417.

## **Database of Original Results from All Experiments in the Study**

Raw data from this study has been provided in the CD, which includes all the results from every experiment involved in the thesis.